# Study of Cell Division Genes *sepF*, *SCO2078* and *divIVA* in *Streptomyces coelicolor*

Sundeep Kaur
4748611

A thesis submitted for the degree of Doctor of Philosophy

University of East Anglia
School of Biological Sciences

September 2018

**Abstract**

*Streptomyces coelicolor* is a model organism for growth and cell division, with a unique advantage for using this organism for studying cell division since this bacterium does not require division for its viability, but only for sporulation. *S. coelicolor* contains a gene cluster of six genes that are key for growth and division. Only two members of this gene cluster, *ftsZ* and *divIVA* has been well characterized, while the role of the other four genes are not yet fully established. FtsZ is a ubiquitous protein for cell division in bacteria, a key for initiating division. FtsZ marks the position of septum formation and recruits a number of proteins to this position forming the so called divisome complex, to complete division. On the other hand, DivIVA has been shown to be essential for growth, which in *Streptomyces* takes place exclusively at hyphal tips. The genetic location of the remaining genes suggests that they may be important for either polar growth or division.

This study investigated different aspects of the biological role of three genes of this cluster, namely *sepF*, *SCO2078* and *divIVA* genes, which encompass one half of the cell growth and division cluster. The phenotypes of the knockout mutants of *sepF* and *SCO2078* were characterised by monitoring cellular development macroscopically on solid medium. In addition, epi-fluorescence microscopy was used to analyse both cell wall and chromosomal DNA in these mutants compared to the wild-type strain. Also, the effect of overproduction of both SepF and SCO2078 proteins in *S. coelicolor* was tested using the vector pIJ6902, one of the few variable inducible overexpression vectors available for *Streptomyces* research. This study identified some of the shortcomings of the pIJ6902 vector, including the accessibility of the inducer to the different cellular compartments within the complex *Streptomyces* colony and the importance of efficient translation of the genes cloned into pIJ6902. It was also shown that the sequences upstream of the translational start points had a major effect on the efficiency of overexpression of proteins. Additionally, polar growth and DivIVA localisation under selected stress conditions was investigated.

**Acknowledgments**

Firstly, I would like to thank my supervisor, Gabriella Kelemen, for her support and guidance during my time in the laboratory. I would also like to thank all those who helped me in my research endeavors.

A special thank you to my friends Elena Tan, Monika Zietek, Rebecca Lo, Alan Lau, Emily Alcock and Gemma Cassettari for all their support in and out of the laboratory. And thank you to Liz Coe, our weekly “science chat” kept me going!

Also, I am deeply grateful for the love and support of my family, who made it possible for me to pursue research.

**Table of Contents**

# Chapter 1: Introduction

## 1.1. *Streptomyces coelicolor*

*Streptomyces coelicolor* is a model organism for cell cycle and development in bacteria. When it was first discovered it was thought to be part of the fungus family due to its complex life cycle; which mirrors a fungal one, as *Streptomyces* starts out as a spore. However, further analysis has shown this complex microorganism is in fact part of the bacterial *Actinomyces* phylum (Bentley et al., 2002).

*Actinomyces* are extremely abundant and the genus *Streptomyces,* like many of the other bacteria in the phylum, consists principally of soil bacterium. It is found throughout the globe and in varying levels of soil (Omura et al., 2001), and includes examples of marine *Streptomyces*. The soil and marine environment can be a harsh one, and requires any successful bacteria to be hardy, as all resources are under a high amount of competition. This helps to highlight how widespread and well adapted the various *Streptomyces* species truly are.

The challenges that the diverse environments present has been met by *Streptomyces*, including the model organism *S. coelicolor*; which with its 8.6 million base pair and GC rich chromosome has numerous traits that have led to its ubiquitous nature (Bentley et al., 2002). Additionally, the genome is linear, which allows it to be marked into three regions. The primary region is the ‘core’ which separates two ‘arm’ regions (Figure 1.1) (Bentley et al., 2002).

The impressive genome, one of the largest seen for bacteria at the time of its genome sequencing, was sequenced in 2002 (Bentley et al., 2002). There were 7,825 genes predicted, giving a fairly uniform coding density of 88.9% with genes of an average length of 991 base pairs. Of these genes, many are kept in its core region as they vital for survival**,** as the core region is less variable than the ‘arms’ of the *Streptomyces* genome. The arms of the *Streptomyces* genome are not highly conserved and their variable nature allows *Streptomyces* to undergo changes and even deletions of up to a million base pairs without compromising its viability (Bentley et al., 2002).

This can allow beneficial mutations to take place resulting in a bacterium, which with its 65 sigma factors many of which are involved in the regulation to

responses to outside stimuli and stresses, can quickly adapt to its varying environment (Kim et al., 2008).

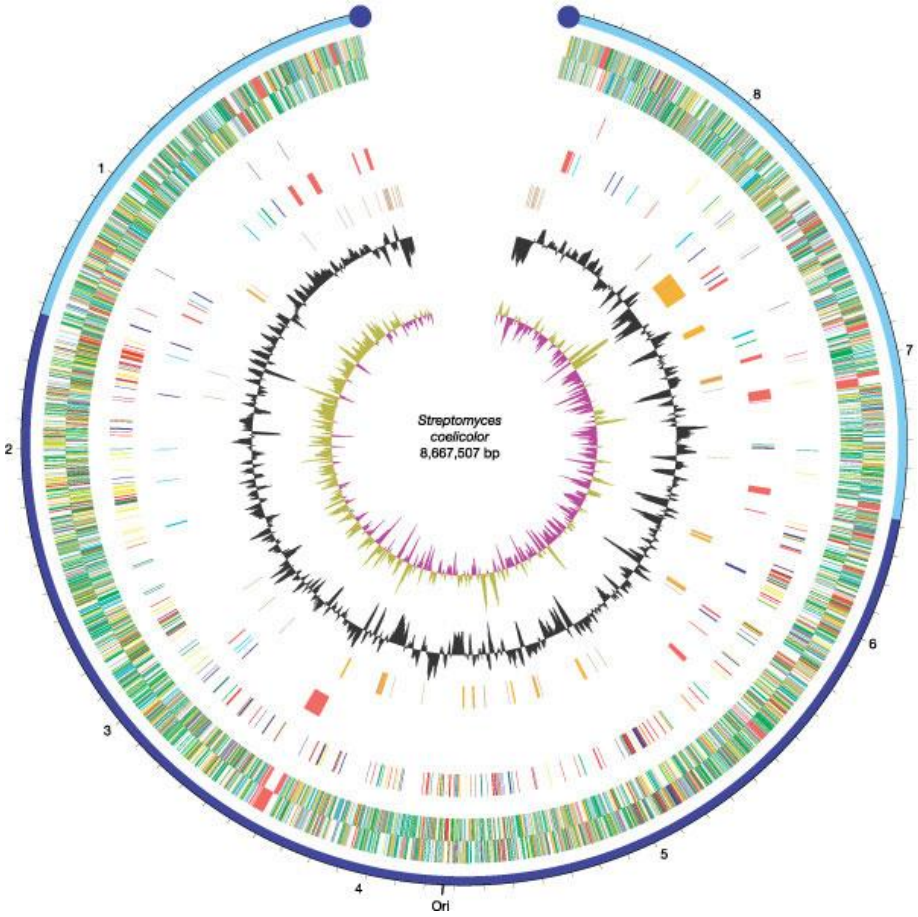


Figure 1.1: The *S. coelicolor* chromosome. The dark blue line shows the core region and the light blue sections show the arms of the chromosome. Image from Bentley *et al*., 2002.

Amongst the 7,825 genes there are a large number of genes with hypothetical function. In addition, some of the genes and pathways are not expressed containing 'sleeping' genes that operate in " silent" secondary pathways (Ikeda et al., 2003).

It is these 'silent' pathways which give *Streptomyces* its competitive edge, as when a resource is in short supply another can be utilised by a secondary pathway to give the same or similar end function (Chater et al., 2010, Ochi and Hosaka, 2013). Secondary pathways are also thought to produce many of the antibiotics and other biologically active substances which have given the *Streptomyces* family much of its fame (Bérdy, 2005).

*Streptomyces* is able to produce a range of antibiotics, with two thirds of antibiotics used being derived from *Streptomyces* alone (Barka et al., 2016, Procópio et al., 2012, Bérdy, 2012). Other secondary metabolites have been utilised as immune-suppressants and anti-cancer agents (Procópio et al., 2012). Other *Actinomyces* can produce substances which can kill parasitic worms and certain insects, evolved for their protection (Yu et al., 2011).

Within *S. coelicolor* it is estimated that there are up to 20 distinct pathways which can produce secondary metabolites. However, only four of these have been accessed under laboratory conditions (Ryding et al., 2002).

*S. coelicolor* is not only an important organism in regard to its potential for secondary metabolites. As mentioned, it is a model organism for cell growth and division. Unlike other bacteria, *Streptomyces* does not rely on cell division to be viable, making it a useful tool to determine proteins required for cell division (McCormick, 2009). Unlike *E. coli* where lots of the cell division genes are essential and therefore hard to study, in *Streptomyces* cell division mutants are viable and are affected mainly at the sporulation stages of development. Additionally, though *S. coelicolor* is not a pathogen, it does share genetic similarities to other actinomycetes such as *Mycobacterium* (Flärdh, 2010). It is estimated that *S. coelicolor* shares up to 3.2 to 4.4 Mbps with *Mycobacterium tuberculosis* and *Mycobacterium leprae*. This means that advances in understanding *Streptomyces* genetics and development could translate to potential advances in *Mycobacterium* knowledge.

### 1.1.1 *Streptomyces* Life Cycle

*S. coelicolor* has a distinctive life cycle, which is complex when compared to standard rod-shaped bacterium.

These Gram-positive bacteria start as a uni-genomic spore, which then grows to form a comprehensive mycelium that is found on below the surface of the growth medium (Jyothikumar et al., 2008) (Figure 1.2).

To do this the spore must first germinate. This involves the formation or one, and occasionally two, germ tubes. The germ tube grows away from the spore via polar growth (Flärdh, 2003b, Flärdh, 2003a). When a sufficient distance has been reached by the germ tube it then under goes a branching event (Flärdh et al., 2012, Richards et al., 2012). The branching is not forked but occurs a distance behind the

growing tip. Branches also grow in a polar manner and can also have branches. This results in an increased growth rate. (Flärdh et al., 2012)

This resulting mycelium is vegetative and is used to collect resources for *S. coelicolor* (Claessen et al., 2006). Its other functions may be protective, as the mycelium is able to secrete proteins. Additionally, the vegetative mycelium is multi-genomic but does not under-go cell division. However, there are septum within the vegetative hyphae, but differ from cell division septa, and thus are called crosswalls (Yagüe et al., 2016). Crosswalls do not completely separate the cell but do form compartments within the mycelium (Celler et al., 2016).

After enough resources have been collected to cause nutrient depletion in the surrounding growth media vegetative growth stops and a new form of growth is triggered (den Hengst et al., 2010, Jyothikumar et al., 2008). This is the aerial growth stage, at which slightly thicker aerial hyphae are formed. As the name suggests, aerial hyphae grow up and out of the growth medium (Gray et al., 1990).

This second mycelium is reproductive and creates spores to allow a new generation of *Streptomyces* to be dispersed (Strakova et al., 2013, Claessen et al., 2006). It also differs from the nutrient collecting hyphae, as it aerial hyphae do not branch.

The aerial hyphae start as multi-genomic structures, but when apical growth stops, aerial hyphae must undergo carefully orchestrated sporulation events to ensure that the chromosomes are segregated fully and packaged to produce spores (Jakimowicz and van Wezel, 2012). These events include the placement of septa along the length of the aerial hyphae. This forms pre-spore compartments, which should only contain one genome. The pre-spores are part of a spore chain which then undergoes a constriction event to separate the spores from one another (Claessen et al., 2006). Each aerial hypha can produce up to 50 spores each (Flärdh and Buttner, 2009).

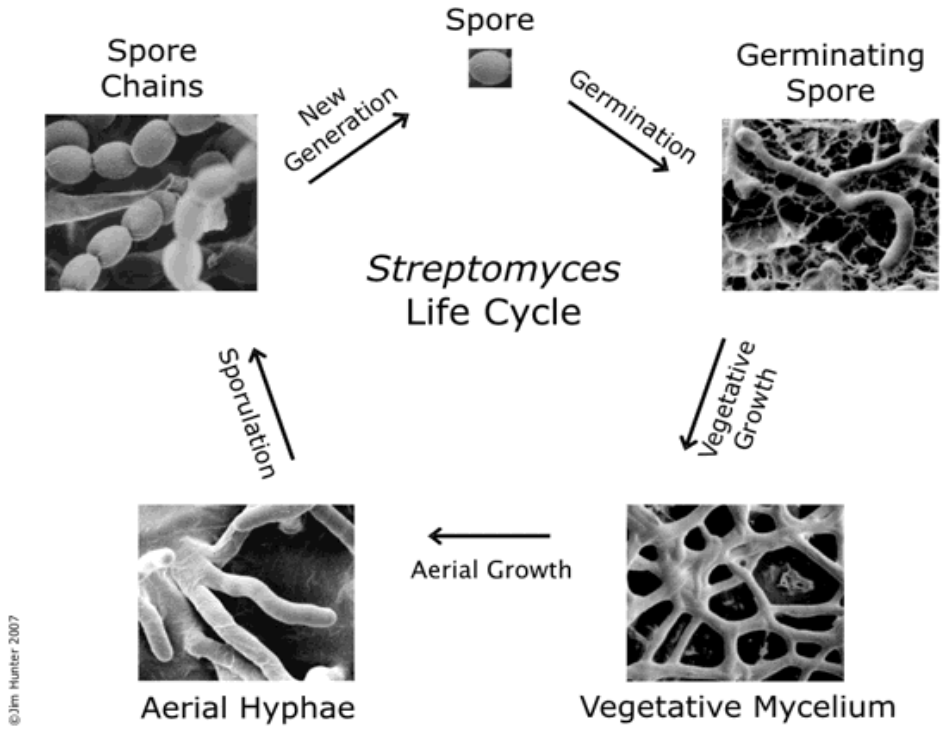


Figure 1.2: The life cycle of *Streptomyces. Streptomyces* starts as a spore which undergoes germination and vegetative growth to produce a vegetative mycelium. Once the mycelium has depleted surrounding resources aerial growth is initiated, and aerial hyphae form. Aerial hyphae then undergo sporulation which is the only cell division event in *Streptomyces*. Images taken by Findlay and Kelemen, 2007.

### 1.1.2. Polar Growth within *Streptomyces*

Vegetative growth and aerial hyphae extension is a result of polar growth. As mentioned, *Streptomyces* has growing tips, which are located one end of the actively growing hyphae (Flärdh, 2003b, Kelemen, 2017, Ausmees, 2013, Flärdh, 2010). The cell wall is not extended laterally, but exclusively at the ends of growing tips. However, growing tips can occur from the lateral cell wall, in order to form branches; each of which has its own growing tip (Hempel et al., 2008, Flärdh et al., 2012, Richards et al., 2012).

The growing tip is governed and driven by the Tip Organising Centre (TIPOC), also known as the polarisome (Flärdh et al., 2012, Fuchino et al., 2013), which is found at the site of each growing tip or pre-branching site (Holmes et al., 2013). The TIPOC is a multiprotein complex, with three players identified; the cytoskeletal proteins DivIVA, Scy, and FilP (Holmes et al., 2013). These three proteins are believed to recruit and organise cell growth machinery and potentially interact with cell division machinery too (Figure 1.3).

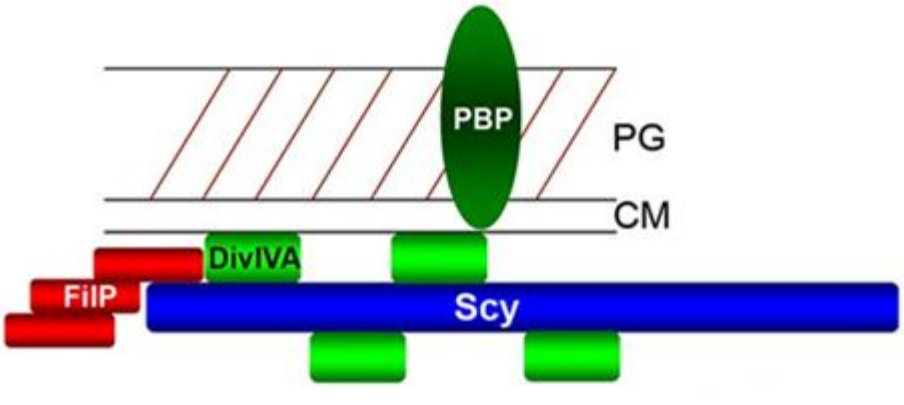


Figure 1.3: The TIPOC of *S. coelicolor,* (Holmes *et al.,* 2013). The proteins Scy, DivIVA and FilP are all coil-coiled and can interact with each to form the TIPOC. Image taken from Holmes et al., 2013.

The most characterised protein within the TIPOC is DivIVA (Flärdh, 2003a, Oliva et al., 2010, Wang et al., 2009, Hempel et al., 2008). *Streptomyces*, like many other Gram-positive bacteria, contains a homologue of *divIVA*, which is an essential gene. DivIVA is believed to be the first protein to the TIPOC and acts as a signal protein to recruit other cell wall machinery (Flärdh, 2010, Flärdh and Buttner, 2009, Hempel et al., 2008). DivIVA in *Streptomyces* contains two coiled coil domains which are present in all DivIVA and a highly conserved 20 amino acid stretch located in the amino terminal domain (Wang et al., 2009). It is thought that it is these conserved areas of DivIVA make the protein functional, as deletions of these stretches affect the cells negatively. The stretch of amino acids 66-201 is *Streptomyces* specific and shown not to be essential, as deletions in this area of *divIVA* did not affect the *Streptomyces* growth (Flärdh, 2003a).

DivIVA has been show to from complexes with itself, with molecular mass ranging from 400-1000kDa (monomeric DivIVA has a mass of 41kDa), and these complexes can be filamentous. It is thought that the second coiled coil structure of DivIVA is essential in multimeric interactions (Wang et al., 2009).

DivIVA has also been shown to localise to small foci along lateral cell walls, marking sites of future branching (Flärdh et al., 2012). These foci have been shown to grow in size as more DivIVA aggregates at future branching sites, some of which comes from the apical growth tip (Hempel et al., 2008). This indicates that DivIVA in *Streptomyces* is a tip marker and potential branch site marker.

It is an essential protein, as knockout mutants are not viable in *Streptomyces*. Additionally, if levels of DivIVA within *S. coelicolor* are increased or decreased the resulting phenotypes are distinctive (Flärdh, 2003a). Studies in which DivIVA was produced at a level 10-fold less than normal the phenotype of the *Streptomyces* differed from the wild-type. The normally smooth looking hyphae were instead curled and kinked in many places. Branching was also affected, with branches appearing in locations close to the hyphae tips and in an irregular fashion. Additionally, a number of cells were lysed. (Flärdh, 2003a)

However, the DNA distribution in the depleted DivIVA strains appeared to be normally spaced and absent in the tips of the hyphae, as seen in the wildtype. The DNA also appeared to be in similar densities and shapes in the two strains. This suggests that DivIVA is involved in branching and apical growth, but not DNA distribution in those branches.

The phenotype of the *Streptomyces* which contained 25-fold more DivIVA than normal, is again highly different when compared to the wild-type. However, western blot analysis showed that DivIVA in these strains was also accompanied by truncated forms of itself which may have affected the phenotype. (Flärdh, 2003a)

The cells observed were shorter and thicker, with a swollen shape, and many were lysed (as seen in the under expression of *divIVA*). The swollen shape of the cells included a larger end, which was pointed away from branches, indicating a form of polarity. They were able to grow into colonies, but at a slower rate than the wildtype. The hyphae were subject to hyperbranching and tip extension was affected. DAPI staining revealed DNA was missing in the larger ends of the cells, and TEM showed that these areas were electron dense, where DivIVA was accumulated. Also, observed were ghost cells which though empty still had a swollen cell shape as seen in the living cells. This indicates that the swollen shape of the cells is not due to DivIVA weakening the cell walls of *Streptomyces*, but instead that DivIVA is also a cell shape determinant. (Flärdh, 2003a)

The other protein of the TIPOC which has been determined to have an important role in cell growth is the *Streptomyces* Cytoskeletal protein (Scy).

The Scy protein affects polarised growth and hyphal geometry, and like DivIVA is a coiled coil protein found in the TIPOC. However, its coil structure differs from that of divIVA, two different types of coils; N-terminal heptad coiled-coils and C-terminal 51mer coiled-coils (Walshaw et al., 2010). It is known to control apical growth and directly interacts with DivIVA (Holmes et al., 2013).

When *scy* is knocked out *Streptomyces* is still able to grow and sporulate, but the mutant strain differs greatly from the wild-type. Mutant colonies are half the size of the wildtype on average and both vegetative and aerial hyphae are affected. Vegetative hyphae show over-branching, tip splitting and formation of tips close to the leading apical tip. Aerial hyphae also exhibit apical branching as well as irregular sporulation, in which septum formation and chromosome distribution are not regular, resulting in fewer spores in mutants. Additionally, the hyphal width is a larger range than that of the wild type and irregular through the hyphae, which could be linked to the unusual cross section shape of the hyphae. The tips of the hyphae were also phenotypically different as they bulged and were not uniform. (Holmes et al., 2013, Kelemen, 2017)

Some of these many changes in the mutant could be due to affect Scy has on DivIVA, which has been shown to directly interact with Scy. It is thought that Scy recruits and organises DivIVA within the tips, and without Scy DivIVA no longer localises exclusively to growing tips or branch sites, but instead can spread to other points in the hyphae. The increased branching in the mutant also suggests that Scy has a large influence on the DivIVA complexes and thus TIPOC formation, though not on the amount of DivIVA itself. (Holmes et al., 2013)

Scy is also able to directly interact with another coiled-coil TIPOC protein; FilP (Holmes et al., 2013). FilP is a form of intermediate filament protein found within *Streptomyces*. It has been shown to have roles in providing hyphae with a rigid structure and also elasticity, using either networks or filament bundles of the self-dimerising protein (Fuchino et al., 2013).

When in the cell, FilP localises strongly at the growing tip and in sites of branching, though it is found throughout the cell as a network (Bagchi et al., 2008). When at tips and branching sites this network of FilP becomes thicker bundles. When hyphae are not growing this strong localisation is not detected.

It has been shown to interact directly with DivIVA and is part of the TIPOC, as shown through localisation studies of growing tips (Fuchino et al., 2013). FilP forms higher order structures when at the apically growing tips, so *in vivo* other

proteins or molecules do affect FilP structures (Bagchi et al., 2008). However, FilP is not reliant on the TIPOC to form networks in order to support cells, as FilP can form networks *in vitro* (Fuchino et al., 2013). It is thought that DivIVA, when in clusters, can recruit and even cause structural remodelling of FilP, as when DivIVA was expressed elsewhere in the hyphae, due to overexpression, FilP was also present in bundle form. Though DivIVA and FilP do interact they do not localise at the exact same points in the growing tips, so interaction is limited to the areas in which FilP and DivIVA are close together, and these areas are not thought to greatly cross over (Ausmees, 2013).

FilP is not an essential gene as knockout studies have shown that will hyphae are affected in terms of elasticity and rigidity, S*treptomyces* is still able to grow with little if any phenotypical differences (Bagchi et al., 2008).

### 1.1.3. Cell Division in *Streptomyces*

In *Streptomyces* cell division is not essential and does not occur until sporulation. Before this, the bacterium is multi-genomic and everything except the spore producing aerial hyphae stays in this state. The chromosomes are found spread and continuous in the mycelium, until sporulation where they condense into single genome 'packets'. Each spore contains only one single chromosome (Hopwood, 2006). This process of chromosome condensation occurs approximately in the same time frame as the cell division septa are formed (Jakimowicz and van Wezel, 2012).

There are two distinct types of septa. The first is septa formed in the vegetative hyphae where they are thought to have a possible structural supporting role. These septa, as known as crosswalls, are formed at fairly regular intervals and enclose compartments with multiple chromosomes (Celler et al., 2016). The second type of septa are found later in development, during sporulation (Jakimowicz and van Wezel, 2012). These septa are evenly spaced within the aerial hyphae forming a 'ladder' which eventually turns into a chain of equally sized spores. This ladder, septation, and chromosome condensation events require many genes, including *ftsZ* and *sepF*.

#### 1.1.3.1. FtsZ in *Streptomyces* Cell Division

As in all bacteria, FtsZ is the driver of cell division, but unlike other bacteria, in *Streptomyces* FtsZ is not essential (McCormick et al., 1994). As previously mentioned, *S. coelicolor* does not require cell division to be viable, as this process only occurs in the later stages of cell development, therefore the lack of cell division is not lethal.

However, as FtsZ does act like its homologues in other bacteria, its absence results in an obvious and distinct phenotype. FtsZ null mutants do not produce spores, as there is no compartmentalisation of chromosomes (Wasserstrom et al., 2013). Compartmentalisation is facilitated by septa, which cannot be formed in *ftsZ* null mutants. Additionally, vegetative crosswalls are not formed, which it thought to contribute to the mutant being unable to grow as the wild-type normally would. This gives *ftsZ* null mutants a 'white' phenotype, opposed to the normal 'grey'. (Flärdh et al., 2000)

The gene itself has three promoters, each with differing expression dependent on the developmental stage. The first promoter, P1, is active during vegetative growth, P2 is upregulated during aerial growth but before division, and P3 is active constitutively (Flärdh et al., 2000).

As suggested by the promoters and shown by knockout mutants, FtsZ is required in both the vegetative and aerial stages of *S. coelicolor*. In aerial hyphae, FtsZ is able to form Z-rings, as seen in other bacteria. These Z-rings form above the basal Z-ring, which divides the aerial hyphae into a spore producing compartment and a sub-apical stem compartment (Dalton et al., 2007). In the sporogenic section of the hyphae up to 50 Z-rings can form synchronously, marking the sites of future septa (Figure 1.4) (Grantcharova et al., 2005). The Z-rings are evenly spaced, giving a ladder like appearance when viewed, ensuring regularly spaced spore compartments can be formed (Schwedock et al., 1997). The appearance of Z-rings is transient, as they mark the sites of septa (Grantcharova et al., 2005).

Before the distinct ladder appearance of the Z-rings, the Z-ring components; FtsZ, has an intermediate form. This is a filament which is spiral-like and spans the sporogenic section of the hyphae. These intermediates are also seen in the vegetative hyphae giving rise to crosswalls (Grantcharova et al., 2005).

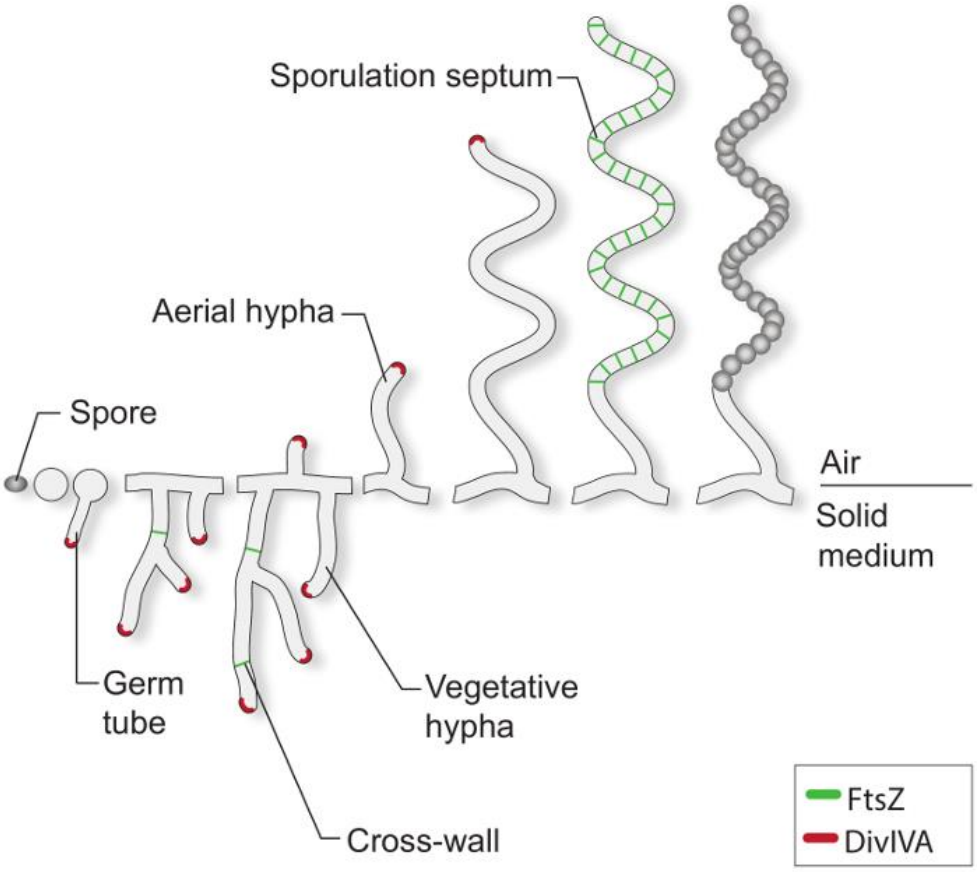


Figure 1.4: The localisation of FtsZ throughout the life cycle of *S. coelicolor.* FtsZ is found in the crosswalls of vegetative hyphae, and in the septum of the aerial hyphae. Image taken from Schlimpert et al., 2017.

**Cell division site regulation via FtsZ**

Though Z-rings are formed in *S. coelicolor* and mark the sites of cell division, there is no known negative regulatory systems, such as the NO or Min system in *Streptomyces*. Instead, a positive regulator of FtsZ positioning, which is specific to *Streptomyces*, controls FtsZ ring formation during sporulation. These are small proteins SsgA and SsgB, which are part of the SsgA-like protein family (Willemse et al., 2011). In addition, SsgA has other roles in *S. coelicolor*, it has been shown to mark the sites of cell wall remodelling during germination, growth and branching.

Prior to cell division, SsgA is localised within the aerial hyphae, and is seen in the young aerial hyphae, before FtsZ been upregulated. At this stage, SsgA is throughout the aerial hyphae in evenly spaced foci (Figure 1.4) (Kormanec and Sevcikova, 2002).

SsgA then recruits SsgB to the cell wall, with localisation studies showing that SsgB is evenly spaced but appears on alternating sides of the hyphae. FtsZ expression is then upregulated, and subsequently FtsZ filaments are formed. These spiral-like filaments span the length of the aerial hyphae (Hopwood, 2006).

SsgB then recruits the FtsZ filament to the future cell division site. It interacts with FtsZ via N-terminal of FtsZ. The filament is still spiral-like but is regular due to its interact with SsgB. At this point, new and smaller SsgB foci can be seen can be seen opposite the original SsgB-FtsZ foci (Barka et al., 2016).

FtsZ then transitions from its filament structure to co-localise with the SsgB foci on both sides of the hyphae. The Z-rings can then form, with evidence that SsgB also forms rings alongside FtsZ (Barka et al., 2016)(Figure 1.5).

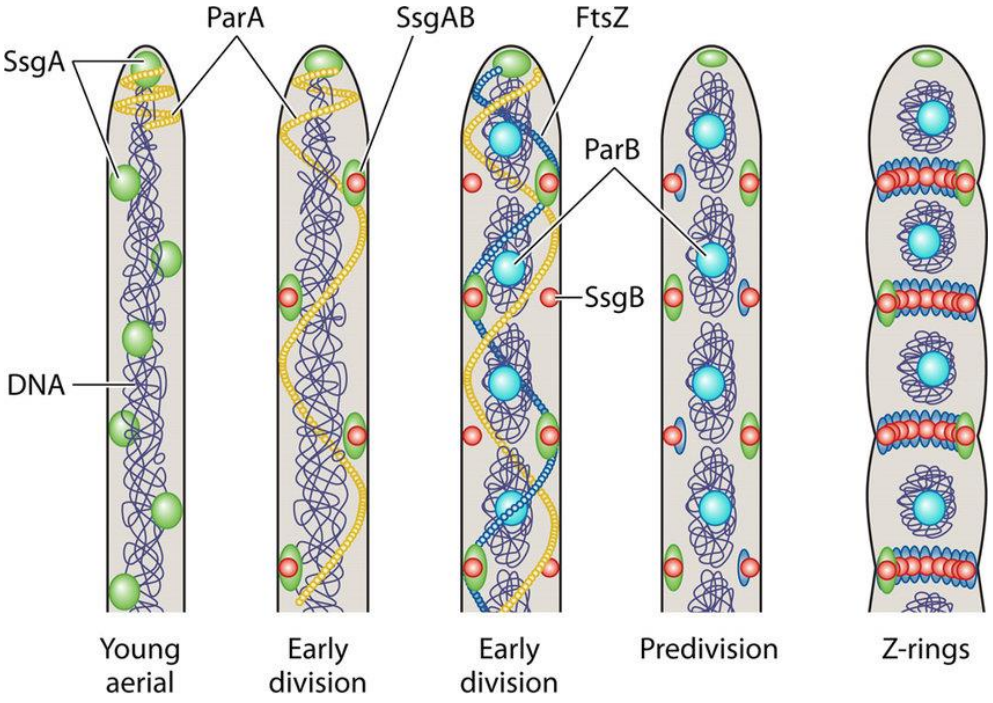


Figure 1.5: The positioning of SsgA and SsgB before and during Z-ring formation in *S. coelicolor*. Image taken from Barka et al., 2016.

## 1.2. Bacterial Growth in Rod Shaped Bacteria

Bacterial growth in rod-shaped bacteria can occur at three main locations within the cell, at the mid-cell, at lateral cell walls, and at the poles (Thanbichler, 2010, Egan et al., 2017). However, first we will focus on the latter two areas and modes of growth. Mid-cell growth is associated with cell division and will be further examined later.

Cell wall elongation, through the addition of new building blocks to the peptidoglycan (PG), a three dimensional polymer built from N-acetylglucosamine (GlcNAc) and N-acetylmuramic acid (MurNAC) monomers of the cell wall (Figure 1.6) at the lateral site of the rod shaped bacterium is known as lateral growth. Lateral growth is seen mostly in rod shaped bacteria and is driven by MreB, a bacterial cytoskeletal protein (Margolin, 2009, Randich and Brun, 2015). The process is characterised by new incorporation of GlcNAc- MurNAC disaccharide into the network of PG at the lateral cell walls, while the poles of the cell are relatively inert in terms of cell wall growth (Egan et al., 2017).

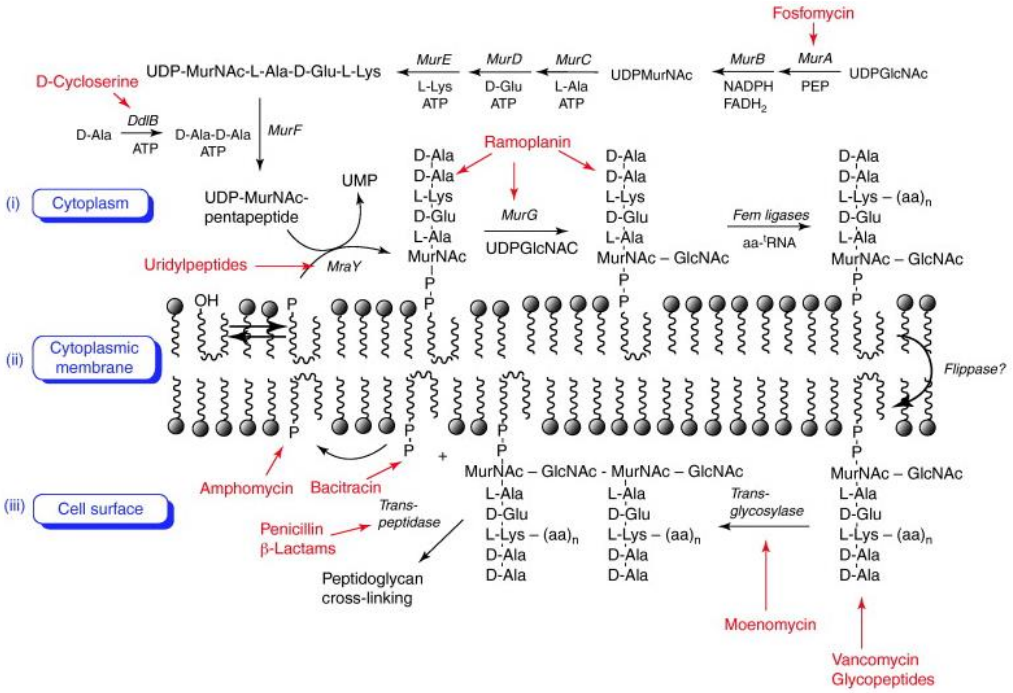


Figure 1.6: Bacterial peptidoglycan biosynthesis, image taken from Bugg et al., 2011. Antibiotics that target peptidoglycan biosynthesis are marked in red.

A different type of growth at the ends of the cell, or at the 'poles', is known as polar growth. Polar growth can be found in some rod shaped bacteria, however, it is prevalent in filamentous bacteria (Cava et al., 2013). Examples of these are *Actinobacteria*, which can vary in form and shape, with generating some relatively complex structures (Brown et al., 2011).

### 1.2.1. Lateral Growth

This form of growth has been described in many bacteria including model organisms such as *Escherichia coli* and *Bacillus subtilis*. It is also known as dispersed elongation, as the introduction of PG precursors can span the whole of the lateral cell wall (Brown et al., 2011).

This growth and insertion of PG into the PG layer is driven by the protein MreB (Schirner and Errington, 2009). MreB is a highly conserved protein, found in the majority of rod shaped bacteria and is a homologue of the eukaryotic protein actin (Juarez and Margolin, 2012). Actin is a microfilament and has a number of important roles within eukaryotes. MreB has a very similar 3D tertiary structure to actin, which allows it form filaments (Daniel and Errington, 2003, Jones et al., 2001). These filaments, or cables, have been shown through subcellular localisation, to form helices (Vats et al., 2009). The helices are singular in *B. subtilis* (Jones et al., 2001), however, within *E. coli* double helices are seen during growth (Figure 1.7) (Kruse et al., 2005).

The MreB helices act as cytoskeletal elements and are thought to interact with a number of different proteins. Some of the proteins include PG synthetic enzymes, such as PBP2 which is dependent on MreB filaments and essential for cell elongation (Varma and Young, 2009, Domínguez-Escobar et al., 2011, Daniel and Errington, 2003), and interactions may promote GT activity of PBPs. Further evidence that MreB drives growth is that cell growth, documented by vancomycin staining of cell wall precursors, which have also been visualised as helices, and thus mirroring the MreB helices (Domínguez-Escobar et al., 2011).

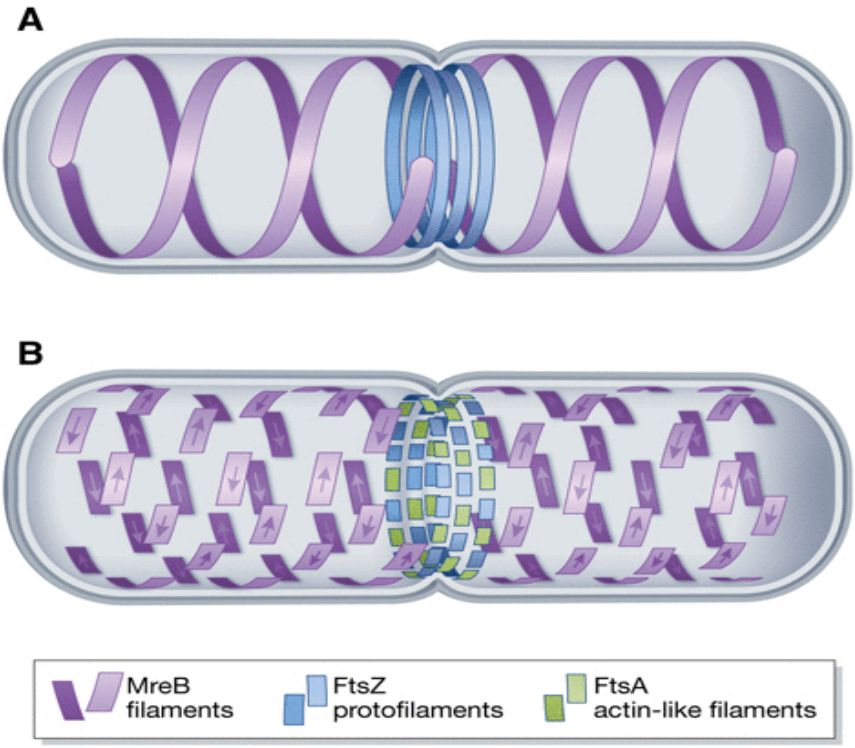


Figure 1.7: Proposed models for MreB localisation during cell growth in *E. coli*. MreB helices are dynamic and their growth is suggested to be through the insertion of MreB filaments throughout the whole of the helix. Image taken from Juarez *et al*., 2012.

MreB also interacts with proteins originating from its operon (*mreBCD*), MreC and MreD (Kruse et al., 2005, Vats et al., 2009), and others such as RodZ (Alyahya et al., 2009, Bendezú et al., 2009) (Figure 1.8). These proteins are thought to act as stabilisers of the MreB helix, through anchoring the filament structure to the membrane. MreB would not be able to do this independently, as it does not contain a membrane anchoring domain. The RodZ protein also interacts with MreB, with proteins forming separate co-dependent helices (Alyahya et al., 2009, Shiomi et al., 2009). The inactivation or overproduction of either protein results in misshapen cells in *E. coli* and in *Caulobacter crescentus* (Bendezú et al., 2009, Alyahya et al., 2009). However, if MreB and RodZ are both equally overproduced then the cell stays rod shaped. They are thought to stabilise the bacterial cell wall, as well as direct the pattern of cell wall growth (Alyahya et al., 2009, Renner et al., 2013, Margolin, 2009).

*E. coli* with defective MreB lose their ability to grow laterally, but instead grow into a spherical shape, similar to that of bacteria lacking MreB (Bendezú et al.,

2009). Therefore, cell growth can be independent of MreB, but requires MreB and the host of other proteins that it directly or indirectly interacts with to ensure lateral growth to give rod-shaped cells.

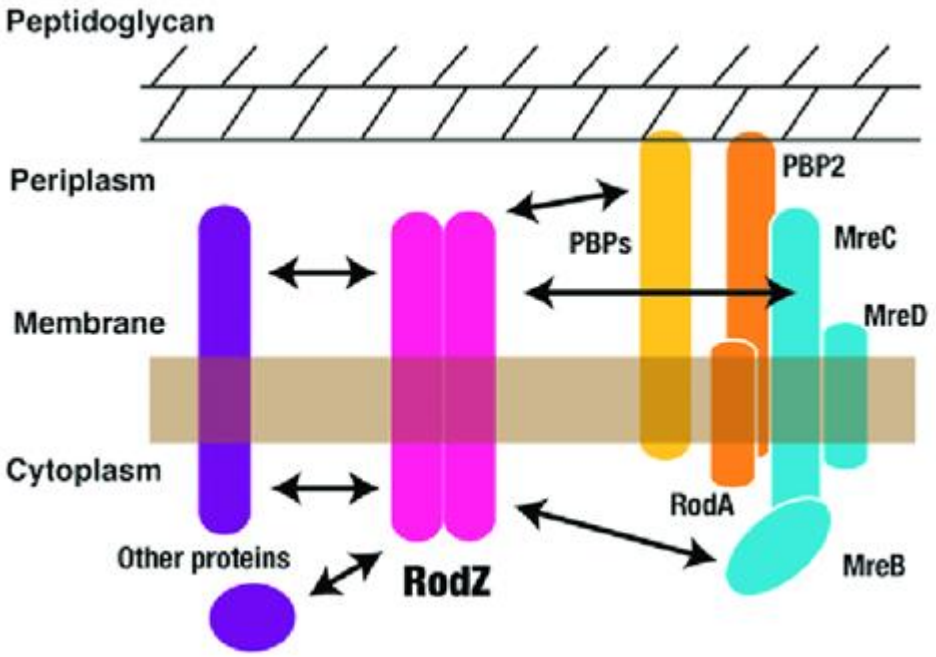


Figure 1.8: The interactions between cell wall machinery in *E. coli*. Taken from Shiomi et al., 2009).

Within *B. subtilis* MreB has two other additional homologs; MreB-like (Mbl) and MreBH (Kawai et al., 2009, Schirner and Errington, 2009). However, additional MreB homologs are not a common feature within Gram-negative bacteria but are seen in Gram-positive species (Schirner and Errington, 2009). The three MreB homologues of *B. subtilis* are able form helices which co-localise thus forming one structure (Carballido-López et al., 2006). It is thought that MreB drives PG synthesis as cell wall precursors have been localised to the MreB helix (Kawai et al., 2009) and has been shown by vancomycin staining (Tiyanont et al., 2006). Null mutants of the different homologues give very different phenotypes, the *mreB* mutants are wide and straight, the *mbl* mutants are wide but twisted, and the *mreBH* mutants are thin and straight, but all are thought to be required to generate a correctly formed rod shape (Kawai et al., 2009, Schirner and Errington, 2009).

### 1.2.2. Polar Growth

Polar growth is a subset of zonal growth, with growing areas restricted to the ends or 'tip' of the cell, and the lateral cell walls are inert (Daniel and Errington, 2003, Laloux and Jacobs-Wagner, 2014, Flärdh, 2010). This form of growth is documented in *Actinobacteria*, with *Streptomyces coelicolor* a model organism for this process (Flärdh, 2010, Ausmees, 2013, Flärdh et al., 2012). However, it can also occur in other bacteria, which due to evolutional niches and pressures have varying forms of polar growth. These forms of polar growth can be exhibited at the ends or poles of bacteria or at one area only, to result in either polar elongation, which can be uni- or bi- directional, budding or stalk growth (Figure 1.9) (Daniel and Errington, 2003, Randich and Brun, 2015, Egan et al., 2017).

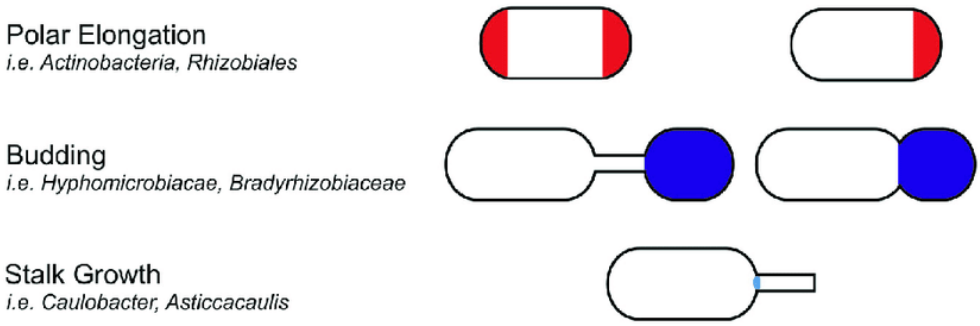


Figure 1.9: Polar growth occurs only at the pole or poles of cell, as shown in red. There are multiple forms of polar growth, with the lateral cell walls staying inert. Image taken from Randich *et al*., 2015.

Polar growth is present in Gram-positives and Gram-negatives, with a number of pathogens, such as *Mycobacterium tuberculosis*, shown to have polar growth (Mukherjee et al., 2009, Kloosterman et al., 2016, Flärdh, 2010). Polar growth is commonly seen in *Actinobacteria*, which are Gram-positive, and contain many different filamentous bacterial species (Flärdh, 2010). Polar growth can also occur in some rod-shaped bacteria, however it differs from polar growth exhibited by non-rod shaped bacteria (Daniel and Errington, 2003). These bacteria are also usually from the *Actinobacteria* group, an example of which is *Corynebacterium glutamicum* (Letek et al., 2008a). These rod-shaped cells are slower growing than their lateral growing rod-shaped counterparts, as growth is restricted to only the cell pole.

The mechanisms of polar growth are unknown, but polar growth within *Actinobacteria* is dependent on the conserved protein DivIVA (Letek et al., 2008b, Kloosterman et al., 2016, Meniche et al., 2014, Saalbach et al., 2013). DivIVA is a key player in cell growth and division, and thus a highly conserved protein, with an homologue found in the model organism *Streptomyces coelicolor* (Flärdh, 2003a, Holmes et al., 2013, Richards et al., 2012). DivIVA is typically associated with cell division, but in bacteria that use polar elongation, it has a role in growth instead. DivIVA is an essential protein for growth for many *Actinobacteria*, though it was first identified as a cell division gene in *B. subtilis* (Cha and Stewart, 1997). In *Actinobacteria*, such as *S. coelicolor* and *Mycobacterium*, DivIVA is a growth protein so localises to the growing end of the cell (Flärdh, 2003a, Kang et al., 2008). Here it can localise other proteins required for cell wall synthesis, such as the penicillin-binding protein 3 (PBP3) (Mukherjee et al., 2009). There is however, indication that DivIVA is not localised to the extreme end of growing cell, but instead a sub-polar location behind the pole, as seen in super-resolution microscopy of *Mycobacterium* (Meniche et al., 2014).

### 1.3. Bacterial Cell Division

Cell division is another highly regulated process, essential to most bacteria. There are varying forms, though the simplest and most well known is division through binary fission.

Binary fission is the propagation process in which a single bacterial cell divides into two identical daughter cells (Wu and Errington, 2004, Haeusser and Margolin, 2016). Once the cell has grown to appropriate size for division, with some exceptions, the bacterial chromosome is replicated and then portioned to separate areas of the cell. A dividing structure known as a septum is formed between the chromosomes, while they are separating (Weiss, 2004, Erickson, 2017a, Jakimowicz and van Wezel, 2012). This process is driven by the divisome, which is a complex of cell division and cytoskeletal proteins (Adams and Errington, 2009). The placement of the septum is regulated so that it is formed at the middle of the cell, so to ensure the resulting cells are even in size (Addinall and Lutkenhaus, 1996, Monahan and Harry, 2013). The septum consists of a cell wall, which is also the site of the start of division. Division usually involves the invagination of the cell wall, till the two cells separate (Errington et al., 2003).

The binary fission process, though relatively simple has a number of players involved. The key protein and driver of binary fission is FtsZ (Erickson, 2017b, Coltharp and Xiao, 2017, de Boer, 2016).

### 1.3.1. FtsZ

The FtsZ protein is a structural homologue of the eukaryotic microtubule forming tubulin (Löwe, 1998, Löwe and Amos, 1998). Though the two primary protein sequences do not share a high amount of homology (~20%), the resulting tertiary structure of the proteins are very similar (Lowe et al., 1998). The *ftsZ* gene, or filament temperature sensitive mutant Z, was first discovered in bacteria in the 1950's (de Boer, 2016). However, it was only in the 1990's when FtsZ was shown to be a cytoskeletal protein, and homologue of tubulin (Mukherjee et al., 1993, RayChaudhuri and Park, 1992, de Boer et al., 1992) .

Structurally, FtsZ is an 388 amino acid long protein, containing two globular domains separated by a central helix and a variable spacer which links the C-terminus to the C-terminal tip (Figure 1.10) (Buske and Levin, 2012). The C-terminus is a tubulin like loop domain, while the N-terminus is a GTPase (Margolin, 2005). The C-terminal tip domain is a conserved peptide which facilitates FtsZ interaction with anchor proteins such as ZipA and FtsA (Du et al., 2015, Buske and Levin, 2012) .

FtsZ has been well studied within *E. coli*, where it is the main driver of cell division and therefore an essential protein (Erickson et al., 2010, Haeusser et al., 2015). Here FtsZ has been shown to locate to the septum in the mid-cell during cell division, through immune-electron microscopy, it is the first protein to be localised to the site of cell division (Bi and Lutkenhaus, 1991), and it is thought to recruit and interact with many other proteins (Margolin, 2005). Importantly, it can also self-interact (Wang et al., 1997), through dimerization. The dimerization events are GTP-dependent and involve the head of one FtsZ interacting with the tail of the other (Mikuni et al., 2015), through the two globular domains. These interactions form protofilaments and can create a ring like structure; the Z-ring (Figure 1.11) (Erickson, 2001, Guan et al., 2018, Haeusser and Margolin, 2016).

The formation of FtsZ polymers is dynamic, as it requires GTP (de Boer et al., 1992, Arjes et al., 2015, Ruiz-Avila et al., 2013). Without it the Z-ring cannot

form, and once the GTP is used up as it is hydrolysed into GDP the FtsZ units stop interacting and cause the Z-ring to dissociate (Wang et al., 1997, Erickson, 2001).

However, while the Z-ring is formed and stable, cell division can occur. This involves the recruitment of other proteins for the stabilisation of the Z-ring, by tethering it to the cell membrane, and maturation of the Z-ring and then for formation of the divisome, which is a large multi-protein complex (Coltharp and Xiao, 2017, Bottomley et al., 2017, Egan et al., 2017). This leads to the division of the cell, as the Z-ring constricts, causing the cytoplasmic membrane to also constrict (Haeusser and Margolin, 2016, Monahan and Harry, 2013). As this layer of the cell is pulled inwards, peptidoglycan synthesis follows, creating the new cell wall for the resulting daughter cells (Erickson, 2017a, Haeusser and Margolin, 2016).

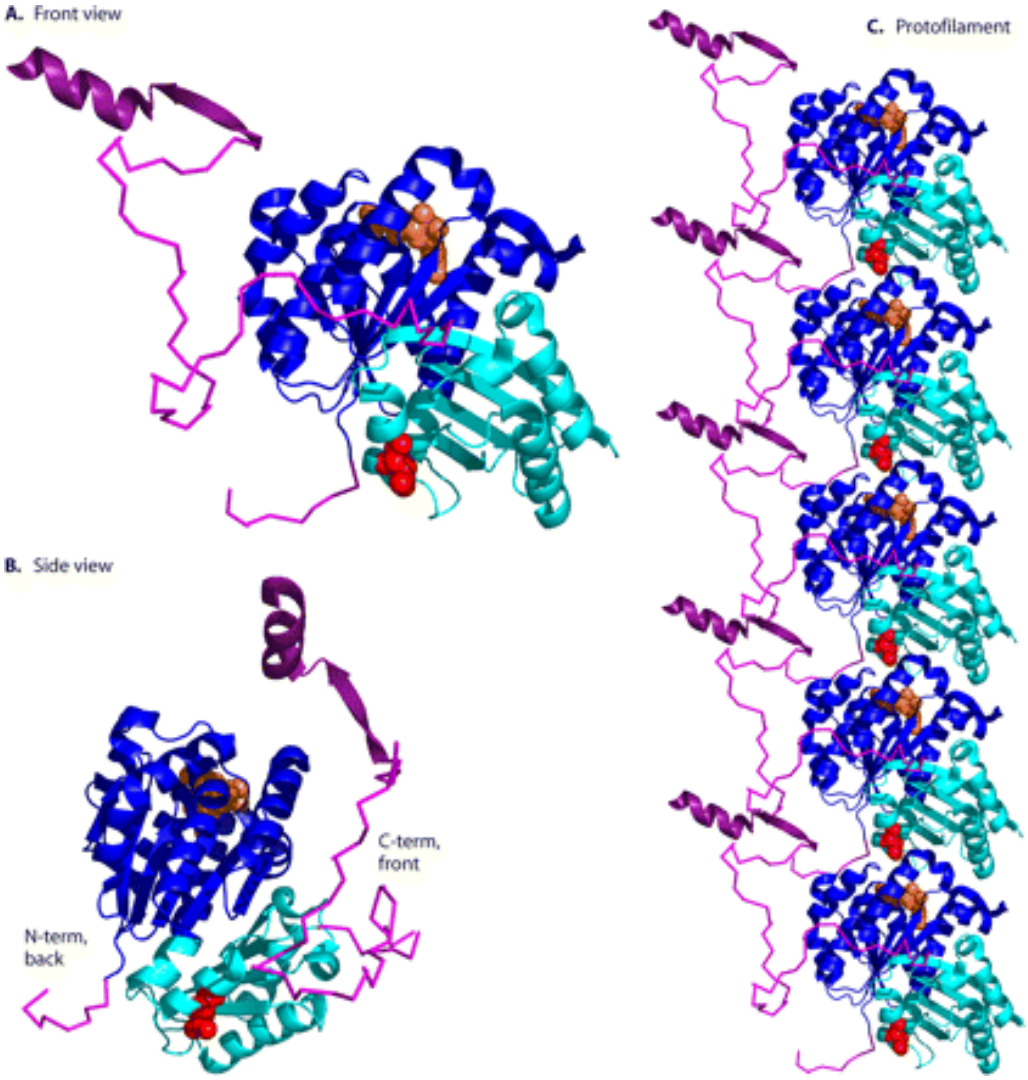


Figure 1.10: The structure of FtsZ in monomeric (A,B) and polymeric forms (C). The two globular domains of FtsZ are shown in dark blue (N-terminal) and cyan (C-terminal), with the remaining linker and C-terminal domains shown in purple. The orange structure represents GDP, and the red region represents the location of a highly conserved synergy loop. Figure taken from Erickson et al., 2010.

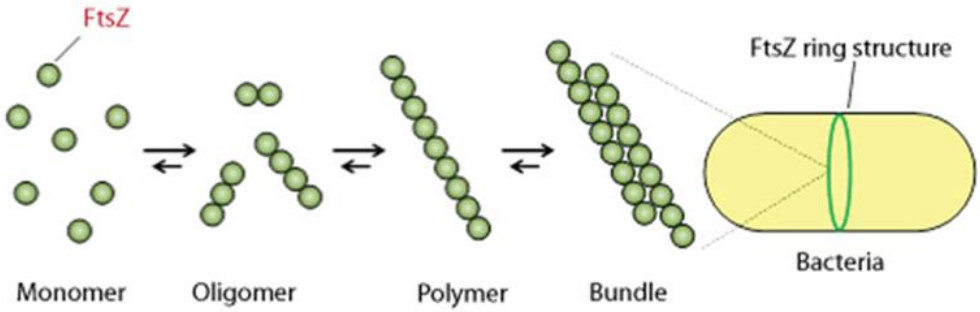


Figure 1.11: FtsZ assembles into pre-filaments before forming filaments required in the Z-ring. Figure taken from Mikuni et al., 2015.

### 1.3.2. Z-ring Regulation

As the Z-ring plays such an important role in cell division it must be carefully controlled, though spatial and temporal regulation. Positive regulation of the Z-ring involves its stabilisation, while negative regulation helps ensure the Z-ring only forms at the mid-cell through the NOC and Min systems (Wu and Errington, 2004, Schumacher, 2017, Monahan et al., 2014).

#### 1.3.2.1. Stabilising FtsZ and the Z-ring

This form of regulation stabilises the Z-ring through anchoring it onto the cell membrane or increasing stability between FtsZ polymers. Within *E. coli* this is facilitated by the trans-membrane proteins ZipA and FtsA (Figure 1.12). They have been shown to localise at the Z-ring, as the Z-ring is forming (Liu et al., 1999, Addinall and Lutkenhaus, 1996). Both proteins are essential in *E. coli,* as they are required for Z-ring formation, but increased activity mutants can compensate for each other's absence (Chen et al., 2017). Additionally, if the proteins are depleted after Z-ring formation then later recruitment of downstream cell division proteins cannot be completed (Pichoff et al., 2012).

FtsA is a member of the actin family (Bork et al., 1992, Mura et al., 2016), and thus can form protofilaments (Szwedziak et al., 2012), and is conserved in many bacterial species (Haeusser and Margolin, 2016). It is one of the first proteins, along with ZipA, to be recruited to the Z-ring (Jensen et al., 2005). It is here where it interacts with FtsZ and the cell membrane (Du et al., 2015). These interactions are thought to be facilitated by the C-terminal of FtsA, as it contains an amphipathic helix which is required for membrane binding (Krupka et al., 2014, Du et al., 2015). FtsA can also self-interact as shown through yeast two-hybrid studies and can form polymers in vitro (Loose and Mitchison, 2014). It has been theorised that FtsA must form dimers or polymers to promote Z-ring assembly, as FtsA monomers generated from non-functional FtsA mutant result in an increased cell toxicity and may inhibit FtsZ polymerisation (Haeusser et al., 2015). However, it was shown that mutations in FtsA which decrease self-interaction, and thus increase the possibility of FtsA in monomer form, can actually bypass the role of ZipA in FtsZ in recruitment of downstream cell division proteins (Pichoff et al., 2012).

ZipA, which is found in γ-proteobacteria and not present in other model organisms such as *B. subtilis* (Margolin, 2003), uses its cytoplasmic domain to

interact with FtsZ via its C-terminal (Mosyak et al., 2000). ZipA is recruited to the cell division site by FtsZ independently of FtsA (Hale and de Boer, 1999, Liu et al., 1999). ZipA, along with tethering FtsZ, also increases Z-ring integrity, and *in vitro* experiments show FtsZ filament bundling is caused by the presence of ZipA (Hale et al., 2000, Krupka et al., 2018). This increase in bundling was seen in straight and curved FtsZ polymers (RayChaudhuri, 1999).

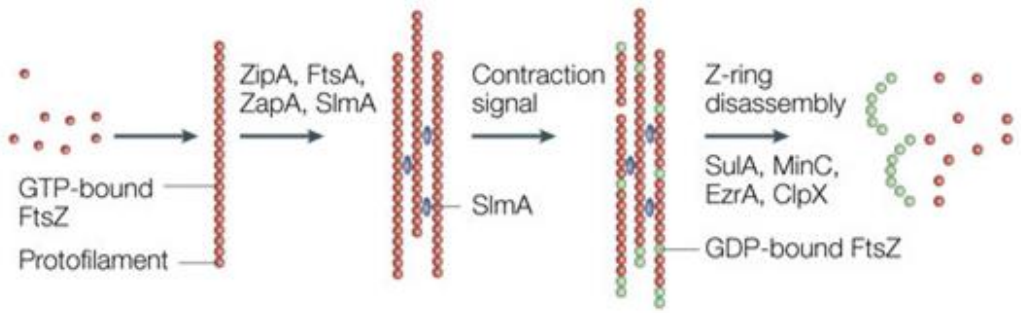


Figure 1.12: Formation and stabilisation of the Z-ring. The Z-ring is stabilised by the ZipA and FtsA proteins. Figure taken from Margolin, 2005.

Though FtsA and ZipA are essential in *E. coli*, *B. subtilis* does not have a homologue of ZipA and *ftsA* mutants are viable (Errington et al., 2003). The *ftsA*-null mutant is slower growing and resulted in filamentous cells (Beall and Lutkenhaus, 1992). Sporulation efficiency is also affected, and this is also seen in another *ftsA* mutant, in which only sporulation, and not vegetative, division is affected (Kemp et al., 2002). In the *ftsA* knockout mutant Z-rings were able to form, but up to 90% of the Z-rings were abnormal. It is thought that the remaining 10% of Z-rings are the sole source of true division in the *ftsA*-null mutants (Jensen et al., 2005). This suggests that the role of FtsA is more critical than previously thought, in respect to Z-ring formation and stabilisation (Jensen et al., 2005). It has also been shown that FtsZ and FtsA associate before Z-ring formation and even FtsZ localisation (Jensen et al., 2005). This suggests that FtsA, in bacteria lacking ZipA, has a vital role.

However, *B. subtilis* has some other proteins, in addition to FtsA, that are involved in Z-ring formation and stabilisation. The Z-ring associated protein, ZapA, is part of the divisome, and is important in Z-ring formation (Buss et al., 2013, Ebersbach et al., 2008). However, it is not essential for septum formation, but its loss of function coupled with other regulatory proteins can block cell division (Gueiros-Filho and Losick, 2002). It has been shown to promote FtsZ polymerisation

*in vitro* and ZapA is able to interact directly with FtsZ (Gamba et al., 2009). It is thought that ZapA forms crosslinks between FtsZ protofilaments, thus increasing lateral stability within the FtsZ filaments (Dajkovic et al., 2010). ZapA is widely conserved, and the *E. coli* ZapA homologue able to localise in the same pattern as the *B. subtilis* orthologue (Gueiros-Filho and Losick, 2002). However, this protein does not tether the Z-ring, so does not share the full role of ZipA in *E. coli*.

Therefore, as *B. subtilis* must have another protein or mechanism to ensure the Z-ring is tethered to the cell membrane, otherwise *ftsA* would be essential for cell division though the *ftsA*-null mutants are viable. This protein would have a similar role within *B. subtilis* than that of ZipA in *E. coli*. SepF, also known as the YlmF, fulfils this role (Ishikawa et al., 2006, Król et al., 2012, Hamoen et al., 2006). SepF is able to interact with FtsZ directly, using a FtsZ-binding site in its C-terminal to bind to the C-terminal of FtsZ (Król et al., 2012). It interacts with the cell membrane via its N-terminal domain, with the first 12 amino acids being highly conserved between SepF homologues. It has been shown that the first 13 amino acids of the *B. subtilis* SepF fold to form an aliphatic helix (Duman et al., 2013). This would allow SepF to anchor FtsZ to the cell membrane, and localisation studies have shown that SepF is present at the cell division site and its localisation is dependent on FtsZ (Hamoen et al., 2006). Additionally, SepF has been shown to bind to lipid membranes and furthermore can recruit FtsZ to the lipid membranes *in vitro* (Duman et al., 2013).

Null mutants of *sepF* have division defects which result in slower cell division, due to some malformation of the septum. The division septum is produced but it is thicker and not smooth looking and is completed later than in the wild-type (Hamoen et al., 2006). Additionally, overexpression of *sepF* can rescue the ftsA-null mutant phenotype, and its deletion in *ftsA*-null mutants is lethal (Ishikawa et al., 2006).

SepF can also self-dimerise, and these dimers can further assemble into large, ~40 nm diameter rings (Duman et al., 2013). These rings are thought to be able to stabilise the Z-ring, by bundling FtsZ protofilaments (Figure 1.13) (Gündoğdu et al., 2011).

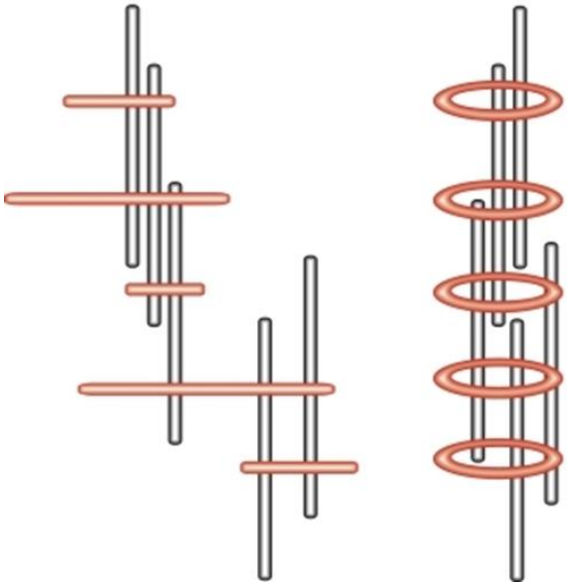

Figure 1.13: SepF (red) can stabilise FtsZ (grey) protofilaments. On the left is model where SepF is linear and supports FtsZ thought crosslinking. The right image shows SepF rings could help stabilise and direct FtsZ protofilaments. Image taken from Gundogdu et al., 2011).

### 1.3.2.2. Negative regulators of FtsZ ring formation: Min system in *E. coli*

The Min system ensures that FtsZ assembly is restricted to the mid-cell in dividing *E. coli* cells, by inhibiting assembly from occurring elsewhere in the cell. It consists of three proteins; MinC, MinD, and MinE (Rowlett and Margolin, 2015, Hajduk et al., 2016, Di Ventura et al., 2013).

The effects of the disruption of the Min proteins was discovered first in the 1960s, with the resulting phenotype of anucleate mini-cells (Adler et al., 1967). Though the Min system is not essential for *E. coli*, without it there are an increase of mini-cells, as FtsZ is able to polymerise and form Z-rings at any position of the cell, often close to the poles (Rowlett and Margolin, 2015).

The MinC and MinD proteins work together to inhibit FtsZ polymerisation, while MinE controls MinD polymerisation and depolymerisation close to the poles (Wu and Errington, 2011).

MinC is the only protein of the system which directly interacts with FtsZ. It consists of two domains (Cordell et al., 2001, An et al., 2013). Though the exact way in which interact occurs is unknown, MinC is able to inhibit FtsZ from forming the Z-ring (Hu et al., 1999).

If MinC was localised everywhere in the cell, it would restrict the formation of the Z-ring, and therefore stop any cell division from taking place. Therefore, to regulate MinC and ensure it is not concentrated at the cell division sites, MinD and MinE are required (Margolin, 2001, Shih and Rothfield, 2006).

MinD is an ATPase able to bind to the cell membrane when bound to ATP (Meinhardt and de Boer, 2001, Hu et al., 2002). Once bound to the membrane MinD can self-interact and polymerise (Taghbalout et al., 2006). MinD localises to one end of the cell, where it becomes bound with MinC. This stops the MinC proteins from being within the vicinity of the mid-cell.

MinD then dissociates from the end of the cell, in an event thought to be triggered by MinE (Hu et al., 2002), and travels to the other end of the cell. Doing so it transports MinC, and thus inhibits Z-ring assembly at this end of the cell. The proteins carry on moving from one cell end to the other, in an oscillating fashion. Though the proteins must move past the mid-point of the cell, and thus inhibit Z-ring formation, relatively the Min proteins spend more time at the ends of the cells than the mid-point (Figure 1.14) (Meinhardt and de Boer, 2001).

The MinE protein stops the MinCD complex from forming throughout the cell. MinE forms a ring which targets the end of the MinCD polymers (Shih et al., 2002) MinE can form dimers which bind to MinD, causing it to dissociate from MinC. MinE also upregulates the ATPase activity of MinD, allowing it to hydrolysis ATP and thus releases MinD from the cell membrane. The monomeric MinD then can travel to the other pole of the cell, which is free of MinE, and can reform into polymers (Suefuji et al., 2002).

The pole to pole oscillation of the Min proteins ensures that the area of lowest inhibition is always the mid-point of the cell (Laloux and Jacobs-Wagner, 2014).

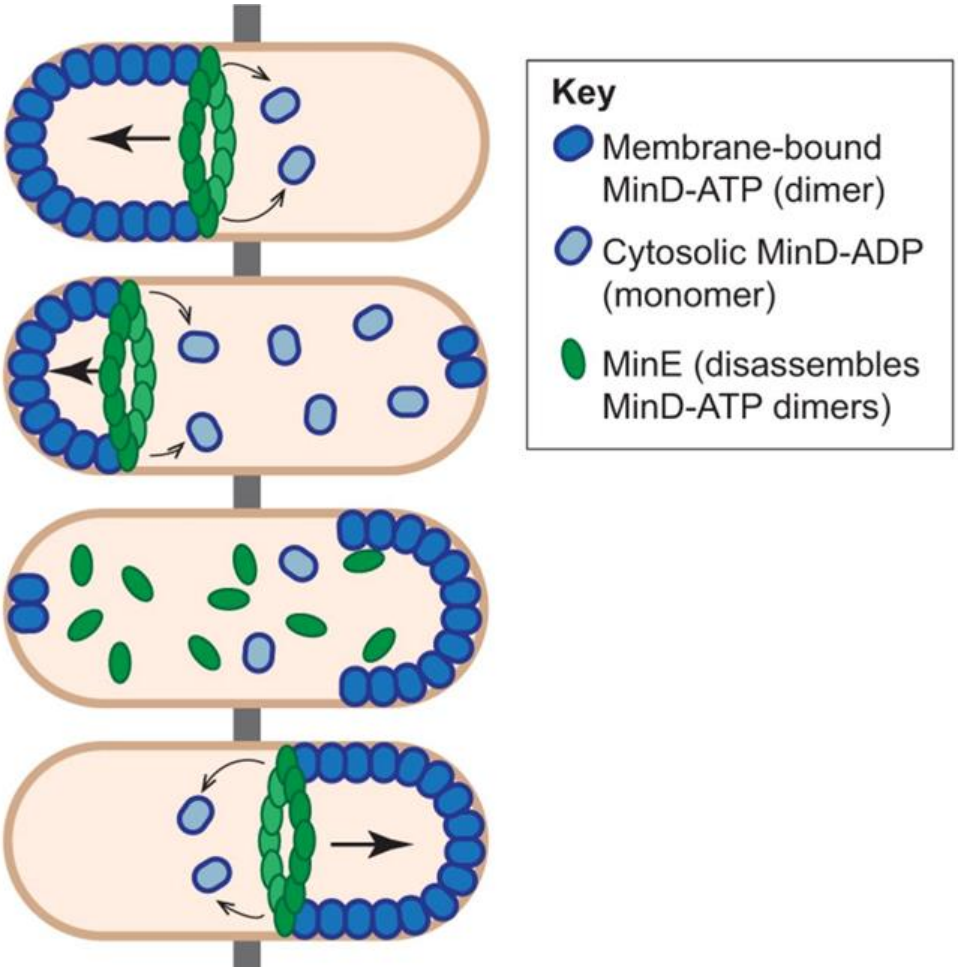


Figure 1.14: The mechanism of the Min system. The Min proteins oscillate between the poles of the cell, with MinE effectively following MinD-ATP to disassemble the membrane bound MinD polymers into free MinD-ADP. The MinD-ADP proteins then travel to the pole furthest from MinE, where they bind to ATP. This allows MinD to bind to the membrane and MinC. MinC concentrations are regulated this way to ensure that the cell poles have the highest concentration of MinC over time. MinC inhibits Z-ring formation through interacts with FtsZ, thus preventing Z-rings from forming at the poles of the cell. Image taken from Laloux *et al*., 2014.

#### 1.3.2.3. Nucleoid Occlusion

Nucleoid occlusion is another system which helps to position the Z-ring by prevention of Z-ring assembly over or in the area that is occupied by the chromosome. Within *E. coli* this is facilitated by the SlmA protein (Cabré et al., 2015, Schumacher, 2017, Cambridge et al., 2014).

SlmA is a member of the TetR family and is able to bind directly to specific DNA sequences (Cuthbertson and Nodwell, 2013). These sequences are SlmA-binding sites (SBS) and are found almost throughout the *E. coli* chromosome (Schumacher, 2017, Cabré et al., 2015). Once bound to these sites, SlmA can spread along the DNA, covering more of the chromosome (Tonthat et al., 2013).

Additionally, once bound to the SBS, SlmA is in a conformation which allows it to interact and bind to FtsZ protofilaments. It is this conformation of SlmA that prevents Z-ring formation, as it stops FtsZ from forming filaments (Figure 1.15) (Bernhardt and de Boer, 2005).

As mentioned, SBS are found in the chromosome, but they are absent at the terminus-containing (Ter) region (Tonthat et al., 2013). When the chromosome segregates, it is this region that is the last to be parted. This leaves a region where FtsZ protofilaments can form, and this region is at the middle of the cell, when the chromosome is being segregated. This means the NO system not only prevents Z-ring formation on the nucleoid, and thus prevents the nucleoid from being fragmented, but also acts to help the timing of the Z-ring formation to when the chromosomes are being segregated (Tonthat et al., 2013, Tonthat et al., 2011, Schumacher, 2017).

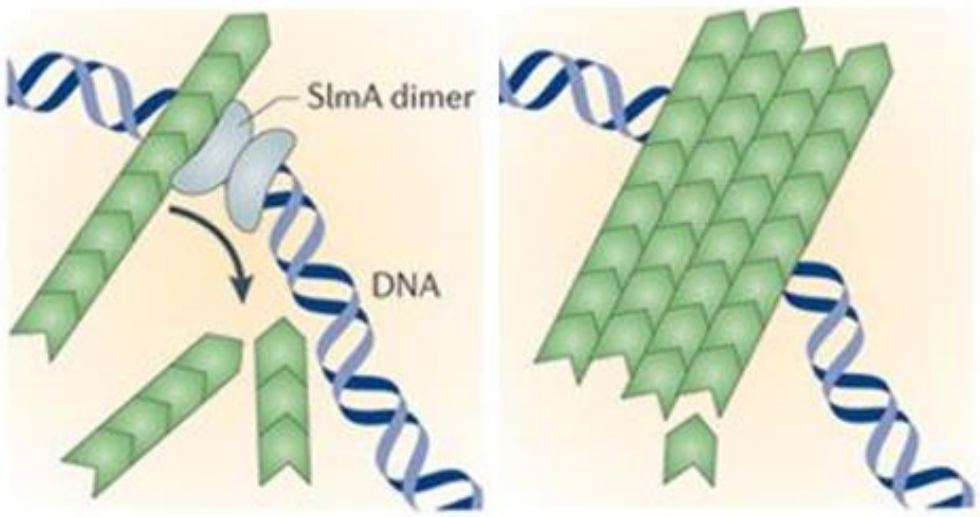


Figure 1.15: The action of SlmA on FtsZ (green units shown as polymers). SlmA binds to a SlmA binding site, before it disrupts filament formation in FtsZ. Image taken from Wu *et al*., 2011).

### 1.3.3. Chromosome Segregation

Another important factor to consider in binary fission is chromosome segregation. As previously mentioned, the replicated chromosomes need to be separated and then packaged into their separate locations for the generation of identical progeny.

To do this the chromosomes are segregated via the ParAB system and then packaged by the protein SMC (Bignell and Thomas, 2001, Kleckner et al., 2018).

#### 1.3.3.1. ParAB system

Chromosome segregation was at first thought to be a passive process, with chromosomes moving with the appointed middle of the daughter cells. However, instead chromosome segregation is an active process and highly regulated. The ParAB system was first and best documented within *E. coli*, however, this system has been seen in many other bacteria (Lutkenhaus, 2012).

The ParAB system consists of three distinct elements which effectively pull apart daughter chromosomes. These are ParA, a weak ATPase, ParB, which binds to DNA (Vecchiarelli et al., 2013), and *parS*, which is a centromere-like site within

the chromosome where ParB can bind (Erdmann et al., 1999). These are also known as ParA-like proteins, SopB, and *parC* (respectively) in other systems (Gerdes et al., 2010). ParA and ParB were first established as proteins involved in plasmid segregation (Bignell and Thomas, 2001).

For plasmid partitioning, the process starts with ParB binding to a *parS* site, which are located close to the origin of replication (Livny et al., 2007). Once bound, ParB can bind to ParA-ATP. However, at this time ParA is not free, but bound to other regions of the chromosome in an ATP dependent manner. ParA then binds with other ParA, forming filaments which spread across the chromosome. Eventually, ParA interacts with ParB-*parS* (Toro and Shapiro, 2010). This interaction upregulates ParA ATPase activity, causing ParA to hydrolyse its ATP. Without ATP ParA is now depolymerised, shortening the ParA filament. This means that the next ParA within the filament can interact with the ParB-*parS* complex. As the filament becomes shorter, it effectively pulls the plasmid to the chromosome (Iniesta, 2014).

The released ParA, which cannot interact with the chromosome, is now monomeric. This free Par-ADP can then assemble another ParA filament, with other free ParA. It does this at the other end of the chromosome, eventually causing the plasmid to be pulled to that region. This process continues and gives an oscillating positioning of the plasmid.

### 1.4. Aims

Within *S. coelicolor* the key cell division cluster contains six genes, two of which, *ftsZ* and *divIVA*, are well known for their importance in division and growth, respectively. The remaining four genes are not well characterised, though *sepF* and *SCO2078* do have homologues which have been highlighted to be involved in cell division. SepF in *B. subtilis* is an FtsZ stabilising protein, which can tether FtsZ and may form rings to stabilise FtsZ filaments (Hamoen et al., 2006, Singh et al., 2008). SCO2078 homologues have been identified outside of prokaryotes, within plants. Here it is found in the chloroplast, a structure originating from cyanobacteria, where it is involved in the distribution of nucleoids (Kabeya et al., 2010).

The aims of this thesis are to characterise *sepF* and *SCO2078*, and further characterise, *divIVA* in *S. coelicolor*.

Firstly, the knockout mutant strains of *sepF* and *SCO2078* will be phenotypically characterised, with emphasis on any impact on cell division and growth. The respective proteins will then be overexpressed to identify any phenotypic changes to the development of *S. coelicolor*. DivIVA will also be investigated, with studies to observe the effects on DivIVA localisation and cell wall growth when exposed to the cell wall synthesis disruptor bacitracin and to low temperatures. This will be completed by using a strain which carries a DivIVA-eGFP fusion protein.

## Chapter 2. Material and Methods

### 2.1. Bacterial strains and plasmids:

Table 2.1: *E. coli* strains used:

| Strain | Genotype | Source or reference |
|---|---|---|
| DH5α | $F^-\lambda^-$ *endA1 glnV44 thi-1 recA1 relA1 gyrA96 deoR nupG Φ80dlacZΔM15* Δ(*lacZYA-argF*)*U169 hsdR17*($r_K^-$ $m_K^+$) | (Hanahan, 1983) |
| ET12567 | *F- dam::Tn9 dcm6 hsdM hsdR* | (MacNeil et al., 1992) |

Table 2.2: *Streptomyces* strains used:

| Strain | Genotype | Source or reference |
|---|---|---|
| M145 | $SCP1^-$ $SCP2^-$ Pgl+ | (Hopwood et al., 1985) |
| M145 KF59 | M145 | |
| Δ*sepF* | M145 *sepF::ApraR* | This work |
| Δ*SCO2078* | M145 *SCO2078::ApraR* | This work |
| M145/pMS82 | M145 containing pMS82 plasmid | This work |
| Δ*sepF*/pMS82 | M145 *sepF::ApraR* containing pMS82 plasmid | This work |
| Δ*sepF*/pMS82-sepF | M145 *sepF::ApraR* containing *sepF* gene under the control of its promoter | This work |
| Δ*SCO2078*/pMS82 | M145 *SCO2078::ApraR* containing pMS82 plasmid | This work |
| Δ*SCO2078*/pMS82-2078 | M145 *SCO2078::ApraR* containing *sco2078* and upstream region | This work |
| M145/pIJ6902 | M145 containing pIJ6902 plasmid | This work |
| M145/pIJ6902-P1sepF | M145 containing *sepF* under the control of its own | This work |

| | | |
|---|---|---|
| | promoter (P1) and the tipA promoter | |
| M145/pIJ6902-2078 | M145 containing *SCO2078* under the contol of the tipA promoter | This work |
| Δ*sepF*/pIJ6902 | M145 *sepF::ApraR* containing pIJ6902 plasmid | This work |
| Δ*sepF*/pIJ6902-P1sepF | M145 *sepF::ApraR* containing *sepF* under the control of its own promoter (P1) and the tipA promoter | This work |
| Δ*SCO2078*/pIJ6902 | M145 *SCO2078::ApraR* containing pIJ6902 plasmid | This work |
| Δ*SCO2078*/pIJ6902-2078 | M145 *SCO2078::ApraR* containing *sco2078* and an upstream region, under the control of the tipA promoter | This work |
| Δ*sepF*/pIJ6902-sepF | M145 *sepF::ApraR* containing the *sepF* gene under the control of the tipA promoter | This work |
| Δ*sepF*/pIJ6902-ERBEsepF | M145 *sepF::ApraR* containing the *sepF* gene and upstream region containing *E. coli* RBS, under the control of the tipA promoter | This work |
| M145/pIJ6902-divIVA | M145 containing *divIVA* and a region containing an *E. coli* RBS under the control of the tipA promoter | This work |
| M145/pIJ6902-filP | M145 containing *filP* and a region containing an *E. coli* RBS under the control of the tipA promoter | This work |
| M145/pIJ6902-parH | M145 containing *parH* and a region containing an *E. coli* RBS under the control of the tipA promoter | This work |

Table 2.3: Plasmids and cosmids used:

| Plasmid | Genotype | Source |
|---|---|---|
| 4A10 | Supercos Cosmid with a 50 Kbp chromosomal fragment containing cell division and growth cluster of *S. coelicolor.* | (Redenbach et al., 1996) |
| 4A10Δ*SCO2078* | Cosmid 4A10 with *SCO2078::ApraR* allele | This lab |
| pMS82 | *ori* pUC18, *hyg*, *oriT* RK2, *int ΦBT1*, *attP* | Gregory et al., 2003 |
| pMS82-*2078* | pMS82 derivative containing *SCO2078* gene | This work |
| pMS82-*sepF* | pMS82 derivative containing *sepF* gene | This work |
| pIJ6902 | *ori* pUC18, *tsr*, *aac(3)IV, oriT* RK2, *int ΦC31*, *attP* | (Huang et al., 2005) |
| pIJ6902-P1sepF | pIJ6902 derivative containing *sepF* and one of its own promoters | This work |
| pIJ6902-sepF | pIJ6902 derivative containing just the *sepF* gene without upstream promoters | This work |
| pIJ6902-ERBSsepF | pIJ6902 derivative containing sepF with an upstream region containing an *E. coli* RBS originating from pET28 | This work |
| pIJ6902-2078 | pIJ6902 derivative containing *SCO2078* | This work |
| pIJ6902-ERBSparH | pIJ6902 derivative containing *parH* with an upstream region containing an *E. coli* RBS originating from pET28 | This work |
| pIJ6902-ERBSdivIVA | pIJ6902 derivative containing *divIVA* with an upstream region containing | This work |

| | | |
|---|---|---|
| | an *E. coli* RBS originating from pET28 | |
| pIJ6902-ERBSfilP | pIJ6902 derivative containing *filP* with an upstream region containing an *E. coli* RBS originating from pET28 | This work |
| pET28 | *ori* pBR322 T7 promoter, His-tag coding sequence, *lacI*, *kan*, *ori* f1 | Novagen |
| pET28-sepF | pET28 derivative containing *sepF* gene | This lab |
| pET28-divIVA | pET28 derivative containing *divIVA* gene | This lab |
| pET28-parH | pET28 derivative containing *parH* gene | This lab |
| pET28-filP | pET28 derivative containing *filP* gene | This lab |

### 2.2. Media and Antibiotics

#### 2.2.1. Solid Media

**SFM**: For general growth and phenotypic analysis of *S. coelicolor* strains.

The 6g mannitol was dissolved in 300 ml tap water, while 6 g soya flour and 6 g agar were measured into 500 ml Duran bottles. The dissolved mannitol media was dispensed into Duran bottles and twice autoclaved.

**MMM**: For growth of *S. coelicolor* strains with Mannitol as a carbon source

L-Asparagine (0.8 g), $K_2HPO_4$ (0.8 g), $MgSO_4.7H_2O$ (0.32 g), $FeSO_4.7H_2O$ (0.016 g), and mannitol (8.0 g) were added to 1600 ml of $dH_2O$. The above ingredients were dissolved in the $dH_2O$, and then measured for a pH of 7.0-7.2 (use orthophosphoric acid). 4 g of agar was measured into 500 ml Duran bottles. The dissolved media was made up to 1600 ml and dispensed in 400 ml aliquots into Duran bottles and autoclaved.

**MMG**: For growth of *S. coelicolor* strains with Glucose as a carbon source

L-Asparagine (0.6 g), $K_2HPO_4$ (0.6 g), $MgSO_4.7H_2O$ (0.24 g), $FeSO_4.7H_2O$ (0.012 g), and glucose (12 g) were added to 1200 ml of $dH_2O$. The ingredients were dissolved in the $dH_2O$, and then measured for a pH of 7.0-7.2 (use orthophosphoric acid). 3 g of agar was measured into 500 ml Duran bottles. The dissolved media was made up to 1200 ml and dispensed in 300 ml aliquots into Duran bottles and autoclaved.

**Lennox Broth (LB) Agar** (Kieser et al., 2000): For growing of *E. coli* strains and spore titres of *S. coelicolor* strains.

Tryptone (16 g), yeast extract (8 g), NaCl (8 g), and glucose (1.6 g) were added to 1600 ml of $dH_2O$. The ingredients were dissolved in the $dH_2O$, while 4 g of agar was measured into 500 ml Duran bottles. The dissolved media was dispensed in 400 ml aliquots into Duran bottles and autoclaved.

### 2.2.2. Liquid Media

**Lennox Broth (LB)** (Kieser *et al.*, 2000): For growing *E. coli* strains.

Tryptone (10 g), yeast extract (5 g), NaCl (5 g), and glucose (1 g) were added to 1000 ml of $dH_20$. Once dissolved, the media was dispensed, either in 10 ml aliquots into universals or in 50 ml aliquots into 250 ml conical flasks, and autoclaved.

### 2.2.3. Antibiotics

Table 2: Antibiotic Concentrations used.

| Antibiotic | Stock (mg/ml) | *Streptomyces* final concentration (µg/ml) | *E. coli* final concentration (µg/ml) |
|---|---|---|---|
| | | SFM | LB |
| Ampicillin | 100 | - | 100 |
| Apramycin | 100 | 50 | 50 |
| Bacitracin | 50 | 25 | - |
| Chloramphenicol | 25 | - | 25 |
| Hygromycin | 50 | 50 | 50 |
| Kanamycin | 100 | 50 | 50 |
| Nalidixic Acid | 25 | 25 | - |
| Thiostrepton | 50 | 50 | - |

## 2.3. Bacterial growth conditions and storage

### *S. coelicolor* strains

*S. coelicolor* strains were grown on SFM containing the appropriate antibiotics and incubated at 30°C until the required developmental stage. For storage (spore preparation), *S. coelicolor* spores were streaked on a single SFM plate to generate a confluent lawn and incubated at 30°C until mature spores developed. Spores were harvested by rubbing spores in a layer of water using a cotton bud. The spore suspension was collected in a 15 ml falcon tube using a pastor pipette. The spores were centrifuged for 10 minutes at 4500 g at 4°C and the supernatant removes. The spores were re-suspended in approximately 1 ml 20% glycerol and stored at -20°C in a 2 ml microcentrifuge tube with a screw cap. The viable spore concentration was determined by plating out a dilution series on LB agar plates containing the appropriate antibiotics.

### *E. coli* strains

*E. coli* strains were grown in either LB solid or liquid media and incubated at 37°C. Glycerol stocks were generated by making a 1:1 mixture of culture to 100% glycerol, and stored at -20°C.

## 2.4. General molecular biology methods:

### 2.4.1. Plasmid DNA isolation from *E. coli*

Solution 1: 50 mM Tris/HCl, 10 mM EDTA pH 8
Solution 2: 200 mM NaOH, 1% SDS
Solution 3: 3 M potassium acetate pH 5.5

A single colony of DH5α containing the desired plasmid DNA was inoculated into 50 ml LB supplemented with the appropriate antibiotic. The inoculum was grown overnight at 37°C (shaking 250 rpm). The overnight growth was collected in a 50 ml falcon by centrifugation for 5 minutes at 5000 g at 4°C. The cells were washed in 40 ml Solution 1 and centrifuged for 5 minutes at 5000 g at 4°C. The supernatant was discarded and cells re-suspended in 1 ml Solution 1, before the addition of 2 ml Solution 2. The cells were mixed gently by turning the falcon tube and incubated for 4 minutes on ice. After incubation 1.5 ml Solution 3 was added and the lysate shaken vigorously. The lysate was incubated for 10 minutes on ice before centrifugation for 10 minutes at 5000 g at 4°C. The supernatant was transferred to a 15 ml falcon and mixed with 500 µl of 1:1 phenol:chloroform. The extract was vortexed for 30 seconds and centrifuged for 5 minutes at 5000 g. After centrifugation the upper aqueous phase was collected in a fresh 15 ml falcon and 7 µl of 30 mg/ml RNase was added. The extract was incubated for 1 hour at 37°C. After incubation another phenol: chloroform extraction was performed as before. After collecting the aqueous phase the DNA was precipitated by mixing 1:1 with isopropanol kept at -20°C, the solution was mixed by inversion and incubated on ice for 30 minutes. The precipitated DNA was centrifuged for 15 minutes at 5000 g at 4°C. The supernatant was discarded and the DNA pellet washed with 2 ml 70% ethanol kept at -20°C. The DNA was centrifuged for 5 minutes at 5000 g at 4°C and the supernatant was discarded. The DNA pellet was allowed to air dry for 5 minutes

before re-suspension in 200-600 µl sterile $dH_20$ dependent on pellet size. The resulting plasmid DNA was stored at -20°C.

### 2.4.2. Chromosomal DNA preparation from *S. coelicolor*

The spores of desired *Streptomyces* strain were plated onto cellophane on SFM containing glycine. The inoculated plate was incubated at 30°C for 22~24 hrs. The cells were collected from the cellophane and divided into two 2 ml Eppendorf tubes. The cells were resuspended in 150 µl Solution 1 on ice, and 20 µl lysozyme (100 mg/ml) was gently added and mixed in the Eppendorf. The solution was incubated on ice for 5 minutes and then immediately incubated at 37°C for 5 minutes. After incubation, 30 µl of 10% SDS was added and gently mixed by inverting the Eppendorf tubes. The tubes were then incubated at 60°C for 10 minutes, before adding 150 µl 1:1 phenol:chloroform. After vigorous shaking, without vortexing, the tubes were centrifuged at 13,000 g for 5 minutes at room temperature. After this, the aqueous phase of the solution was transferred into a fresh Eppendorf and the phenol:chloroform extraction was repeated. The transferred aqueous phase then had 200 µl chloroform added to it and mixed gently. The tubes were then centrifuged at 13,000 g for 2 minutes at room temperature. The resulting aqueous phase was then transferred into a fresh Eppendorf to precipitate the chromosomal DNA by adding 300 µl isopropanol kept at -20°C. The tubes were gently inverted and incubated on ice for 10-20 minutes and centrifuged at 5000 g for 10 minutes at 4°C. The supernatant was discarded and the DNA pellet washed with 300 µl 70% ethanol kept at -20°C. The pellet was centrifuged for 3 minutes and the supernatant was discarded. The DNA pellet was allowed to air dry for 5 minutes before re-suspension in 50-100 µl $dH_2O$ dependent on pellet size. The resulting chromosomal DNA was stored at -20°C.

### 4.2.3. Agarose gel electrophoresis of DNA

50x TAE: 2M Tris acetate, 50 mM EDTA pH 8

10x Loading dye: 50 mM Tris, 50 mM EDTA, 50% Glycerol pH 7.4 -Autoclave- 0.05% Xylene Cyanol, 0.05% Bromophenol Blue

Agarose gels were cast using the Bio-Rad Mini-Sub and Sub-cell trays. Gels were made in a range between 0.7% and 1% agarose in 1x TAE buffer with the addition of 0.5 µg/ml ethidium bromide. DNA was mixed with 1x loading dye and run in gels

submerged in 1x TAE buffer. Gels were imaged with UV light using a Bio-Rad trans-illuminator. A size marker of λ DNA digested with *Hin*dIII, and *Eco*RI was used to estimate band sizes.

### 4.2.4. PCR

All PCR reactions were performed using a BioRAD DNA Engine® Peltier Thermal Cycler.

Hi-Fidelity PCR using Phusion High-Fidelity DNA Polymerase (Thermofisher) was used for the generation of PCR fragments used for cloning.

Reaction conditions: 1x Phusion GC Buffer, 200 µM of each of the four dNTPs, 1.5 mM $MgCl_2$, 3% DMSO, 1 µM of each primer, 0.02 U/µl Phusion DNA polymerase.

Low-Fidelity PCR using Go Taq DNA Polymerase (Invitrogen) was used for diagnostic purposes and for the generation of disruption cassettes.

Reaction conditions: 1 x Go Taq polymerase buffer, 200 µM of each of the four dNTPs, 2.5 mM $MgCl_2$, 5% DMSO, 1 µM of each primer, 0.02 U/µl Go Taq DNA polymerase.

Table 2.5: Oligonucleotide sequences used:

| Primer | 5'-3' Sequence |
|---|---|
| Apra 5' REV | GGCGGGATGCGAAGAATGCG |
| Apra 3' forward | CGCACCTGGCGGTGCTCAACG |
| 2078 3' END | TCGTTCTCGCGGAGCAGTCGG |
| 2078 XbaBgl Prom FRW | GATCACTCTAGATCTAACACTTCCGTGAGGGCACTCC |
| SepF XbaBgl Prom FRW | GATCACTCTAGATCTCGGGTAACGTCGCCAAGAAGTCG |
| SepF 3' END | GCCTTGCCGGGTTGCCACGAGC |
| T0 | GAGCGTTCTGAACAAATCCAGATGG |
| Tfd | GATTTTCAACGTGAAAAAATTATTA |

| | |
|---|---|
| pET28 XbaFRW | CCGATCTTCCCCATCGGTGATGTCG |
| Sco2079_EcoRI UTC | GGATCAGAATTCTCTCAGCTCTGGTTGAAGAACC |
| sco2079_XbaNde | GGATCATCTAGAGCATATGGCCGGCGCGATGCGCAAGATGG |
| THDiv_F | GGATCATCTAGAGCATATGCCGTTGACCCCCGAGGACG |
| THDiv_R | GGATCAGAATTCTCAGTTGTCGTCCTCGTCGATCAGGAACC |
| THAbps Rev | GGATCAGAATTCTCAGCGGGACTGCTGGGCCG |
| sco1772 EcoUTC | GGATCAGAATTCTCTCACTCGGCGTGACACCGGGC |
| DIR | CGCCAGGGTTTTCCCAGTCACGACG |
| REV | TTTACACATTTATGCTTCCGGCTCG |

### 4.2.5. Restriction Digest

Were carried out in a total volume of 20 µl, with 10 U of each restriction enzyme in 1x of the optimum digestion buffer (enzyme and buffer from Roche), or a volume of 100 µl, with same ration of enzyme. The incubation was carried out at 37°C for the 4 hours, and then stopped by heating the entire reaction mix to 65°C for 50-10 minutes. The restriction digest was then cooled on ice, before loading onto an agarose gel.

Table 2.6: Concentration and restriction sites of enzymes used

| Restriction enzyme | Concentration (U/µl) | Restriction site |
|---|---|---|
| *Eco*RI | 10 | 5'..G↓AATTC..3'<br>3'..CTTAA↑G..5' |
| *Xba*I | 10 | 5'..T↓CTAGA..3'<br>3'..AGATC↑T..5' |
| *Eco*RV | 10 | 5'..GAT↓ATC..3'<br>3'..CTA↑TAG..5' |

### 2.4.6. A-tailing of DNA fragments

The DNA fragments were purified PCR products, and A-tailing was carried out in a total volume of 10 µl:

| | |
|---|---|
| DNA fragment | 6.5 µl |
| GoTaq buffer | 2.0 µl |
| $MgCl_2$ | 0.5 µl |
| dATP | 0.5 µl |
| GoTaq Polymerase | 0.5 µl |

The mixture was incubated at 72°C for 20 minutes, and then cooled on ice. Reagents and enzyme were from Promega.

### 2.4.7. Isolation of DNA fragments by agarose

Agarose gels containing desired DNA fragments were view under long-wavelength UV light (310 nm). The fragments were then excised using a scalpel, and DNA was extracted, purified and concentrated using a Qiagen QIAquick Gel Extraction kit. The resulting DNA was filtered into sterile $dH_2O$ and stored at -20°C.

### 2.4.8. Ligation of DNA fragments

Ligations were carried out in volumes of 15 µl, with the DNA fragments suspended in sterile water (of linearised vector and insert fragments) at a total of 11.5 µl. The fragments were mixed and incubated at 65°C for 3 minutes. They were then immediately cooled on ice, and once cool 3 µl of 5x ligation buffer and then 0.5 µl of T4 DNA ligase (from Invitrogen) were added. Ligations were desalted via G75 sephadex columns.

### 2.4.9. Transformation of competent *E. coli* cells by electroporation

To prepare the cells, a single colony of the *E. coli* strain was inoculated into 10 ml liquid LB supplemented with the appropriate antibiotics and grown overnight at 37°C with shaking at 350 rpm. After overnight growth, the culture was used to subcultured fresh media, using 1% of the volume of the fresh media, into either 10 ml or 50 ml

liquid LB supplemented with the appropriate antibiotics. The fresh culture was incubated at 37°C with shaking until it achieved an OD600 ~0.7. The cells were collected by centrifugation for 5 minutes at 5000 g at 4°C. The supernatant was removed, and the cells washed twice in 10% glycerol centrifuging for 5 minutes at 5000 g at 4°C. The pellet was re-suspended to a final total volume between 100 µl and 250 µl in 10% glycerol. For transformation 50 µl of cells were mixed with either 1 µl of plasmid or cosmid DNA, or 5 µl of ligation. Electroporation was carried out in an ice cold 0.2 cm electroporation cuvette using a BioRad Gene Pulser 2 set to 200 Ω, 25 µF and 2.5 kV. After electroporation, cells were mixed with 1 ml ice cold LB and allowed to recover during a 1 hour incubation at 37°C before plating onto LB agar plates supplemented with the appropriate antibiotics. Plates were incubated overnight at 37°C.

### 2.4.10. Transformation of competent *E. coli* cells by chemical competence

To produce chemically competent cells, a single colony of the *E. coli* strain was inoculated into 10 ml LB supplemented with the appropriate antibiotics and grown overnight at 37°C with shaking. After overnight growth, the cells were subcultured by transferring 500 µl into fresh 50 ml LB supplemented with the appropriate antibiotics. The fresh culture was incubated at 37°C with shaking until it achieved an OD600 ~0.4-0.6. The cells were collected by centrifugation for 5 minutes at 5000 g at 4°C. The supernatant was removed, and the cells washed with 10 mM NaCl centrifuging for 5 minutes at 5000 g at 4°C. The pellet was re-suspended in 30mM $CaCl_2$, 10 mM $RbCl_2$ solution and incubated on ice for 1 hour at 4°C. After incubation, the cells were centrifuged for 5 minutes at 5000 g at 4°C and the supernatant discarded. The pellet was re-suspended with 500 µl of 30 mM $CaCl_2$, 10 mM $RbCl_2$ solution. For transformation, 50 µl of the competent cells were mixed with either 0.5-1 µl of plasmid or cosmid DNA, or 5 µl of ligation and incubated for 30 minutes on ice. The cells were then heat shocked at 42°C for 1 minute before being placed immediately in ice. After heat shock, the cells were mixed with 500 µl LB and allowed to recover during a 1 hour incubation at 37°C with shaking, before plating onto LB agar plates supplemented with the appropriate antibiotics. Plates were incubated overnight at 37°C.

### 2.4.11. Conjugation into *S. coelicolor*

Conjugation of vectors containing *oriT* into *S. coelicolor* was achieved using the *E. coli* strain ET12567/pUZ8002. A single colony of ET12567/pUZ8002 containing the desired plasmid or cosmid for conjugation was inoculated into 10 ml LB containing kanamycin, chloramphenicol and the antibiotic for which the plasmid or cosmid confers resistance, and grown overnight with shaking at 37°C. After overnight growth the cells were subcultured by transferring 100 µl into fresh 10 ml LB supplemented with the appropriate antibiotics. The fresh culture was incubated with shaking at 37°C until it achieved an OD600 ~0.4-0.6. The cells were collected by centrifugation for 5 minutes at 5000 g at 4°C. The supernatant was removed and the cells washed twice with 10 ml LB by centrifuging for 5 minutes at 5000 g at 4°C. The pellet was re-suspended in 250 µl LB and kept on ice. Approximately $10^8$ spores of the desired *S. coelicolor* strain were added to 500 µl LB and germination activated by heating at 50°C for 10 minutes before cooling on ice. After cooling the germinating spores were mixed with re-suspended ET12567/pUZ8002 cells containing the plasmid/cosmid and centrifuged for 2 minutes at 16,000 g at 4°C. The supernatant was removed and the pellet re-suspended in 300 µl sterile $dH_20$. A dilution series was set up in which three 10x dilutions were made. The stock and 3 dilutions were then plated into SFM and incubated at 30°C. After overnight incubation the plates were overlaid with 500 µl sterile $dH_20$ containing nalidixic acid and the appropriate antibiotics. The plates were then incubated at 30°C until the appearance of colonies which had developed mature spores (5-8 days). Successful ex-conjugants were selected streaked for single colonies on SFM supplemented with nalidixic acid and the appropriate antibiotics and grown at 30°C until spores were produced. Spore preparations of the strain were then generated, originating from a single colony of the streaked plate.

### 2.4.12. Generation of *S. coelicolor* knockout strains

The knockout mutants Δ*sepF* and Δ*SCO2078* were generated using REDIRECT PCR-directed mutagenesis (Gust et al., 2003, Gust et al., 2002) (Figure 2.1). The target genes were replaced with an apramycin resistance cassette.

The process firstly requires an apramycin resistance cassette to be excised from the plasmid pIJ773 by restriction enzymes. The cassette is then amplified using primers which are complimentary to the flanking regions of the gene to be knocked out. The

primers are designed to contain 39 nt of the gene region and either 20 nt or 19 nt of the cassette, to ensure an in-frame deletion of the gene. The amplified apramycin resistance cassette is then able to undergo homologous recombination with the target gene. To knockout *sepF* and *SCO2078* the amplified cassette was not introduced directly to *Streptomyces*, but instead to a cosmid. The cosmid, 4A10, contains are stretch of DNA which encompasses *sepF* and *SCO2078* alongside other surrounding genes. The target gene is knocked out in the cosmid by homologous recombination. The cosmid, now null of either *sepF* or *SCO2078*, was then transformed into a series of *E. coli* species and then conjugated into *S. coelicolor* M145. Another double crossover recombination event knocks out the native target gene, replacing it with the apramycin resistance cassette.

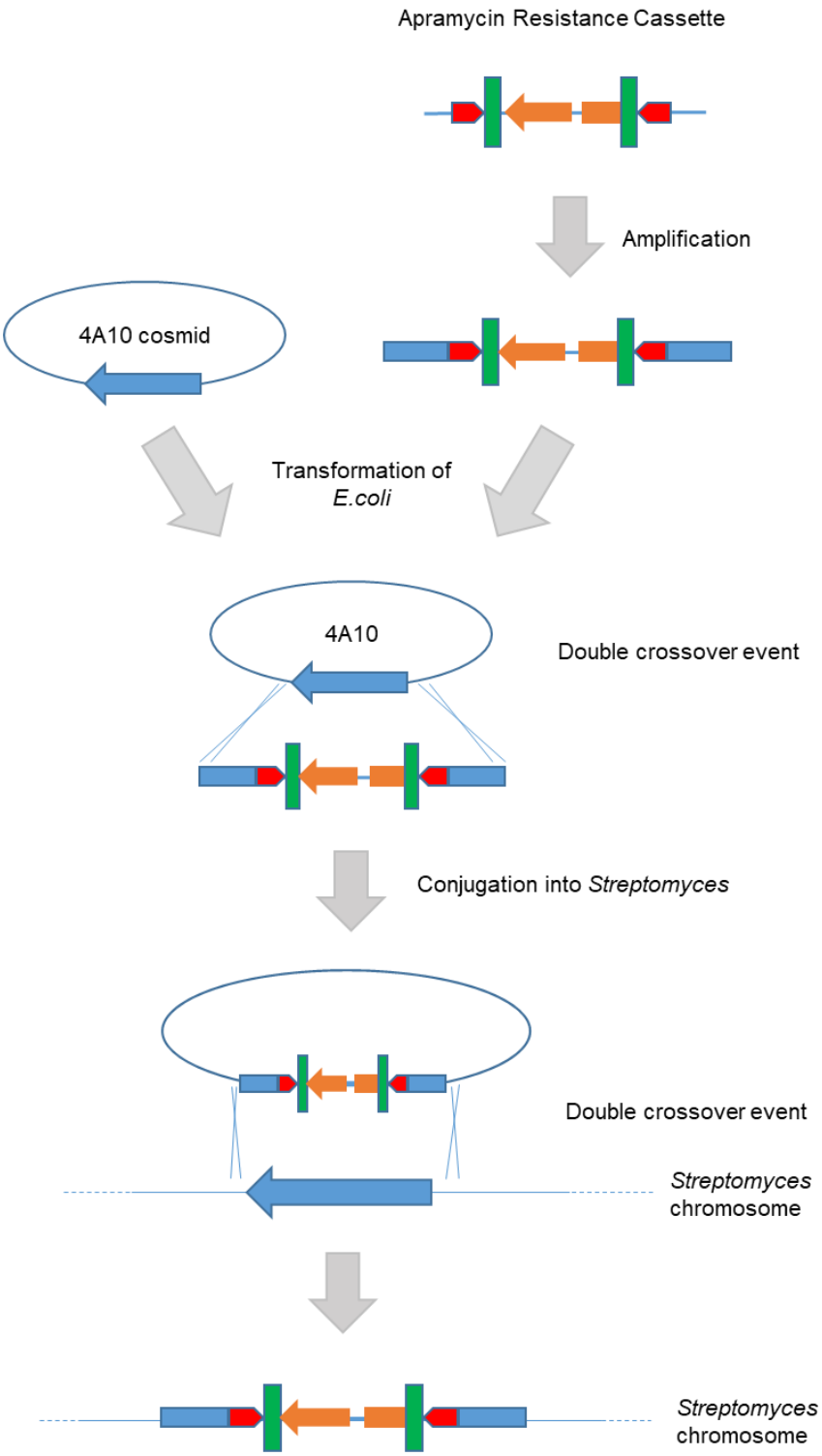


Figure 2.1: A simplified REDIRECT process for the replacement of a target gene (blue) by an apramycin resistance cassette. The apramycin resistance cassette also contains the resistance gene and an oriT (both in orange) and FLP recognition targets (FRT, in green). The FRT would be used if the apramycin resistance cassette required excising but were not used in this study.

### 2.5. Microscopy of *S. coelicolor*

All microscopy of the *Streptomyces* strains was visualised using an Axioplan 2 Imaging E (Carl Zeiss) Universal light microscope with a Zeiss AxioCamMR camera. Strains were viewed via brightfield microscopy or fluorescence microscopy, dependent on strain and if stained. The images were processed using Carl Zeiss AxioVision (Release 4.8) software.

#### 2.5.1. Coverslip microscopy

Approximately $10^5$ spores of an *S. coelicolor* was plated in a 1 $cm^2$ confluent patch (0.5 cm by 2 cm) on a deep SFM plate (40 ml of media used per plate) containing the appropriate antibiotics. A UV sterilised glass coverslip, 22 mm x 22 mm with a thickness of 0.13-0.17 mm, was inserted into the patch at an approximate angle of 60˚-70˚ to the horizontal plain of the medium. Plates were incubated at 30°C with coverslips removed at regular intervals after approximately 48 hours growth, to visualise the developmental stages of *S. coelicolor*.

**Staining of Coverslip**

Plates containing coverslips were dried for 30 minutes to ensure that aerial hyphae stuck to the surface of the coverslip. Coverslips were removed from the media and placed on filter paper with the sample (growth line) face up. The sample was fixed with 100% methanol (stored in the freezer) for 1 minute, after which the excess methanol was removed, and the remainder allowed to evaporate. The sample was stained with the application of WGA-Alexa Fluor 488 conjugate (50 µg/ml) and propidium iodide (25 µg/ml) to each coverslip on the growth line. The samples were incubated for 20 minutes in total darkness at room temperature. The coverslips were then washed 4 times by pipetting 1 ml PBS onto the surface before allowing the slides to dry. After drying the coverslips were mounted face down onto microscope slides (76 mm x 26 mm, thickness 1.0 – 1.2 mm) with an 8 µl drop of 20% glycerol on the surface. Excess liquid was removed from the edge of the coverslip before it was sealed with a fine coat of nail varnish applied around the edge.

### 2.5.2. Cellophane microscopy

Approximately $10^5$ spores of *S. coelicolor* was plated on a cellophane placed on a SFM plate. The plates were incubated at 30°C for 18 hrs. After incubation, a $1cm^2$ square of cellophane was extracted and mounted facedown onto microscope slides (76 mm x 26 mm, thickness 1.0 – 1.2 mm) with a 7 µl drop of 20% glycerol on the surface of the slide and then on the cellophane. The coverslip was then mounted and pressed to expel excess liquid and flatten the sample. Excess liquid was removed from the edge of the coverslip before it was sealed with a fine coat of nail varnish applied around the edge.

**Staining of Cellophane**

After the cellophane square containing the sample had been scored but not extracted, the sample was stained with the application of 20 µl vancomycin. The samples were incubated for 5 minutes in total darkness at the temperature at which the cellophanes had been previously stored. The cellophane square was then extracted and mounted onto a slide (as above).

### 2.5.3. Coverslip Imprint microscopy

Spores were plated onto SFM, in sufficient numbers to confluently plate the surface. The plates were then incubated at 30°C for 5-7 days, to allow for aerial hyphae and spores to form. The plates were then dried for 30 minutes to remove any visible moisture. A UV sterilised coverslip was then placed onto the surface of the plate. Pressure was applied to the whole of the coverslip and it was left on the plate for 2 minutes. After 2 minutes of contact with the aerial hyphae, the coverslip was removed and passed quickly through the top of a Bunsen burner flame to fix the material on the coverslip. The coverslip was then placed material side up and fixed again with 300 µl 100% methanol for 1 minute. The coverslip was then allowed to air dry to remove remaining methanol. The coverslip was then mounted onto a slide face down with 7 µl 20% glycerol. Pressure was applied to the coverslip to remove excess liquid and it was sealed with a coat of nail varnish.

**Staining of Coverslips**

After the coverslip had been fixed with methanol, the sample was ready to be stained. The coverslip had 30 µl of WGA-Alexa Fluor 488 and PI mixture added

carefully to the centre. The sample was then incubated for 20 minutes in darkness at room temperature.

## Chapter 3. Bioinformatic analysis and Characterisation of SepF

### 3.1. Introduction

The SepF protein has been shown to be involved in septum formation during cell division in *Bacillus subtilis* (Hamoen et al., 2006, Ishikawa et al., 2006). SepF is found in Gram-positive and Gram-negative bacteria, and though not essential, it does play an important role in cell division. In *B. subtilis,* SepF is thought to act as a membrane anchor for the key cell division protein FtsZ, as *sepF* knockouts in *B. subtilis* effect septum formation, with septa being malformed and irregular (Hamoen et al., 2006). The septa formed in the *sepF* knockout mutant was thicker and completed slower than in the wild-type *B. subtilis* cells, but cell division was still able to take place.

Yeast two-hybrid interaction studies have shown that SepF can interact with itself as well as interacting with FtsZ. SepF protein that has been overexpressed and purified has been shown *in vitro* to form 'SepF rings', which are higher order structures of SepF dimers (Duman et al., 2013). It has been theorised that these rings anchor and stabilises the FtsZ rings (Gündoğdu et al., 2011). SepF has also been shown to have an affinity for lipid membranes which pertain to its anchoring role during cell division (Duman et al., 2013).

SepF has been shown to localise at the site of cell division, when viewed using GFP tagged fusions, with this localisation dependent on FtsZ. Without sufficient levels of FtsZ (in FtsZ depleted strains) SepF-GFP cannot be viewed within the cells, as SepF is recruited by FtsZ and not by any proteins of the later cell division machinery (Duman et al., 2013).

*B. subtilis* also contains other FtsZ-interacting proteins which are thought to have overlapping roles with SepF. One key protein is FtsA which directly interacts with FtsZ during cell division but is also non-essential. FtsA is a highly conserved protein, acts as a Z-ring cell membrane anchor and is one of the first proteins recruited to the Z-ring. Null mutants of *ftsA* of *B. subtilis* result in inefficient Z-ring formation and elongated cells (Kemp et al., 2002). A double knockout mutant with both *ftsA* and *sepF* is not viable, though overexpression of SepF can rescue this double mutant to wild-type (Duman et al., 2013). This suggests, that SepF has overlapping function with FtsA.

While FtsA helps to maintain Z-ring formation, EzrA is a proposed negative regulator of FtsZ ring formation. This is because in the *ezrA* mutant additional Z-rings are formed within the cell, some of which are located not just at the middle of the cells but also at the cell poles. This is thought to occur as the critical concentration of FtsZ required for Z-ring formation is lower in the absence of EzrA (Levin et al., 1999). As EzrA is known to interact with FtsZ in vitro, it is thought that its negative regulation is due to the protein blocking FtsZ dimerisation or FtsZ filaments from forming lateral interactions (Haeusser et al., 2004). Interestingly, when *sepF* and *ezrA* are both knocked out in *B. subtilis* cells are not viable (Duman et al., 2013). EzrA and SepF are not thought to interact with one another, as shown by yeast two-hybrid studies, but may have some overlap in their roles controlling FtsZ polymerisation.

These observations have been seen in *B. subtilis*, however, in *Streptomyces* and other bacteria SepF has not been as widely researched.

This chapter will investigate the role of SepF and gage its importance, by conducting a number of bioinformatic searches and comparisons. An additional focus of this chapter is to characterise the phenotype of the previously generated knockout mutant (Alan Lau and Xiao Tan, unpublished). To determine the role of *sepF* within *S. coelicolor* a knockout strain was generated within the lab, using REDIRECT technology. This is based on a PCR-generated cassette which was used to replace the gene of interest, in this case the *sepF* gene, with an apramycin resistance cassette. As *sepF* is part of a gene cluster located between *ftsZ* and *divIVA*, it is important that introduction of the apramycin cassette does not affect the expression of any downstream genes. This was achieved by removing only the first 159 amino acids from the total of 213 amino acids, leaving a 165 bp long sepF sequence that likely contains the promoter for the downstream gene, *SCO2078*, based by the large scale transcription start analysis by Jeong et al. (2016).

The generated Δ*sepF* strain was viable and was confirmed to have its *sepF* gene deleted by PCR-tests using chromosomal DNA isolated from the *sepF* mutant (Alan Lau and Xiao Tan, unpublished).

In this chapter *sepF* is investigated bioinformatically and the characterisation of the *sepF* knockout strain is shown using both macroscopic and microscopic observations to record its distinctive phenotype.

## 3.2. Bioinformatic Analysis of SepF

### 3.2.1. SepF domain presence within *Streptomyces* and other organisms

The *B. subtilis* SepF homologue was used as a starting point for bioinformatic analysis, as most of the research on *sepF* has been conducted using this homologue. It has previously been shown that SepF is wide-spread and conserved in Gram-positive bacteria and also found in some Gram-negative bacteria. To identify which bacterial families contain *sepF* homologues, the amino acid sequence of *B. subtilis* SepF was ran on pFam (http://pfam.xfam.org/family/PF04472#tabview=tab0). This identified a domain, DUF552, which is uniquely associated with SepF.

This domain of unknown function, was used to identify other SepF homologues. These homologues were present not only in bacteria but also amongst archaea (Figure 3.1). A total of 1846 species were identified, using the pFam search, to contain the SepF motif and be part of the SepF family. The majority of these were found in bacteria, 1254 species, and the remaining 127 species belonged to archaea.

Additionally, a number of these bacteria and archaea had multiple homologues of SepF within a single species. Though the number of identified species containing SepF was 1846, the number of sequences was larger than that, at 2163. Many *Streptomyces* species contained two to three homologues, including *S. coelicolor*, which contains three SepF homologues. These homologues have been previously identified, and the sequences of all three were obtained using StrepDB. To identify which of the *S. coelicolor* SepF homologues were more closely related to the *B. subtilis* SepF, pairwise comparisons were performed using the three *S. coelicolor* SepFs and SepF of *B. subtilis*.

Though the model organism for cell division of Gram-positive bacteria, *B. subtilis*, has only one *SepF* homologue, *Streptomyces coelicolor*, which is also Gram-positive, contains three *SepF* homologues. It is this difference that is important to discuss and to find any possible reasons why *S. coelicolor* contains three copies of this gene.

To answer this, the three SepF homologues of *S. coelicolor* were investigated to give an insight on their possible functions. The information gathered, to address the possible reasons for the number of *sepF* homologues, was the amino

acid composition of each, their genomic location in relation to their surrounding genes, and their secondary structures. This information was then compared to other SepF, with emphasis on their comparisons with the *B. subtilis* SepF. It should also be noted that *S. coelicolor* does not contain an EzrA or FtsA homologue, therefore it may be possible that SepF homologues fulfil the roles of these two proteins.

A


B

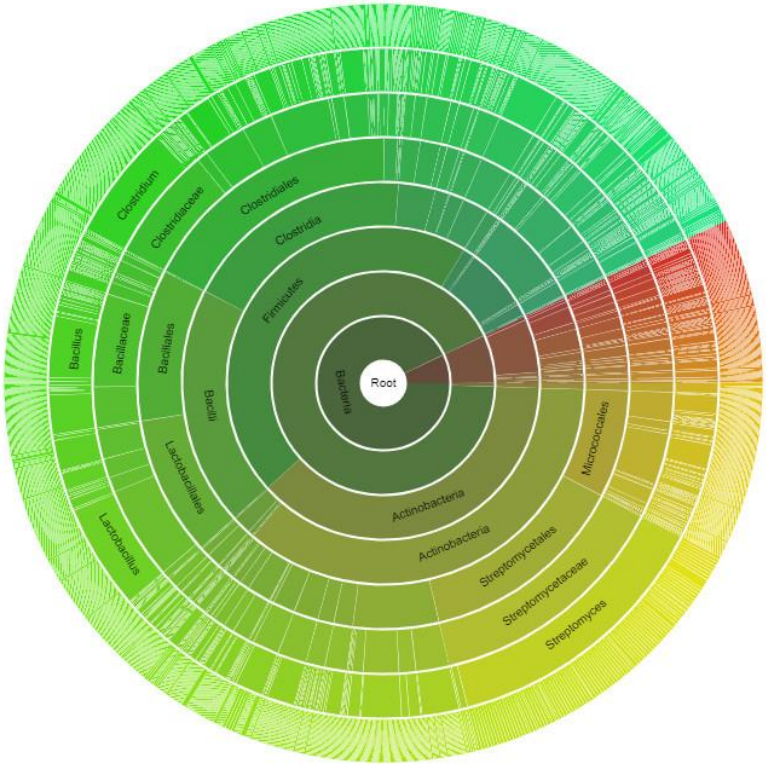


Figure 3.1: Graphical trees of SepF homologue distribution within species recorded in the pFam database, with green and yellow colouring indicating bacteria and red indicating archaeal species (trees generated by pFam sunburst). A: Shows the SepF distribution via number of individual species. B: Shows the SepF distribution via number of sequences. The representation of *Streptomyces* is greater compared to other species when viewed via number of sequences because Streptomyces species often contain multiple SepFs.

### 3.2.2. *S. coelicolor* has three *sepF* genes

To investigate this, the amino acid sequences of the three SepF proteins from *S. coelicolor* were obtained using the database StrepDB. The *sepF* homologues are named SCO1749, SCO2079, and SCO5967, and will be referred to as SepF1, SepF2, and SepF3 respectively from hence onwards. All three homologues differ in size, with SepF2 at 213 amino acids in length being clearly the largest of the group. SepF1 and SepF3 are closer in size at 146 and 136 amino acids (respectively). Using the *S. coelicolor* SepF homologues amino acid sequences, each was compared to the *B. subtilis* SepF homologue in a pair wise comparison using Clustal Omega (https://www.ebi.ac.uk/Tools/msa/clustalo/). The amino acid sequence of *B. subtilis* SepF was obtained from UniProt, O31728. This identified regions of similarity between the four sequences (Figure 3.2), particularly at the C-terminal ends of the SepF proteins. Interestingly, all of the amino acid residues that has been shown to be important for SepF binding to FtsZ in *B. subtilis* are identical and conserved in all three *Streptomyces* SepFs (Gupta et al., 2015, Duman et al., 2013). This might suggest that all three *Streptomyces* SepFs could interact with FtsZ.

```
b.sub       -MSMKNKLKNFFS-MEDEEYEYEYIETER---------------------ESHEEHEQKE    37
SCO5967     ----------------------------------------VKSGEPV-NSHDVTDEQW    17
SCO1749     -MGSVRKASAWLGLVDDNNDDERYYDDDYSEGPESGDA----------------------    37
SCO2079     MAGAMRKMAVYLGLVEDDGYDGRGFDPDDDFEPELDPEPERDHRRHEPAHQSHGAHQSQR    60

b.sub       K-PAYNGNK-------------------------------------PAGKQNVVSLQSVQ    59
SCO5967     E-GLAQVVPLRGRDAWPS--------------------------AVGHRAMPEA-ETE    47
SCO1749     ----WV---------------------------------------TDPRVKVASDVAEE    53
SCO2079     DEEVRVVQPPAQREPMPRAASLAAESSRPARIAPVASITQERASLEKSAPVIMPKVVSER    120
                                                                 : .    .

b.sub       KSSKVVLSEPRVYAEAQEIADHLKNRRAVVVNLQRIQHDQAKRIVDFLSGTVYAIGGDIQ    119
SCO5967     RRRRFVVLRINVFADAREVAETLMAGIPVLLDLTSAEGEVAKRVLDFSTGVVFGLASGMH    107
SCO1749     KGRRIATVTPDSFRDARAIGELFRDGVPVIVNLTAMEGTDAKRVVDFAAGLIFGLRGSIE    113
SCO2079     EPYRITTLHPRTYNEARTIGEHFREGTPVIMNLTEMDDTDAKRLVDFAAGLVFGLHGSIE    180
            .  :..      : :*: :.: :     *:::*   :    **::** :* ::.: ..:.

b.sub       RIGSDIFLCTPDNVDVSGTISELISEDEHQRW-     151
SCO5967     RVDRNVFLLTPAGTEVNGLMESAAGVPGV----     136
SCO1749     RVSTRVFLLSPADTQVISGESAAHRSDGFFNQS     146
SCO2079     RVTQKVFLLSPANVDVTAEDKARIAEGGFFNQS     213
            *:   :** :* ..:* .  .
```

Figure 3.2: The amino acid alignment of the three SepFs from *S. coelicolor* (SCO1749, SCO2079 and SCO5679) and SepF of *B. subtilis* (B.sub) UniProt number O31728, using Clustal Omega. Conserved amino acids are shown by * and :, with . indicating amino acids with similar properties. Residues that are indicated to be important for SepF binding to FtsZ are highlighted in the blue boxes (Gupta et al., 2015; Duman et al.,2013)

As can be seen from Table 3.1, SepF2 shows the highest level of homology to SepF of *B. subtilis*. This suggests that SepF2 and *B. subtilis* SepF may share similar roles, but all three *S. coelicolor* SepF homologues contained regions which showed highly conserved amino acids.

Table 3.1: The percentage identity of the SepF homologues of *S. coelicolor* when compared to *B. subtilis* SepF, UniProt number O31728. The percentage identity was generated using Clustal Omega (rounded to the nearest whole number). (https://www.ebi.ac.uk/Tools/msa/clustlo).

| Compared sequences | Percentage identity |
|---|---|
| **SepF1** **_B. subtilis_ SepF** | 24 |
| **SepF2** **_B. subtilis_ SepF** | 30 |
| **SepF3** **_B. subtilis_ SepF** | 21 |

### 3.2.3. Comparison of the three *S. coelicolor* SepF homologues to the SepF of *B. subtilis*

The predicted secondary structures of each *S. coelicolor* SepF was compared with the SepF of *B. subtilis*, as previous research had concluded that the β-strands present at the C-terminus of the protein are important for SepF function. It is believed that five β-strands form a β-sheet between two α-helices at the C-terminus which facilitates the interactions between SepF and FtsZ, and with other SepF proteins, as without this structure SepF is unable to form rings through dimerization (Duman et al., 2013).

Then the PSIPRED programme (Buchan et al., 2013) was used to predict the secondary structure of the *S. coelicolor* homologues (Figure 3.3). For *B. subtilis* SepF, at present, only the last 88 amino acids of the C-terminus have been overexpressed, purified and crystallised. The structure of the C-terminus has been solved through X-ray diffraction (Duman et al., 2013), though the full length *B. subtilis* SepF has not yet been crystallised, possibly due to unordered regions and the membrane binding N-terminus within SepF. A truncated SepF protein was used for X-ray diffraction and consists of the majority of the C-terminus and contains the amino acids 61 to 140, which have been identified as FtsZ binding regions through yeast two hybrid screens (Duman et al., 2013). This truncated version of the *B.*

*subtilis* SepF homologue has also been observed to form a ring-like structure in vitro when viewed using transmission electron microscopy, suggesting that the C-terminus amino acids 61-151 are also responsible for SepF self-interaction. As the structure of *B. subtilis* SepF does not encompass more than the C-terminus, the full *B. subtilis* SepF structure was predicted and analysed using PSIPRED. The predicted structure generated by PSIPRED was then cross referenced with existing information from the X-ray diffraction patterns of the crystallised C-terminus of *B. subtilis* SepF. The predicted structure closely matched the confirmed C-terminus structure, with the location of predicted and actual β-strands and α-helices being shared (Duman et al., 2013).

The predicted secondary structure (Figure 3.3) of each *S. coelicolor* homologue was very similar, with all three containing β-sheets at their C-terminus. This reinforces the conclusions of Duman et al that the C-terminus of SepF is conserved. It also implies that all three SepF homologues could potentially dimerise or interact with FtsZ.

However, Gundogdu et al (2011) state that destroying the last α-helix of *B. subtilis* SepF abolishes SepF ring formation. This α-helix is only predicted for SepF1, which suggests that only this homologue can dimerise and form rings. On the other hand, all three homologues contain the β-strands which are believed to be the dimerisation interface in *B. subtilis* SepF (Duman *et al.,* 2013). It may be possible that without the second α-helix the β-strands and the leading α-helix are not able to form a tight enough structure to allow SepF-SepF interaction to take place.

Though SepF dimerisation may not be feasible for all the *S. coelicolor* SepF homologues, there is the potential that they can all interact with FtsZ. This is possible as the C-terminals of each are mostly conserved and contain the amino acids identified by Duman et al to be important in FtsZ binding such as G109, A100, and F126. Additionally, other amino acids have been shown to be important for growth by testing these mutations in a *ftsA* knockout background causing lethality (Duman et al., 2013). These residues are also conserved within all three *Streptomyces* SepF homologues. These amino acids were G109, F106, D105, F126, F126, G116, I118 and Y72, though the last three amino acids where not conserved within SepF3.

Literature suggests that the N-terminus, though not widely conserved, may allow the anchoring role of SepF, through interaction with the cell membrane. This

interaction may be facilitated by the α-helices. Duman et al (2013), identified that the first 13 amino acids of the N-terminus of *B. subtilis* SepF are membrane binding, as truncated proteins lacking amino acids 1-13 show no lipid interaction with SepF. The predicted secondary structures also showed that the N-terminus may contain α-helices for SepF1 and SepF2 (Figure 3.3). This is a feature that they share with *B. subtilis* SepF, though this latter contains two α-helices in its N-terminus as opposed to one in SepF1 and SepF2 of *Streptomyces*. As they both have an α-helix predicted within the first 13 amino acids, this suggests that SepF1 and SepF2 are able to interact with the cell membrane and could potentially bind to it to help anchor FtsZ during cell division.

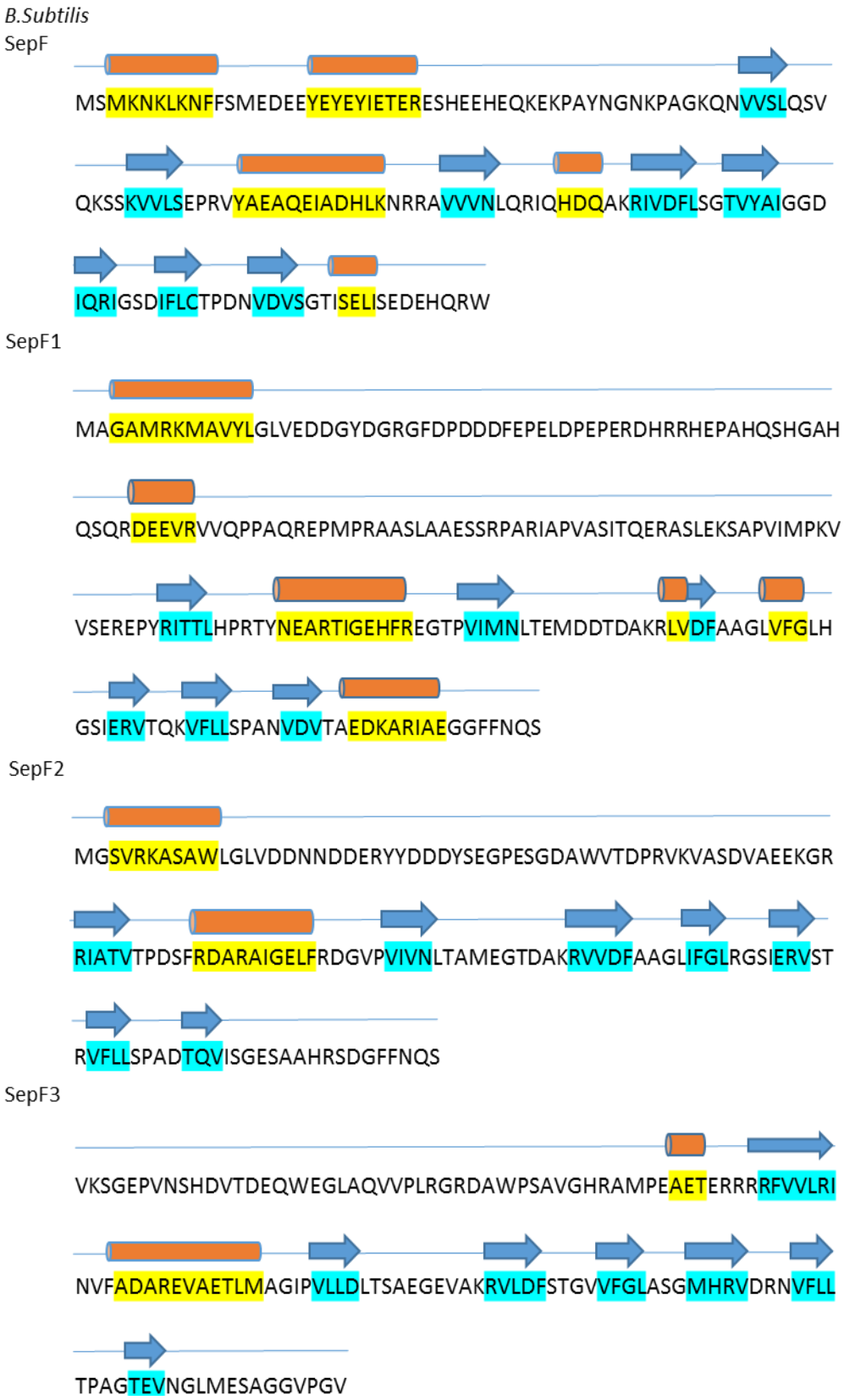


Figure 3.3: The predicted secondary structures of the three SepF homologues of *S. coelicolor* compared to that of the *B. subtilis* SepF. The blue arrows represent β-sheets and the orange rods represent α-helices, with their respective amino acids highlighted in blue (β-sheet forming) or yellow (α-helix forming). The predicted secondary structure was obtained using PSIPRED, from sequences taken from StreptDB (for *S. coelicolor* SepF1, SepF2 and SepF3) and UniProt (for *B. subtilis* SepF).

### 3.2.4. Genome Organisation adjacent to the three *S. coelicolor sepF* genes

As the previous analysis did not greatly differentiate between the three SepF homologues, we compared each *sepF* gene's genomic locations to that of *B. subtilis sepF*. In bacteria gene density is high and often adjacent genes are involved in related biological pathways. To compare the gene organisation around the *sepF* genes five to six genes upstream and downstream of the *sepF* genes homologues were identified and information was gathered on their functions or predicted roles using StreptDB and BLAST searches (Appendix I).

Using this data, it became apparent that the gene organisation adjacent to *sepF2* was very similar to that of next to *B. subtilis sepF* as both genes were in the conserved cell division cluster spanning between *ftsZ* and *divIVA* genes (Figure 3.4). The gene orientation of *sepF1* is opposite to that of its neighbouring genes and so it is not part of a gene cluster. The genes *SCO1748, SCO1747* and *SCO1746* are directed in the opposite direction from *sepF1*. Whilst it is possible that *SCO1748* encodes a repressor protein that could in principle regulate the expression of *sepF1*, it is more likely that this repressor regulates the expression of *SCO1746* which encodes a protease as it is annotated as a repressor of protease expression. Therefore, the genes surrounding *sepF1* do not give any insight as to the possible function of SepF1. The gene for SepF3 could be part of an operon, which starts with sepF3 and includes downstream genes between *SCO5968*-5972. There are 96 bp between the 3' end of *sepF3* and the 5' prime end of *SCO5968* which encodes a possible bldA regulated nucleotide binding protein. The 96 bp distance between the two genes might contain a separate promoter or *SCO5968*, which could separate this gene functionally from the *sepF3* gene. However, the 96 bp distance is short and could also allow co-transcription starting upstream of *sepF3*. In the absence of transcriptional data, we cannot exclude the possibility of a link between *sepF3* and *SCO5968* and the further downstream genes.

In summary, SepF2 is the true homologue of SepF of B. subtilis, as it not only has the highest percentage identify sharing 30% of amino acid residues when compared, but also the gene organisation surrounding the two *sepF* genes is highly conserved (Figure 3.4).

The other two *sepF* genes, *sepF1* and *sepF3* encode proteins that could potentially interact with FtsZ (Appendix I), but their locations in the chromosome do not give any additional insight to their location. If they are involved in controlling FtsZ, it is not clear why these genes ae located so far apart in the chromosome.

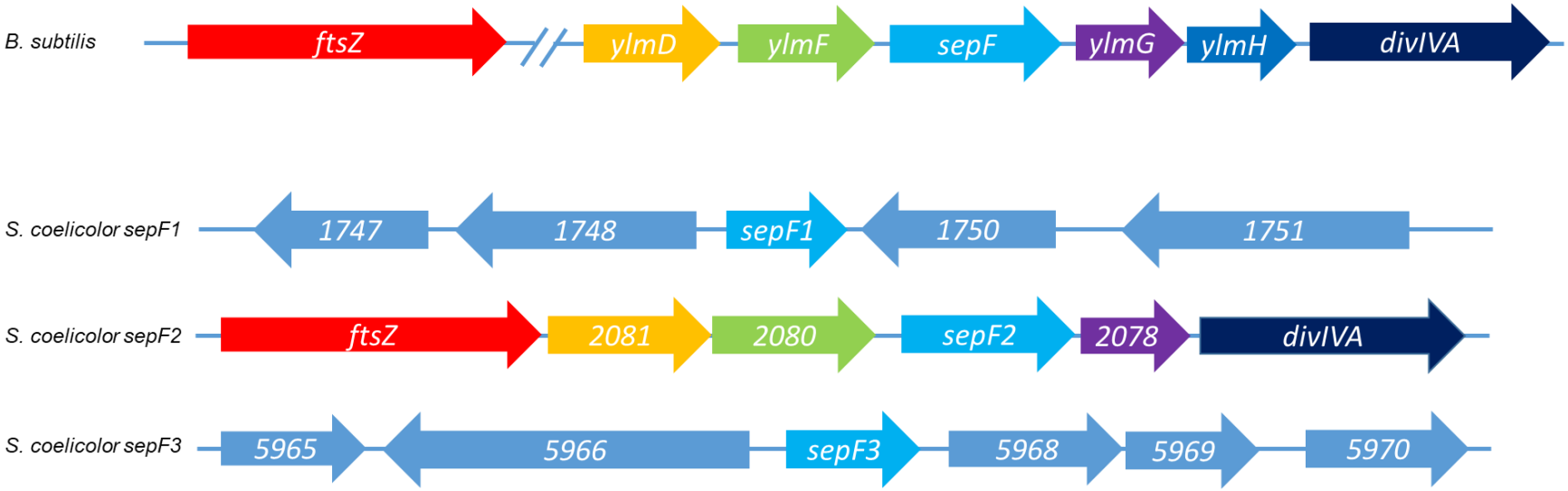


Figure 3.4: The gene organisation surrounding the three *sepF* genes in *S. coelicolor* compared to the gene organisation surrounding *sepF* from *B. subtilis*. The genes are described by either their SCO number or gene names. The gene organisation surrounding *sepF* for *B. subtilis* and *S. coelicolor sepF2* is similar, and homologues between the two sets of surrounding genes can be seen by matching colours.

### 3.2.5. Comparisons of the three SepFs of *S. coelicolor* with SepF found in other bacteria

To further investigate the distribution of SepF in bacteria, all three *S. coelicolor* SepFs were compared against SepF from other bacteria. Clustal Omega (https://www.ebi.ac.uk/Tools/msa/clustalo/) was used to conduct pair wise comparisons of each combination to establish whether SepF2 shows the highest similarity to SepFs from other bacteria.

Firstly, bacteria which contained only one SepF homologue and represented the *Cyanobacteria, Firmicutes* and *Actinobacteria* families were chosen for comparsion. The phyla chosen contain a large number of SepF containing bacteria (Table 3.2).

Table 3.2: The percentage identity of the SepF homologues of *S. coelicolor* when compared to other bacterial SepFs from organisms containing only a single copy of SepF. The percentage identity was generated though pair wise comparisons of the respective amino acid sequences using Clustal Omega (Rounded to the nearest whole number).

| | *Synechococcus sp.* | *Corynebacterium glutamicum* | *Mycobacterium marinum* | *Gloebacter violaceus* | *Bifidobacterium bifidum* |
|---|---|---|---|---|---|
| **SepF1** | 22 | 31 | 41 | 30 | 43 |
| **SepF2** | 23 | 24 | 41 | 30 | 42 |
| **SepF3** | 21 | 23 | 29 | 29 | 28 |

As Table 3.2 shows, SepF1 and SepF2 showed a higher homology than SepF3 when compared to the single SepFs from other bacteria.

Then *S. coelicolor* SepFs were compared against SepF homologues from bacteria also containing multiple SepF homologues. There are a number of bacteria that have been predicted to contain multiple SepF homologues. A significant number of these are other species of *Streptomyces* genus, with many containing two or three homologues. Multiple SepF homologues are also found in *Cyanobacteria*, *Firmicutes*, *Fusobacteria* and other *Actinobacteria*. Therefore, the three SepF homologues from *S. coelicolor* were compared against SepF sequences from other *Streptomyces*, to see if SepF1 and SepF3 are conserved within *Streptomyces*. Then the *S. coelicolor* SepF homologues were compared against other non-*Streptomyces* bacteria which contained multiple SepF homologues. This would test if SepF1 and SepF3 were conserved, if at all, in a wider range of bacteria.

The sequences required were identified and obtained using the pFam database (Finn et al., 2016), Kegg database (Kanehisa et al., 2016, Kanehisa and Goto, 2000) and BLAST searches. The gene locations of the *Streptomyces* SepF homologues were noted in relation to nearby genes so to determine which homologues where more likely to be a 'primary' SepF in order to compare each correctly. SepF2 homologues where chosen as their genes are close to *ftsZ* and/or *divIVA* homologues, while SepF1 homologues where distinguished by their lack of cluster identity. This was attempted for all the bacteria listed in Table 3.3, however, some of the SepF homologues are significant distances away from the other identifying genes, so were labelled by the order in which they appear in their respective genomes.

As Table 3.3 suggests, SepF1, SepF2 and SepF3 are conserved within *Streptomyces*. Though SepF3 is not present in all *Streptomyces* strains, such as *Streptomyces bingchenggensis BCW 1*, many *Streptomyces* strains carry all three SepF homologues.

Table 3.3: The percentage identity of the SepF homologues of *S. coelicolor* when compared to other *Streptomyces* species with multiple SepF homologues. The percentage identity was generated though pair wise comparisons of the respective amino acid sequences by Clustal Omega (rounded to the nearest whole number).

| | *S. bingchenggensis* SepF 1 | *S. bingchenggensis* SepF 2 | *S. griseus* SepF 1 | *S. griseus* SepF 2 | *S. griseus* SepF 3 | *S. Scabiei* SepF 1 | *S. Scabiei* SepF 2 | *S. Scabiei* SepF 3 | *S. Venezuelae* SepF 1 | *S. Venezuelae* SepF 2 | *S. Venezuelae* SepF 3 | *S. Avermitilis* SepF 1 | *S. Avermitilis* SepF 2 | *S. Avermitilis* SepF 3 |
|---|---|---|---|---|---|---|---|---|---|---|---|---|---|---|
| **SepF1** | 49 | 78 | 49 | 83 | 31 | 50 | 81 | 30 | 50 | 81 | 29 | 49 | 85 | 32 |
| **SepF2** | 88 | 78 | 88 | 48 | 29 | 93 | 91 | 48 | 88 | 46 | 30 | 92 | 48 | 31 |
| **SepF3** | 32 | 32 | 30 | 32 | 64 | 28 | 32 | 23 | 30 | 34 | 70 | 31 | 33 | 87 |

Table 3.4 suggests that the overall percentage identity is much lower when the *Streptomyces* SepF were compared to the multiple SepF homologues found in bacteria other than *Actinobacteria*. The designation SepF1 was given to the homologues which were encoded in the vicinity of the *ftsZ* gene. Overall, SepF2 of *S. coelicolor* shows highest identity to SepF1 of these other bacteria with some exception (Table 3.4). However, it is not possible to make a convincing statement

about the second sepF in these bacteria, which sometime shows high similarity to SepF1 at other times to SepF2 of *S. coelicolor*.

Table 3.4: The percentage identity of the SepF homologues of *S. coelicolor* when compared to bacteria other than *Streptomyces* which contain multiple SepF homologues. The percentage identity was generated though pair wise comparisons of the respective amino acid sequences by Clustal Omega (Rounded to the nearest whole number).

| | *Pleurocapsa* SepF 2 | *Pleurocapsa* SepF 1 | *Cyanothece* SepF 1 | *Cyanothece* SepF 2 | *Cyanothece* SepF 3 | *Ilyobacter polytropus* SepF 1 | *Ilyobacter polytropus* SepF 2 | *Dialister* SepF 1 | *Dialister* SepF 2 | *Frankia* SepF 1 | *Frankia* SepF 2 |
|---|---|---|---|---|---|---|---|---|---|---|---|
| **SepF1** | 25 | 19 | 24 | 19 | 22 | 24 | 22 | 25 | 24 | 50 | 25 |
| **SepF2** | 24 | 23 | 24 | 20 | 21 | 22 | 24 | 31 | 28 | 58 | 28 |
| **sepF3** | 24 | 19 | 25 | 15 | 25 | 20 | 21 | 27 | 21 | 29 | 30 |

### 3.2.6. SepF in other organisms

As previously mentioned, the SepF-like proteins have been identified in many bacteria and archaea. The many bacterial phylum includes Cyanobacteria, Actinobacteria, Firmicutes and Fusobacteria.

It is important to note that the phyla that were chosen, all contain bacterial species which carry only one copy of the SepF and other species which contain at least two SepF homologues. The bacterial phyla covered and investigated are Cyanobacteria, Actinobacteria and Firmicutes. A brief look into archaeal SepF will also be provided.

#### SepF in *Actinobacteria*

*Streptomyces,* as part of the Streptomycetales, belongs to the *Actinobacteria* phylum, but this is not the only notable family it contains, with others including Corynebacterialies, Micrococcaceae, Mycobacteriaceae. These diverse bacteria come in different cell shapes including spherical, rod, club and filamentous bacteria and with different characteristics ranging from the human pathogen *Mycobacterium* to the producers of secondary metabolites, such as the *Streptomyces* species.

A pFam search has identified 587 species within *Actinobacteria* which contain the SepF. However, the individual number of SepF sequences within the genomes ranged from just one to six, with the total of identified sequences being

796. These multiple *sepF* sequences were mostly restricted to *Streptomyces* species, however, nine other species were also found to contain multiple homologues. Of these, two contained three homologues each, *Thermobispora bispora* and *Frankia sp*. (strainEI5c), with others, such as *Saccharopolyspora erythraea* and *Micromonospora rosaria*, containing two SepF homologues.

A large proportion of *Streptomyces* species (a total of 106 documented) contained three *sepF* homologues, but 11 species containing only two were also found. Additionally, there were five *Streptomyces* species which contained only one SepF homologue, *Streptomyces rubellomurinus, Streptomyces griseolosporeus, Streptomyces spNRRL S-495, Streptomyces sp AA4,* and *Streptomyces thermoautotrophicus.*

**SepF in *Cyanobacteria***

Cyanobacteria are quite distinct from *Streptomyces* and other *Actinobacteria*, being Gram-negative. Cyanobacteria are known for their roles in nitrogen fixing and photosynthesis.

Of these, 99 different species contained a SepF homologue (pFam 12.04.18), with 132 SepF sequences between them. Of the bacteria which contain multiple SepF, the majority contain two homologs as opposed to the typical three SepF found in various *Streptomyces* species. Remarkably, some cyanobacterial species contain much higher numbers of SepF with *Cyanothece* sp (strain PCC7822) containing four SepF homologues and *Acaryochloris marina* (strain MBIC 11017) containing the largest number of homologues seen in the SepF pFam search at nine homologues. It should be noted that *A. marina* is known for gene duplication as it adapts to various niches (Miller et al., 2011), and is thought to remove unneeded genes. As the strain contains a high number of SepF homologues it suggests that SepF is important for its survival and that the multiple SepFs have beneficial effects that outweigh any negative ones. *A. marina* and *Cyanothece sp* do not contain any FtsA or EzrA homologues when searched for using the pFam and KEGG databases.

Cyanobacterial growth is varied throughout the phylum, with individuals being unicellular, filamentous, or colony forming. Additionally, their forms of cell division as well as growth is complex, with examples of polar growth, and regular and irregular cell division on a variety of planes. These multiple forms of growth and division are seen in the SepF containing *Cyanobacteria*, with *A. marina* with nine SepF homologues being unicellar and dividing in one plane and *Fischerella* sp.

JSC-11, which contains only one SepF homologue, being filamentous and branching (pFam and Komarek et al.,). *Fischerella* does not contain FtsA or EzrA homologues, suggesting that one SepF homologue is sufficient for anchoring FtsZ in this organism. The varied forms of SepF containing bacteria suggest that *sepF* is not a deciding factor in cellular shape and architecture, but it still has an important role to play in cell division in these bacteria.

**SepF in *Firmicutes***

In addition to *Actinobacteria*, this was the other major phylum identified to contained SepF homologues, with 934 species logged. The number of species containing multiple homologues was relatively low, as the number of sequences was only 982. Multiple SepF homologues occurred in various bacteria which did not share any obvious pattern in families or groups, including *Dialister* species which all contained two SepF homologues, and Selenomonadaceae, which has two subgroups both containing two homologues. Both of these groups of bacteria are within the Negativicutes class, and Gram-negative as opposed to the majority of firmicutes which are Gram-positive. The major sub group of firmicutes containing SepF were *Bacilli*. Only single SepF homologues were found in the 418 species listed.

**SepF is also found in *Archaea***

SepF has been shown to be present within *Archaea* which contain FtsZ, which happens to be a component of the cell division machinery in major lineages (Bernander, 2003). This shows that SepF has been involved with FtsZ and therefore cell division, for quite some time. Additionally, Makarova *et al*. 2010, noted that other partners associated with FtsZ are not present within Archaea, such as FtsA and MreB, with one exception for FtsA (Makarova et al., 2010). Using the pFam database, it was suggested that 127 species of Archaea contain at least one SepF orthologue. This number may be greater, as presently access to archaeal genomes is limited. When independently searched for via the pFam database, no homologues for FtsA or EzrA were found, bar one exception for EzrA. Lack of any FtsA and EzrA identified within all the Archaeal species searched, suggests that SepF is the sole membrane anchoring partner for FtsZ.

Additionally, some *Archaea* were identified on pFam to contain two orthologues of SepF, though this was rare, with only two species exhibiting this. This suggests that any roles provided by the multiple SepF in bacterial species are potential covered by the one SepF homologue in archaea.

### 3.3. Characterisation of a *sepF* knockout mutant

Based on the bioinformatics studies it is clear that the *sepF2* gene is located in the cell division gene cluster, similarly to the *sepF* gene of *B. subtilis*. Therefore, we hypothesise that *sepF2* might possess similar functions and characteristics as the *B. subtilis sepF*. In this work we only focused on one *sepF* gene, the *sepF2* gene of *S. coelicolor*, therefore, from this point the '*sepF*' designation will be used for *sepF2*.

The *sepF* knockout strain was generated by replacing *sepF2* with an apramycin resistance cassette, and the strain was confirmed to be *sepF2* null through PCR (not shown).

#### 3.3.1. The Δ*sepF* strain was distinct from the wild-type M145 strain when observed macroscopically

Samples of Δ*sepF* and the wild-type M145 strains were streaked onto SFM medium to generate both confluent and "single spore" areas on a single plate. The strains were grown at 30°C for 7 days, while being observed daily and scanned every 24 hours.

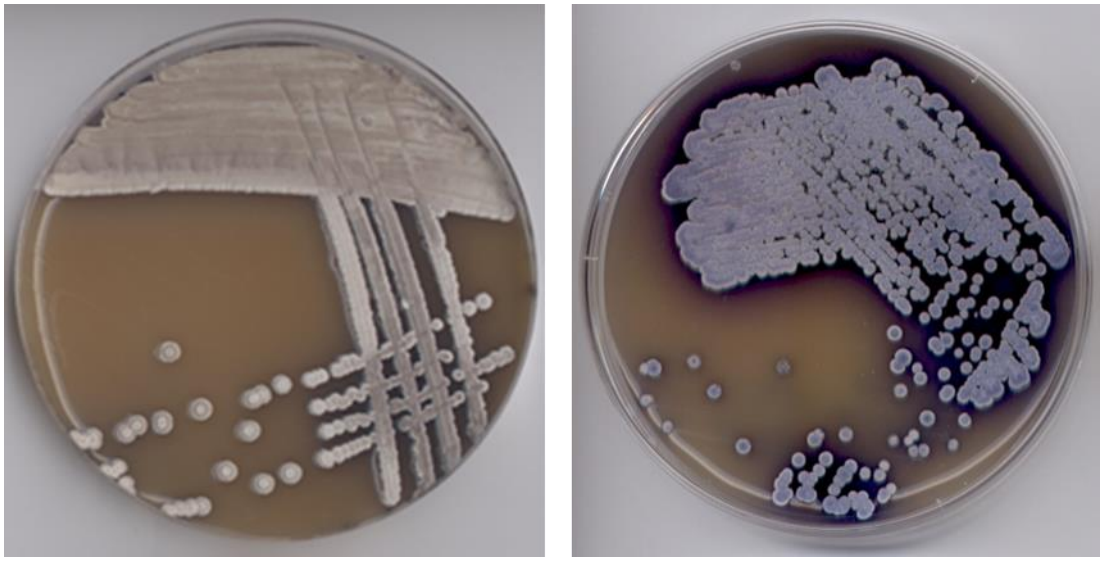

Figure 3.5: **M145 Δ*sepF* (right panel) and M145 (left panel) grown on SFM and imaged after 7 days of growth at 30°C.**

The wild-type M145 strain had a grey powdery appearance after 4 days growth, which is indicative of sporulation and the production of the grey coloured spore pigment. The *ΔsepF* mutant failed to produce the grey colour suggesting that the sepF mutant might not be able to sporulate. Instead, the *sepF* mutant showed blue pigment production both secreted into the medium around the colonies and also on the surface of the bacterial lawn (Figure 3.5). this blue pigment Is likely to be actinorhodin, one of the weak antibiotics produced by *S. coelicolor*.

**The Δ*sepF* strain has delayed growth**

The two strains grew at different rates, with Δ*sepF* growing slower than M145 and producing smaller colonies after the same period of growth (Figure 3.5). Also, Δ*sepF* did not produce as much colony producing material as M145, which can be seen on Figure 3.5 as the single spore stage occurred at a dilution closer to the confluent area.

**The Δ*sepF* strain has arrested development**

The most noticeable difference was at the mature stage of development, with colonies of Δ*sepF* staying white, though M145 colonies went through the normal white to grey colouring (Figure 3.5). This suggests that the development of Δ*sepF* stalls. It seems to be able to produce vegetative hyphae and aerial hyphae as the white colonies for Δ*sepF* were slightly 'fuzzy' in appearance, similar to those produced by M145 when at an early stage of aerial hyphae development. This is distinct from 'bald' mutants of *Streptomyces* which are also developmentally stalled but are unable to produce aerial hyphae.

The Δ*sepF* strain was observed for a period of two weeks, twice the normal growth time, to see if it would eventually transition from white to grey, however, this did not occur. The aerial hyphae of Δ*sepF* remained white, instead of turning to the wild-type grey, a colour which is associated with mature spores as they are covered with a grey 'sheaf'. This indicated that Δ*sepF* was unable to produce spores and the white colonies were not only due to slower development.

**The Δ*sepF* strain overproduces actinorhodin**

Though Δ*sepF* colonies were originally white, after seven days of growth on SFM the white colonies turned blue and the surrounding media also shows blue pigmentation. When grown for longer, blue droplets formed on top of the colonies. This is thought to be due to the overproduction of actinorhodin, one of the many antibiotics produced by *S. coelicolor*. The role of actinorhodin in *Streptomyces* has

not been fully defined but the product itself turns blue in alkaline conditions and red in acidic conditions and it has a weak antibiotic activity against Gram-positive bacteria. Actinorhodin production is well documented in *S. coelicolor* with overproduction observed under several different conditions. Some these include exposure of *S. coelicolor* to rare earth metals, disruption of glycolysis enzymes, or exposure to other bacteria such as *Myxococcus xanthus.*

**Summary of Macroscopic Observations**

These apparent differences suggested that Δ*sepF* mutants were unable to complete the last stage of *Streptomyces* development, the production of spores. While spore production is not essential for *Streptomyces* viability, as a variety of non-sporulating mutants are viable, this phenotype does indicate that *sepF* is necessary for spore production, and thus synchronous cell division.

As the white colonies are 'fuzzy', this indicated that the vegetative stage of development was completed, and aerial hyphae was also produced. Macroscopic observations cannot give detailed analysis of a knockout phenotype, therefore microscopic analysis was performed to monitor morphological differentiation of the *sepF* mutant.

### 3.3.2. The Δ*sepF* strain was distinct from the wild-type M145 when observed using epi-fluorescence microscopy

Based on the macroscopic phenotype we suspected that Δ*sepF* was not producing spores, hence Δ*sepF* samples were preserved by collecting all hyphal fragments grown on a cellophane sheet covering the SFM medium using storage media. This preparation was used to inoculate patches in solid medium grown next to microscope cover slips. As a control, spore preparations of M145 were also inoculated at the same time. Both inoculum were spread onto deep SFM plates in a small rectangle area that is slightly wider than a cover slip. Then a microscope cover slip was inserted into the medium at an angle of approximately 60 degrees at the location of the inoculum. This would allow aerial hyphae to grow onto either side of the cover slip. By pulling out the coverslips and staining, it was possible to investigate the aerial hyphae at different points of development. Several time points for the strain was tested, so to collect different stages of aerial development covering before, during and after potential sporulation. The time points were chosen based on the wild-type M145 developmental cycle, though additional later time

points were tested for the M145 Δ*sepF* strain to factor in any slower developmental changes. The hyphae were fixed to preserve the time point's developmental stage, and then stained. To observe any differences in cell wall and DNA distribution, two different fluorescent dyes were used on each cover slip sample. The dyes were Wheat Germ Agglutinin (WGA) with an Alexa Fluor 488 conjugate, and propidium iodide (PI). The stain WGA – Alexa Fluor 488 selectively binds to N-acetylglucosamine and N-acetylneuraminic acid (sialic acid). These targets are part of the bacterial cells walls, with N-acetylglucosamine being a major cell wall component as it is a principle part of peptidoglycan, and sialic acid is a precursor of cell wall synthesis. Therefore WGA-Alexa Fluor 488 stains areas of the bacterial cell wall and especially areas of cell wall growth. Its emission maximum is 519nm and therefore gives a green colour. PI is a DNA intercalator and therefore targets the chromosome. It has little sequence preference so double stranded areas are equally stained, with PI intercalating every four to five base pairs. PI is a red stain with an emission maximum of 617nm when bound to DNA. WGA-Alexa Fluor 488 and PI monitor both cell wall and DNA distribution during *Streptomyces* development.

The cover slips were viewed using fluorescence light microscopy at x100 magnification using a phase contrast filter and under two different waves of UV light so to highlight areas of cell wall growth and DNA, with images of all three phases (Figure 3.6-3.9).

When observed under the microscope, the aerial hyphae of the Δ*sepF* strain showed a clear difference in the phenotype, when compared to the wild-type: there is a complete absence of septation in the mutant strain (Figure 3.6.). This was observed at all time points tested, including later time points. M145 presented the expected results of irregular septation during vegetative growth and clear, regular and complete septum formation within the aerial hyphae transitioning to spore chains. The aerial hyphae seemed otherwise unaffected, though there were notably more lysed cells for Δ*sepF* compared to the wild-type (Figure 3.7).

Samples taken after 48 hours growth, when septum formation and therefore spore production takes place in the wild-type strain, showed no septa present in the Δ*sepF* strain. Interestingly, some aerial hyphae did show signs of chromosome segregation (Figure 3.8). The chromosomes seemed to compact into spore like packages, though the chromosome distribution was not uniform, and the chromosome packages still appeared to be linked though tenuously. In addition, at some places the cell wall was also affected, it was no longer smooth but appeared

to be constricted in places, though not fully, potentially due to contractile forces. However, this was a rare observation, with most aerial hyphae observed having smooth hyphae and no chromosome packaging.

**Crosswalls are absent in the Δ*sepF* strain**

To observe if this lack of septation also affected the vegetative hyphae, in which the wild-type contains crosswalls periodically, vegetative growth was also investigated. To do this Δ*sepF* samples were grown on a layer of cellophane placed on SFM plates. The samples were grown at 30°C with early time points (22 hrs, 24 hrs, and 26 hrs) being collected. At each time point cellophane squares, where Δ*sepF* had been grown, were cut and removed from the plate, fixed and then stained with WGA-Alexa 488 and PI. This process was done in a high moisture environment so to prevent the cellophane from drying which would have negatively affected the *Streptomyces* strains grown on it. The cellophane slides where then viewed under a fluorescence light microscope using phase contrast filter and UV light.

Analysis of the vegetative hyphae revealed that vegetative septa, or crosswalls, were missing throughout the mycelium (Figure 3.6). This was observed at all time points tested. The rest of vegetative mycelium seemed otherwise unaffected.

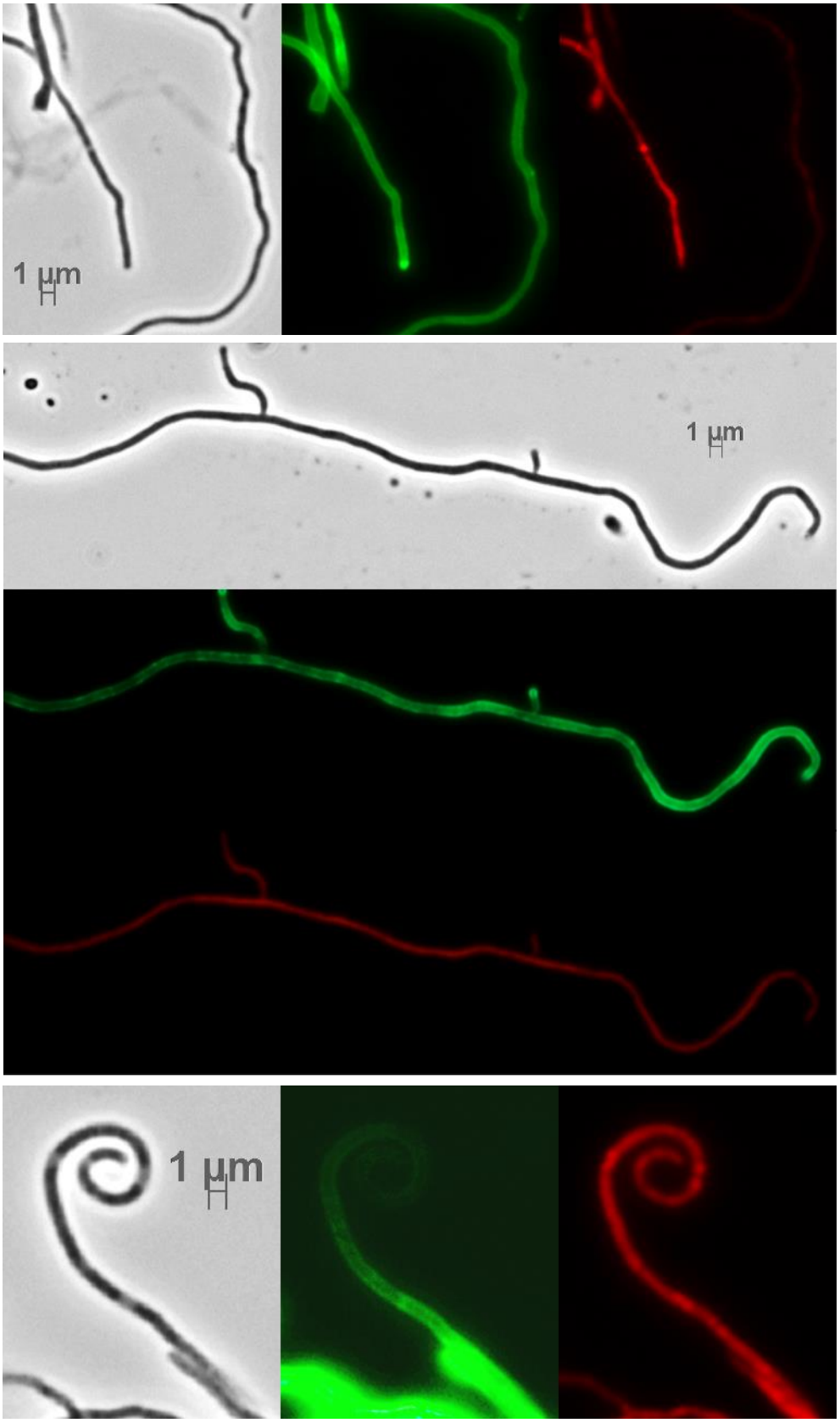


Figure 3.6: The **Δ*sepF* strain viewed under confocal microscopy.** The Δ*sepF* mutant has no septa or other cell wall structures present within the aerial and vegetative hyphae. Δ*sepF* was imaged under normal light (grey panels, left/top), UV light to excite green fluorophore of WGA-Alexa 488 (middle panels), and UV light to excite red fluorophore of PI (right/bottom panels). The first panel shows vegetative hyphae, imaged after 22 hrs of growth. The middle panel shows late vegetative and aerial hyphae. The bottom panel shows aerial growth and was imaged after 56 hrs of growth.

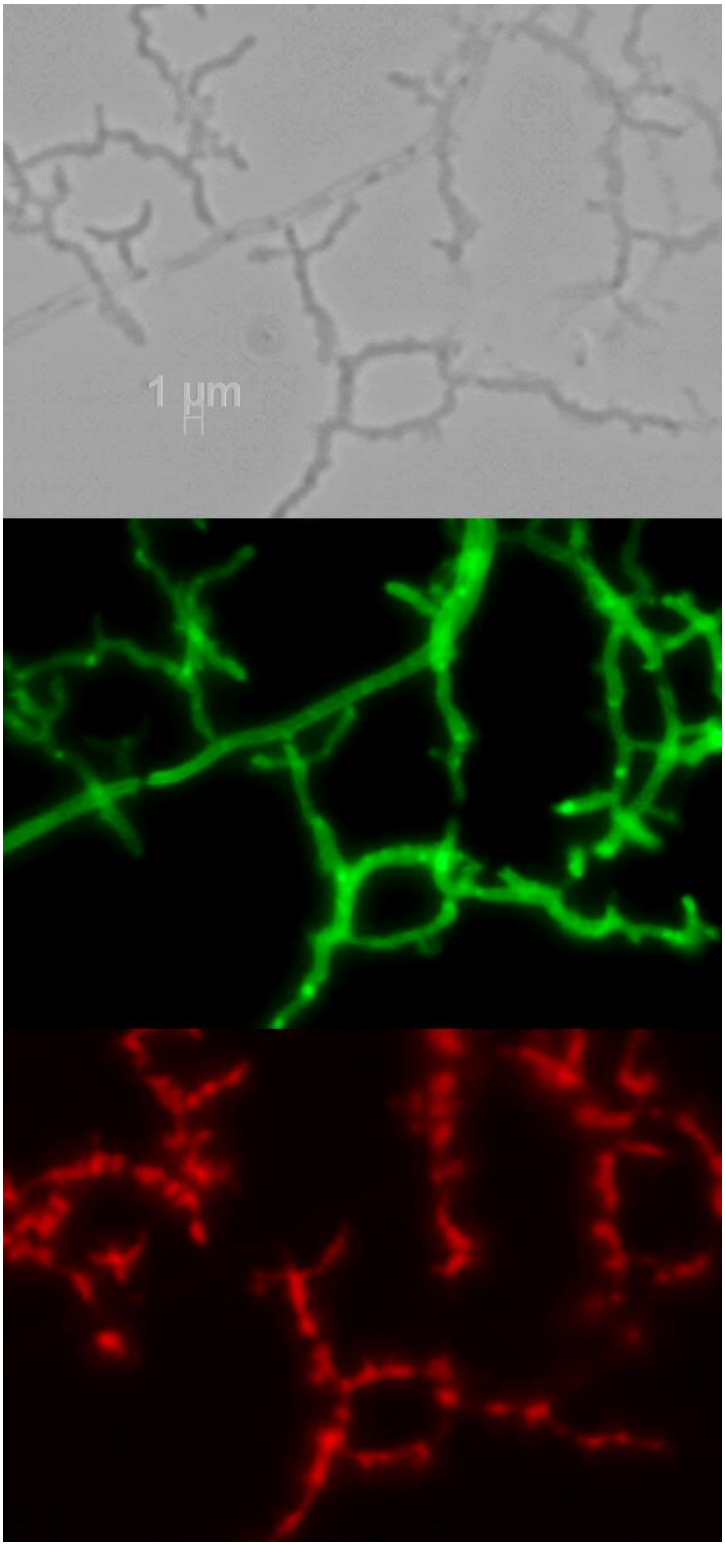


Figure 3.7: The Δ*sepF* strain viewed under confocal microscopy. Example of lysis within the vegetative hyphae of the Δ*sepF* strain. Δ*sepF* was imaged under normal light (top), UV light to excite green fluorophore of WGA-Alexa 488 (middle), and UV light to excite red fluorophore of PI (bottom). The images were taken after 22 hrs of growth.

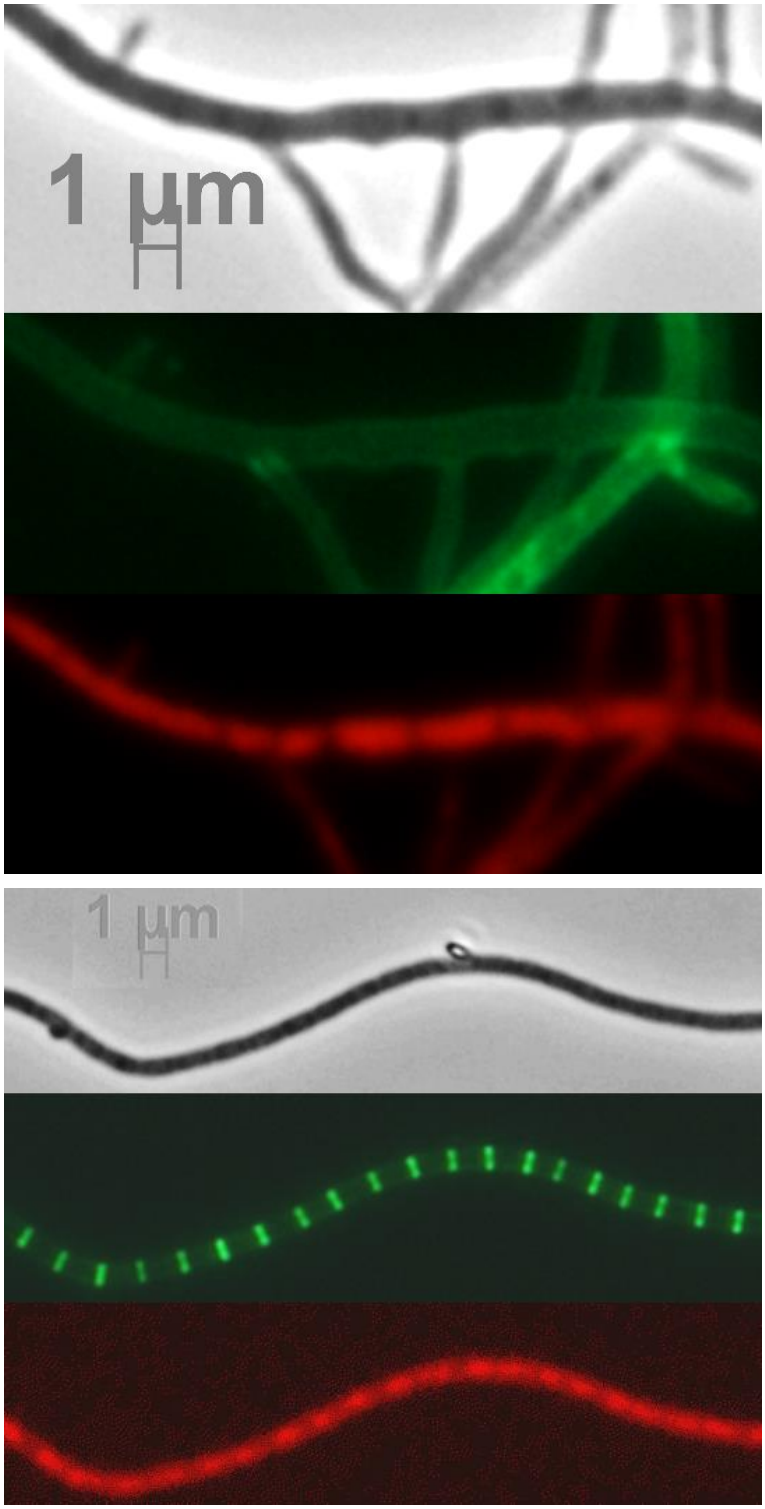


Figure 3.8: Examples of chromosome segregation within the aerial hyphae of Δ*sepF* (top panel), compared to septa and chromosome segregation seen in M145 (bottom panel). The samples were imaged under normal light (top), UV light to excite green fluorophore of WGA-Alexa 488 (middle), and UV light to excite red fluorophore of PI (bottom). The wild-type M145 shows regularly spaced septa within the aerial hyphae and evenly sized chromosomes. Δ*sepF* does not have any septa, but the chromosomes do show signs of segregation, though these DNA packages are irregularly sized.

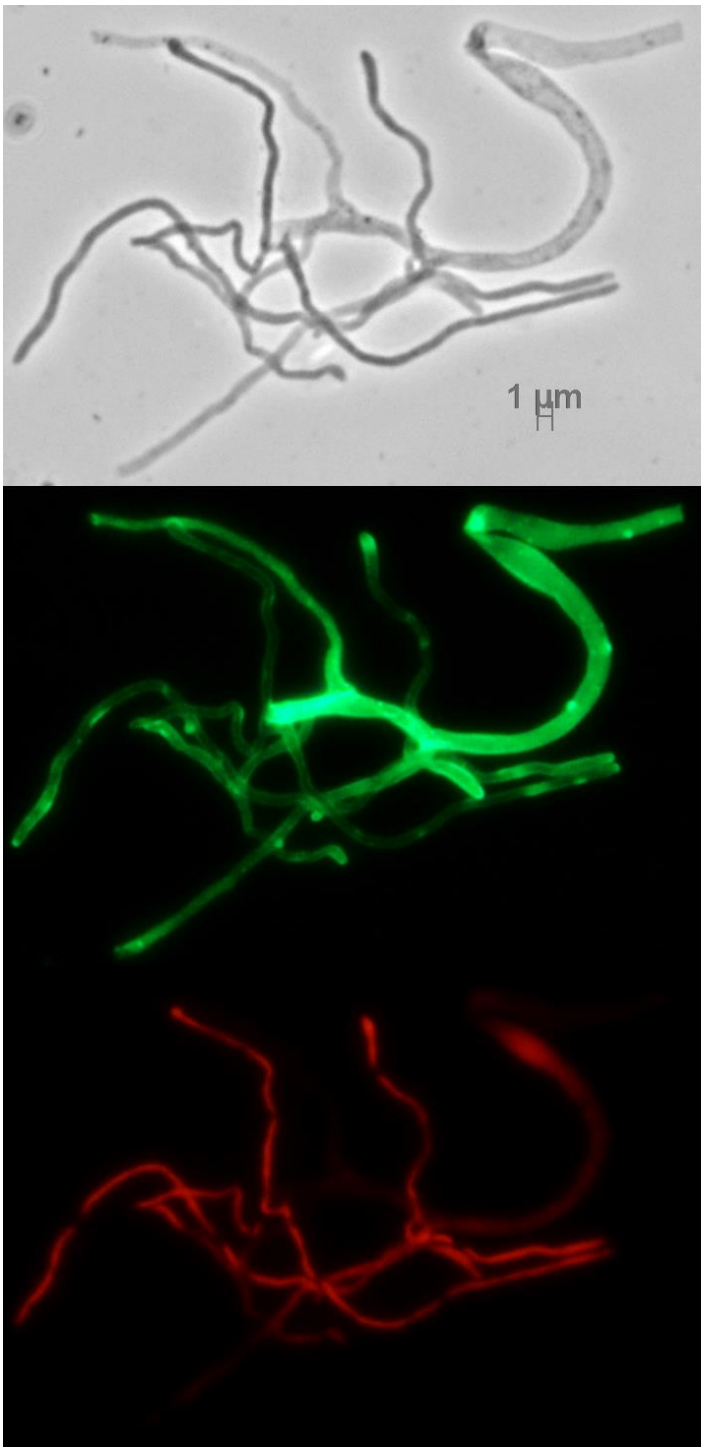


Figure 3.9: An example of Δ*sepF* at the vegetative developmental stage. There is evidence of lysis, in the lighter coloured hyphae which seems to have spilt. Δ*sepF* was imaged under normal light (top), UV light to excite green fluorophore of WGA-Alexa 488 (middle), and UV light to excite red fluorophore of PI (bottom).

### 3.3.3. Summary of the phenotype of the *sepF* knockout mutant

The lack of septa within both the vegetative and aerial hyphae suggests that *sepF* is vital for septum formation throughout development. In addition to FtsZ and SsgA, it seems that SepF is an instrumental protein for septation and therefore cell division in *Streptomyces*.

Without septation spores cannot be produced in the aerial hyphae. The *sepF* mutant is capable of producing aerial hyphae and therefore not 'bald' as colonies have a 'fuzzy' appearance. However, these 'fuzzy' colonies do not become grey, as they fail to sporulate and fail to produce the spore-specific grey pigment.

The absence of septa in the vegetative hyphae may also play a part in explaining why Δ*sepF* is slower growing and may be more prone to lysis. It is thought that crosswalls may be structurally important and give support to the vegetative hyphae. Maybe without this extra internal support hyphae are slightly more vulnerable to damage and lysis, and slower growing as they are not as structurally stable as the wild-type. Also, crosswalls generate compartments and compartmentalisation might be essential for normal development. Cell lysis might be part of *Streptomyces* development, where isolated compartments can lyse without effecting the well-being of the colony, or even providing nutrients for the expanding colony. However, in the *sepF* mutant, the lack of crosswalls means that when lysis occurs, it spread without any restriction by the crosswalls. This might explain the extensive areas of cell lysis in the *sepF* mutant. Similarly, the blue antibiotic, actinorhodin production is also compartmentalised and restricted to the vegetative hyphae in wild-type colonies. In the *sepF* mutant actinorhodin overproduction or the produced actinorhodin spread to the aerial hyphae, likely because of the lack of compartmentalisation.

## 3.4. Partial complementation of the *sepF* knockout using a '*sepF* fragment'

To confirm the mutant as a true knockout a construct containing *sepF* was generated and introduced into the mutant Δ*sepF* strain. The restoration of the wild-type phenotype in complemented strains would indicate that the absence of septa was the direct result of the deletion of *sepF*, and not due to secondary mutations, which may have accumulated in the knocking out process.

The construct produced was designed to contain a DNA fragment including the *sepF* gene and was amplified using PCR. Instead of using the genomic DNA as a template, a cosmid, 4A10, was utilised. The 4A10 cosmid carries ~40kb DNA of *S. coelicolor* and was generated as part of the cosmid library of *S. coelicolor*. This cosmid DNA was used instead of genomic DNA to reduce the possible annealing events during the construct generation, which could have been a potential problem for *sepF* as it has two other homologues within the *S. coelicolor* genome.

It was expected that after introduction of the construct into the *sepF* mutant strain, the phenotype of the knocked-out strain would be restored to the wild-type phenotype. The restoration of the wild-type phenotype will be observed by either macroscopically or microscopically. Initial macroscopic observations will test whether the *sepF* mutant produces dark grey aerial surface after complementation, which is indicative of sporulation.

Additionally, the *sepF* construct was also introduced into the wild-type M145 strain, to test whether an extra copy of *sepF* had any effect on development.

### 3.4.1. Construct Generation

#### Plasmid selection

To deliver the *sepF* gene we used the plasmid pMS82, which can replicate within *E. coli* but not in *Streptomyces*. In *Streptomyces* pMS82 integrates into the *attB* site in a single copy and it is able to carry inserts up to 8Kb in size (Gregory et al., 2003).

It is 6108 bp in size and contains the selectable marker *hyg*, which is a hygromycin resistance gene (Figure 3.10). It also contains the *int* gene, which is an integrase gene which originates from the *Streptomyces* phage ΦBT1 and promotes the integration of this plasmid into the *Streptomyces* genome. The plasmid has a multiple cloning site and various restriction sites, though pMS82 has not been fully sequenced.

The pMS82 plasmid was chosen as its hygromycin resistance is a selectable marker which differs from the marker used during the knockout generations. The knockouts were generated in a way in which the *sepF* gene was replaced by an

apramycin resistance cassette, therefore a different resistance gene was required to deliver the complementing clone.

Additionally, the plasmid is able to replicate in *E*. *coli*, this is important as two *E. coli* strains are used in this experiment. One strain, DH5α is used to generate the complementing clone and the other, ET12567 (pUZ8002), is used as a donor in the conjugation itself.

The pMS82 plasmid can be introduced into *Streptomyces* via a conjugation event due to it containing an OriT (Origin of Transfer), and it is able to integrate into *Streptomyces* via a ΦBT1 attachment site using the *attB* site in *Streptomyces*. This attachment site is located at *SCO4848*, which means that when it is used in M145, the wild-type *S. coelicolor*, it contains the construct and the original gene, where the construct used in this experiment are downstream of the original DNA stretch by over 2500 gene.

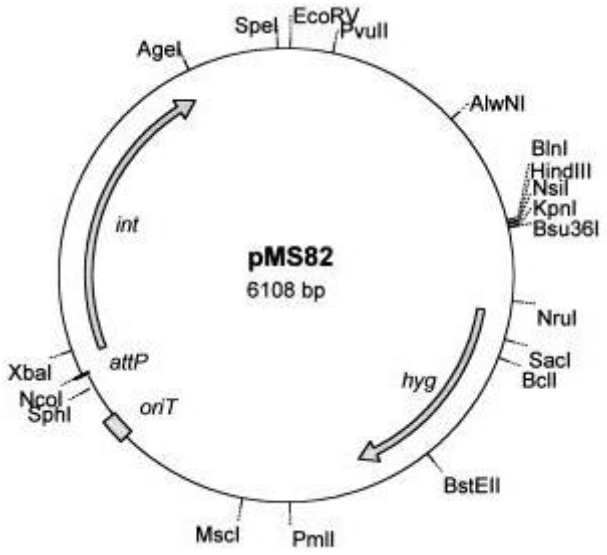


Figure 3.10: The plasmid map of the vector pMS82. The plasmid is 6108 bp in length with limited cloning sites. We have used the blunt end *EcoRV* site for cloning. It contains the hygromycin resistance gene (*hyg*) which acts as a selectable marker and the integrase gene (*int*) which originates from the *Streptomyces* phage ΦBT1. (Gregory et al., 2003)

**Primer design**

The primers were designed to anneal to sequences either side of the *sepF* gene (Table 3.5 and Figure 3.11). The construct was designed to contain 136 bp of upstream sequence to allow any potential close promoters to be included in the

construct fragments. As the promoter or potentially multiple promoters for *sepF* had not yet been identified, an estimation on the promoter location had to be made, but there was possibility that the fragments generated for the complementation will not contain all the promoters, which could be located further upstream.

The forward oligonucleotide sepF XbaBgl Prom FRW was designed previously and contain Xba and Bgl restriction sites, however, these sites were not used in this set of experiments.

Table 3.5: The oligonucleotide primer pairs and the expected size of the PCR product when using the wild-type 4A10 cosmid DNA as a template.

| | **Primer Pair** | **Expected size of fragment** |
|---|---|---|
| sepF | sepF XbaBgl Prom FRW<br>sepF 3 END | 978 bp |

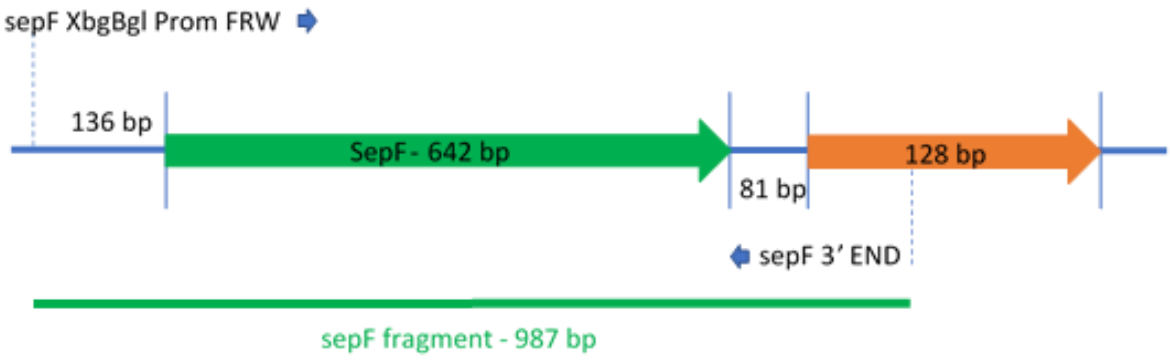


Figure 3.11: The Gene Organisation of *sepF*. The oligonucleotide arrangements used to generate the construct *sepF* from the 4A10 cosmid are shown. The oligonucleotides are shown by the dotted lines, with the arrows indicating the oligonucleotide directions. Measurements shown are based from one line to the next.

### Generation of the Construct

The construct corresponding to *sepF* was generated using the specific primer pairs shown in Table 3.5, in a high fidelity Phusion PCR.

The PCR product was confirmed through gel electrophoresis, in which the band produced was the correct size expected for the construct (Figure 3.12).

The PCR product generated was a blunt ended product. Blunt ended cloning is not as efficient then sticky end cloning and to increase the ligation efficiency we decided to dephosphorylate the vector fragment to block re-ligation of the vector. However, the blunt ended PCR product did not have phosphate groups at its 5' end which would have made ligation to an unphosphorylated vector impossible. Therefore, the PCR fragment was phosphorylated with T4 kinase to enable ligation.

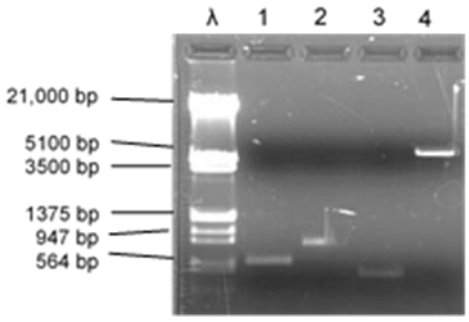


Figure 3.12: The Gel Electrophoresis of the Phusion PCR product. Lane 1: The size of the PCR Phusion product corresponds with the predicted '*sepF'*. Lane 4: The pMS82 plasmid after digestion with EcoRV and gel extraction. The other lanes are not relevant. Lambda DNA was digested with EcoRI and HindIII and used as a size marker.

Once confirmed, the DNA fragment was introduced into the pMS82 vector which had been digested with EcoRV (Figure 3.12) and was dephosphorylated.

The ligation was then desalted via a column and electroporated into the *E. coli* strain DH5α.

**Confirmation of the Recombinant Clones**

The transformed DH5α cells were selected on LB medium lacking salt with hygromycin. The resulting colonies were screened using colony PCR.

The colony PCR used the same primer pairs that were used to produce of the construct, therefore the expected size should be as shown in Table 3.5. After a series of colony PCRs positives were found for the clones containing pMS82-sepF (Figure 3.13).

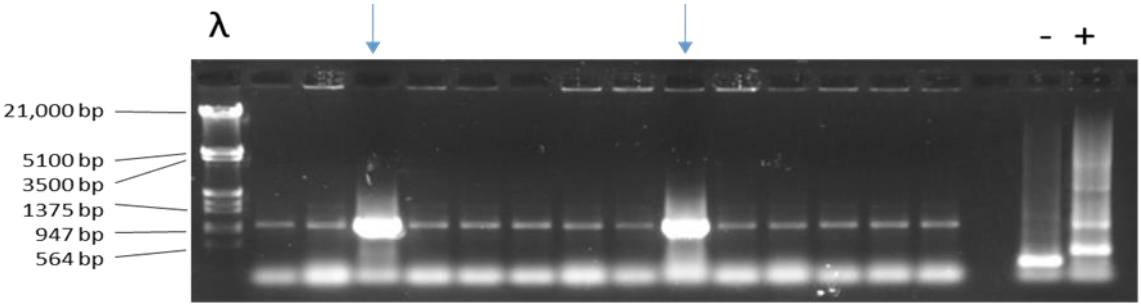


Figure 3.13: Colony PCR containing the correct fragments for *sepF*. Lambda DNA digested with EcoRI and HindIII was used as a size marker. The positive clones are recognised by their strong bands and are the same size as the positive controls. Two positive clones for *sepF* were detected as shown by the blue arrows. The positive control was pGEM-sepF and the negative control was pMS82-ftsZ.

### Sequencing and confirmation of the fragments within pMS82

To confirm the putative positive clones, plasmid preps for each were generated and sequenced. The sequencing confirmed the clones and their presence within the preps generated.

### Conjugating the fragments into *S. coelicolor*

The plasmid, pMS82-sepF was introduced into the *E. coli* strain ET12567 (pUZ8002), which acts as the donor during conjugation. This *E. coli* strain contains the pUZ8002 plasmid which facilitates the conjugation of pMS82 by providing the *tra* gene which is required in to transfer the DNA between the donor ET12567 and receiver *Streptomyces*. This mobilises the pMS82, but pUZ8002 is not able to cross into *Streptomyces* ensuring only the plasmid of interest is transferred. Additionally, *Streptomyces* does not readily accept all donors during conjugations, due to a system in which it will restrict certain methylated DNA (González-Cerón et al., 2009). ET12567 (pUZ8002) is able to bypass this problem as it is methylation deficient (Gregory et al., 2003).

The conjugations set up were using the *Streptomyces* strains Δ*sepF* and M145. Each of these strains were conjugated with ET12567 (pUZ8002) carrying pMS82-sepF, and an empty pMS82 vector to act as control.

The *Streptomyces* exconjugants were selected using hygromycin and nalidixic acid, this latter was used to restrict *E. coli* growth. Two independent hygromycin resistant exconjugants were used to generate spore stocks.

### 3.4.2. Characterisation of the Resulting Strains

The resulting strains were viewed and monitored for any macroscopic differences. Each strain was plated in near equal amounts (estimations of colony producing material were calculated for non-spore producing strains), onto the same media plate. They were then observed for 4 days and imaged every 24 hours (Figure 3.14). The media used was SFM, so to observe the strains when on a balanced media, minimal media with glucose (MMG), and minimal media with mannitol (MMM), so to see if the strains developed differently. SFM contains a plentiful carbon source in the form of mannitol and other nutrients in relatively high levels compared to the minimal media. Minimal media contains restricted amounts of nutrients, and a sole carbon source. It has been previously shown that the carbon source available to *Streptomyces* can affect development and growth of different strains. Mannitol has been shown to rescue certain phenotypes when strains, such as those with a bld phenotype, were grown on it (Viollier *et al*., 2001). Glucose on the other hand has been shown to repress certain systems within *Streptomyces*, dependent on the species (Van Wezel *et al*., 1997). Glucose repression and its full effect on the morphology and metabolites of *Streptomyces* is not well understood, but it has been shown to affect actinorhodin production (Romero-Rodriguez *et al*., 2016). Therefore, it is important to observe the strains when grown on either mannitol or glucose, as it is possible that the different medias would allow for alternative pathways for growth or morphology to be utilised by *S. coelicolor*. Hygromycin was added to the media to ensure the presence of the plasmids.

The conjugated strains were also investigated though microscopy analysis to see if they had been restored fully to the wild-type phenotype. From the stock preparations 1 µl of each strain was used to grow material on SFM medium for coverslip microscopy. Several time points were tested so to compare. Each coverslip was stained with WGA-Alexa 488 and PI, as before, to detect any change in cell growth and DNA distribution. The morphology of stage was also noted, so to detect any unexpected differences due to the conjugations. Additionally, septa to septa distances for the spore producing strains were measured to quantify any changes between the strains.

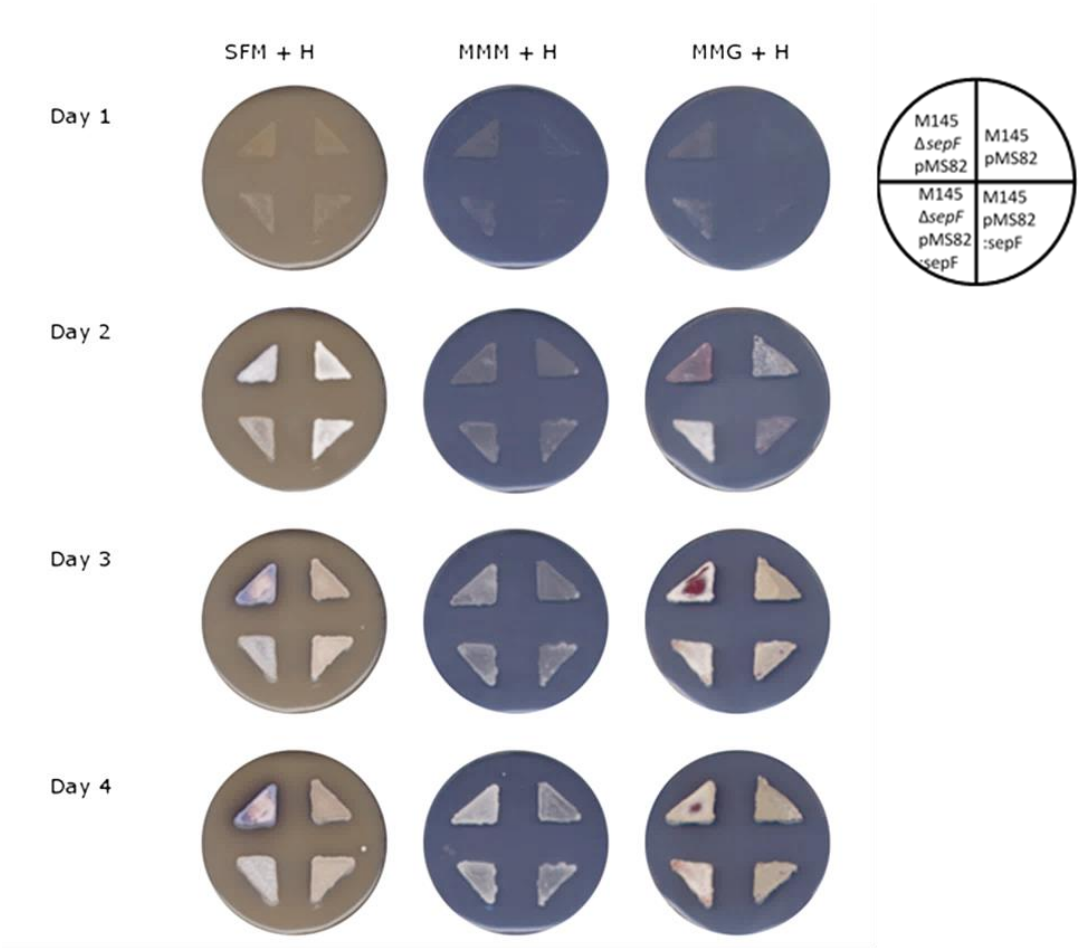


Figure 3.14: The strains M145 carrying pMS82, M145 carrying pMS82-sepF, Δ*sepF* carrying pMS82, and Δ*sepF* carrying pMS82-sepF were grown on selected media containing hygromycin. The plates were viewed every 24 hours after inoculation on SFM, MM and mannitol, and MM and glucose. The control strain M145/pMS82 and M145/pMS82-sepF do not differ in growth rate or phenotype, even when plated on MM. The Δ*sepF*/pMS82 develops as a Δ*sepF*. Δ*sepF*/pMS82-sepF does produce spores as seen on SFM, though when grown on MM with glucose it shows a phenotype which seems a mix of the phenotypes seen for the two control strains (Δ*sepF*/pMS82 and M145/pMS82).

**M145 carrying pMS82**

This strain was generated to see if the presence of pMS82 vector affected development of *S. coelicolor*, and so to verify that any differences seen in the other conjugated strains were due to the introduced *sepF* gene and not interference from the vector.

The wild-type and M145/pMS82 are very similar macroscopically, with M145/pMS82 producing spores (Figure 3.14), though septa to septa length analysis has shown that there are no significant differences between the two strains (Figure 3.15). The mean of the septa to septa distances are 1.1 µm. The M145/pMS82 strain seems to have a modal length 0.2 µm smaller than the wild-type, and the average length is not as pronounced as in the M145.

Therefore, we concluded that the presence pMS82 did not alter the wild-type phenotype and the septation during sporulation.

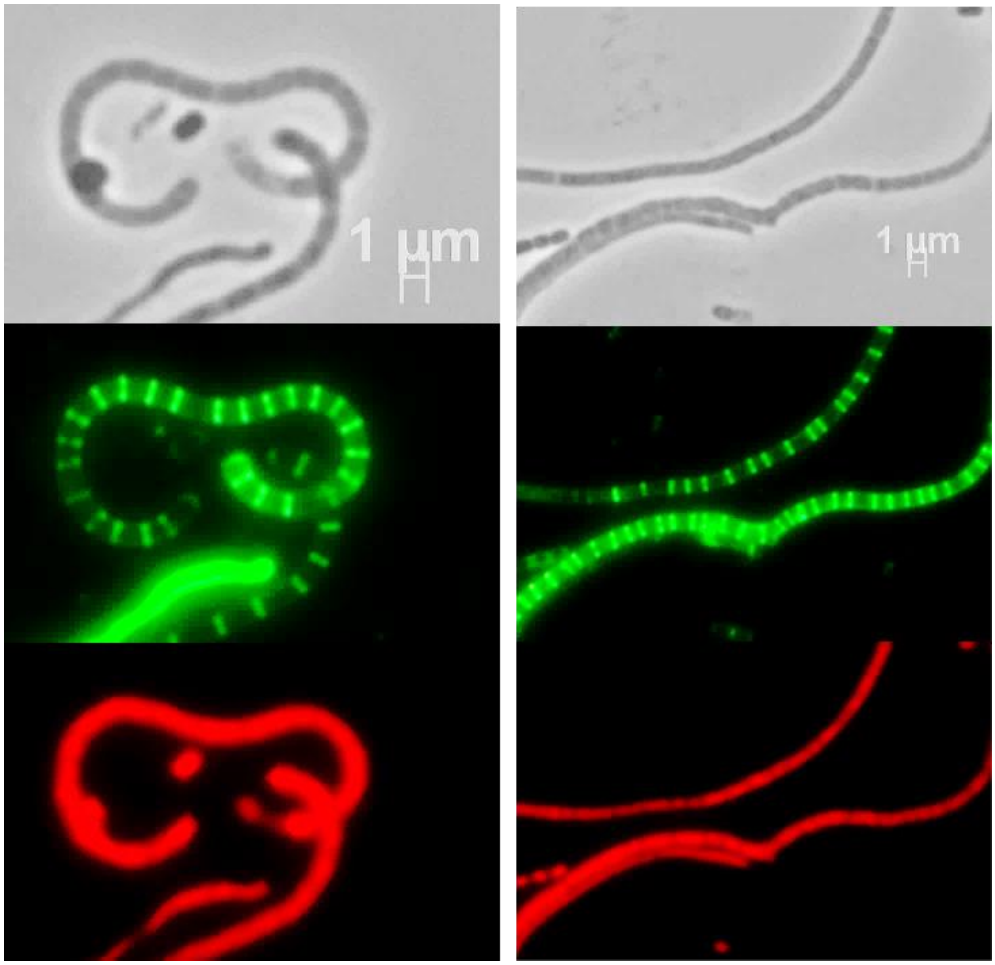


Figure 3.15: M145/pMS82 viewed under confocal microscopy. Examples of septa within aerial hyphae and chromosome segregation. The samples were imaged under normal light (top), UV light to excite green fluorophore of WGA-Alexa 488 (middle), and UV light to excite red fluorophore of PI (bottom).

**Δ*sepF* carrying pMS82**

The resulting strain did not seem to differ macroscopically from Δ*sepF* with both strains resulting in a blue lawn and an overproduction of actinorhodin. The strain, when observed microscopically, behaved as expected with an absence of spores within the aerial hyphae, or crosswalls within the vegetative mycelium (Figure 3.16). This suggests that pMS82 did not affect the *sepF* mutant phenotype.

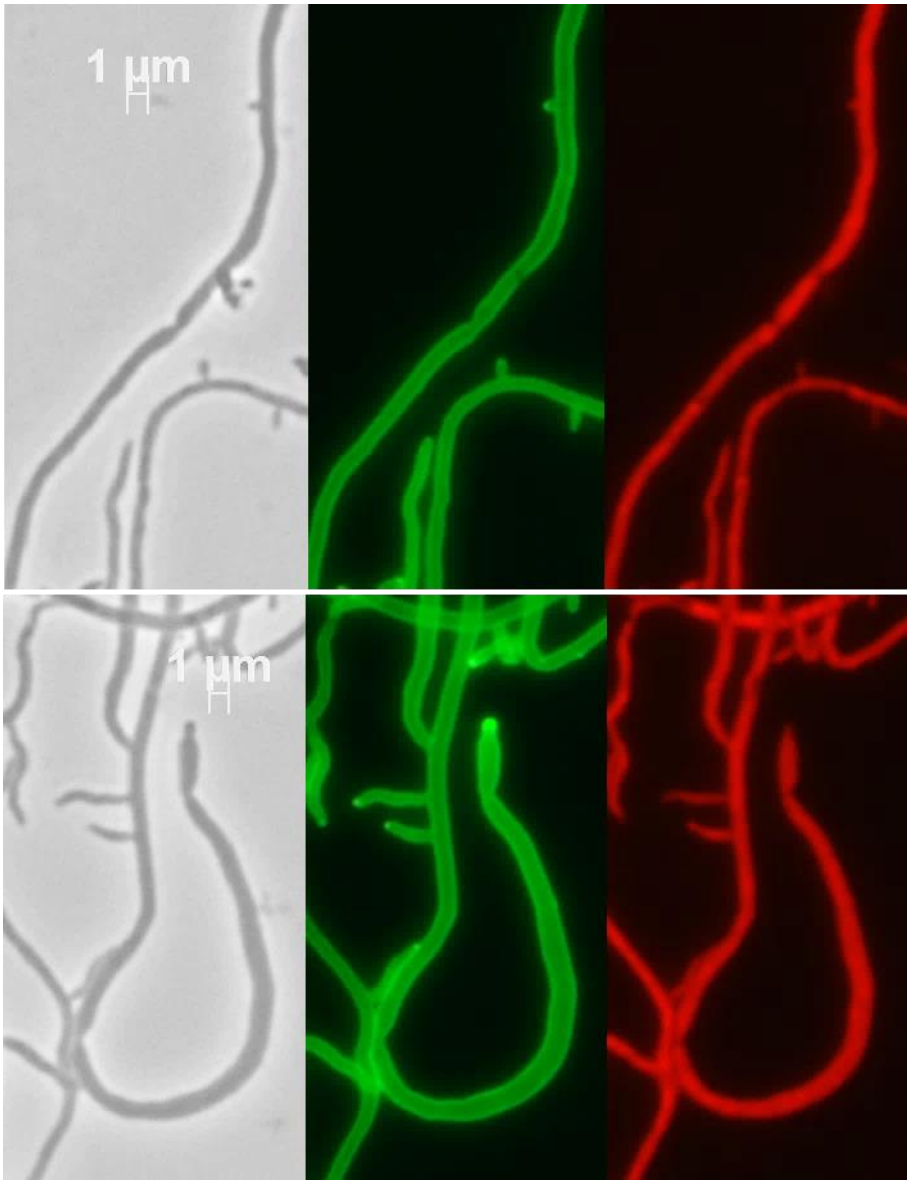


Figure 3.16: Δ*sepF*/pMS82 viewed under confocal microscopy. As expected, there is an absence of septa within the aerial (top) and vegetative (bottom) hyphae. There are examples of attempted and partial chromosome segregation. The samples were imaged under normal light (top), UV light to excite green fluorophore of WGA-Alexa 488 (middle), and UV light to excite red fluorophore of PI (bottom).

**M145 carrying pMS82-sepF**

This strain was tested to see the effect of overproduction from an extra *sepF* copy. When grown on SFM, the extra *sepF* gene does not seem to affect the morphology in any way macroscopically when compared to M145/pMS82 (Figure 3.14). This was also the case when comparing the M145/pMS82-sepF strain to M145/pMS82 on MMM and MMG when grown over four days.

Microscopic analysis shows that characteristic wild-type like septa ladders can be clearly seen during septation. The septa to septa lengths did not show any significant differences when compared with the wild-type or M145/pMS82 strains (Figure 3.20). Additionally, chromosome segregation does not seem to be affected either, with distinct 'packages' of DNA being visible in Figure 3.17.

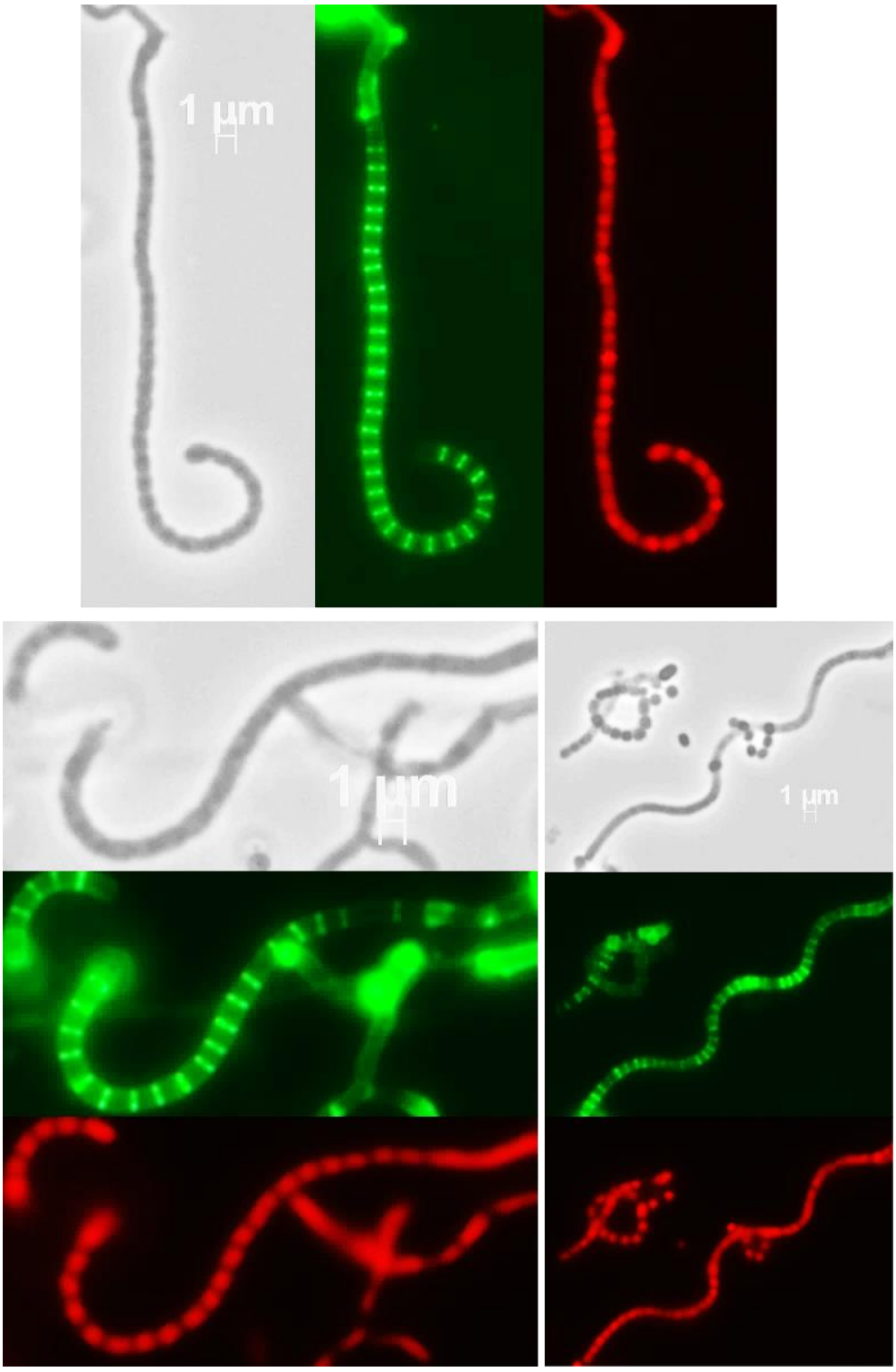


Figure 3.17: M145/pMS82-sepF viewed under confocal microscopy. The samples show evenly spaced septa and chromosome segregation can occur within the aerial hyphae. The samples were imaged under normal light (left/top), UV light to excite green fluorophore of WGA-Alexa 488 (middle), and UV light to excite red fluorophore of PI (right/bottom).

**Δ*sepF* carrying pMS82-sepF**

**The Δ*sepF* carrying pMS82-sepF strain was similar to the wild-type M145 macroscopically**

The Δ*sepF* mutant when conjugated with pMS82-sepF resulted in a clear phenotypic change, where the previously spore-less mutant returned to a spore producing state. Macroscopically, this conjugated strain looks similar to the wild-type and is able to produce the grey spore related pigment that it lacked before. However, the strain does not fully resemble the wild-type, with its grey colour being less pronounced as M145 or M145/pMS82 (Figure 3.14).

As spores were produced, spore stocks were collected and quantified. This allowed for the comparison of equal amounts of Δ*sepF* carrying pMS82-*sepF* against M145, something that was not possible to accurately do with the non-sporulating Δ*sepF* strain.

Additionally, the growth rate of Δ*sepF* carrying pMS82-*sepF* was very similar to that of the wild-type strain. This was seen when equal amounts of the spores were streaked onto SFM medium, and when used to generate confluent plates. Both strains were observed for seven days and reached developmental points at similar times.

The strain Δ*sepF* carrying pMS82-sepF does not produce excessive actinorhodin unlike Δ*sepF* strain. Its growth and development mirrors that of M145 and does not overproduce any obvious secondary metabolites, such as actinorhodin.

When grown on MMM, Δ*sepF* carrying pMS82-sepF showed little difference from the control strains. However, there are phenotypic differences between Δ*sepF* carrying pMS82-sepF and the other conjugated strains when grown on MMG. Each strain is able to grow confluently, though Δ*sepF* carrying pMS82-sepF seems to develop at an accelerated rate during early growth. By the second day of growth on MMG the strain is distinct, with a strong white colour. This colouring slowly turns pink on the edges of the confluent area. The M145 carrying pMS82 and M145 carrying pMS82-sepF strains are both grey at this stage, while Δ*sepF* carrying pMS82 is changing from to pink to white.

**The Δ*sepF* pMS82-sepF strain is different when compared to the wild-type M145 microscopically**

When the Δ*sepF*/pMS82-sepF strain was investigated microscopically there were significant differences between the spores produced when compared to the wild-type (Figures 3.18 and 3.19). Unlike the very even spore size in the wild-type strain, the spores of Δ*sepF*/pMS82-sepF were irregular, with spore sizes ranging from mini to double spore compartments. This resulted in a large range of spore sizes, with septa distances ranging from 0.28 µm to 3.71 µm (Figure 3.20). Additionally, when large number of septa to septa distances were measured, there were four small peaks for the septa to septa lengths. The peaks at 1.2 µm and at 2.0 µm could represent for the single and double spore compartments, respectively.

This irregularity with spore development may also be linked to the subtle change in the colour of Δ*sepF*/pMS82-sepF when compared to M145, M145/pMS82 and M145/pMS82-sepF.

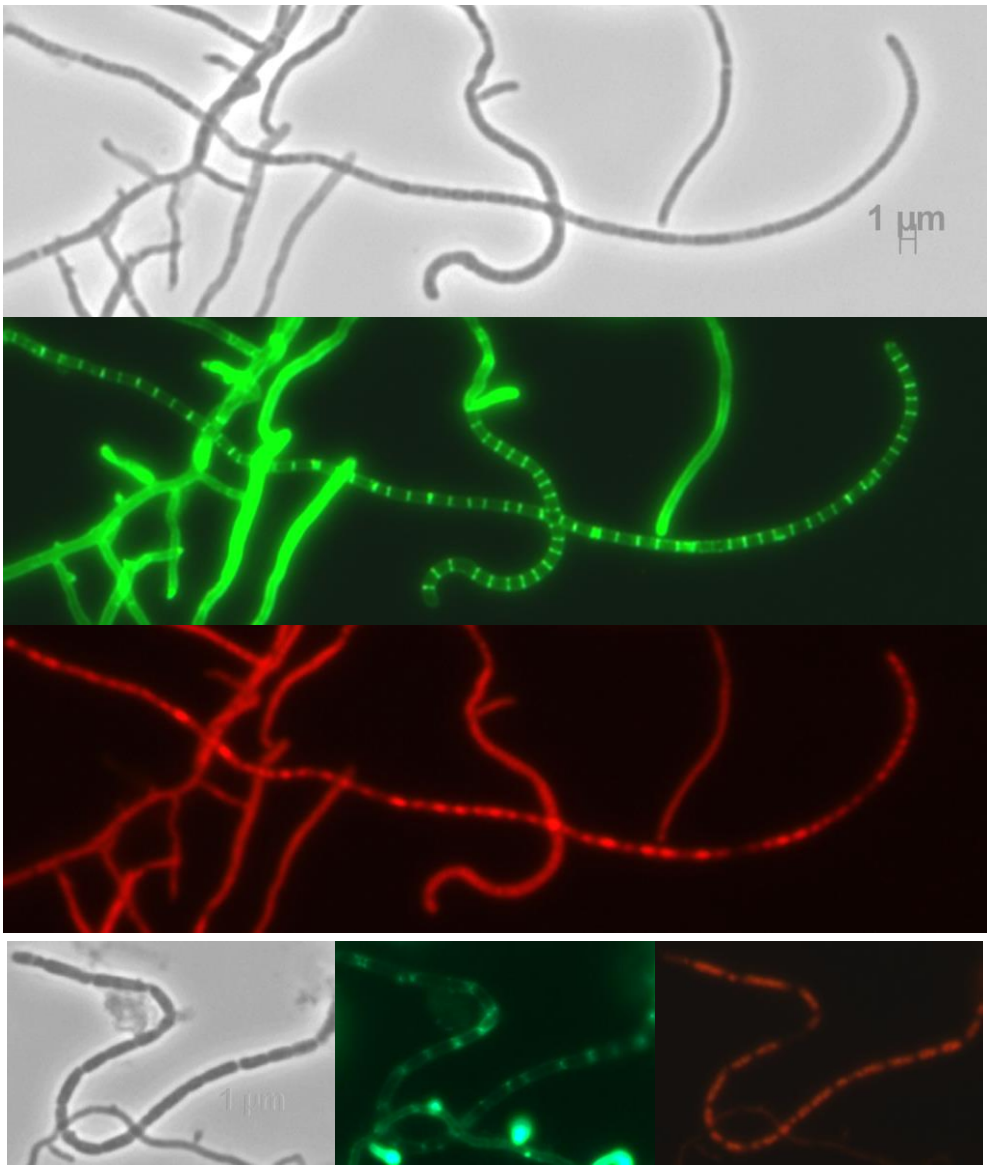


Figure 3.18: Δ*sepF*/pMS82-sepF viewed under confocal microscopy. Septa and chromosome segregation can take place, with some samples seeming similar to the wild-type M145. However, there are examples of spore compartments that are larger or smaller than the normal, especially in the bottom set of images. The samples were imaged under normal light (top), UV light to excite green fluorophore of WGA-Alexa 488 (middle), and UV light to excite red fluorophore of PI (bottom).

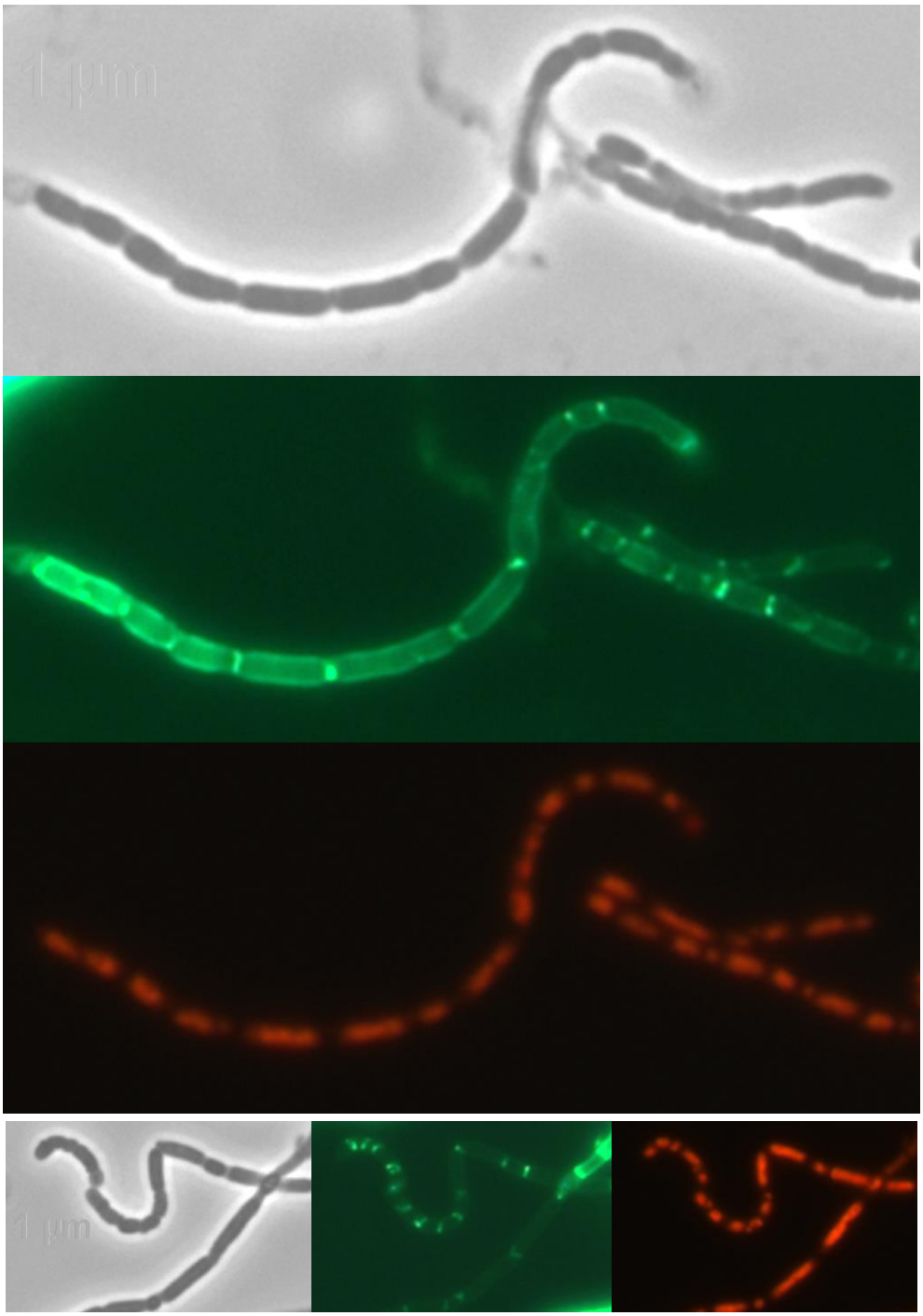


Figure 3.19: Δ*sepF*/pMS82-sepF viewed under confocal microscopy. The samples are nearing the end of the sporulation process, with the hyphae constricted in areas for cell division. The samples were imaged under normal light (top/left), UV light to excite green fluorophore of WGA-Alexa 488 (middle), and UV light to excite red fluorophore of PI (bottom/right).

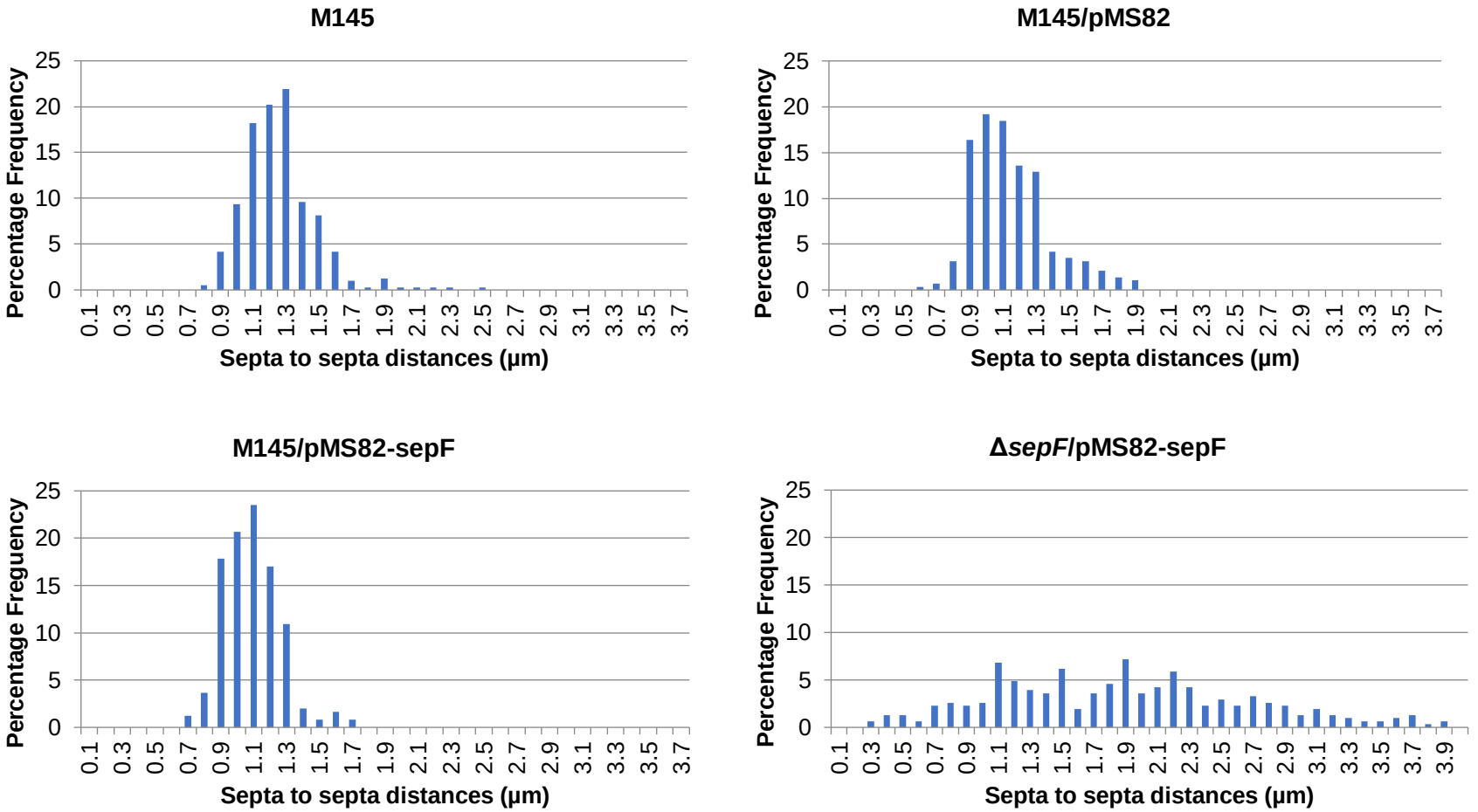


Figure 3.20: The percentage frequency of the septa to septa distances measured for the spore producing strains; M145/pMS82, M145/pMS82-sepF, Δ*sepF*/pMS82.-sepF and M145. There is no data for Δ*sepF* as it does not produce septa.

### 3.5. Summary

The *Streptomyces* SepF2 protein is highly conserved and is encoded in a gene cluster which is also highly conserved amongst different groups of bacteria such as Firmicutes and Actinobacteria. SepF is wide-spread amongst Gram-positive bacteria with a few examples amongst Gram-negatives. Analysis of the amino acid sequences of the three SepF of *S. coelicolor* established high similarity to SepF of *B. subtilis* suggesting a similar role in anchoring FtsZ polymers to the cell membrane during cell division. This would be especially important in *Streptomyces* as it does not contain homologues for other anchoring proteins such as FtsA or EzrA. The absence of other anchoring proteins might be compensated by the presence of two other SepF homologues found within *S. coelicolor*.

Additionally, the *sepF* mutant was characterised, and an attempt to the complementation of the mutant using a DNA fragment carrying *sepF* and short upstream sequence was carried out.

The *sepF* mutant is distinct from the wild-type M145 both macroscopically and microscopically. Compared to the wild-type the Δ*sepF* strain is very slow growing and has a developmental stall which stops it from being able to sporulate. This means that the strain cannot mature to a 'grey' wild-type colouring, as this is associated with spore production. Instead the resulting knockout strain is white, the colour of immature aerial hyphae, and this itself changes as the strain turns blue. The blue colouring is thought to be the result of overproduction of the naturally occurring weak antibiotic actinorhodin. This colour change due to antibiotic production again shows the difference between the Δ*sepF* strain and M145. Healthy *S. coelicolor* colonies would not overproduce actinorhodin unless grown in specific conditions. This suggest that there are other negative effects of knocking out *sepF* other than stopping sporulation.

These effects are due to the phenotype observed microscopically in the *sepF* mutant. When viewed using epi-fluorescence microscopy, it became clear that the *sepF* mutant did not contain septa in the aerial hyphae or crosswalls in the vegetative mycelium. A lack of septa in aerial hyphae is the cause for the developmental stall in the *sepF* mutant. Without SepF and therefore without septa, spores cannot be formed. The absence of crosswalls in the vegetative hyphae could be the cause for the slower growth and increased lysis of the colonies. The function of crosswalls has not been fully understood, but it is believed that they have a role in

compartmentalising the mycelium. Without these barriers harmful substances can, once within the hyphae, spread easily and affect the whole of the bacterium.

The complementation experiment also had an interesting result. Whilst macroscopic observations suggested that the addition of the *sepF* fragment had restored the mutant due to the grey sporulation specific pigment production, microscopic observations suggested that the complementation was only partial. Spores and septa were observed for the Δ*sepF*/pMS82-sepF strain, however, the spores were irregular due to the irregular spacing of the septa.

This partial complementation suggests that the DNA prior to *sepF* included in the construct contained a promoter for the gene. Otherwise we would have not seen any change when introducing this construct to the Δ*sepF* mutant. However, as the complementation was partial, as the strain was not returned to the wild-type phenotype, it is possible that *sepF* has multiple promoters further upstream of the selected fragment used in this experiment.

This idea was confirmed by the publication of Jeong et al, which predicted two promoters for *sepF*. Whilst our complementation effort using pMS82-sepF to complement the *ΔsepF* mutant phenotype generated only partial complementation, we can report that the *ΔsepF* mutant phenotype was fully complemented when the DNA fragment cloned into pMS82 contained a larger upstream region of the *sepF* gene, presumably carrying the full promoter activity that is required for *sepF* expression (Xiao Tan and Gemma Cassettari, unpublished).

## Chapter 4. Overexpression of *sepF*

### 4.1. Introduction

After the *sepF* knockout phenotype has been characterised, the next step to further assess the role *sepF* has in growth and development was to overexpress *sepF* within *S. coelicolor*. To do this a plasmid would have to be constructed which would allow for the overexpression of an *sepF* containing DNA fragment, when fully introduced into *S. coelicolor*. Overexpression would give some insight to the role of *sepF* as well as addressing if the amount of SepF is precisely controlled, which may not be the case when *sepF* is overexpressed. Overexpression of *sepF* would be assessed at different developmental time points, as growth is dynamic in *S. coelicolor*. Additionally, *sepF* would be overexpressed in wild-type and Δ*sepF* strains, primarily to see the changes *sepF* overexpression may bring and secondarily to see if Δ*sepF* could be fully complemented through *sepF* overexpression. Interestingly, in *B. subtilis*, where there are multiple proteins that anchor FtsZ to the cell membrane, namely FtsA, ZipA and SepF (Chen et al., 2017, Pichoff and Lutkenhaus, 2002, Hamoen et al., 2006), an *ftsA* knockout is lethal but this mutation can be rescued by the elevated expression of *sepF (Duman et al., 2013)*. In *Streptomyces*, there is no FtsA or ZipA homologues, instead, there are three SepF homologues.

However, overexpression in *Streptomyces* can be challenging, and previous work in the lab has shown that gene overexpression systems which may work for one gene may not necessarily work for another. The cause, or causes, for this are not fully understood, but work shown in this chapter may bring light to two possible causes: placement and availability of upstream promoter regions and ribosomal binding sites, and the timing and placement of overexpression inducers.

Overexpression systems in *E. coli* make use of the lacZ promoter, which is inducible by IPTG and are widely used in protein overexpression vectors (Marschall et al., 2017). However, this promoter cannot be used in *Streptomyces* because of the presence of five endogenous beta-galactosidase homologues encoded in the genome of *S. coelicolor*. In addition, the inducer IPTG cannot enter the *Streptomyces* hyphae (King and Chater, 1986). Recently an overexpression system relying on the T7 RNA polymerase was developed, however, this system requires a modified strain that harbours the gene encoding the T7 RNA polymerase under the control of the tipA promoter (Lussier et al., 2010).

For efficient overexpression often an inducible promoter is required, which allows monitoring of the effect of no induction vs induction. Alternatively, a strong constitutive promoter can also be used to generate elevated expression of a protein. In *Streptomyces* there are a limited number of inducible promoters that are successfully used for overexpression studies. One of these is the tipA promoter that is used in this study (see more detail below). It is a very strong promoter that can be induced with a minimum of 5 µg/ml of thiostrepton (Takano et al., 1995). Some of the identified disadvantages of using thiostrepton is that it is not soluble in water based media and only soluble in DMSO. Also, the tipA promoter is 'leaky', which means that transcription can take place even in the absence of the inducer, thiostrepton (Chiu et al., 1999).

Another inducible promoter is the cpkO promote, which is inducible by *S. coelicolor* gamma-butyrolactones (SCBs). Only nanomolar concentrations of the inducer are required for induction and the inducer is not toxic to the cells (Hsiao et al., 2009). However, as *S. coelicolor* contains the biosynthetic cluster for the production of SCBs, a host strain that does not produce these inducers must be used (Takano, 2006).

Finally, the terR promoter is induced by tetracycline and anhydrotetracycline and consists of the -10 and -35 regions of the strong ermEp1 promoter (Bibb et al., 1985) with the tetO1 and tetO2 operator sequences from the *E. coli* transposon Tn10. Promoter activity has a good response to the concentration of the inducer and anhydrotetracycline is not toxic to the cell (Rodríguez-García et al., 2005, Dangel et al., 2010).

A constitutive strong promoter, the promoter call ermE* includes a point mutation in the ermE promoter of the erythromycin resistance gene rendering it with enhanced promoter activity (Bibb et al., 1985). This ermE* promoter is also suitable for monitoring the effect of elevated expression of a protein. However, this promoter is not inducible.

This chapter will show the overexpression of *sepF* in wild-type and Δ*sepF* strains, and the evaluation of the changes due to this, in relation to levels of overexpression, timing of induction of overexpression the way in which the inducer of the overexpression is applied.

### 4.2. Construct design

The *sepF* overexpression construct shares some similarities with the complementation construct described in Chapter 4. As generation of the overexpression construct was conducted in the same time as the generation of the complementing clone, the first overexpression construct carried a very similar DNA fragment containing the whole *S. coelicolor sepF* gene and an 136 bp upstream region which is likely to contain only one promoter for *sepF*, but does not contain the full promoter region that drives *sepF* expression throughout development, this we did not know at the time of designing this construct, but it will be important when we interpret the results generated using this construct.

The *sepF* fragment was generated by PCR using primers SepF XbaBgl FRW and SCO2079 EcoRI UTC. The fragment size for the PCR product is 781 bp, which is shorter than the *sepF* fragment that was used for complementation, though the upstream promoter containing region is the same (Figure 4.1). The shorter *sepF* fragment was used as the reverse primer, SCO2079 EcoRI UTC, contains an EcoRI site which would be necessary for inserting this fragment into the overexpression vector.

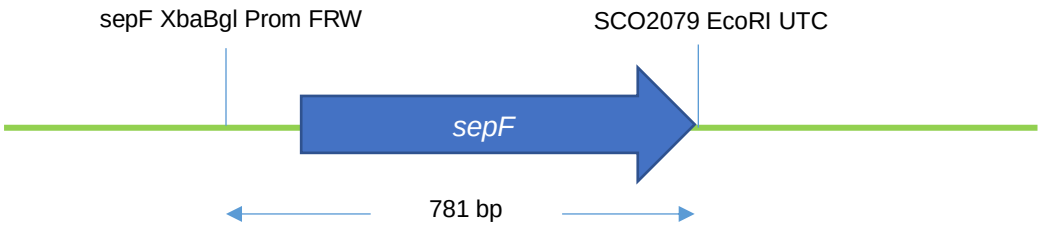


**Figure 4.1**: Schematic of the *sepF* gene with primers, sizes, and surrounding area shown. The construct was generated using a forward primer which contains an XbaI site. This would be necessary for the ligation into pIJ6902, which also contains an EcoRI and an XbaI site.

This fragment design means that *sepF* would have a low level of natural expression, as it contained a native promoter, though this would only partially complement knockout strains, as we confirmed in the previous chapter.

**Plasmid selection**

The vector used for the overexpression series of experiments is pIJ6902 (Huang et al., 2005). This 7406 bp vector is a shuttle vector that can replicate as a high copy number plasmid in *E. coli* and it can integrate into the *S. coelicolor* genome as a single copy at the *attP* site within the chromosome by the integrase encoded within pIJ6902. The location of the integration of pIJ6902 is within SCO3748, encoding a putative chromosome condensation protein (Combes et al., 2002). This plasmid contains an inducible promoter, tipA, which can be induced by thiostrepton and will be used to overexpress cloned genes downstream of this promoter. The upstream of the tipA promoter and downstream of the multiple cloning site there are transcriptional terminators that prevent any unwanted transcriptional activity. These are the bidirectional Tfd, originating from the major terminator from *E. coli* phage fd (Ward et al., 1986), and t0, the lambda phage T0 terminator (Scholtissek and Grosse, 1987). As thiostrepton is an antibiotic and wild-type *S. coelicolor* is sensitive to thiostrepton, pIJ6902 also carries the thiostrepton resistance gene, together with an apramycin resistance gene. This latter is used for selection of the plasmid in the absence of the inducer. The plasmid also carries the *oriT* site, which facilitates conjugation between *E. coli* and *Streptomyces* and will facilitate the delivery of the constructed clone into *Streptomyces*.

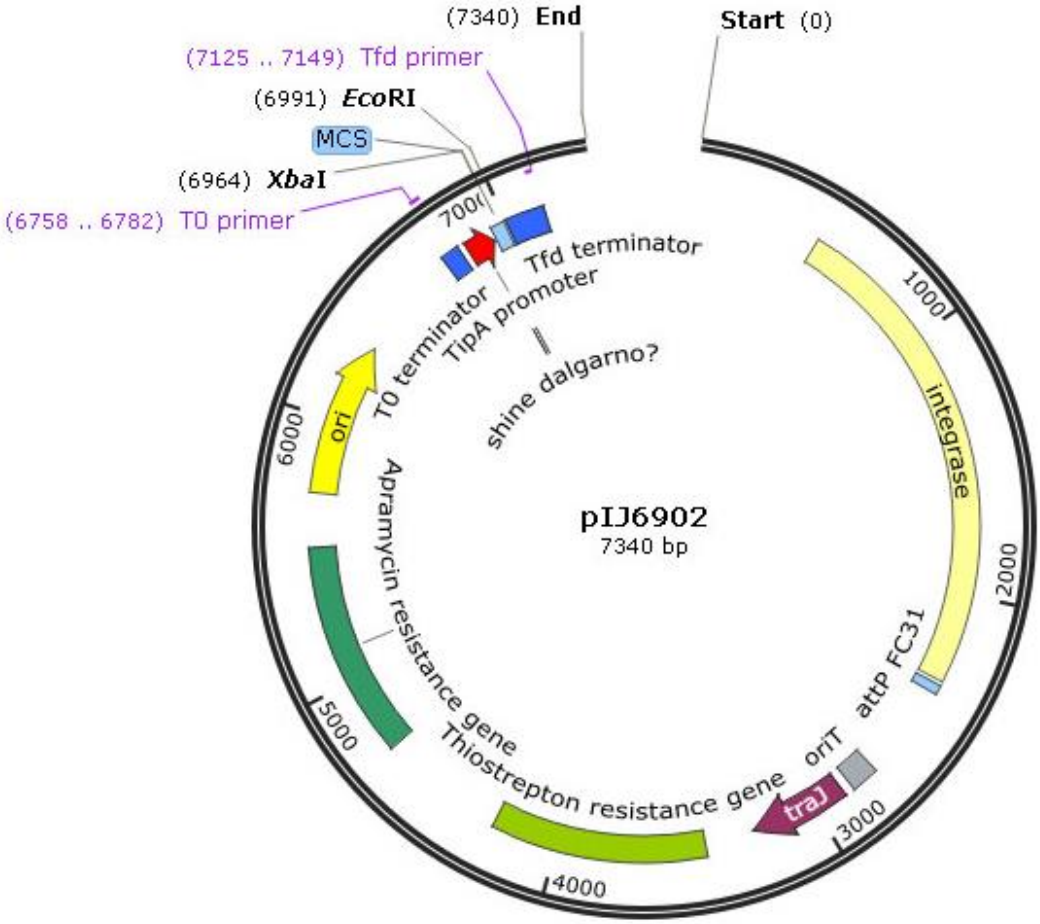


**Figure 4.2**: The plasmid map of pIJ6902. The pIJ6902 vector contains an *attP* site, which allows it to integrate into *Streptomyces* and an *oriT* site to allow conjugation between *E. coli* and *S. coelicolor*. It also contains the *tsr* gene to confer thiostrepton resistance. The enzymes EcoRI and XbaI were used to digest the plasmid.

The pIJ6902 vector was chosen to overexpress the constructs as contains the tipA promoter upstream of its multiple cloning site (Figure 4.2). The tipA promoter is inducible by thiostrepton, therefore when bacteria containing pIJ6902 are grown on thiostrepton containing media the genes driven from the tipA promoter are expressed at higher levels. The exact level of induction and thus gene expression is unknown, however for some genes it can be up to 50 times the original level. In theory, when thiostrepton is not present the tipA promoter should not be induced and therefore the downstream genes induced by tipA should not be expressed. However, in practise it seems that there is a low level of tipA activity even when thiostrepton is not present (Flärdh, 2003).

When integrated into wild-type *S. coelicolor*, the inducible promoter of pIJ6902 will only be used as a tool to test the effect of *sepF* overexpression. However, when the same construct is conjugated into the Δ*sepF* strain, the inducible promoter will also take on an additional role: it will be used to mimic the second promoter of *sepF* in an attempt to fully restore the strain to a wild-type phenotype (Figure 4.3). This full complementation will only be possible if we can control the tipA promoter in the same way as the native P2 promoter operates.

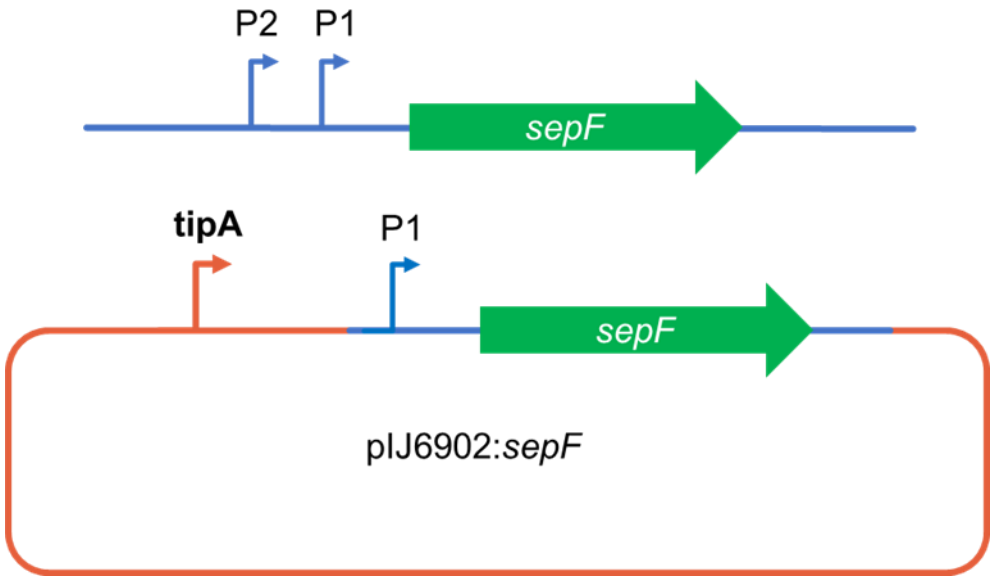


**Figure 4.3**: The *sepF* gene had been predicted to contain two promoters. The cloned fragment used in this study only contains one promoter for *sepF*, hence this fragment alone can only give partially complementation. If the tipA promoter is used in conjunction with the native promoter of *sepF* it could be possible to use this construct to full complement the Δ*sepF* phenotype.

### Fragment Generation

The *sepF* fragment was generated using the primer pair from Figure 4.1, in a Phusion PCR with St4A10, a *S. coelicolor* cosmid, acting as template. The *sepF* PCR fragment was phenol extracted and run on an ethidium bromide gel, to be subsequently purified via gel extraction.

### Ligation of pIJ6902 and the fragment

The pIJ6902 plasmid and the *sepF* fragment were digested with EcoRI and XbaI. After the digestion the *sepF* fragment and pIJ6902 were run on gels to confirm their sizes and gel extracted to concentrate the DNA. Ligations between the fragment and pIJ6902 then took place, with the ligations were desalted through

columns twice before being electroporated into *E. coli* DH5α cells. The cells were then plated onto LB media with an apramycin selective pressure.

### Confirmation of the Recombinant Clones

Colonies that were grown on media containing apramycin, thus confirming that they contained pIJ6902, were screened for clones with the fragment inserts using colony PCRs. The primers, t0 and SCO2079 EcoRI UTC were used, where the t0 primer anneals within the pIJ6902 plasmid and the SCO2079 EcoRI UTC primer anneals within the cloned PCR fragment.

Screened via colony PCRs, positive clones for the construct were found (Figure 4.4).

| | **Primer Pair** | **Expected size of fragment** |
|---|---|---|
| *sepF* | t0<br>SCO2079 EcoRI UTC | 981 bp |

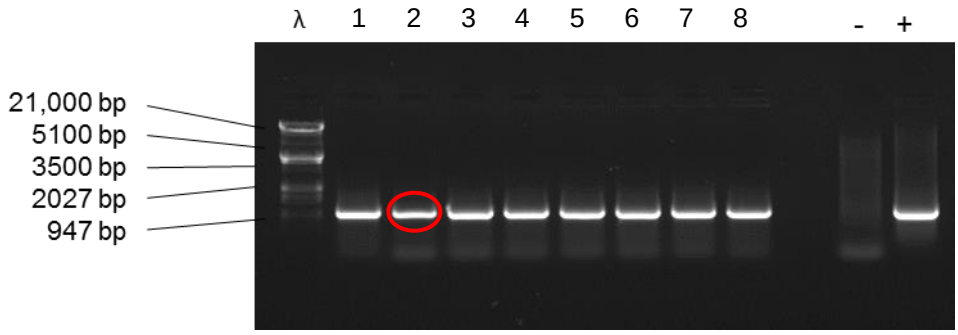


**Figure 4.4: Gel electrophoresis of colony PCRs for *sepF*.** The expected size was 981bp for the *sepF* fragment. Lambda DNA digested with EcoRI and HindIII was used as a size marker, with colonies tested in lanes 1-8. Positive colony carried forward is lane 2 and circled in red. The positive control for *sepF* was confirmed by a previously generated pIJ6902 *sepF-2078* clone and the negative control was an empty pIJ6902 vector.

### Sequencing and confirmation of the fragment within pIJ6902

Colony number 2 (Figure 4.4) was chosen to carry further and a large plasmid preparation was generated, which was then sequenced to confirm no mutation had been introduced into the inserts during PCR.

The *sepF* clone was sequenced with the oligonucleotides tfd and t0, which anneal to the pIJ6902 vector. These primers anneal a small distance from either side of the insert (Figure 4.5). The sequencing confirmed that the clones were correct.

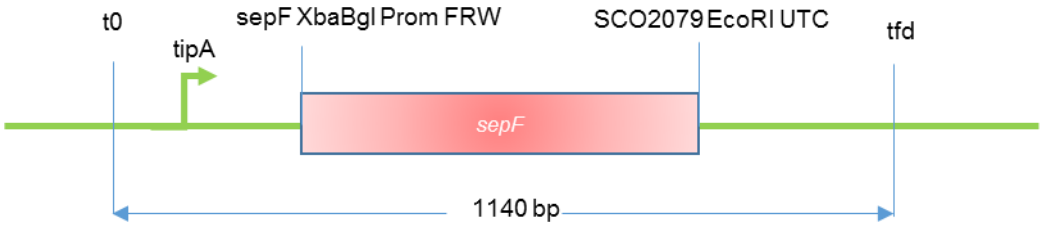


**Figure 4.5: The *sepF* fragment (pink) in pIJ6902 (green).** The t0 and tfd primers used to confirm the presence of the fragment are marked, as well as the primers which were used to construct the *sepF* containing fragment.

### Conjugating the overexpression clone into *S. coelicolor* strains

The confirmed plasmid, pIJ6902-P1sepF was introduced into the wild-type and Δ*sepF* strains using conjugation. The plasmid was named pIJ6902-P1sepF as it became known that the cloned region used in this study contained the *sepF* gene plus the upstream region containing one of its two predicted promoters due to the publication of Jeong et al. The wild-type exconjugants were selected using apramycin. However, as the Δ*sepF* strain is resistant to apramycin because of the way this mutant was generated by the replacement of the wild-type allele with the apramycin resistance cassette, exconjugants could not be selected with using apramycin. In this case I used thiostrepton to select colonies that carried the overexpression construct. This is not optimal, as the presence of thiostrepton will potentially induce the expression of *sepF*. Selected exconjugants were used to generate spore stocks for both the wild-type and the Δ*sepF* derivatives.

### 4.3. The placement and availability of thiostrepton affects its ability to act as an inducer of tipA within *Streptomyces*

#### 4.3.1. Thiostrepton within growth media does not induce *sepF* expression in the aerial hyphae

The initial experiment was to observe any macroscopic differences between the strains, which were M145/pIJ6902-P1sepF and Δ*sepF*/pIJ6902-P1sepF, and empty vector versions of these strains to act as controls. The Δ*sepF*/pIJ6902-P1sepF strain was used to see if overexpression of the construct could restore the strain to wild-type phenotype. This is as the P1sepF fragment is not enough to completely restore the Δ*sepF* strain to a wild-type phenotype, as shown before in previous experiments, likely due to a missing promoter for *sepF* in the cloned fragment. The M145/pIJ6902-P1sepF strain should give the true effects of the overproduction of the *sepF* fragment, and could also be used to compare against the Δ*sepF*/pIJ6902-P1sepF strain if it was not returned to a wild-type phenotype.

To do this the aim was to inoculate even numbers of cells of each of the strains. This can be easily done when the strain sporulates as we can inoculate with identical numbers of spores. However, strains that do not sporulate such as the Δ*sepF*/pIJ6902 and Δ*sepF*/pIJ6902-P1sepF strains, it is impossible to be quantitative. Strains were plated on different growth media including SFM medium, minimal medium with mannitol (MMM) and minimal medium with glucose (MMG) plates. Three different growth mediums were chosen, as this would give a range of growth conditions. The SFM plates are routinely used in the laboratory because strains exhibit fast growth rates and a full developmental cycle when grown in this medium. Therefore, any large phenotypic differences such as colour and texture of the colonies should be visible, as well as differences in growth rates. The MMM and MMG plates present a different, less rich, environment for the strains, as these medias are low in nutrients. It is expected that on MMM and MMG plates the growth of the strains will differ greatly compared to their growth on SFM.

Each strain was tested in two different media, one set containing the apramycin and the other with the addition of both apramycin and thiostrepton. The thiostrepton was present to enable us to see the effects of overproduction, as its presence should induce the promoter resulting in an increased transcription of the *sepF* fragment. Apramycin was also included in the medium together with

thiostrepton, to allow a clear comparison and evaluation of the effects of *sepF* overexpression as opposed to the additional effects of having apramycin present.

The non-thiostrepton plates were used as a control where no induction takes place unless the tipA promoter leaky. Additionally, the promoter within the *sepF* fragment used would also be active, providing some expression of the *sepF* gene. However, if *sepF* overexpression is achieved the expected result was phenotypic differences in the presence and absence of the thiostrepton in the growth medium.

The plates were grown at 30°C and observed every 24 hours for 8 days after their inoculation, as in these conditions the wild-type strain would normally mature in 5 days. The plates were observed for longer than the normal growth period so to allow for any slower growing strains. Additionally, the presence of thiostrepton in growth medium can slow growth, which was taken into consideration during the observation. If too large an amount of thiostrepton was used the strains may not grow as the minimum inhibitory concentration would be reached, and too little may not induce the promoter enough, therefore a 10 mg/ml concentration was used.

As can be seen from Figure 4.5, Δ*sepF*/pIJ6902 differs from M145/pIJ6902, as it exhibits a 'white' phenotype as opposed to the normal wild-type 'grey'. The Δ*sepF*/pIJ6902 does not look white after day 4, as it is then producing a blue secretion; the antibiotic actinorhodin. As predicted it does not achieve the brown colouring of the wild-type M145 strains. This is seen in both the SFM containing apramycin and SFM containing apramycin and thiostrepton plates, with the growth of Δ*sepF* pIJ6902 and M145 pIJ6902 mirroring their counterparts, as expected of the controls.

The Δ*sepF*/pIJ6902-P1sepF and M145/pIJ6902-P1sepF differ also, with the Δ*sepF*/pIJ6902-P1sepF not achieving the brown-grey colour of the M145/pIJ6902 and M145/pIJ6902-P1sepF strains. This is the case in both the un-induced and induced plates.

However, the addition of the P1sepF fragment to the M145 strain seems to have an effect in the induced and overproducing plate, SFM containing apramycin and thiostrepton. The early stages of growth seem to be slightly accelerated, as the amount of vegetative material is increased. This is suggested by the clear triangle seen clearly by day 2, when compared to the non-induced plate. The day 3 and 4 samples are also darker then that seen on the SFM containing apramycin plate, suggesting that the strain has moved into the aerial hyphae stage earlier.

While the SFM plates did not show many differences between the induced and non-induced strains, the MMM plates show differences between the strains when plated on the mediums. This was not expected as the controls were also affected by the addition of thiostrepton. All the strains grew better on the MMM containing apramycin and thiostrepton plates, while the non-induced plate resulted in non-confluent growth (Figure 4.6). These differences among all the strains suggests that thiostrepton may positively affect growth in certain stress conditions.

The MMG set of plates (Figure 4.7) show a different picture. The Δ*sepF*/pIJ6902-P1sepF and M145/pIJ6902-P1sepF strains show differences on the inducer containing plates and the non-inducing plates. The controls are similar, though maybe not identical, on each plate, suggesting that any differences on the strains is due to the *sepF* fragment. On the MMG containing apramycin media the Δ*sepF*/pIJ6902-P1sepF and M145/pIJ6902-P1sepF strains are confluent and can clearly be seen by day 3, and by day 8, though Δ*sepF*/pIJ6902-P1sepF is more pronounced, both are distinct. However, on the MMG containing apramycin and thiostrepton plate both strains are at a disadvantage and struggle to grow. The Δ*sepF*/pIJ6902-P1sepF strain is no longer confluent, even at day 8, with individual colonies easily visible. The M145/pIJ6902-P1sepF strain is greater affected, with only a few colonies able to grow, each covering a small area.

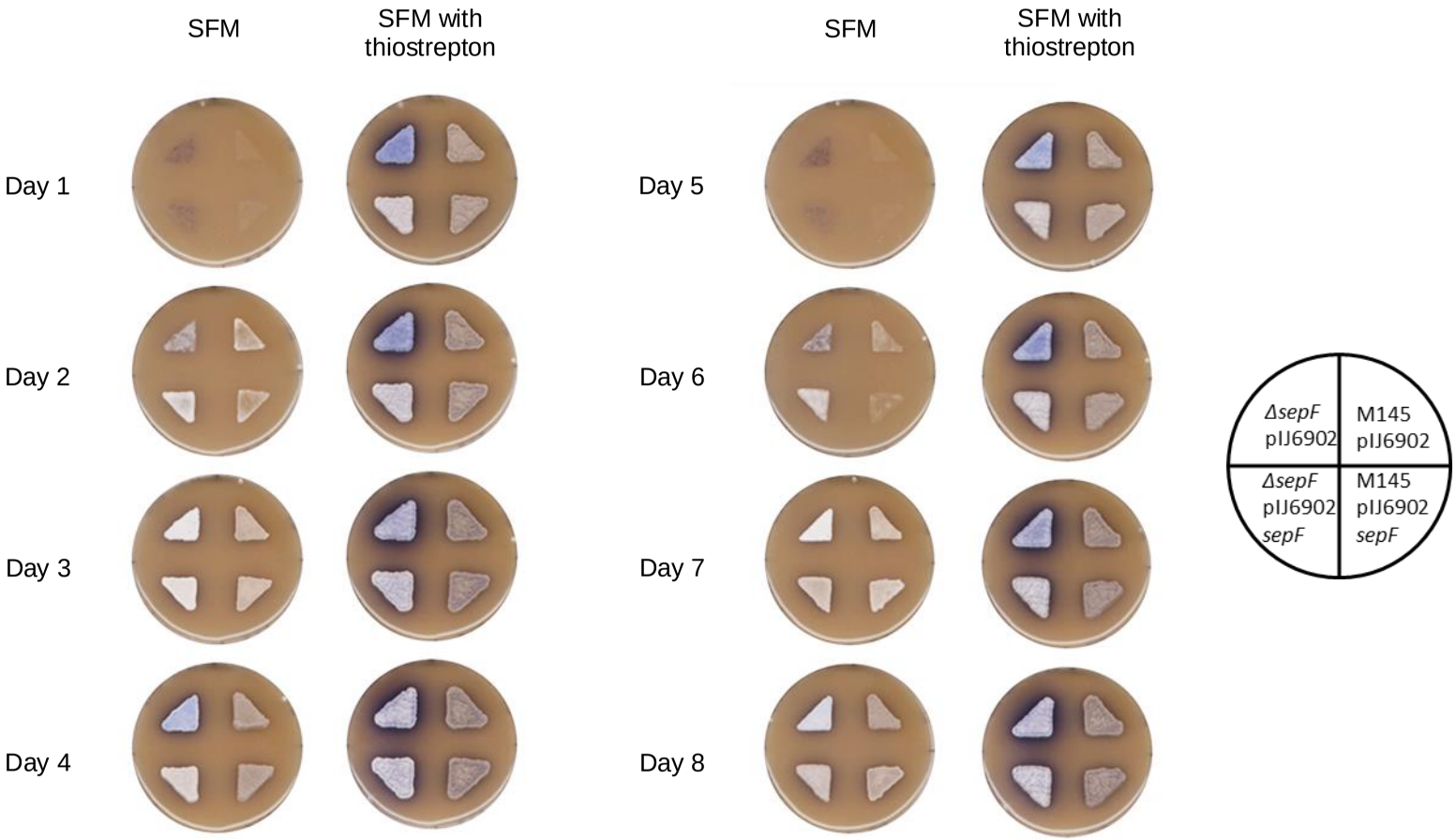


Figure 4.6: Scanned images of the strains, Δ*sepF*/pIJ6902, Δ*sepF*/pIJ6902-P1*sepF*, M145/pIJ6902 and M145/pIJ6902-P1*sepF*, plated onto SFM containing apramycin and SFM containing apramycin and thiostrepton plates, over the course of 8 days

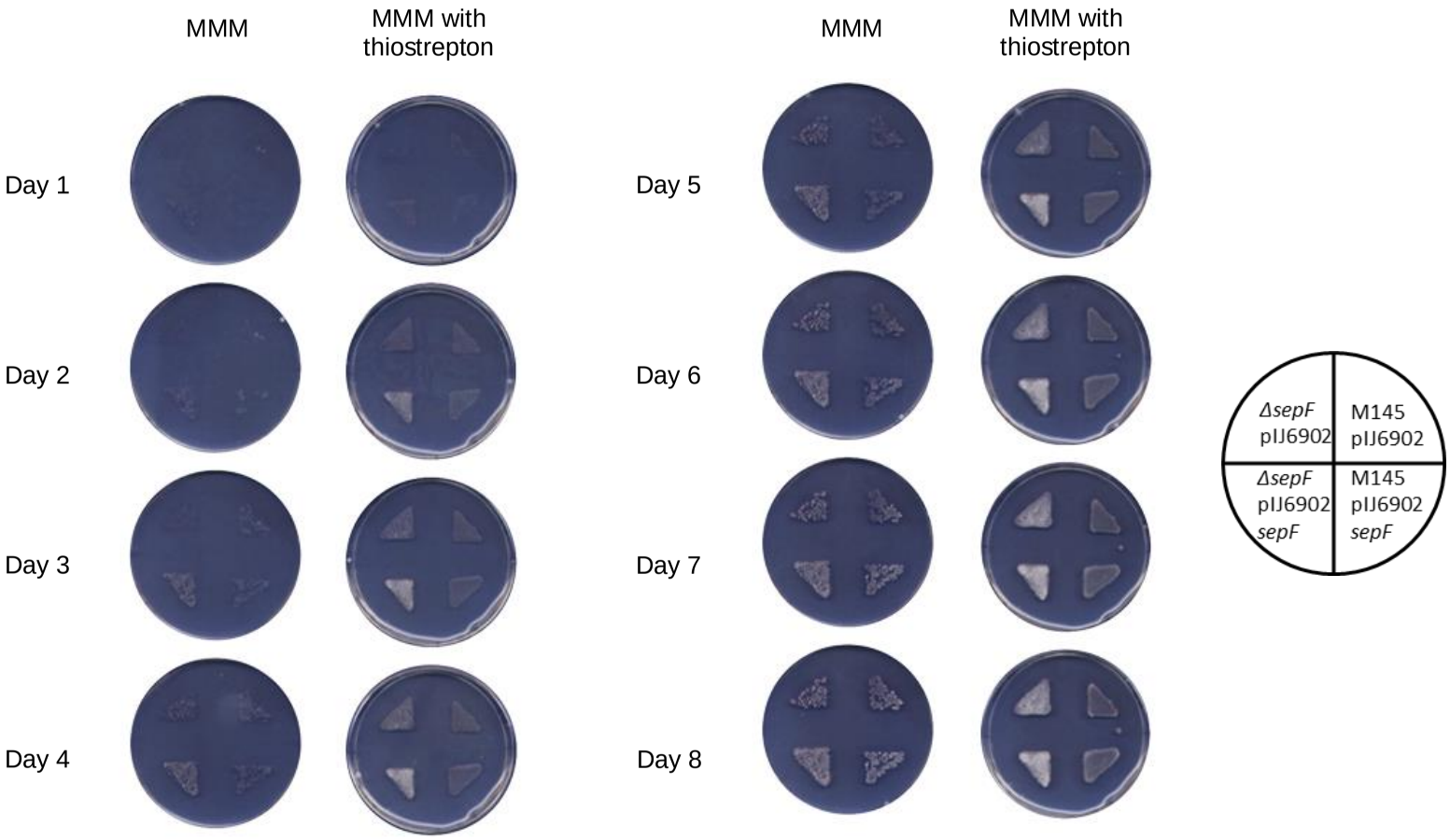


Figure 4.7: Scanned images of the strains, Δ*sepF*/pIJ6902, Δ*sepF*/pIJ6902-P1sepF, M145/pIJ6902 and M145/pIJ6902-P1sepF, plated onto MMM containing apramycin and MMM containing apramycin and thiostrepton plates, over the course of 8 days.

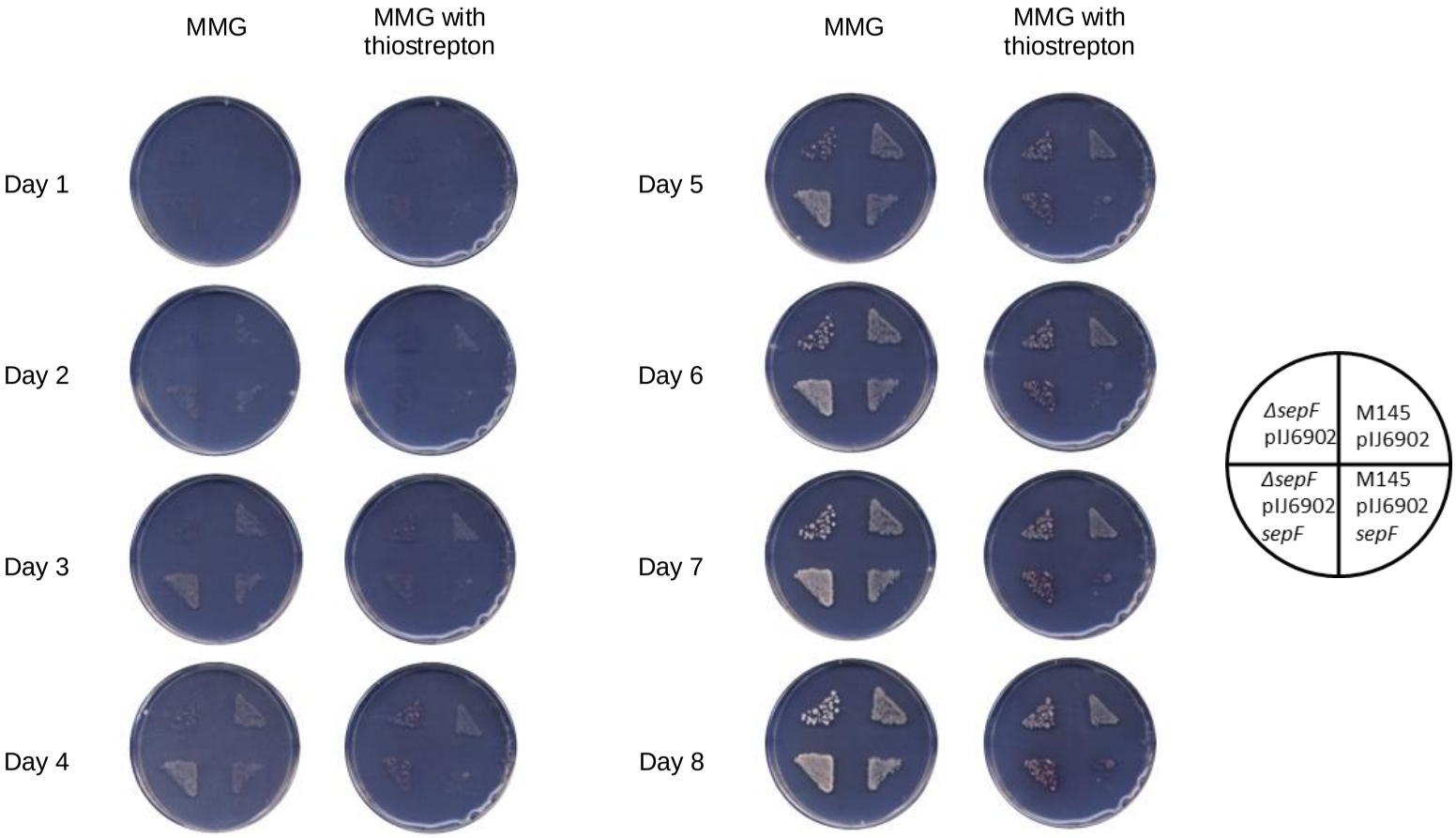


Figure 4.8: Scanned images of the strains, Δ*sepF*/pIJ6902, Δ*sepF*/pIJ6902-P1sepF, M145/pIJ6902 and M145/pIJ6902-P1sepF, plated onto MMG containing apramycin and MMG containing apramycin and thiostrepton plates, over the course of 8 days.

While having the *sepF* fragment at low levels of induction or as an extra copy of *sepF* it seems not to affect growth on the MMG containing apramycin media, overproduction of the *sepF* fragment on thiostrepton containing media does seem to be slightly detrimental.

All the differences observed seem to be minimal, with no distinguishable macroscopic change seen at all in the strains grown on the optimal growth media of SFM. These could suggest two things, either that *sepF* overexpression does not affect growth and development, or that *sepF* overexpression did not take place. The former seems less likely as knocking out *sepF* gave a pronounced phenotype, which had suggested that maintaining levels of *sepF* was important. The latter could be due to a number of reasons.

Firstly, consider the issue concerning the access of thiostrepton to all parts of the developing *Streptomyces* colony. SepF is utilised within the aerial hyphae, as it affects septum formation and thus sporulation. Therefore, the effects of *sepF* overexpression should be most distinguishable in the aerial hyphae. However, the only area of *Streptomyces* which was being exposed to the inducer, which is required for overexpression in this system, were the areas in contact with the media: the vegetative hyphae (Figure 4.9). The vegetative hyphae could be affected by *sepF* overexpression, but the inducer and its influence would have to be able to pass to the aerial hyphae and we have very limited information about the transfer of molecules between different compartments within the *Streptomyces* hyphae that are separated by crosswalls. Firstly, *Streptomyces* grows in a polarised fashion, and the aerial hyphae are as their name suggests above the vegetative hyphae, meaning that the inducer would need to be transported. The inducer is not native to *S. coelicolor*, so there may have not been mechanisms available for its transport. Secondly, *Streptomyces*, though it does not undergo chromosome segregation till sporulation, it does have some irregularly spaced semi-permeable cross-walls. These cross-walls are present in the vegetative hyphae, and thought their function is not greatly explored, they are thought to have roles in structural integrity and acting as a barrier between spaces, thus compartmentalising *Streptomyces*. It is possible that the inducer may have been compartmentalised into sections of the vegetative hyphae, and thus retained in only these areas. Additionally, as seen in the previous chapter, knocking out *sepF* causes these vegetative septum, or cross-walls, to not appear, so it is possible that overexpressing *sepF* in the media caused more cross-walls to form, which would have resulted in more comparts within

*Streptomyces*, thus making it even harder for the inducer to travel (if it can) to the aerial hyphae.

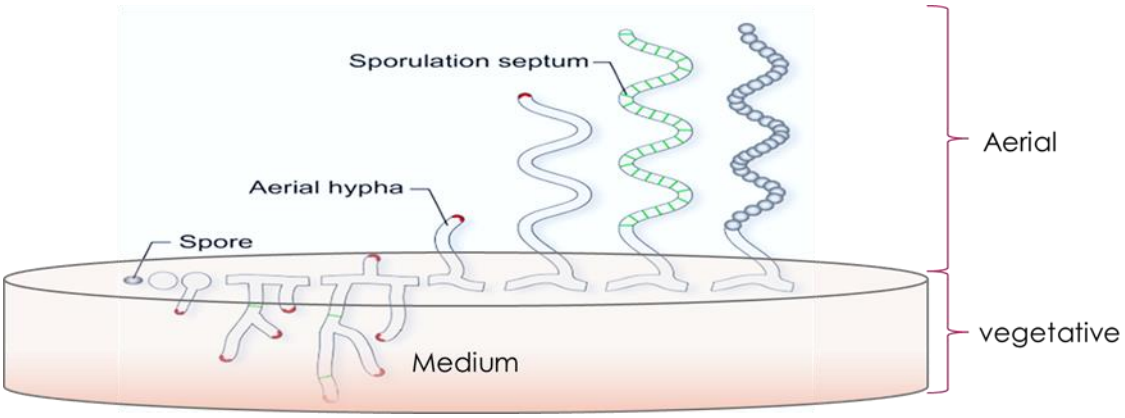


Figure 4.9.: Thiostrepton was added directly to the aerial hyphae, as opposed to the vegetative hyphae through thiostrepton exposure through the media. (Image adapted from Schlimpert et al., 2016)

This all means that the inducer may have never reached the aerial hyphae, and this could be the reason that the overexpression of *sepF* did not seem to have any affect in the initial overexpression experiment. Therefore, to compensate for thus effect, thiostrepton (the inducer) would then be added directly to the 'compartments' of *Streptomyces* which would be affected by it, to the aerial surface.

### 4.3.2. Thiostrepton when applied directly can induce *sepF* expression in the aerial hyphae

The second set of *sepF* overexpression experiments involved using the same constructs and strains but directly adding the tipA inducer thiostrepton to plated *Streptomyces* in a drop over the aerial surface of the colonies.

Initially four strains were chosen; M145/pIJ6902, M145/pIJ6902-P1sepF, Δ*sepF*/pIJ6902 and Δ*sepF*/pIJ6902-P1sepF. The M145/pIJ6902 and Δ*sepF*/pIJ6902 strains were controls for the M145/pIJ6902-P1sepF and Δ*sepF*/pIJ6902-P1sepF (respectively). After initial experiments only Δ*sepF*/pIJ6902 and Δ*sepF*/pIJ6902-P1sepF were further investigated, as these two strains that showed obvious macroscopic differences. As these strains were visibly affected, further refinement of the experiments allowed for differences in the concentration of

the inducer and the time at which the inducer was added to the strains. These conditions where then used to test and observe the strains macroscopically and microscopically. What is described next is the effect of adding equal amounts of inducer to strain at different time points after inoculating the strain.

#### 4.3.2.1. The developmental time points at which *sepF* expression is induced affects development

Approximately equal cell material of each strain was plated onto SFM plates, so cover the whole plate minus the outermost borders. Approximations had to be made for Δ*sepF*/pIJ6902, as this control strain is not sporulating, therefore stock concentrations cannot be accurately measured. However, the inoculation resulted in confluent growth, which was then subjected to thiostrepton. Each plate was divided into four equal sections, in which a different condition was tested. To three of these sections thiostrepton was added to the centre in a circular area and kept from the edges of their respective sections so not to interfere with the other adjacent sections of growth. The amount of thiostrepton added to each of these three sections was equal at 87.5 µg thiostrepton. The three thiostrepton sections differ as the thiostrepton was introduced at different time points, 28 hours, 51 hours and 69 hours after inoculation and growth at 30°C, corresponding to different stages of growth. At 28 hours cell are in late vegetative growth stage, at 51 hours cells have completed the is after vegetative growth and they are in the early aerial stage. The 69 hour time point represents a later mature stage, aerial growth, when the hyphae become highly hydrophobic. The fourth section was not exposed to thiostrepton directly, and acts as a control.

The plates were images at each time point to observe any macroscopic differences. Additionally, after 82 hours each section was also observed microscopically, to observe any additional or non-apparent changes in the aerial hyphae.

To observe microscopically, coverslips were pressed onto the surface of the plates at the areas at which the thiostrepton had been added and to the centre of the control section, in order to collect hyphae. The coverslips were then heat fixed, and further fixed with methanol, and then stained. Each coverslip was stained with wheat germ agglutinin conjugated to the fluorescent Alexa-488 (WGA) and propidium iodide (PI), which fluoresce green and red (respectively) after excitation. WGA attaches to areas of cell wall growth, and PI intercalates in DNA, allowing

differences in cell shapes and septation (WGA) together with chromosomes (PI) to be easily observed. Only the samples from the aerial surface of the colonies were collected, however, as *sepF* is a septation protein which has a key role in the septation of the aerial hyphae, this is appropriate.

Firstly, the control strain Δ*sepF*/pIJ6902 generated a lawn that failed to develop a grey surface, but instead developed a blue aerial surface (Figure 4.10). this is expected, as the Δ*sepF* strain fails to sporulate, but produces elevated levels of the blue antibiotic, actinorhodin. At the positions where thiostrepton was applied, the growth is very similar to the areas where no thiostrepton was added. Perhaps, the only exception to this is the patch where thiostrepton was added at 28 hrs, where there is less blue colouration. But other all, the presence of pIJ6902 plasmid n the control strain did not affect growth or development not even when the thiostrepton was applied. On the other hand, administering thiostrepton did have an effect on the development of the Δ*sepF*/pIJ6902-P1sepF strain. This effect was dependent on the time and developmental stage when the thiostrepton was applied.

**Figure 4.10:** The effects of thiostrepton on Δ*sepF*/pIJ6902-P1sepF (top) and Δ*sepF*/pIJ6902 (bottom) at different time points after 5 days growth at 30°C. The SFM plates carrying apramycin were inoculated at the same time, and both received 87.5 µg thiostrepton at 28 hrs (top left), 51 hrs (top right) and 69 hrs (bottom right) time points. The remaining (bottom left) segment is the control area.

When thiostrepton was added at early stages, at 28 hrs, there is a strong inhibition of growth (Figure 4.10), however, at later time points of 51 hrs and 69 hrs the hyphae exhibit a grey colour, which is normally the sign of sporulation because of the production of the spore-specific grey polyketide pigment. The patch where thiostrepton was applied shows a grey colour compared to neighbouring areas that stay less grey.

The fact that the induction of the overexpression of *sepF* at 51 hrs results in a near wild-type phenotype, at least macroscopically, suggests that overexpression of the *sepF* fragment can rescue the Δ*sepF* phenotype when induced at this stage of development. The 69hrs segment also shows a darker phenotype, suggesting that even later in growth overexpression of *sepF* can allow the complementation of the Δ*sepF* strain to develop spores.

To determine if the grey colour was indeed indicative of spore formation and whether the Δ*sepF* phenotype was potentially restored to a wild-type phenotype, the spores and aerial hyphae were investigated using fluorescent microscopy, with samples from all four patches viewed.

The samples were taken directly from the plates tested above, using the clearly affected hyphae, using 'coverslip drop' technique. The coverslips were first pressed firmly into the hyphae where the thiostrepton had been added, but without being moved from their original positions. For the control segment, the coverslip was added to the middle of the segment. The coverslips were then removed and heat fixed, followed by an additional methanol fix.

To view any developing septa and cell wall growth, to see the effects on septa and spore size and development, the coverslips were stained using WGA-Alexa 488 and PI as before. The samples were collected 24 hr after the last addition of thiostrepton and then viewed under the microscope.

The control samples behaved as expected, having septa present, and these are irregularly spaced with a mix of larger and small septa to septa distances. These samples also had less material collected on the coverslips, than the induced coverslips (Figure 4.11).

The samples viewed for the 28 hr induction time point showed a different septa arrangement. These septa seem to be more widely spaced than the control samples, and are distinct. The DNA within the hyphae can also be clearly viewed,

and have not formed separate single chromosome packets, but instead fills each septum to septum compartment.

The samples for the 51 hr induction time point show uneven septation but the septa to septa distances are shorter than the 28 hrs sample, and some of the distances closer to wild-type distances of ~1.2 µm. This is also the case for the 69 hr induction time point, however, these hyphae also show examples of two septa very close together. Additionally, some of the hyphae observed seem to have septa which where oddly angled – giving an askew appearance.

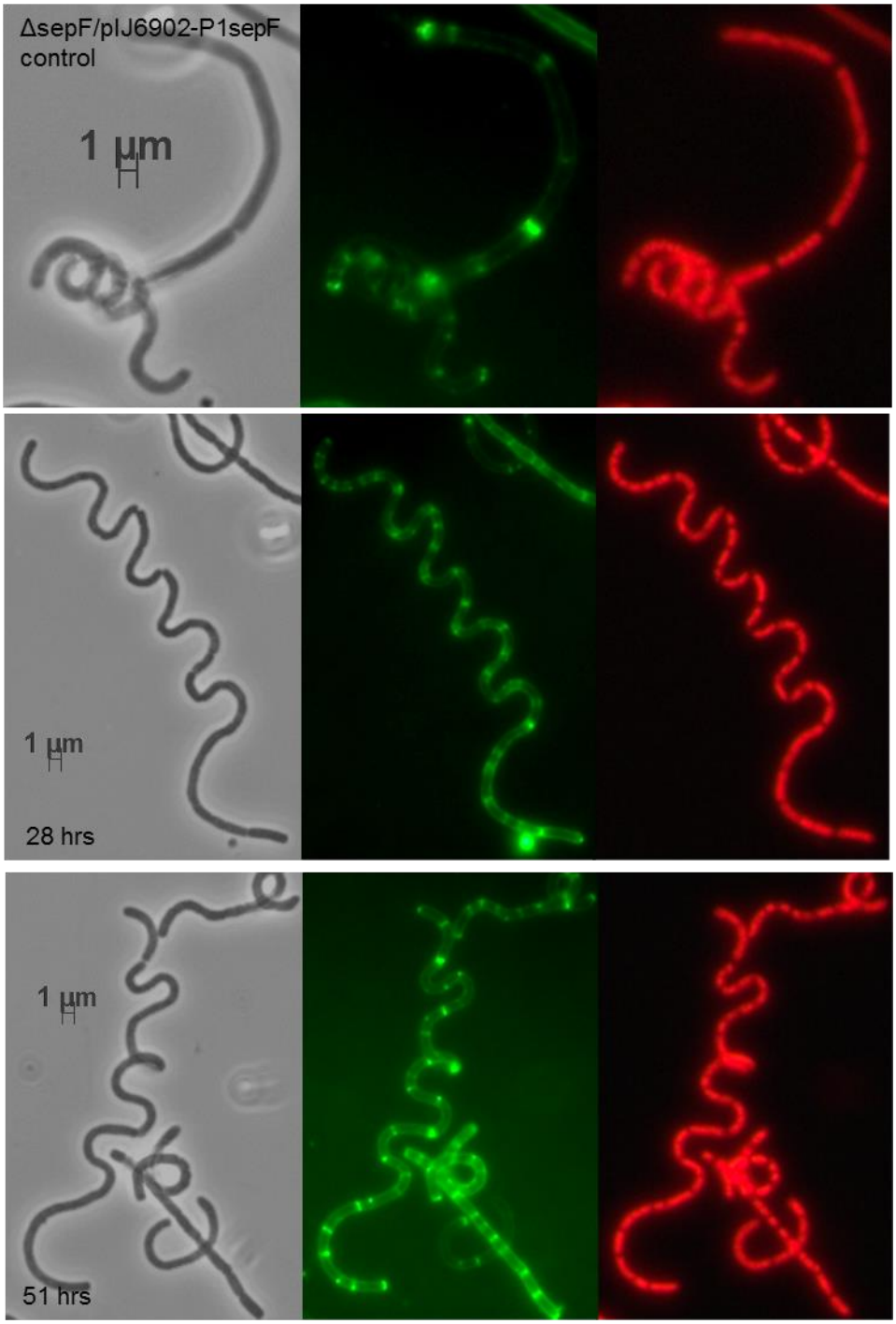
ΔsepF/pIJ6902-P1sepF
control
1 µm
1 µm
28 hrs
1 µm
51 hrs

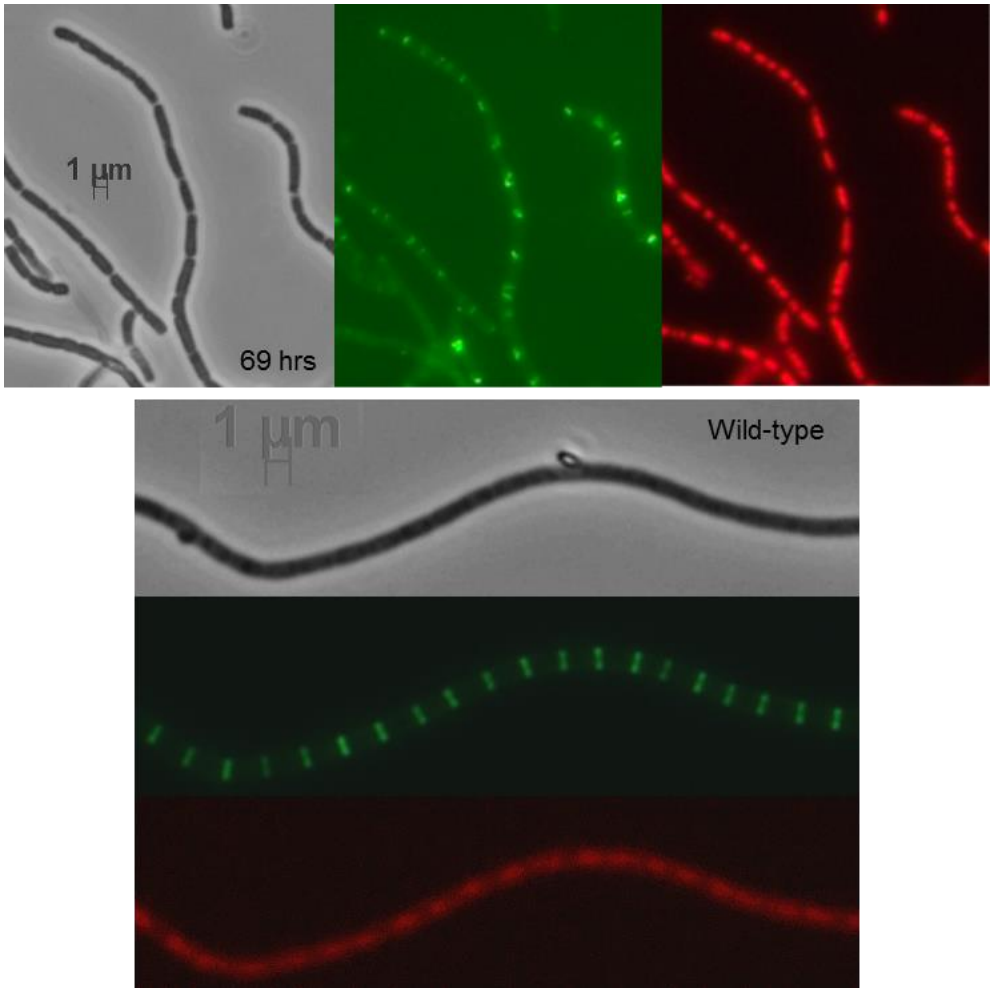


Figure 4.11: Microscopy images of the samples collected 83 hours after inoculation of Δ*sepF*/pIJ6902-sepF viewed using epi-fluorescence microscopy. The images are phase contrast (left), WGA stained (middle) and PI stained (right). The top panel shows images of the control segment, which was not exposed to thiostrepton. The panels are the images of samples taken from areas which had 1.75 ul of thiostrepton added to them at 28, 51 and 69 hrs after inoculation. A wild-type M145 control is also shown in the bottom panel.

**Discussion for adding thiostrepton at different developmental time points**

There are significant differences between the induced and uninduced samples, and even between the different time points of induction, though none of these exhibited the even septation event seen in the wild-type strain.

The common distinction between the induced samples is that the septa seem to be slightly wider spaced, with the chromosomes filling these larger compartments fully. There are exceptions, especially within the 69 hr samples, which do show a number of septa that are closer together than normally seen.

Although it seems that the overproduction of SepF induced sporulation septation, it did not mimic the wild-type scenario as the phenotype after overexpression was not restored to wild-type.

This is interesting and might suggest that excess of SepF must be interfering with septa development. As SepF is an anchoring protein for FtsZ, which is the scaffold for septa development when formed into Z-rings, it would be easy to assume that extra SepF would mean extra FtsZ would be anchored resulting in more septa. However, when SepF is overproduced, the FtsZ levels are not expected to change.

It is possible that SepF, which can, as well interact with FtsZ, self-dimerise to form rings, which are thought to be used to anchor FtsZ, when in high amounts forms extra rings or larger rings. These larger SepF rings would have more areas at which FtsZ could interact and bind. This would lead to more FtsZ in one place, which would mean that septa would be limited, as less free FtsZ would be present for Z-ring, and thus septa, development.

Additionally, having extra FtsZ in one place could mean that the Z-ring is assembled faster, which would mean septa could also form earlier. This would help to explain why the areas induced by thiostrepton seem to develop faster as shown by their hyphae turning brown before the control.

#### 4.3.2.2. The amount of thiostrepton affects development

The next step was to determine if the effects of *sepF* overexpression differed depending on the level of overexpression. To do this, different concentrations of thiostrepton were tested on confluent plates, and each concentration was tested at the same time points as previously used as well as one additional earlier time point. The previous amount of thiostrepton was 87.5 µg per application and as this amount seemed detrimental to the strains when added to early developmental stages, lower amounts were also tested. The different amounts were 50 µg, 25 µg, 10 µg, 5 µg, 2.5 µg, 1 µg and 0.5 µg thiostrepton delivered in 15 µl volumes to individual patches on the plate.

The strains tested were Δ*sepF*/pIJ6902-P1sepF and Δ*sepF*/pIJ6902, with a similar amount of inoculum being plated in the same fashion as used in the previous experiment on SFM plates carrying apramycin. One plate contained the amounts 50 µg, 25 µg, 10 µg, and 5 µg thiostrepton along with a water control. The other plate

contained the amounts 5 µg, 2.5 µg, 1 µg, 0.5 µg thiostrepton and the water control. The 5 µg thiostrepton was applied on both plates acted as a control and point of reference for the two sets of plates.

Each set of the thiostrepton concentrations were added to four plates for each strain. The plates were inoculated at the same time and each was used to represent a different time point after inoculation. The time points were 0 hr, 28 hrs, 51 hrs and 69 hrs. The earlier time point of 0 hrs after inoculation was used to determine if the addition of thiostrepton at a pre-germination time point is detrimental or if a lower concentration, and thus a lower level of SepF, could give different effects to the detrimental ones seen before.

The spores were inoculated onto SFM plates and were grown at 30°C, while being monitored and imaged every 24 hrs over 5 days.

**Macroscopic observations for lower thiostrepton amounts**

As seen in Figure 4.12 and 4.13, low levels of thiostrepton are able to affect the germinated hyphae, with darker 'brown' areas for some of the areas at which the inducer, thiostrepton, was added.

The 5 µg amount of thiostrepton has an effect on Δ*sepF*/pIJ6902-P1sepF, at all times points, including the 0 hr time point. This is interesting as all the other amounts do not seem to have an obvious macroscopic effect at 0 hrs. At later time points all the amounts of thiostrepton affect the hyphae, most notably at the 51 hr time point. This figure also shows that the higher amounts of thiostrepton result in darker patches, with the 0.5 µg area being the lightest. In fact, the 0.5 µg thiostrepton amount only has a visible effect at the 51 hr and 69 hr time points.

The 1 µg amount of the tipA inducer seems to have a small effect at the 28 hr stage, which becomes more pronounced for the subsequent time points.

Development of the control plates of Δ*sepF*/pIJ6902 showed very little morphological differences when low levels of thiostrepton was applied. The patches that were exposed to thiostrepton did not develop the grey phenotype although when thiostrepton was applied at late stages at 69 hrs, there were some lighter patches that lacked the blue pigmentation.

These lighter patches are not seen for any amounts under 5 µg except once for the 28 hr plate with the 1 µg thiostrepton area.

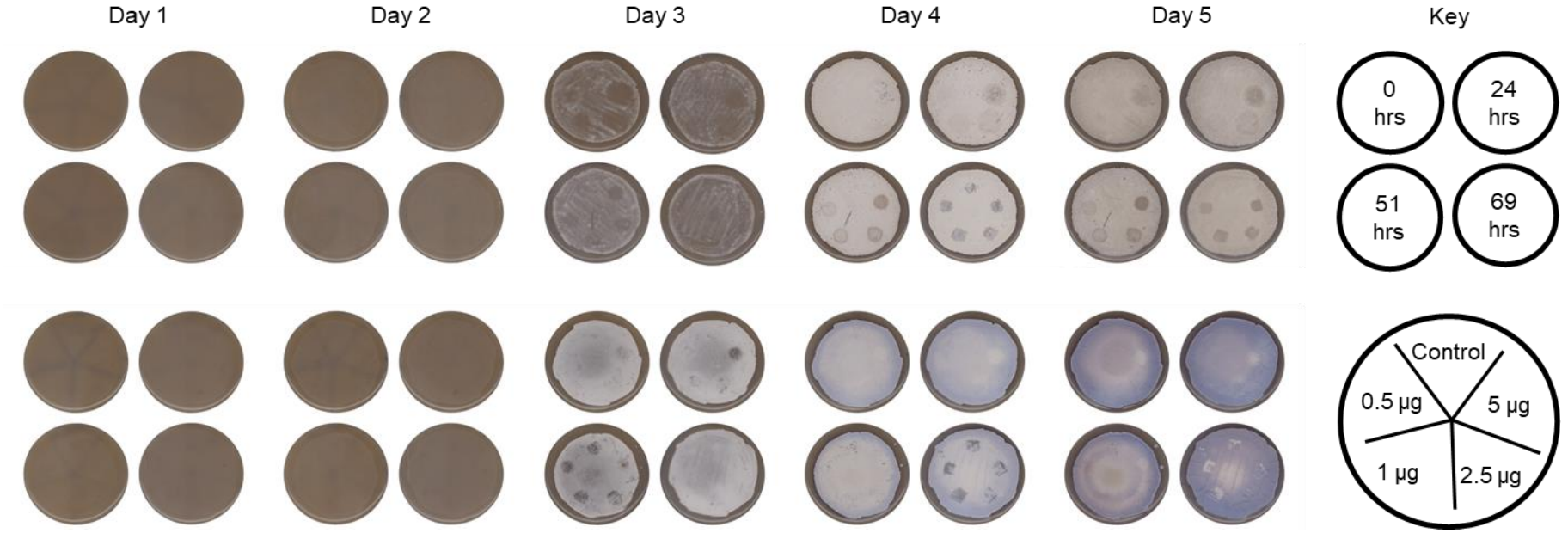


**Figure 4.12**: The effects of low amounts of Thiostrepton on Δ*sepF*/pIJ6902-P1sepF (top row) and Δ*sepF*/pIJ6902 (bottom row) when administered at different times within *S. coelicolor* development. The images were taken every 24 hours of growth, and plates were SFM and grown at 30°c. The amounts of thiostrepton were 0 (top segment), then 0.5 µg, 1 µg, 2.5 µg and 5 µg (anticlockwise manner). The time points when thiostrepton was added 0 hrs, 28 hrs, 51 hrs and 69 hrs after inoculation, and are represented by individual plates which were inoculated in an identical manner and time.

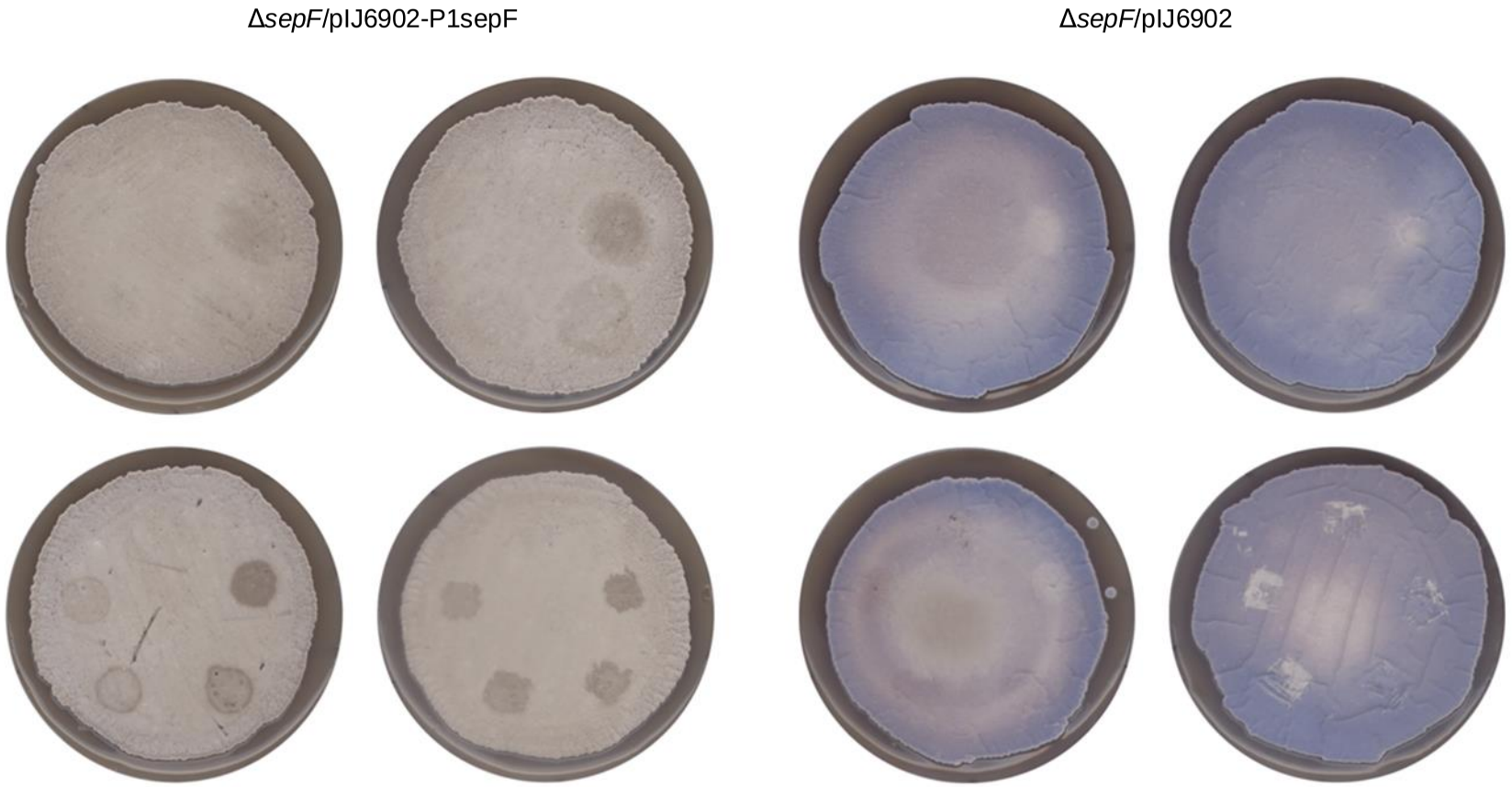


**Figure 4.13**: The effects of low amounts of thiostrepton on Δ*sepF*/pIJ6902-P1sepF (left) and Δ*sepF*/pIJ6902 (right) when administered at different times within *S. coelicolor* development. The images were taken 24 hours after the last addition of thiostrepton, at approximately 93 hours of growth at 30°C on SFM. The amounts of thiostrepton were 0 (top segment), then 0.5 µg, 1 µg, 2.5 µg and 5 µg (anticlockwise manner). The time points when thiostrepton was added 0 hrs (top left), 28 hrs (top right), 51 hrs (bottom left) and 69 hrs (bottom right) after inoculation and are represented by individual plates which were inoculated in an identical manner and time.

**Macroscopic observations for the higher amounts of thiostrepton**

The higher amount of thiostrepton set differs from the lower set (Figures 4.14 and 4.15). All the different amounts of thiostrepton used had a phenotypic effect on all the time points for Δ*sepF*/pIJ6902-P1sepF. Though the effects do differ. When the inducer was added at 0 hr time point the addition of the inducer results in dark 'black' areas, which later have a 'halo' of brown hyphae and then at later time points are filled with white colonies. This is seen for the amounts 50 µg, 25 µg and to some extent 10 µg. The 5 µg amount of thiostrepton has the same effect as seen in the lower amount set.

At all the other time points the hyphae do not show this 'black' phenotype but instead show the 'brown' phenotype. The areas affected all seem to be a similar colour for the 28hr point and 69 hr point. For 51 hrs there seems to be a slight difference, with the areas of lower amounts of thiostrepton, such as 5 µg and 10 µg, having lighter brown hyphae than the 25 µg and 50 µg areas. This was also seen in the lower concentration set, though the difference in colours was more noticeable.

The Δ*sepF*/pIJ6902 plates showed differences between time points. All the areas with thiostrepton were affected at the 0 hr and 28 hr time points, with hyphae being lighter. At the 51hr and 69 hr time points the addition of thiostrepton, even at high concentrations, did not seem to affect the hyphae.

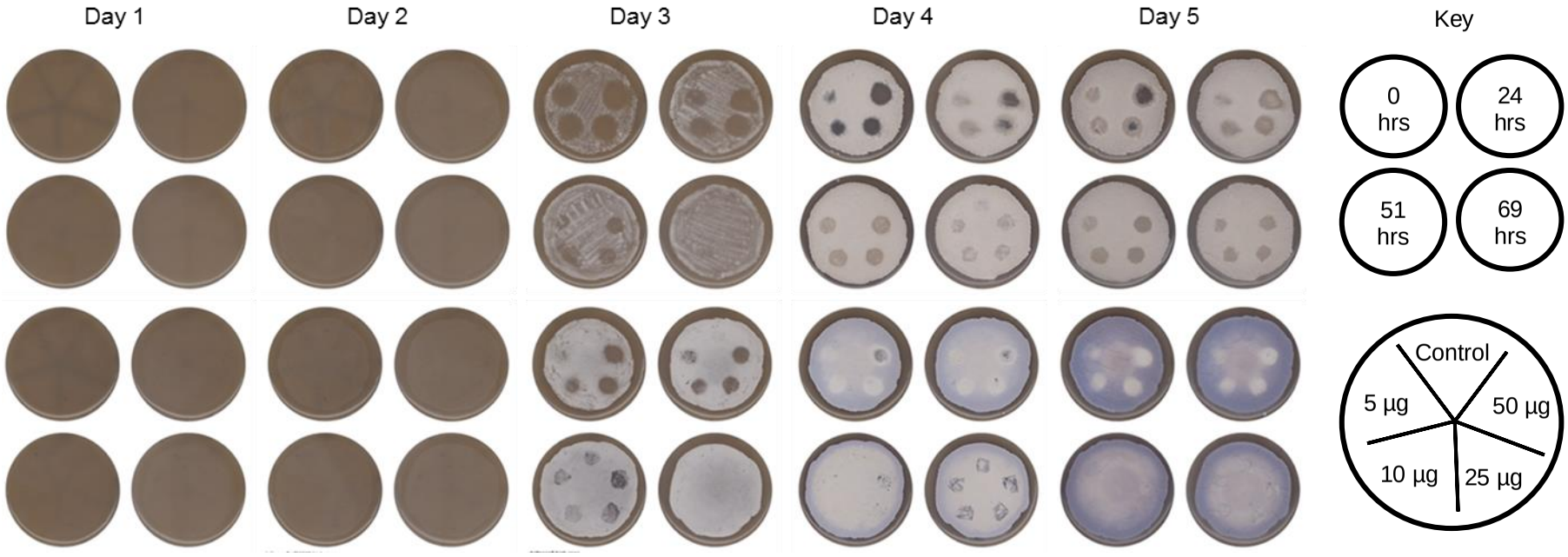


**Figure 4.14:** The effects of high amounts of thiostrepton on Δ*sepF*/pIJ6902-P1sepF (left) and Δ*sepF*/pIJ6902 (right) when administered at different times within *S. coelicolor* development. The strains were grown on SFM at 30°C. The images were taken every 24 hours after the last addition of thiostrepton, till 93 hours of growth. The amounts of thiostrepton were 0 µg (top segment), then 5 µg, 10 µg, 25 µg and 50 µg (anticlockwise manner). The time points when thiostrepton was added were 0 hrs (top left plate), 28 hrs (top right plate), 51 hrs (bottom left plate) and 69 hrs (bottom right plate) after inoculation, and are represented by individual plates which were inoculated in an identical manner and time.

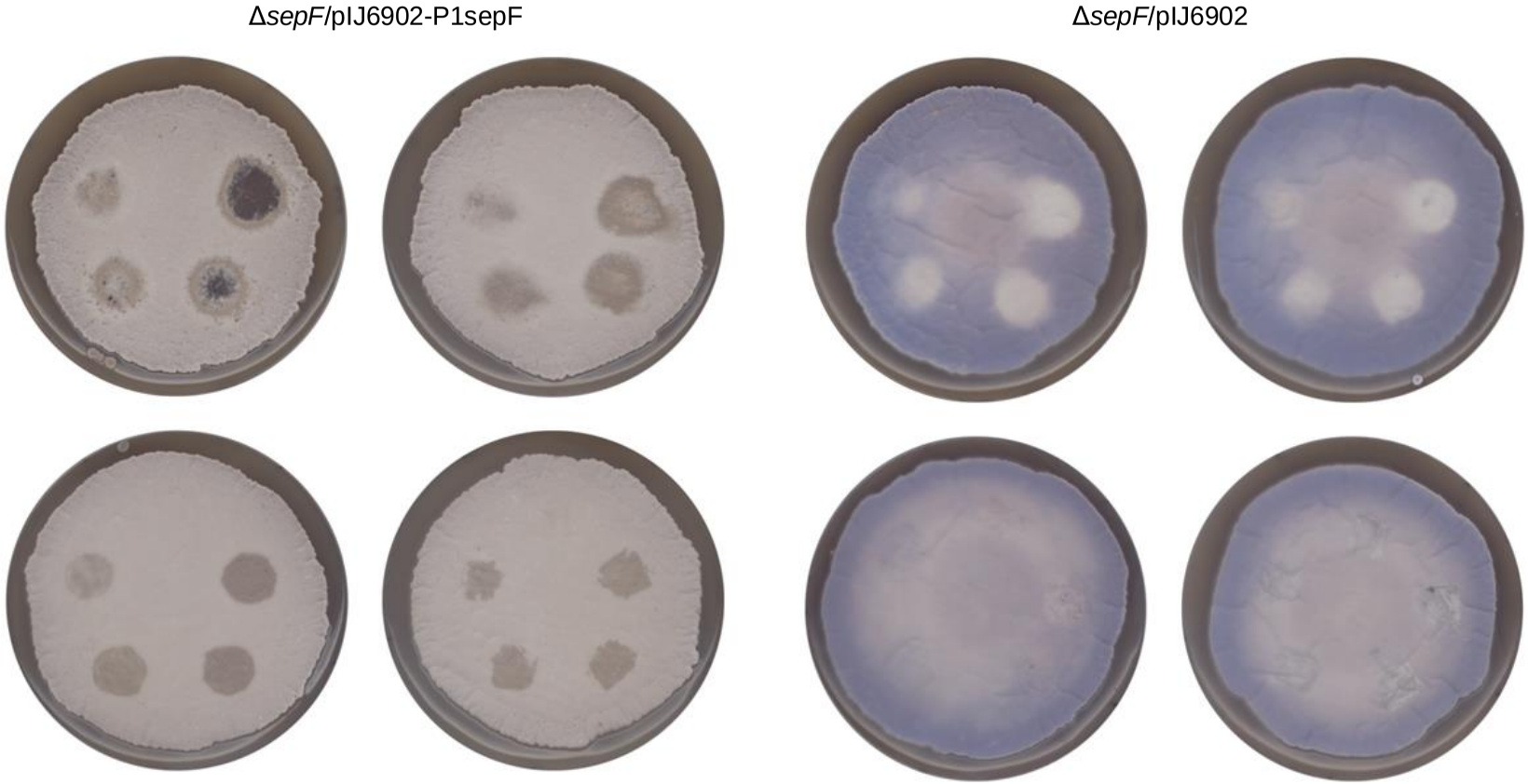


**Figure 4.15:** The effects of high amounts of thiostrepton on Δ*sepF*/pIJ6902-P1sepF (left) and Δ*sepF*/pIJ6902 (right) when administered at different times within *S. coelicolor* development. The images were taken 24 hours after the last addition of thiostrepton, at 93 hours of growth at 30°C on SFM. The amounts of thiostrepton were 0 µg (top segment), then 5 µg, 10 µg, 25 µg and 50 µg (anticlockwise manner). The time points when thiostrepton was added were 0 hrs (top left plate), 28 hrs (top right plate), 51 hrs (bottom left plate) and 69 hrs (bottom right plate) after inoculation, and are represented by individual plates which were inoculated in an identical manner and time.

**Discussion**

The most significant effect of adding thiostrepton was observed on the Δ*sepF*/pIJ6902-P1sepF plate when exposed to high levels of the inducer at 0 hrs. The black phenotype seen could be due to the antibiotic effect of thiostrepton, which at too high a concentration could be inhibiting growth of *S. coelicolor*, even with the resistance conferred by pIJ6902. However, the Δ*sepF*/pIJ6902 0 hr plate does not exhibit this phenotype. Therefore, it is possible that the black phenotype seen in at 0 hrs for Δ*sepF*/pIJ6902-P1sepF is the result of the overexpression of the *sepF* gene. The high levels of *sepF* at this early stage maybe be excessive and seem to be detrimental to growth. Though the areas affected by this do seem to recover to a certain extent after 5 days, it would have been interesting to monitor the phenotype of these "black" patches using microscopy to characterise growth in these zones.

Additionally, as this 'black' phenotype is not seen in the later time points tested, it can be assumed that the effects of high levels of SepF are not as, if at all, detrimental after germination.

The other effect of the inducer seen was the grey phenotype of the affected hyphae, particularly seen in the high level thiostrepton set. The grey phenotype suggests that the Δ*sepF*/pIJ6902-P1sepF strain is producing spores that synthesize the grey spore pigment. Though Δ*sepF*/pIJ6902-P1sepF does produce aerial hyphae and some light grey spores, the areas induced by thiostrepton are a deeper colour than the surrounding area and turn grey ahead of their expected time. This shows that the overproduction of *sepF* may accelerate development of aerial hyphae and spores. This in turn suggests that SepF is a key driver of aerial hyphae development, and its presence may be a 'start signal'. Conversely, it could be affecting the vegetative stage, causing it to end prematurely so allowing the aerial stage to start earlier.

At low amounts of thiostrepton the strains are not as affected as their high concentration counterparts, though the effects are similar especially when the inducer was added at 51hr. As the grey colouring of the hyphae becomes deep the higher the thiostrepton levels applied, it suggests that this phenotype is dependent on the amounts of *sepF* produced.

Additionally, the time point, at which the Δ*sepF*/pIJ6902-P1sepF strain showed the strongest response to thiostrepton addition seemed to be the 51 hr time point, as demonstrated by both sets of thiostrepton amounts. This suggests that this 51 hr stage, at which aerial hyphae is beginning to develop, benefits or is more

affected by the overproduction of *sepF*. This seems logical as this is the stage as which SepF is normally required for septa development. Maybe as SepF is being utilised at this stage, the extra SepF is needed to promote the development of septa and thus spore chains and spores, hence the acceleration of development when compared to the other time points tested.

**Microscopy of Δ*sepF*/pIJ6902-P1sepF when exposed to different levels of the inducer**

Next, phenotypical changes in response to thiostrepton induction were monitored and recorded using microscopy. This was done using 'coverslip drop' microscopy, where a coverslip is pressed onto the surface of the strains for each of the different amounts of thiostrepton used. This would collect material including aerial hyphae and spores. The coverslips were then carefully heat treated so to fix the material without damaging it. To further fix and allow for the subsequent staining, the coverslips then had methanol added for one minute. After this the material on the coverslips were dyed with WGA-Alexa 488 and PI, to show areas of cell wall growth and to chromosomal DNA when viewed under UV light.

Different amounts of thiostrepton were added to the strain after 51 hours growth on SFM medium containing apramycin. The strain, now exposed to thiostrepton, was then allowed to grow at 30°C until 83 hours growth. At 83 hours the strain material was collected via 'coverslip drop' microscopy.

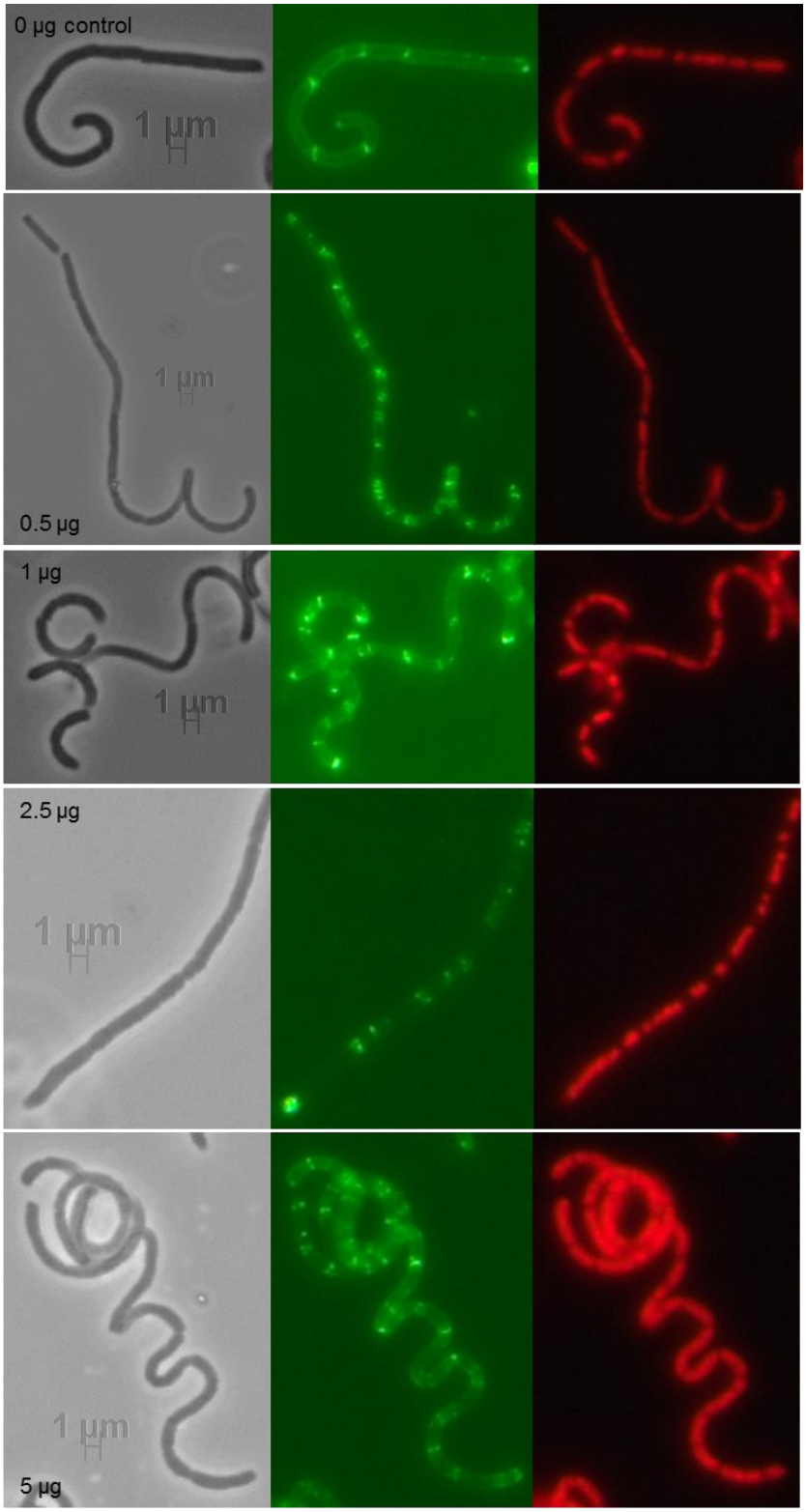


**Figure 4.16**: Microscopy images of the samples collected 83 hours after inoculation of Δ*sepF*/pIJ6902-P1sepF with epi-fluorescence microscopy, phase contrast images (left), WGA stained fluorescent (middle) and PI stained fluorescent images (right). The top panel is an image of the control, which was not exposed to thiostrepton. The panels are the images of samples taken from areas which had 0.5 µg, 1 µg, 2.5 µg, or 5 µg of thiostrepton added to them at 51 hrs after inoculation.

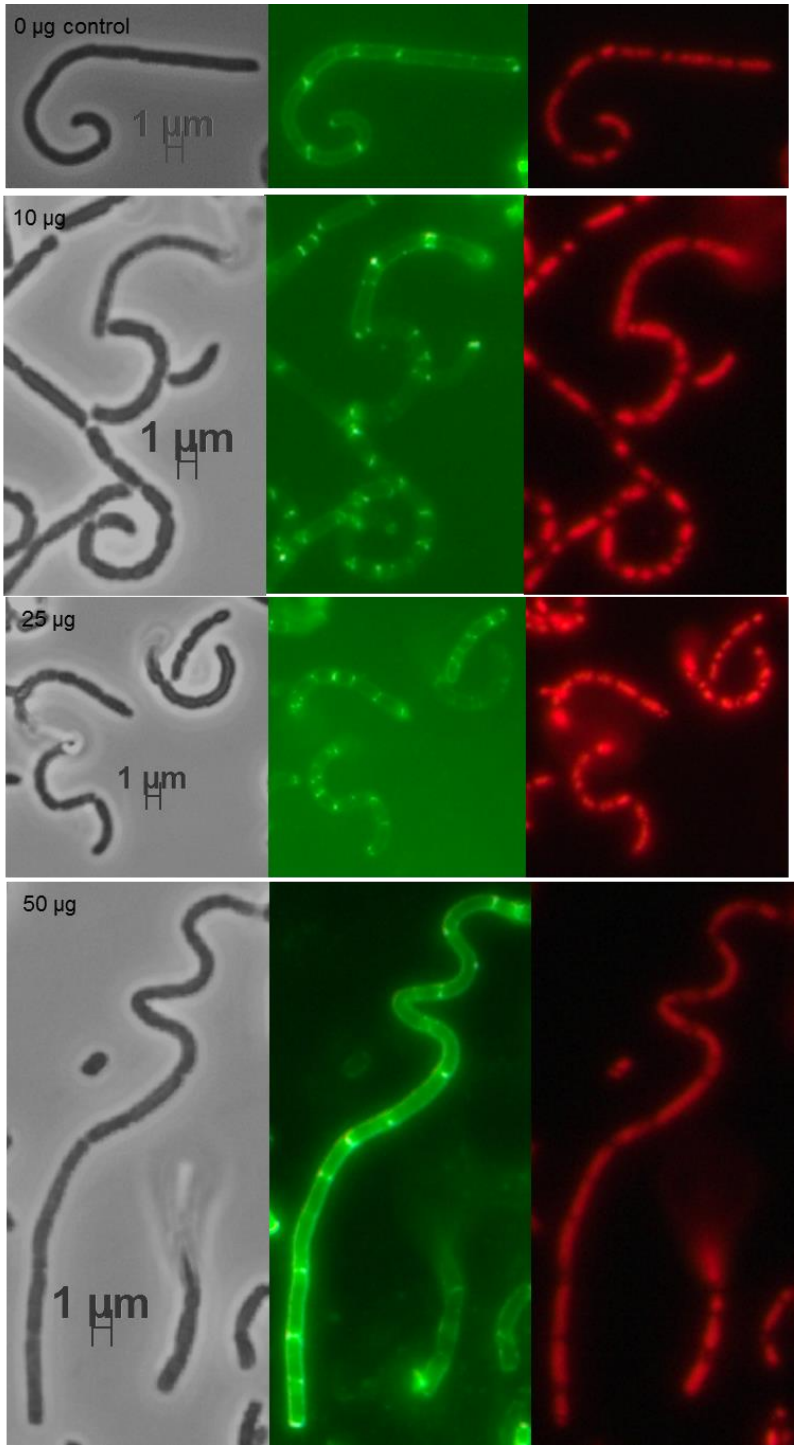


**Figure 4.17**: Microscopy images of the samples collected 83 hours after inoculation of Δ*sepF*/pIJ6902-*sepF* with epi-fluorescence microscopy, phase contrast images (left), WGA stained fluorescent (middle) and PI stained fluorescent images (right). The top panel is an image of the control segment, which was not exposed to thiostrepton. The panels are the images of samples taken from areas which had 10 µg, 25 µg and 50 µg of thiostrepton added to them at 51 hrs after inoculation.

As expected, the control samples show hyphae which have irregular septation that corresponds to a partially complemented Δ*sepF* phenotype, where *sepF* expression is driven from a single native promoter and the uninduced tipA promoter. This irregularity is also seen in the samples with 0.5 µg thiostrepton added, which resemble the thiostrepton null control samples. The 1 µg and 2.5 µg samples are irregular, but also have some septa which seem to be spaced normally (Figure 4.16). The 5 µg thiostrepton samples have septa which are spaced more regularly and are very clear.

The samples to which higher amounts of thiostrepton had been added were observed have a mix of septa distances, some being very short, and others approximately double the normal length (Figure 4.17).

**Discussion**

The amount of thiostrepton does affect the septa development and, as suggested earlier, the amount of thiostrepton, and thus SepF produced, does seem to affect the septa incrementally, not in an on/off switch threshold pattern.

As all the amounts of thiostrepton tested are lower than the original used in the initial time point experiments, the effects are different too. Lower amounts of thiostrepton give septa patterns which are similar to the control, though increasing the amount of SepF does give slightly more uniform septa patterns, with the amount of 5 µg thiostrepton giving results which seem similar to the wild-type. Therefore, it is possible that a level of thiostrepton, and thus *sepF* overexpression, close to this amount could possibly restore the wild-type phenotype, even without the presence of the *sepF* gene's other promoter.

Above this thiostrepton level, larger septa to septa distances are seen, though smaller and normal distances are also seen. This suggests that thiostrepton at 10 µg and over result in excessive amounts of SepF for correct aerial hyphal development.

### 4.4. The expression properties of pIJ6902 can be affected by construct design

The experiments using Δ*sepF*/pIJ6902-P1sepF suggested that in the presence of the inducer, thiostrepton expression of *sepF* was elevated and partial complementation of the Δ*sepF* mutant was observed. However, full complementation was not observed even when the thiostrepton concentration used

was changed or the timing the inducer was added was varied. In addition, previous attempts to use pIJ6902 for the overexpression of *divIVA* and *scy*, encoding two components of the TIPOC (tip organising centre; Holmes et al., 2013) for polar growth, gave mixed success: only *scy* was successfully overexpressed exhibiting a super-branching phenotype (Holmes et al., 2013). It is known that *divIVA* overexpression leads to multiple branch formation (Flardh, 2005) however, when the *divIVA* ORF was cloned between the NdeI and EcoRI sites of the pIJ6902 plasmid (Figure 4.2), during previous experiments within the laboratory, no signs of the over branching phenotype were detected. Therefore, it was considered that although in the presence of thiostrepton the tipA promoter upregulates transcription from this promoter, this transcript must also be efficiently translated into active proteins in order to exert a phenotype.

As the *sepF* overexpression construct was shown to be successful, it was theorised that this was due to the presence of the upstream region of *sepF* within the construct. This region is thought to contain one of the two promoters for *sepF* and it must also contain a native ribosome binding site (RBS), which will recruit ribosomes for efficient translation initiation.

For expression genes must be first transcribed and translated, therefore a problem with either stage would negatively affect expression. Transcription for the constructs within pIJ6902 should be initiated by the vector's inducible tipA promoter. As the *sepF* and *scy* constructs have been successfully overexpressed, this suggests that both transcription and translation were efficient. However, the efficiency of translation can be affected by the ease of access of the ribosomes to the transcript for translation initiation. Ribosomes may not be able to bind to transcripts, and the ATG site might be buried in a double stranded stretch of mRNA. The mRNA transcripts are able to form loop and stem structures, with ribosomes only being able to efficiently access the loops. If area around and including the start site is stem-like due to strong base pairing, this would lower the ribosome binding efficiency and lower translation initiation rates (TIRs).

This lowering of TIRs due to mRNA secondary structures may be the reason why *divIVA* was not overexpressed previously.

To test this two additional constructs for *sepF* were produced. One contained the *sepF* gene but lacking the upstream native DNA. This construct would rely on the putative weak ribosome binding site immediately downstream of the inducible tipA promoter (Figure 4.18) immediately upstream of the ATG translation

initiation site of *sepF*. This construct would mirror the constructs for *divIVA* and *scy* produced previously in lab as they were cloned in the same way. The other construct would contain *sepF*, also without any native DNA upstream of the gene, instead a non-native RBS would be included upstream of the gene (Figure 4.18).

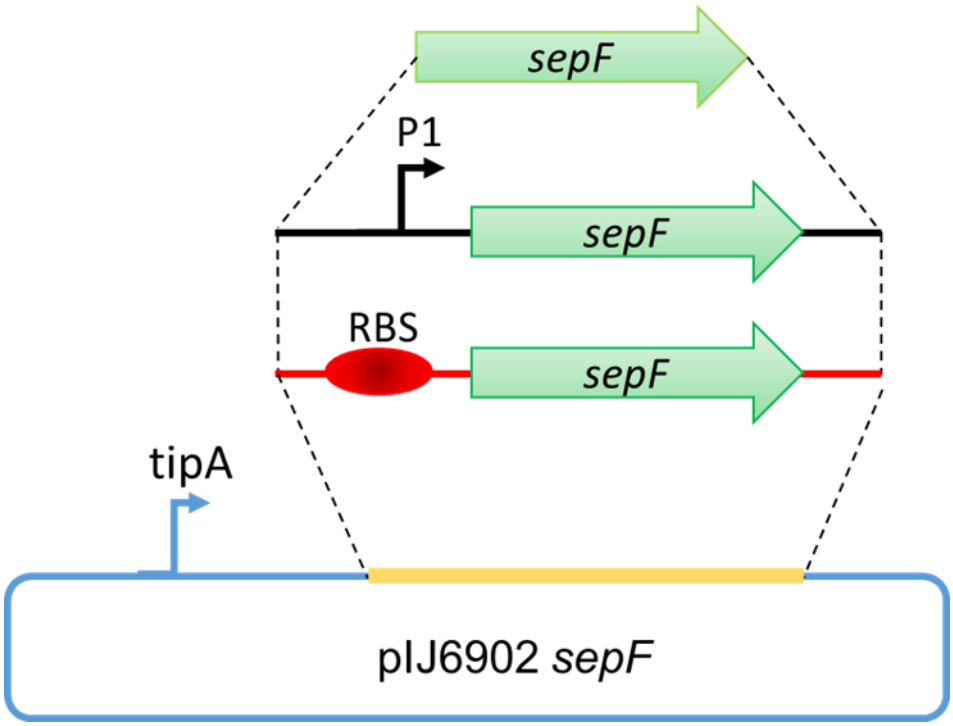


**Figure 4.18**: The three *sepF* overexpression constructs generated using pIJ6902. The top construct corresponds to pIJ6902-sepF and just contains the *sepF* gene with no upstream region. The middle construct is the original pIJ6902-P1sepF construct has already been tested and contains one native *sepF* promoter upstream of the gene. The bottom construct corresponds to pIJ6902-ERBSsepF and contains an *E. coli* RBS site upstream of the *sepF* gene.

The non-native sequence originates for the *E. coli* overexpression plasmid pET28a and carries the ribosome binding site for *E. coli*. The RBS should act to increase the efficiency of ribosome binding, and thus increase translation. The optimal ribosome binding site for translation initiation in *E. coli* is ACCTCCTA and this sequence differs only in a single nucleotide (A -T) from the optimal ribosome binding site for *Streptomyces*, ACCTCCTTT (Salis et al., 2009, Espah Borujeni et al., 2014). Therefore, the *E. coli* RBS should also provide a strong RBS in *Streptomyces*. In addition, as the sequences around the RBS in the pET28a vector are AT rich, they are less likely to generate stem structures with the *Streptomyces* DNA fragment which is GC rich. So in principle, although the *Streptomyces* sequences will vary depending on the gene sequence to be overexpressed, higher

translation initiation rates are expected using this construct, as less secondary structures are predicted between an AT rich and a GT rich sequence.

Testing the two new *sepF* constructs would address whether the construct design could affect translation efficiency.

### 4.4.1. Construct generation

The construct containing just the *sepF* clone was generated using an existing pET28-sepF clone. The pET28 plasmid (Figure 4.19) that was generated before for His-tagged protein overexpression and purification in *E. coli* (Alan Lau, unpublished).

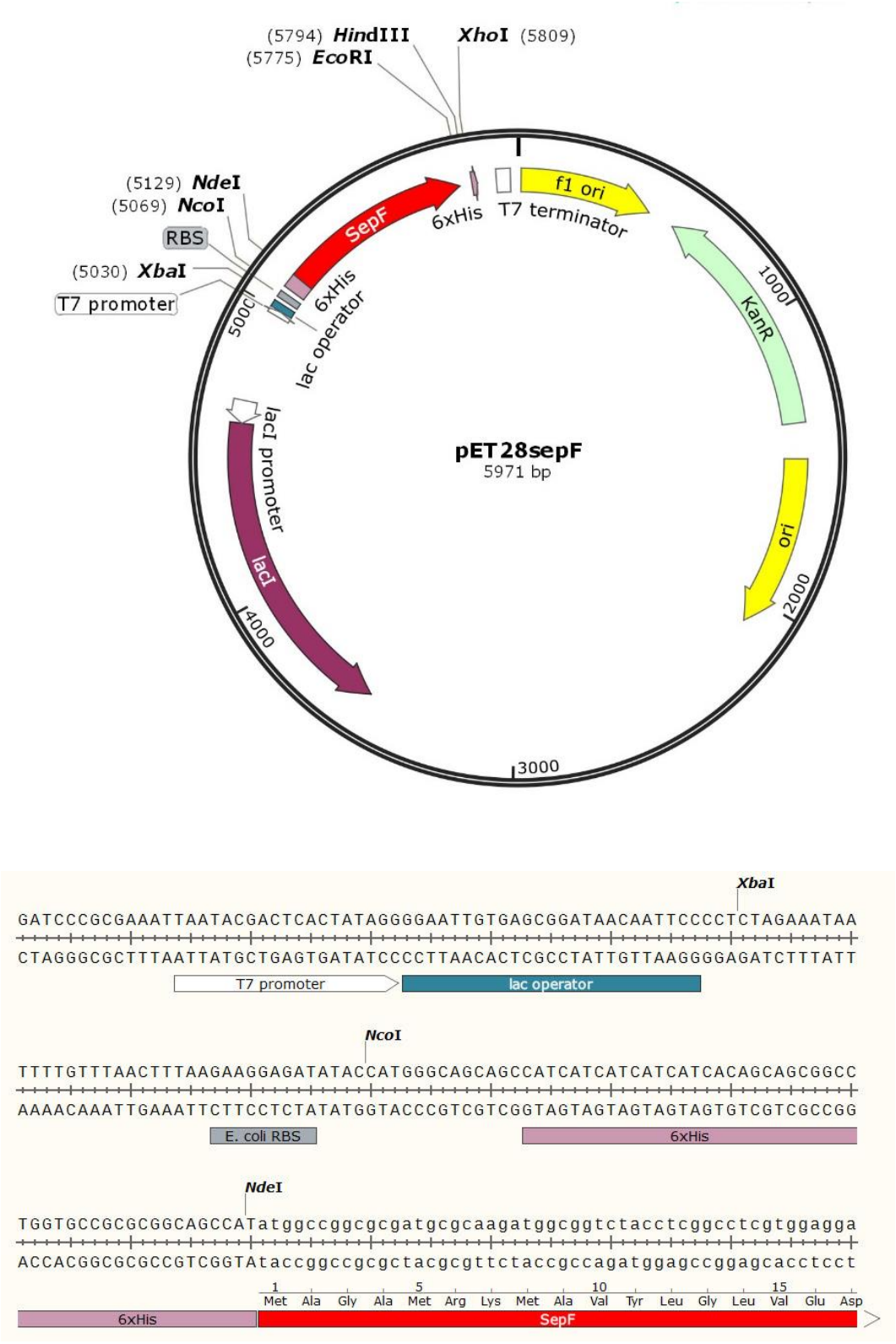


**Figure 4.19**: The plasmid map of pET28-sepF and the sequences around the *E. coli* RBS and the start site of *sepF* are shown.

The pET28-sepF was digested by the restriction enzymes NdeI and EcoRI, where the ATG sequence of the NdeI site overlaps with the translation initiation site for *sepF* and EcoRI is at the immediate end of *sepF*.

The digest was run on an agarose gel and the digest product was excised and purified. The gel extracted fragment was then ligated with pIJ6902, which had also been digested with NdeI and EcoRI, and the mixture was transformed into *E. coli* DH5α competent cells. The apramycin resistant colonies were tested for the correct recombinant clone using colony PCR with the primers 2079 XbaNde FRW and 2079 EcoUTC (Figure 4.20). One of the positive clones, number 1, was confirmed by sequencing. The final construct pIJ6902-sepF and the sequences around the transcription and translation sites are shown in Figure 4.21.

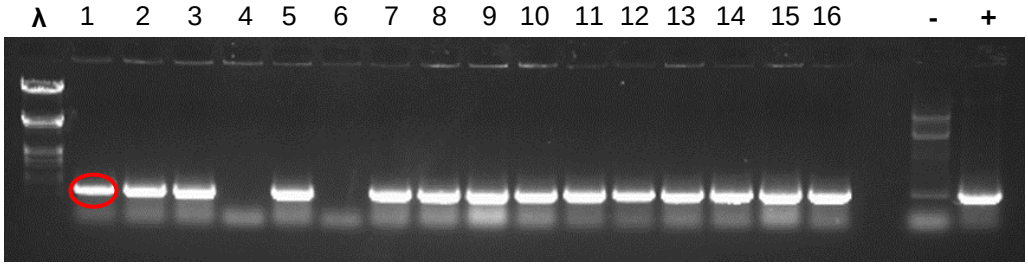


**Figure 4.20:** Gel electrophoresis of colony PCRs for pIJ6902-sepF. The expected product size was 642 bp. Lambda DNA digested with EcoRI and HindIII was used as a size marker. Lane 1-16 contained tested colonies, with the colony carried forward circled in red. The positive control was confirmed by a pET28-sepF clone and the negative control was an empty pIJ6902 vector.

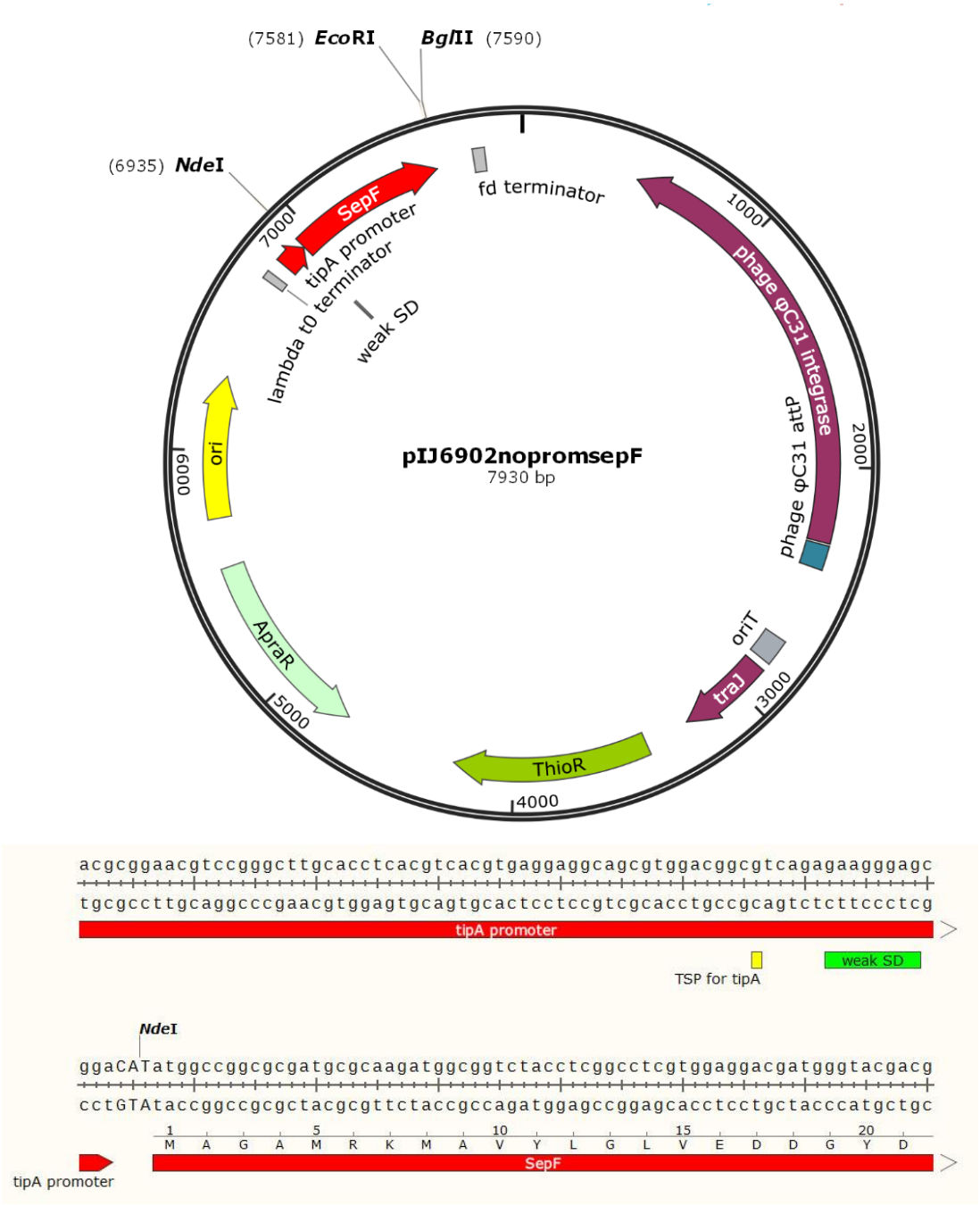


**Figure 4.21**: The plasmid map of pIJ6902-sepF and the sequences around the transcriptional and translational start points. The transcriptional start point (TSP) for the tipA promoter, the weak ribosome binding site (SD) and the translated SepF sequences are shown.

The construct containing *sepF* with an *E. coli* RBS; pIJ6902-ERBSsepF was generated similarly. The fragment used was digested from the existing pET28 *sepF* clone using the restriction enzymes XbaI and EcoRI. This was resulted in a 785 bp fragment, which is larger than the 642 bp of the *sepF* gene. A 99 bp stretch of pET28 was included upstream of the gene, as region contained the *E. coli* RBS. This fragment, when introduced into pIJ6902 will overexpress a His-tagged SepF protein.

After ligation of the XbaI-EcoRI fragment with pIJ6902 digested with the same enzymes, transformation was performed and the transformants were screened using colony PCR with the primers 2079 XbaNde and 2079 EcoUTC (Figure 4.22). We selected colony 3 for the generation of a larger plasmid preparation, which was confirmed by sequencing using the primer T0 which anneals outside the fragment and in the pIJ6902 vector. The construct pIJ6902-ERBSsepF and the sequences around the transcriptional and translational start sites are shown in Figure 4.23.

Both pIJ6902-sepF and pIJ6902-ERBSsepF were introduced into the wild-type and Δ*sepF* mutant *Streptomyces* using conjugation. Selected exconjugants of the wild-type M145 and Δ*sepF* were propagated and collected into stocks.

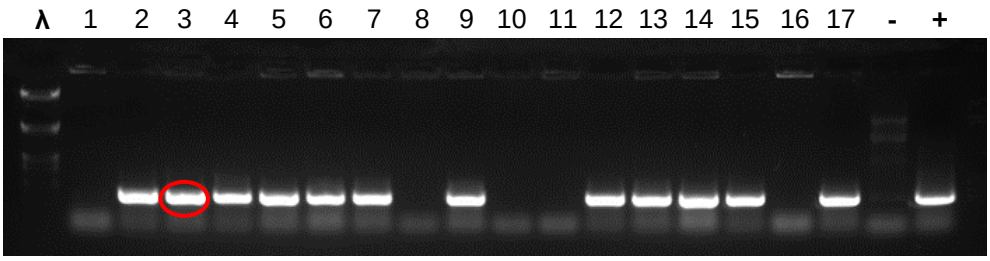


**Figure 4.22:** Gel electrophoresis of colony PCRs for pIJ6902-ERBSsepF. The expected product size was 642 bp. Lambda DNA digested with EcoRI and HindIII was used as a size marker. Lane 1-16 contained tested colonies, with the colony carried forward circled in red. The positive control was confirmed by a pET28-sepF clone and the negative control was an empty pIJ6902 vector.

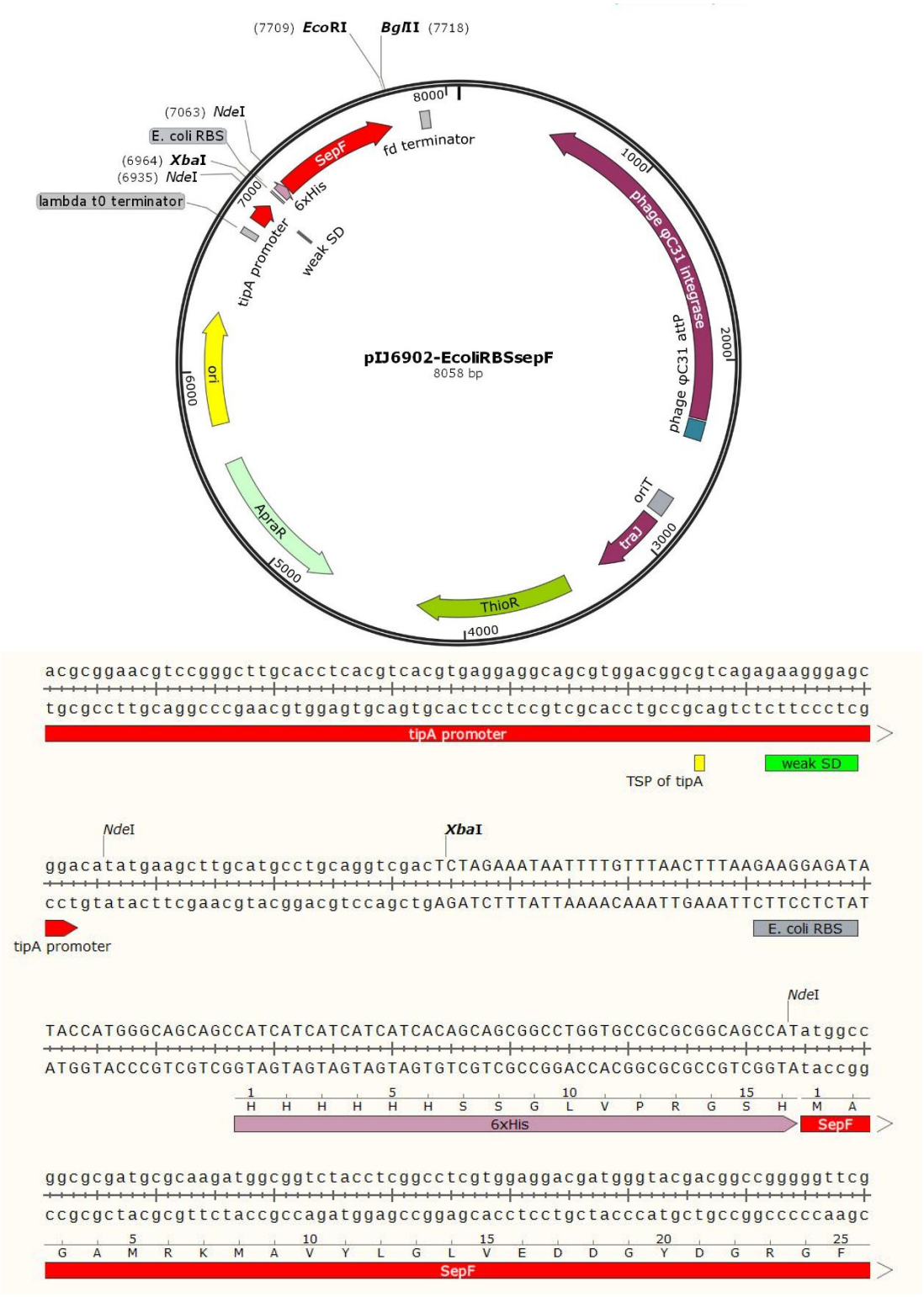


**Figure 4.23**: The plasmid map of pIJ6902-ERBSsepF and the sequences around the transcriptional and translational start points. The transcription start point (TP) for the tipA promoter, the weak ribosome binding site (SD) downstream of tipA, the *E. coli* RBS and the translated His-SepF sequences are shown.

#### 4.4.2.1 The phenotype of the strains carrying pIJ6902-*sepF* and pIJ6902-ERBSsepF in the absence of the tipA inducer, thiostrepton

Firstly, the phenotypes of the Δ*sepF* strain carrying the two new constructs grown in the absence of thiostrepton was observed macroscopically (Figure 4.24). Without the inducer, the promoter is not expected to be active, unless there is some leaky expression, therefore, no complementation of the Δ*sepF* phenotype was expected.

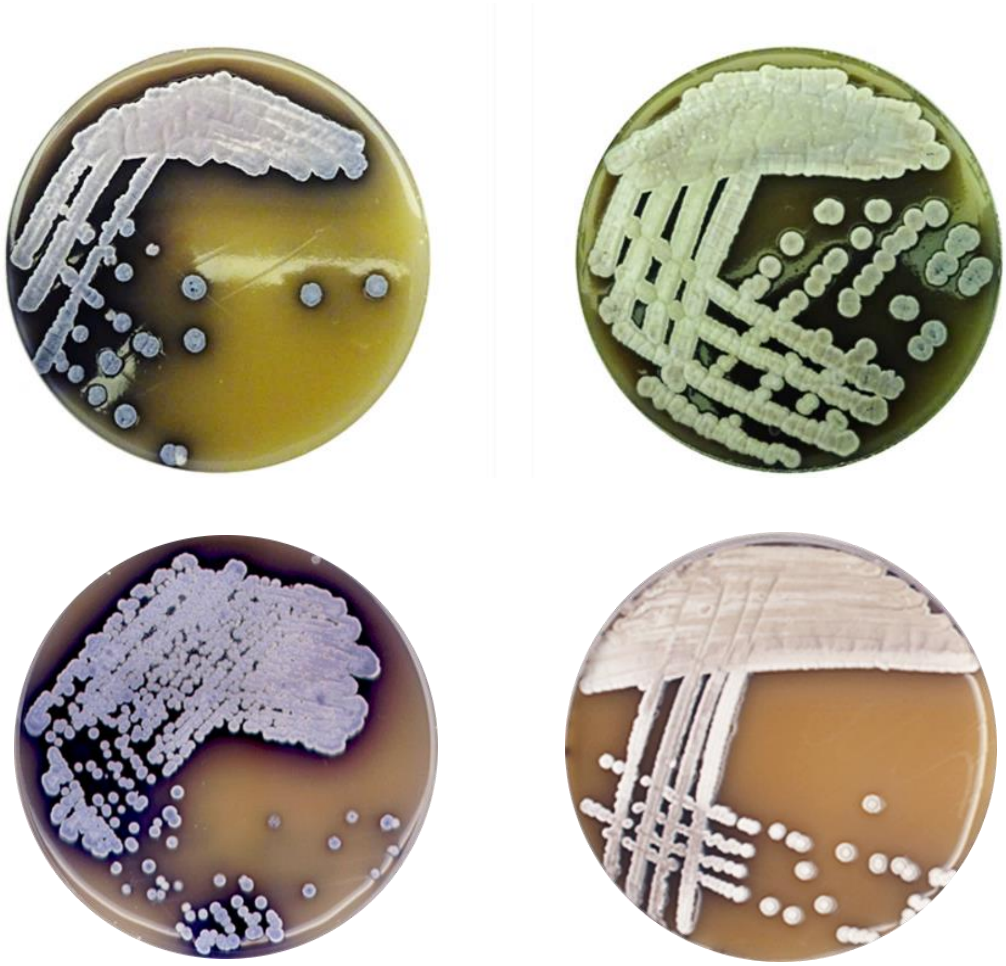

**Figure 4.24:** The Δ*sepF*/pIJ6902-sepF (top left) and Δ*sepF*/pIJ6902-ERBSsepF (top right) strains, grown on SFM over 7 days at 30°C. The control strains in the bottom row are Δ*sepF* (left) and the wild-type M145 (right).

**Δ*sepF*/pIJ6902-sepF**

The Δ*sepF*/pIJ6902-sepF strain exhibited a phenotype which is similar to the Δ*sepF* mutant. When grow on SFM for 7 days, in the absence of thiostrepton, the colonies did not turn into grey but developed a blue colour (Figure 4.24). When initially plated and grown, it developed slowly, and the aerial hyphae did not

transition from white to grey. Instead hyphae stay white till they eventually turn blue, which starts at day 4.

At 7 days of growth the strain is completely blue, but unlike the *sepF* mutant, it does not produce any blue droplets. Therefore, it does not seem to overproduce actinorhodin on the same level as *ΔsepF*. However, the media directly below or close to the inoculated area did turn dark blue, which suggests excess actinorhodin in the vegetative hyphae.

Aerial hyphae were collected from the mature seven-day cultures, through coverslip imprint techniques, and viewed under the microscope. The hyphae were stained with the cell wall and DNA stains WGA-Alexa 488 and PI.

There was some evidence of few spore-like structures (Figure 4.25), which were comparable with the spore-like structures in old Δ*sepF* cultures. The spores were sparse, relative to a wildtype strain or to Δ*sepF*/pMS82-P1sepF. The spores which were present were irregular in size and did not resemble wild-type spores. Additionally, individual spores were rare, with most examples being part of a spore chain. The spore chains were also unusual, as the majority were short and contained spore compartments of different sizes.

Each spore contained a packet of genetic material, which differed in size dependent on the size of the spore itself. The spore compartments were filled completely with the genetic material, and only contained one packet no matter how big the spore was.

Compared to Δ*sepF*/pIJ6902-P1sepF, the spore material was very limited, but the irregular sizes of the spores were similar to the Δ*sepF* strain. Additionally, there seemed to be more lysed material for Δ*sepF*/pIJ6902-sepF though no evidence of spore lysis was documented.

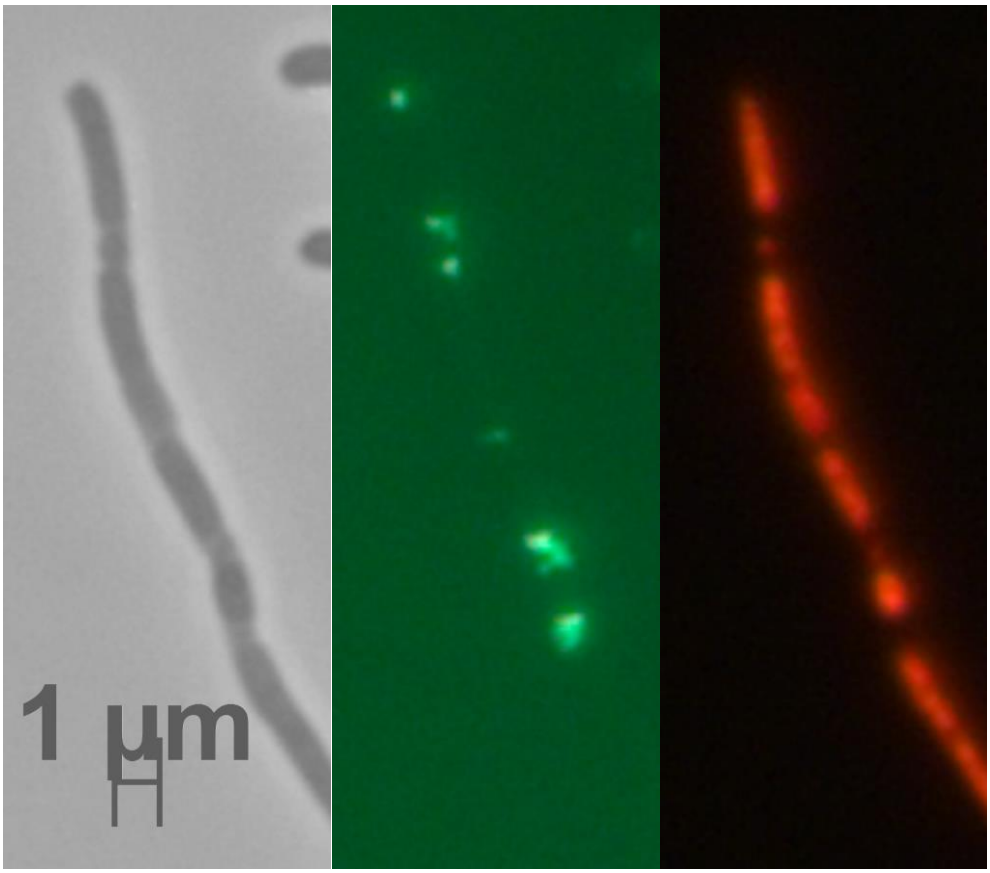


**Figure 4.25**: Microscopy images of the samples of Δ*sepF*/pIJ6902-*sepF* with epi-fluorescence microscopy, phase contrast images (left), WGA stained fluorescent (middle) and PI stained fluorescent images (right). Grown on SFM at 30°C.

**Δ*sepF*/pIJ6902-ERBSsepF**

The strain containing only the *sepF* gene with an upstream region of *E. coli* DNA containing a non-native RBS was grown on SFM for 7 days (Figure 4.24). This strain does not completely resemble the wild-type M145 and differs from both the Δ*sepF* and Δ*sepF*/pIJ6902-*sepF* strains. After five days of growth the mutant is off-white with a slight colour at the edges of the plated areas. It is not grey like the wild-type, but it is not blue like Δ*sepF* or Δ*sepF*/pIJ6902-ERBSsepF. The strain grows like Δ*sepF*/pIJ6902-*sepF* up to day 5, when early aerial hyphae are formed. The hyphae are white, but by day 4 they show some of the off-white colouring mentioned previously. This is also when the smooth surface of the confluent area of growth starts to show areas of wrinkling. The outer edges of the growth areas were wrinkled creating dips in the growth medium. This is more apparent at day 5, with

the ‘wrinkles’ reaching further into the centre of the colony. The colony did not show any more macroscopic differences as it matures from day 5 to 7.

The aerial hyphae were collected and viewed after seven days of growth. The material was stained using WGA-Alexa 488 and PI.

The imprint microscopy was able to collect a lot of material, with the majority of the material being irregularly spaced spores (Figure 4.26). The spores were irregular in length, with many examples of spores longer than the wildtype standard.

The spores did contain packets of DNA, which was divided clearly between the spores. Some areas between septa did not contain any DNA, as seen through the lack of red fluorescence, but these were rare and only occurred between septa which were relatively close together. Interestingly, there were examples of very small genetic packets, which were separated from other DNA foci within the spore chain. When the samples were viewed for septa they were either not obvious or apparent, or the septa seemed to be directly on top of the DNA foci.

The spores themselves were found either in spore chains or individually, as opposed to the very few spore chains of Δ*sepF*/pIJ6902-sepF. Additionally, the spore chains were much longer than those seen in Δ*sepF*/pIJ6902-sepF, with their lengths being comparable with that of the Δ*sepF*/pIJ6902-P1sepF strain.

There was also an absence of spore or hyphae lysis, making it distinct from Δ*sepF* and Δ*sepF*/pIJ6902-sepF.

It is very interesting that we observed differences between the Δ*sepF*/pIJ6902-sepF and Δ*sepF*/pIJ6902-ERBSsepF strains. This suggest that some transcription and translation of *sepF* did take place in the Δ*sepF*/pIJ6902-ERBSsepF strain even in the absence of the inducer. On the other hand, *sepF* expression was not observed in the Δ*sepF*/pIJ6902-sepF strain which exhibited the Δ*sepF* phenotype.

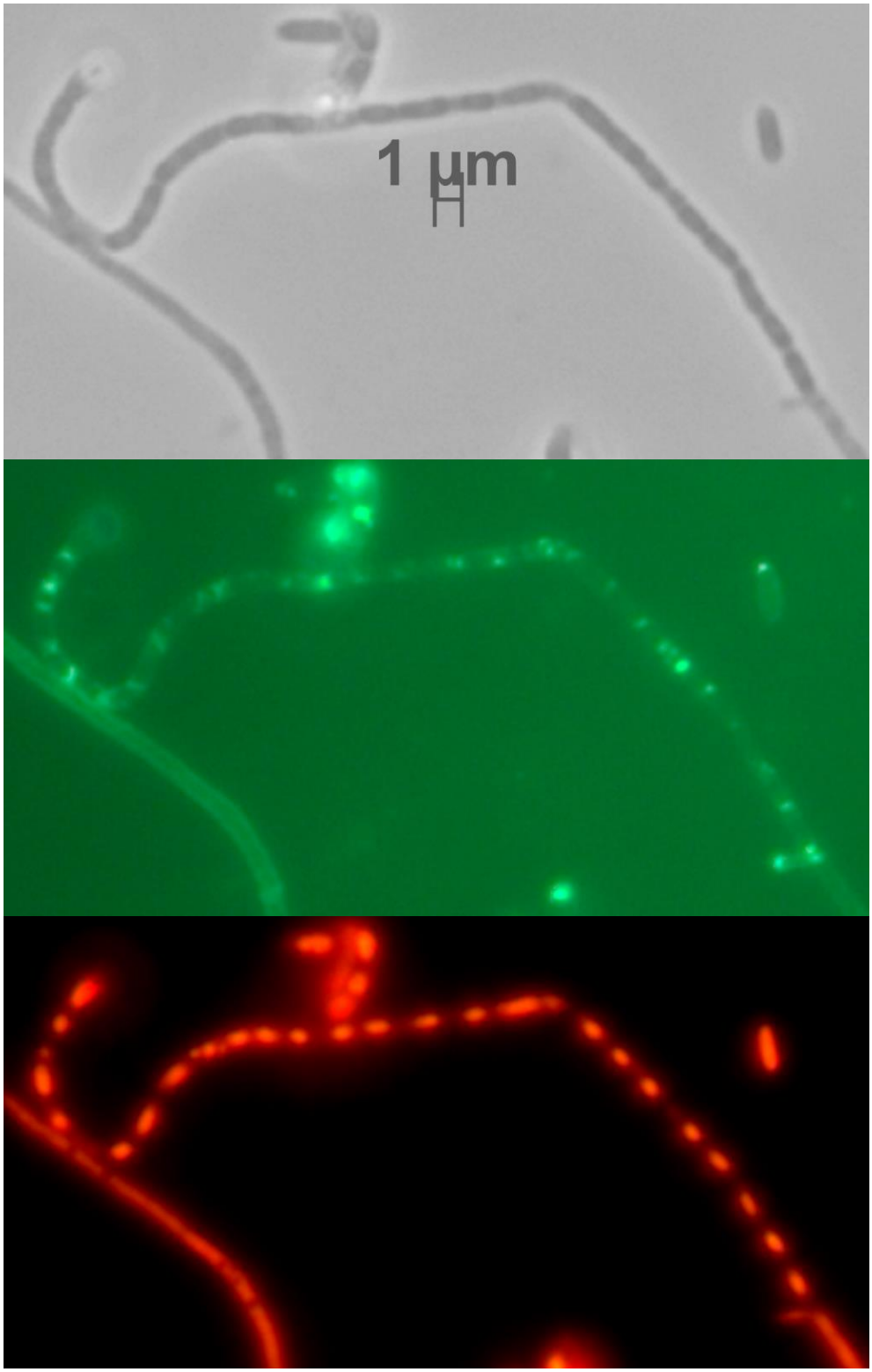


**Figure 4.26**: Microscopy images of the samples of Δ*sepF*/pIJ6902-ERBS*sepF* with epi-fluorescence microscopy, phase contrast images (left), WGA stained fluorescent (middle) and PI stained fluorescent images (right). Grown on SFM at 30°C.

#### 4.4.2.2. Phenotype of the alternative *sepF* constructs within strains in the presence of thiostrepton

Both of the strains, Δ*sepF*/pIJ6902-sepF and Δ*sepF*/pIJ6902-ERBSsepF, were grown confluently on SFM for five days and were exposed to thiostrepton through dropping the tipA inducer directly onto the hyphae (Figure 4.27). The same conditions used to test the first *sepF* construct were used for the additional *sepF* constructs. The strains had a water control and the higher amount of thiostrepton added to them at different development stages after inoculation, 28 hrs after inoculation represented vegetative hyphae, 51 hrs after inoculation represented early aerial, and 69 hrs after inoculation represented late aerial hyphae formation. The set of lower amounts of thiostrepton was not tested for these strains due to the minor differences that resulted when it was tested on Δ*sepF*/pIJ6902-P1sepF. The plates were viewed and imaged daily after inoculation (Figure 4.27).

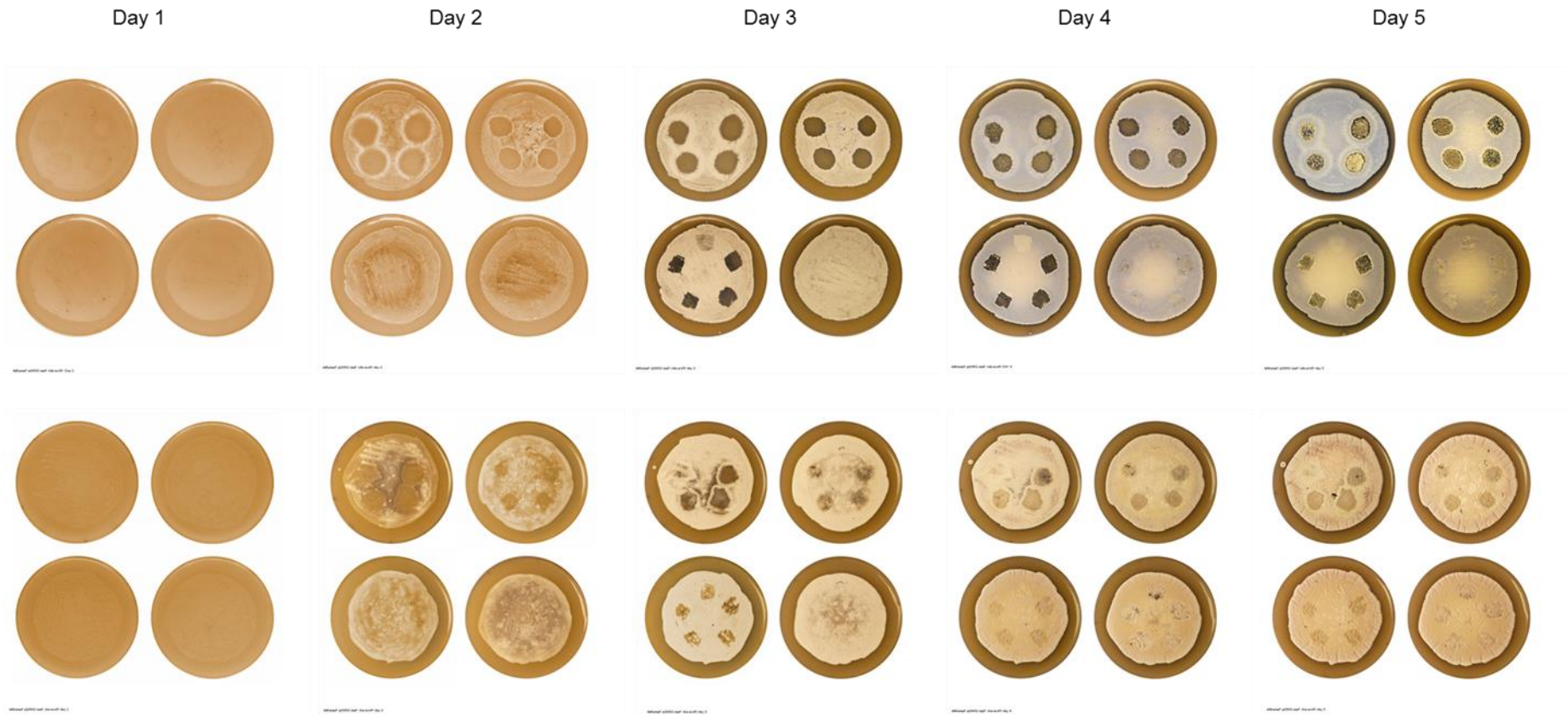


Figure 4.27: The effects of various amounts of thiostrepton on Δ*sepF*/pIJ6902-*sepF* (top) and Δ*sepF* pIJ6902-ERBSsepF (bottom) when administered at different times within *S. coelicolor* development. The images were taken 24 hours after the previous addition of Thiostrepton, till approximately 93 hours of growth at 30°C. The amounts of thiostrepton were 0 (top segment), then 5 µg, 10 µg, 25 µg and 50 µg (anticlockwise manner). The time points when thiostrepton was added 0 hrs, 28 hrs, 51 hrs and 69 hrs after inoculation, and are represented by individual plates which were inoculated in an identical manner and time.


Figure 4.28: The effects of various amounts of thiostrepton on Δ*sepF*/pIJ6902-sepF (left) and Δ*sepF*/pIJ6902-ERBSsepF (right), at day 5, grown on SFM at 30°C.

**Δ*sepF*/pIJ6902-sepF**

The strain shows a similar phenotype to that seen for Δ*sepF*/pIJ6902 and Δ*sepF*/pIJ6902-P1sepF for days 1 to 3 (Figure 4.27). There is an absence of visible growth within the areas in which the thiostrepton had been dropped. This is the case for all the different amounts of thiostrepton tested. There area affected by the thiostrepton is greater for the plates to which thiostrepton was added earlier (timepoints: 0 hr and 28 hr). This is as the thiostrepton solution spread farther when applied at early growth and spread less when applied at the stages of aerial development, possibly, because of the hydrophobicity of the aerial hyphae does not promoter spreading of aqueous solutions.

At day 4 the phenotype of the Δ*sepF*/pIJ6902-sepF strain did differ from that of Δ*sepF*/pIJ6902-P1sepF and Δ*sepF*/pIJ6902-ERBSsepF. The areas affected by the thiostrepton drops still showed no visible growth. At this point the Δ*sepF*/pIJ6902 and Δ*sepF*/pIJ6902-P1sepF strains did show some sort of hyphae recovery, or individual colonies within the areas initially affected negatively by thiostrepton. At day 5 there is some evidence of colonies within the thiostrepton areas, with the 0 hr inoculation plate showing a greater area recovered than the other plates (Figure 4.28).

**Δ*sepF*/pIJ6902-ERBSsepF**

The Δ*sepF*/pIJ6902-ERBSsepF strain also shows similarities to the Δ*sepF*/pIJ6902-P1sepF and Δ*sepF*/pIJ6902-sepF strains for the first two to three days (Figure 4.27). There is an absence of visible growth in the areas where thiostrepton was dropped, but these areas show signs of recovery after day 3. At day 4, the areas where the thiostrepton was added the lawn is darker and has a brown-grey hue. By day 5, the plates tested when thiostrepton was added at 0 hr, 28 hrs, and 51 hrs after inoculation, all have grey spots in the areas thiostrepton was added. An exception to this is the sample tested at 0 hrs with 5 ug of thiostrepton. Though the area to which thiostrepton was added is visible it does not resemble the other areas, as it lighter and not darker than the surrounding hyphae. The plate to which thiostrepton was added at 69 hr also does not show any evidence of grey or brown hyphae, for all the different amounts of thiostrepton tested. This differs from the original Δ*sepF*/pIJ6902-P1sepF, which at day 5 showed grey areas for all the concentration of thiostrepton added to the 69 hr plate (Figure 4.28). The hyphae in the test areas differ slightly to the surrounding hyphae but resemble the control (top section of each plate).

In conclusion, it seems that the two additional *sepF* overexpression strains differ in their success to express *sepF*, and they also differ compared to expression of *sepF* seen in the original overexpression construct pIJ6902-P1sepF. The constructs all contained the whole of the *sepF* gene but differed in their upstream regions. Constructs containing an RBS site, pIJ6902-P1sepF and pIJ6902-ERBSsepF, were more successful in producing spores when induced in the mutant *sepF* strains.

### 4.4.3. Utilising synthetic software for construct generation

All three *sepF* constructs resulted in various phenotypes when introduced into the Δ*sepF* strain, likely due to the differences in the levels of SepF expression due to differences in the DNA fragments upstream of the translational start of *sepF*. The construct pIJ6902-sepF lacked a native promoter or native RBS, and we hypothesise that relied entirely on our interpretation of the SepF protein production was limited, as translation of the *sepF* transcripts could not take place efficiently.

The pIJ6902 expression system does seem to contain an effective and inducible promoter, however, it does not guarantee an efficient translation of genes under the control of that promoter. It seems that native upstream gene regions or artificial RBS can alter gene expression, by increasing the efficiency of translation.

The improvement that mRNA sequence or RBS can give to the pIJ6902 expression system when used in construct design can be predicted through synthetic software (Salis et al., 2009, Espah Borujeni et al., 2014). This software can also be used to design synthetic mRNA transcripts for optimised translation. Moreover, the software can predict or optimise RBSs and translation initiation rates (TIRs) of the mRNA transcripts.

One such system for biological engineering and synthetic biology which specialises in prokaryotes is the Salis Lab DNA complier, which contains software such as the ‘RBS calculator’ (https://salislab.net/software/forward). It is a widely used and has been validated in many microbes, with specific data on *Streptomyces* as well as others. The software allows for the automatic design and prediction of RBSs and TIRs, which it does for each codon start site.

The model is thermodynamic based, and accounts for hybridization of RNA, mRNA, and tRNA, inhibitory mRNA structures, the effects on the ribosome due to

start codon and ribosomal RNA binding site distances, and, other interactions between ribosomes and mRNA.

This software can be used specifically for assessing TIRs for translation in *Streptomyces*. Additionally, validation of the software included bacteria which had been grown at different temperatures, including the optimum temperature for *Streptomyces* at 30°C.

The Salis system should allow for the accurate prediction of the constructs TIRs, and thus show any differences in the rate of translation initiation. Therefore, it is a good tool to predict the TIRs of the *sepF* constructs produced. By using the Salis system, it can be suggested that the translation efficiency of each construct, as shown through the TIR values, is the rate limiting step for the production and utilisation of SepF. Additionally, this software was used to predict TIRs for the various *divIVA* constructs which had been previously been tested in the lab, as another example to verify if translation rates and construct design are affecting overproduction of *Streptomyces* genes when using the pIJ6902 vector. The Salis software was also used to predict an optimal RBS for *sepF* translation and this RBS is compared by its TIR to those of the other constructs used in this study.

#### 4.4.3.1. TIRs of the three *sepF* constructs

To predict the TIR of each construct produced, the Salis RBS calculator (Version 2.0 – Predict: RBS Translation Rates) was used. This required the mRNA sequence data for each construct. This would include the mRNA sequence starting at the tipA promoter and include 300 nt of the coding sequence (Figures 4.21 and 4.23).

The organism in which this mRNA was to be tested was also required, so to allow the correct ribosome to be used in the modelling. At present three *Streptomyces* species are available for organism selection on the Salis programme. None of these are *S. coelicolor*, however, *Streptomyces* species as a whole have similar 16s rRNA sequences (https://scialert.net/fulltext/?doi=jm.2018.13.20) . Therefore, as the *Streptomyces* species chosen would not have too large an impact, *Streptomyces avermitilis* was chosen as the organism for the TIR to be modelled in. The calculated TIR are shown in Table 4.1.

Table 4.1: The TIR of the various constructs predicted using Salis software.

| Gene and construct | TIR (au) |
|---|---|
| pIJ6902-P1sepF | 352.40 |
| pIJ6902-ERBSsepF | 6275.40 |
| pIJ6902-sepF | 84.60 |
| pIJ6902-scy | 503.90 |
| pIJ6902-divIVA | 72.80 |
| pKF58 divIVA (Flardh et al.,) | 343.10 |

The constructs tested were the three separate *sepF* clones, the successfully overexpressed *scy* construct which had been previously generated in lab, and two previously generated *divIVA* constructs. Only one construct for *divIVA* gave gene overexpression, pKF58-divIVA which contains an upstream region to the gene, while pIJ6902-divIVA which only contained the cloned gene region had not shown any evidence of gene overexpression.

The constructs pIJ6902-scy and pIJ6902-divIVA had been generated in the same way as pIJ6902-sepF. But macroscopic and microscopic observations suggested that only *scy* had been overexpressed. When comparing the TIRs of the constructs, the TIR for pIJ6902-scy is higher than pIJ6902-divIVA and pIJ6902-sepF, by an order of magnitude. The TIR values of pIJ6902-divIVA and pIJ6902-sepF are relatively close at 72.80 au and 84.60 au (respectively). This suggests constructs which give TIR values similar to or lower than these will not be efficiently translated due to relatively low TIRs.

The constructs pIJ6902-scy and pKF58-divIVA had previously been identified to successfully overexpression their genes within *Streptomyces*. The TIR values of each construct are higher than pIJ6902-divIVA and pIJ6902-sepF by an order of 10. This therefore suggest that TIR similar to or above that of pKF58-divIVA at 343.10 au would be successfully translated.

The original pIJ6902-sepFP1 construct, which gave *sepF* overexpression, has a predicted TIR of 352.40 au. This is slightly more than the TIR of pKF58-divIVA, and therefore would suggest that the TIR is high enough to allow efficient translation due to successful ribosome binding to mRNA transcripts. As mentioned, the pIJ6902-sepF construct did not result in *sepF* overexpression and this was

thought to be due to problems in ribosome binding, this idea was reinforced by the low TIR predicted which is as expected for a construct resulting in inefficient translation of mRNA transcripts. The construct containing an *E. coli* RBS, pIJ6902-sepFERBS, had the highest TIR predicted for the constructs tested. At 6275.40 au, the construct is an order of magnitude more efficient than the other constructs which were able to result in gene overexpression.

The increase in *sepF* transcript translation initiation for pIJ6902-sepFERBS compared to the original pIJ6902-sepFP1, suggests that having a strong RBS can optimises translation and can potentially be more efficient in translation than native upstream regions of the genes being expressed. Furthermore, it suggests that the addition of an RBS, such as the *E. coli* RBS in pIJ6902-sepFERBS, can be used to overcome the problem of genes not being overexpressed in the pIJ6902 overexpression vector.

#### 4.4.3.2. Using a non-native RBS for overexpression constructs

As constructs containing either a native RBS or the *E. coli* RBS upstream of the translational start of the gene had a relatively high TIRs, for example pIJ6902-P1sepF and pIJ6902-ERBSsepF have TIRs of 352.4 au and 6275.4 au, compared to 84.6 au for the pIJ6902-sepF construct which has a weak ribosome binding site originating from the pIJ6902 plasmid itself and which is located also at sub-optimal distance from the translational start site (Figure 4.21). The highest TIR of 6275.4 au was predicted for pIJ6902-ERBSsepF which suggests that designing the *E. coli* RBS and surrounding sequences upstream of the translational start site of genes for overexpression might be an effective strategy for generating constructs with elevated protein levels. Therefore, further constructs were generated using an *E. coli* RBS were produced for a range of other genes, such as *parH*, *divIVA*, *hyp* and *filP*, which are involved in either polar growth (*divIVA* and *filP*) or in chromosome organisation (*parH* and *hyp*). The clones were constructed in a very similar way that was done for pIJ6902-ERBSsepF (Figure 4.29). An XbaI-EcoRI digestion of a previously generated pET28 clone for overexpression of the appropriate proteins in *E. coli* was performed to liberate a DNA fragment that carried the genes downstream of an optimised *E. coli* RBS for efficient translation. The TIRs of each was predicted and the construct was then subsequently produced. The TIRs of constructs could have been higher, if a *Streptomyces* RBS was used instead of one

originating from *E. coli*. However, it was simpler to use existing pET28 clones of the genes to generate the new overexpression constructs.

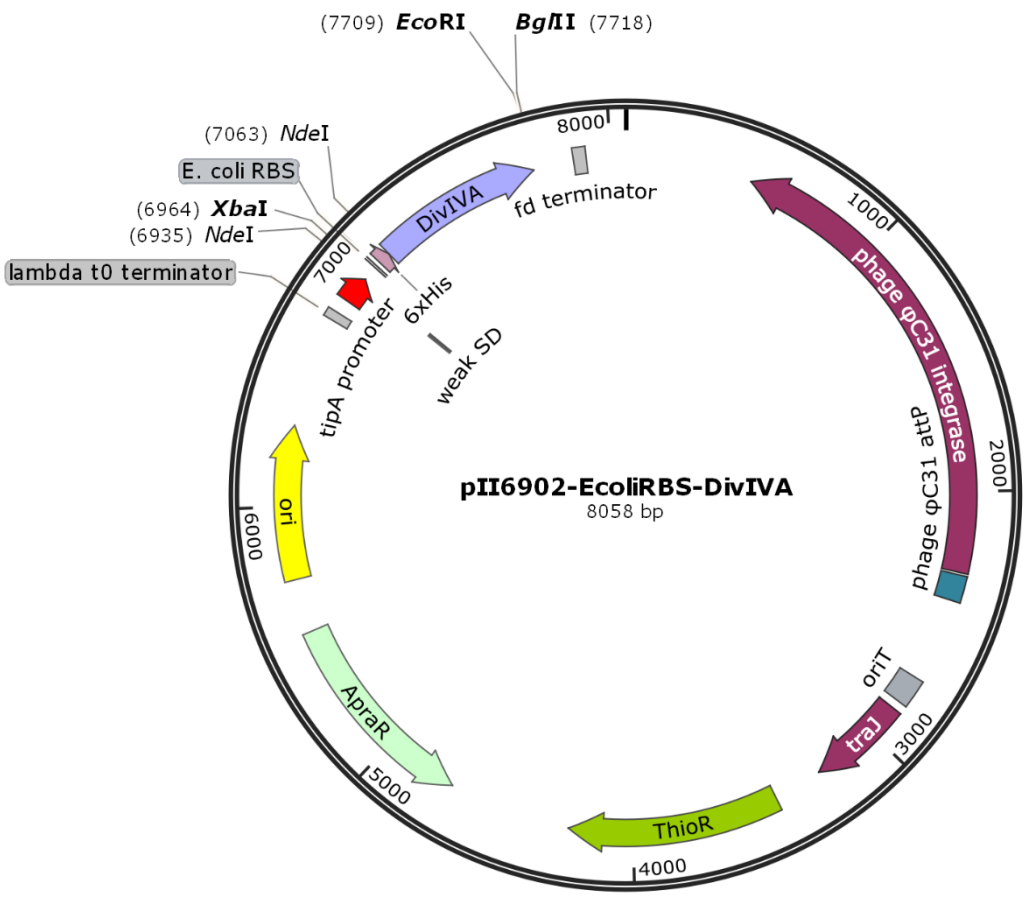


Figure 4.29: The plasmid map of pIJ6902-ERBSdivIVA. The additional overexpression constructs of *hyp*, *parH* and *filP* where generated in the same way, and all have identical upstream regions and His tags.

Interestingly, the predicted TIRs of each construct were identical and matched the TIR of pIJ6902-ERBSsepF of 6275.40 au. This initially seemed odd, however, all constructs share the same upstream region, which therefore contains the same transcription start site and RBS. The distances and sequence between the respective gene and their transcriptional and translational important sequences would be the same and would give the same mRNA when transcribed. The mRNA would have the same structure around the RBS and therefore should give the same value for the predicted TIR when using Salis software.

The constructs were generated in the same fashion as the previous pIJ6902-ERBSsepF. They were then conjugated into the M145 wild-type strain. The exconjugants were screen for viability on thiostrepton containing medium as well as apramycin containing medium, and preliminary characterisation was carried out. However, due to time constraints full characterisation of the strains could not be completed. Therefore, the resulting strains have been generated as a source for the lab and further work will be carried out in the future.

### 4.6. Summary

Overexpression of the P1sepF fragment was attempted for two main reasons, one to determine the effects of *sepF* overexpression, and secondly to determine if the Δ*sepF* mutant phenotype could be rescued.

It became apparent that full complementation of Δ*sepF* was not achievable with the P1sepF fragment, in Chapter 4. This is because the fragment only contained one promoter for *sepF*, not the two necessary for proper *sepF* expression. Therefore, the P1sepF fragment was put under the control of the inducible tipA promoter, which was to act as the second native promoter of *sepF*. However, the expression of P1sepF was not sufficient for full complementation yet again. Even when varying the amount of thiostrepton, the tipA inducer, to change the levels of *sepF* expression did not give a wild-type phenotype to the strain Δ*sepF*/pIJ6902-P1sepF. The times at which *sepF* was induced was varied also, in conjunction with the different amounts of thiostrepton, but none of the combinations of timing and amount of thiostrepton resulted in a wild-type phenotype when viewed microscopically. Macroscopically, the strain seemed similar to the wild-type M145, as it produced spore associated pigment, but this was not true indicator of the stain returning to a wild-type phenotype.

Therefore, it seems that the proper levels and times of expression of *sepF* is well defined and must be controlled. Additionally, that emphasises the importance of the presence of two native promoters for *sepF*, as without the promoters septa produced in aerial hyphae are not formed properly and are irregular.

Attempts to overexpress *sepF* also highlighted the importance of directly applying the tipA inducer thiostrepton to the areas, or ‘tissues’, that will utilise the SepF produced. When thiostrepton was present within the growth medium of Δ*sepF*/pIJ6902-P1sepF the SepF protein was not produced sufficiently in the aerial

hyphae, and the strain resembled the Δ*sepF*/pMS82-P1sepF strain. When thiostrepton was applied to the top of the hyphae and to the aerial hyphae via droplets, it induced the tipA promoter to allow *sepF* expression. The thiostrepton present in the medium was only in direct contact with the vegetative hyphae. The vegetative hyphae are compartmentalised, and this may have prevented the inducer from travelling to the aerial hyphae. Therefore, in *Streptomyces* when using the overexpression system pIJ6902, thiostrepton should be added to the tissues that will utilise the resulting gene product.

Another factor which can affect overexpression when using the vector pIJ6902 is construct design. Certain constructs will not be able to produce overexpression of the desired genes, but may be successful when the same method is used for other genes. Expression is dues to transcription, which must be inducible, and translation, which should be efficient. However, in the pIJ6902 system translation may not be efficient, this is due to construct design resulting in lower TIRs. This was displayed by comparison of the three overexpression constructs, pIJ6902-sepF, which contained only the *sepF* gene, pIJ6902-P1sepf, which contains a native promoter of *sepF*, and pIJ6902-ERBSsepF which contains a *E. coli* RBS upstream of the *sepF* gene. Only the constructs, pIJ6902-P1sepF and pIJ6902-ERBS which contained a site which allowed efficient ribosome binding, were expressed. When the constructs were run through TIR prediction software, the respective TIRs of each indicated that the construct design affects translation, which in turns determines if the gene which should be overexpressed is efficiently expressed.

## Chapter 5: Initial characterisation of the gene *SCO2078*

This chapter will cover the gene *SCO2078*, which is of interest due to its proximity to both *sepF* and *divIVA,* which raised the possibility of a function related to either cell division or polar growth. There is very little literature about protein homologues to SCO2078.

This chapter will present some bioinformatic analysis in relation to gene location, structure and homologues will be covered first, to suggest possible functions for the gene. Following on, a gene knock out was generated and the mutant was confirmed. The phenotype of the *SCO2078* null mutant was characterised, but no major differences between the phenotype of the *SCO2078* mutant and the wild-type strains were found. The *SCO2078* gene was then introduced back into the knock out strain generated and wild-type *Streptomyces*, first to complement the knockout and then to see the effects of overexpression of SCO2078. Overexpression of *SCO2078* was tested further by generating a range of overexpression constructs. However, these experiments were met with varied success, as discussed later.

### 5.1. Bioinformatic analysis of *SCO2078*

*SCO2078* is a small gene, encoding 94 amino acids, and is located in the *ftsZ-divIVA* operon of *S. coelicolor* (Figure 5.1). It shares this operon with the well-known cell division and growth genes *ftsZ*, *sepF* and *divIVA*.

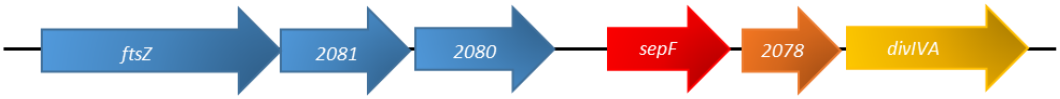


Figure 5.1: The gene arrangement within the *ftsZ-divIVA* operon of *S. coelicolor*.

The function of *SCO2078* is unknown, however, its suggested to be a putative membrane protein on StrepDB, the web server specialised on *Streptomyces* sequences (http://strepdb.streptomyces.org.uk). When the amino acid sequence was analysed using transmembrane prediction software TMpred (Hofmann and Stoffel, 1993), and TMHMM (Krogh et al., 2001)), the possibility of

two transmembrane helices was considered significant. The helices were predicted to be on the outer regions of the putative protein, with approximately 41 amino acids between the two transmembrane domains. This was seen in the preferred and alternative model produced by TMpred, and in the TMHMM prediction plot (Figure 5.2). However, TMHMM also suggested that a potential N-terminus alpha helix may not be a transmembrane domain but a signal sequence. Therefore, a server which can detect the possibility of signal peptides in a sequence, SignalP-4.1 (Petersen et al., 2011), was used to predict the possibility of *SCO2078* containing a signal peptide, by inputting the amino acid sequence and using the parameters for Gram-positive bacteria which may contain a transmembrane domain (TMD). The SignalP-4.1 result did not reach the cut off threshold for the indicator for signal peptides and therefore the N-terminal sequence might not function as a secretion signal.

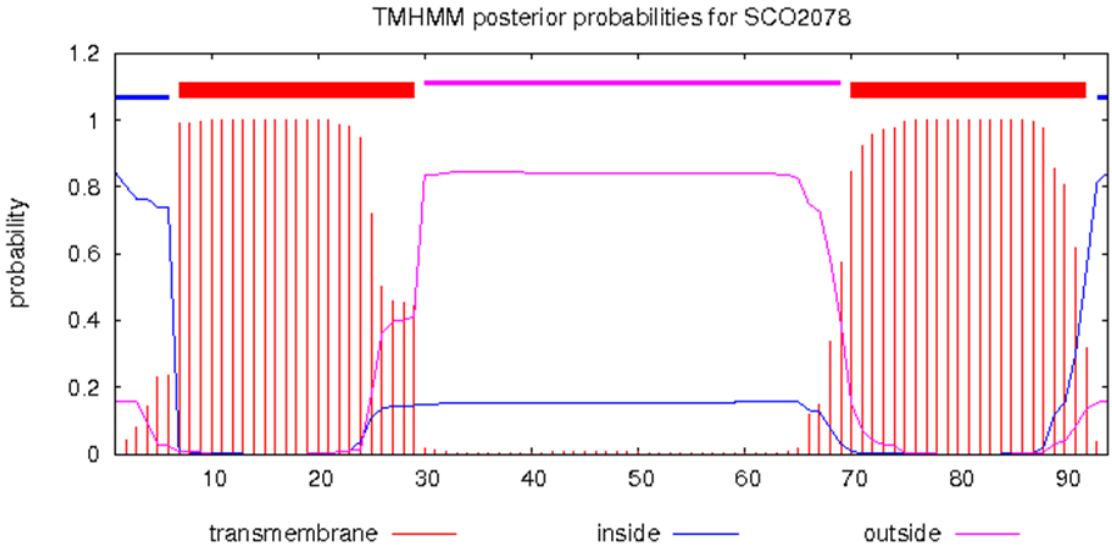


Figure 5.2: *SCO2078* sequence strongly suggests two TMDs. The image was generated using the TMHMM programme. (Image from TMHMM)

The TMHMM programme's prediction (Figure 5.2) is quite unusual, as the two transmembrane domains are suggested to surround the middle fragment, which in the preferred model, is on the outside of the cell membrane.

The protein sequence analysis software PSIPRED (Buchan et al., 2013) also predicted aliphatic helices (Figure 5.3) within the protein, two of which overlap with the TMDs predicted. As transmembrane domains are usually alpha helices this reinforces the model of SCO2078 being a transmembrane protein with two TMDs.

Intriguingly, the amino acids between the two TMDs are thought to be cytoplasmic, when calculated by TMpred and Phobius (Käll et al., 2005) (Figure 5.4) which predicts transmembrane topology and signal peptides. This is the exact opposite that the TMHMM programme predicted, which questions the topology predicted for this protein. Additionally, the Phobius software did not suggest that the sequence contained a signal peptide, reconfirming the prediction from the SignalP-4.1 program. The PSIPRED model also predicted that the amino acids contained within the middle of the protein could potentially form two helices (Figure 5.3).

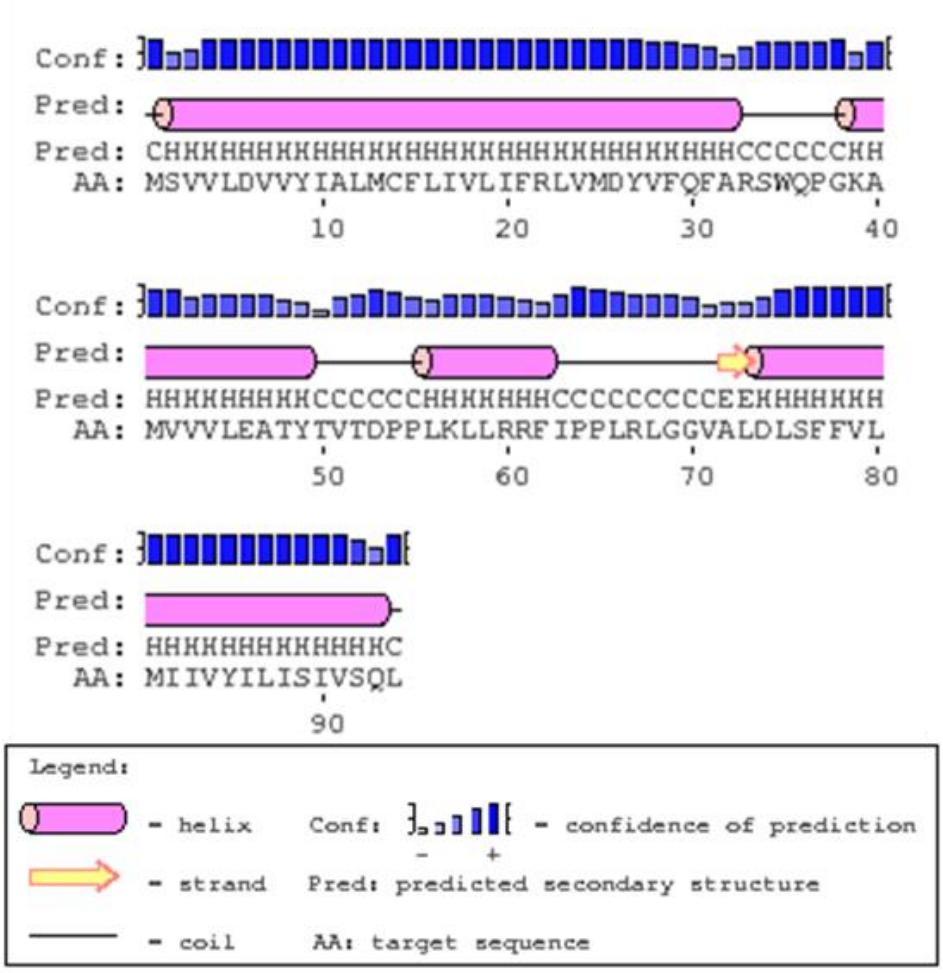


Figure 5.3: PSIPRED results for SCO*2078* show a number of helices.

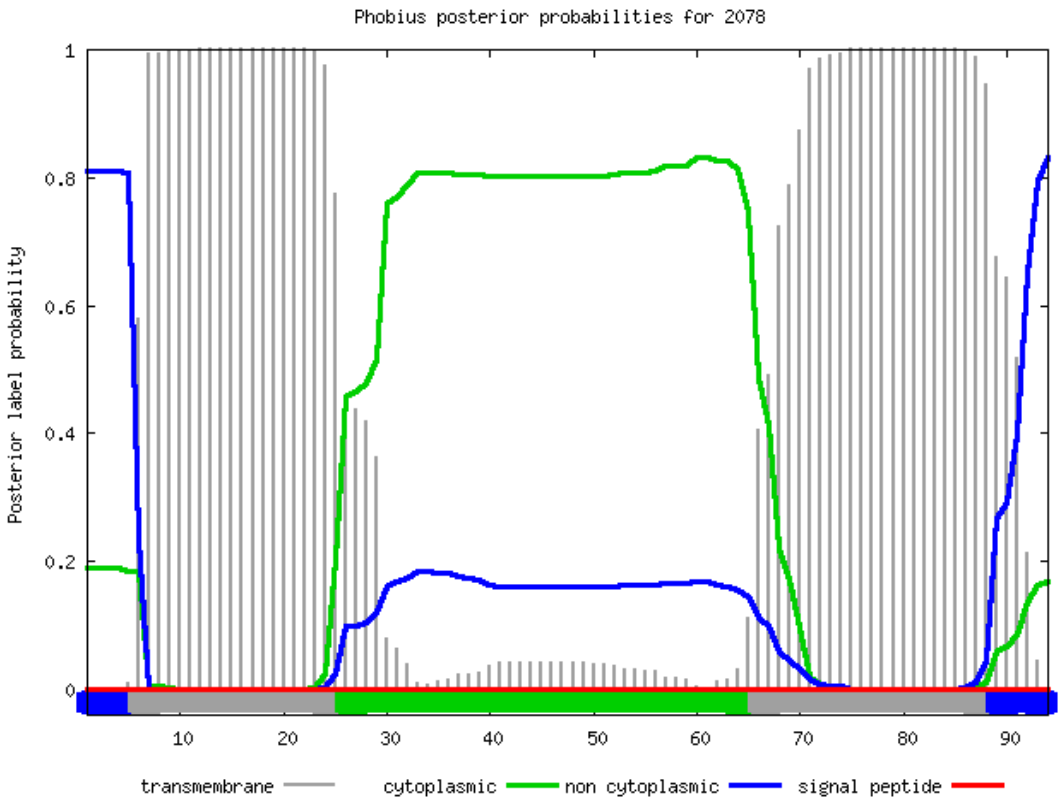


Figure 5.4: Phobius generated chart of probabilities of SCO2078 containing transmembrane domains and cytoplasmic stretches.

To determine if there were any *SCO2078* homologues and their possible roles, *SCO2078* was searched for on the pFam database (Figure 5.5) (Finn et al., 2016). This revealed that *SCO2078* was part of the YGGT family, and that *SCO2078* homologues are documented as *YGGT* in other organisms. The YGGT family is simply defined as containing a repeat conserved in hypothetical integral proteins. There are a number of domain architectures associated with the YGGT family, but this study is focused on architecture which is similar to that of SCO2078. The sequences in the chosen domain architecture were grouped together as they contain one repeat of approximately 80-90 amino acid residues. This is similar to SCO2078 which contains 94 amino acids in total, as opposed to the other architecture groups which were all double the size of SCO2078 or larger. Additionally, the architectural group chosen contains the highest amount of SCO2078 homologues, with a surprising 4054 homologues detected in the pFam database. The other 9 architectural groups containing wither one or two homologues each (with the exception of one architectural group which is defined by containing two YGGT repeats, which contained other 1000 SCO2078 homologues).

Of the species identified by the pFam search the majority were bacterial, however, approximately 93 eukaryotic species contained a YGGT homologue. The eukaryotes species identified contained a total of 288 homologues which contained the YGGT domain. The eukaryotic species were plants, and the genes containing the YGGT repeat have been assigned the name *ylmG*. There is very limited information about role of the YlmG protein, but the sequences are believed to be found within chloroplasts. YlmG has been investigated in the plant *Arabidopsis thaliana* and also in the cyanobacterium, *Synechococcus elongatus.* Interestingly the *Arabidopsis* gene, AtYLMG1 has been identified as a result of a search for genes affecting chloroplast division (Kabeya et al., 2010). Evolutionally chloroplasts are thought to have derived from a bacterial endosymbiont, which was likely an ancient cyanobacteria. Chloroplast division, similarly to bacterial cell division, relies on an FtsZ protein (Osteryoung et al., 1998, Vitha et al., 2003), which forms a ring at the chloroplast division site. Moreover, similarly to *E. coli*, MinD and MinE-like proteins control FtsZ localisation in the chloroplasts (Colletti et al., 2000, Itoh et al., 2001), suggesting that chloroplast division is controlled by a mechanism inherited from bacteria. Both the knockdown and overexpression of AtYLMG1 affected chloroplast nucleoid partitioning, whilst the overexpression of AtYLMG1 also affected chloroplast division (Kabeya et al., 2010). The Δ*sylmG1* knockout mutants of the cyanobacterium *S. elongatus* showed more compact nucleoids whilst the overexpression of *SylmG1* generated longer cells with uneven DNA distribution, suggesting that the nucleoid segregation defects in the overexpression strain also affected division (Kabeya et al., 2010).

Within plants YlmG has a role in cell division, where it is involved in the distribution of nucleoids. It is thought that this role may be conserved in cyanobacteria as well as chloroplasts, as the gene has a bacterial origin. The *ylmG* homologue of *SCO2078* in plants seems to have a clear function and this may be conserved within *S. coelicolor*.

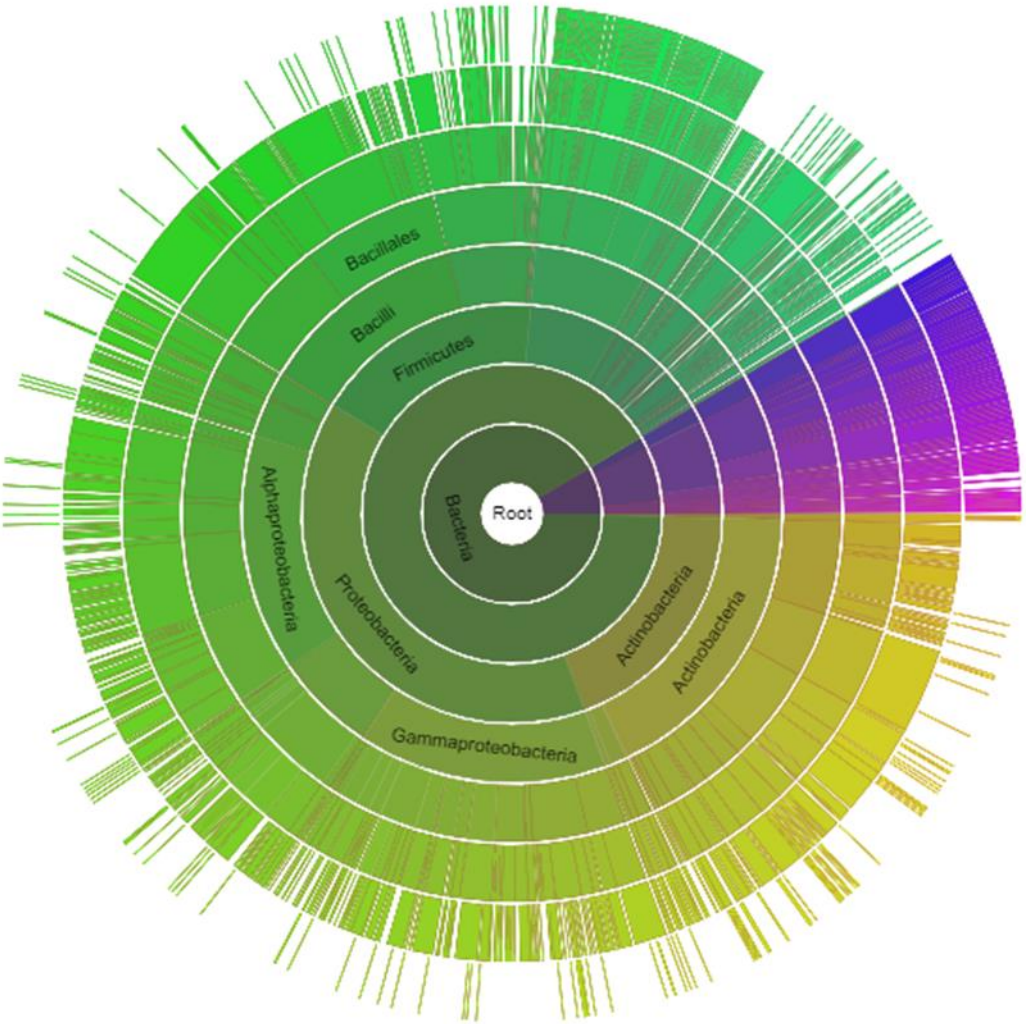


Figure 5.5: The sequence distribution of SCO2078 homologues with organisms. Green and yellow areas are bacterial species and the purple and blue show eukaryotic species (sunburst generated by pFam).

Then STRING DB (Szklarczyk et al., 2017), a database which protein-protein interaction networks, was searched to determine if any other known homologues of *SCO2078* have putative or known functions. Searches used the terms YGGT and YlmG. Both searches were necessary as each gave different set of hits, with only a small amount of overlap (12 homologues).

Many of the protein descriptions of the homologues were noted as putative or hypothetical, though *ylmG* was noted to be a gene encoding a cell shape determination protein for Carnobacterium sp. 174, an integral membrane protein for *Chlamydophila felis* and *Leuconostoc gasicomitatum*, membrane protein for *Parachlamydia acanthamoebae* and *Simkania negevensis*, and a cell division

protein for *Lactobacillus rhamnosus* and *Melissococcus plutonius*. However, there were no publications associated with these statements, therefore, the reason for the allocation of these specific functions are questionable.

The YGGT search also gave similar results, though there were notably a greater number of hits. In addition to YGGT being noted to have the various functions mentioned in the previous search, it was also noted to be an integral membrane resistance protein, inner membrane protein, resistance protein, an endopeptidase, 'required for the proper distribution of nucleoids in chloroplasts' which 'may be related to chloroplast division processes', and an 'integral membrane protein YggT, involved in response to extracytoplasmic stress' (Ito et al., 2009).

As large number of homologues have been identified, and variation of possible functions, several bacterial representatives were chosen to be compared (Table 5.1). Eukaryotes were excluded in this comparison, as Kabeya et al (2010) have described three groups in the YGGT family, with emphasis on the two eukaryote containing groups. The comparison uses bacteria which would be part of the third group. The bacteria chosen are model organisms and carry an *SCO2078* homologue.

Table 5.1: The location of *SCO2078* homologues within other bacteria. The proposed gene functions of the homologues as referenced in KEGG (Kanehisa et al., 2016) or STRINGDB (Szklarczyk et al., 2017) are also included.

| Organism | Gene name | Characterised or predicted function | Nearby *ftsZ* and *divIVA* genes | Possible transmembrane domains |
|---|---|---|---|---|
| *Streptomyces coelicolor* | *SCO2078* | Putative membrane protein | Between *sepF* and *divIVA* | 2 transmembrane helices (6-25, 66-88) |
| *Staphylococcus aureus* | *ylmG* | Hypothetical protein | *SepF*, *ylmH*, *ORF* (*divIVA*) | 2 transmembrane helices (12-33, 59-80) |
| *Corynebacterium glutamicum* | *cg2362* | Hypothetical protein | *SepF* | 2 transmembrane helices (6-25, 75-94) |
| *Mycobacterium tuberculosis* | *MT2205* | Transmembrane protein | *SepF* and *wag31* (*divIVA*) | 2 transmembrane helices (33-57, 107-127) |
| *Bacillus subtilis* | *ylmG* | Transmembrane protein | *SepF, ylmH, divIVA* | 2 transmembrane helices (6-25, 56-76) |

All the compared homologues of *SCO2078* are encoded by genes located in the vicinity of *sepF* and *divIVA*.

Though the function of SCO2078 is not clear, it may be important within the genome for other reasons. In a genome wide search for promoters by Jeong et al (2016), a potential transcription start site (TSS) for the downstream gene *divIVA* was identified within the *SCO2078* gene. The TSS has been mapped to the position

2231962 bp. This places it roughly in the middle of *SCO2078*, which starts at 2231834 bp and ends at 2232118 bp.

The *SCO2078* gene has also been identified as potentially producing three transcripts, a primary, which was shown to produce a relatively high abundance, a secondary transcript, which has a much lower abundance, and an antisense transcript, which has the lowest abundance (mapped reads) of the three (Jeong et al., 2016).

### 5.2. Characterisation of a *SCO2078* knockout mutant

To understand the role of *SCO2078* a knockout strain was produced in lab by other lab members. The generated knockout mutant was then characterised macroscopically and microscopically.

#### 5.2.1. Characterisation through macroscopic observation

Macroscopic observation was carried out to test if the knockout strain Δ*SCO2078* differed from the wild-type M145 strain. To do this, spore preparations of both M145 and Δ*SCO2078* were generated and were streaked onto soya flour media (SFM), to produce confluent and single colony areas. This would allow to distinguish any differences between the strains at different stages of growth. The spores were inoculated at the same time and grown in the same conditions of 30°C for 7 days.

The two strains grew at similar rates. The Δ*SCO2078* strain was initially white, progressing to a brown and then grey pigmented state, much like the wild-type M145 strain. This indicates that Δ*SCO2078* can progress through all the developmental stages of vegetative and aerial growth, as indicated by the white and brown stages (respectively). The grey stage, which occurs when the aerial hyphae have matured into spore chains, leads us to believe that Δ*SCO2078* is able to sporulate (Figure 5.6).

Though there were no observable differences macroscopically, it is possible that there were microscopic differences during hyphal development or spore production. To test this would require microscopy to note any changes to hyphal and spore morphology due to the Δ*SCO2078* knockout.

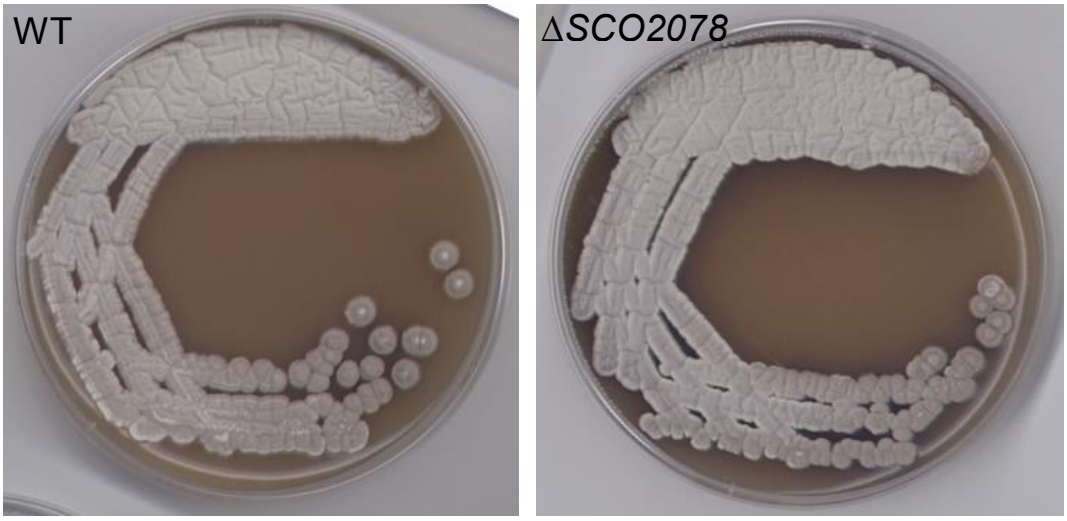


Figure 5.6: **Δ*SCO2078* (right panel) and the wild-type M145 (left panel) when grown on SFM medium at 30°C for 7 days.** The two strains are very similar in appearance.

### 5.2.2. Microscopy analysis of the Δ*SCO2078* knockout strain

To test if there were indeed any differences between the wild-type M145 and Δ*SCO2078* strains, a series of microscopy experiments were performed.

This was achieved through cover slip microscopy, were 1 µl of spore preparations was spread onto deep SFM plates in a small rectangle area that is slightly larger than a cover slip. Then a cover slip was inserted into the media at an angle of approximately 60-70 degrees at the location of the spore rectangle. This would allow aerial hyphae to grow onto either side of the cover slip. Therefore, it was possible to investigate the aerial hyphae at different points of development. Several time points for each strain where tested, so to collect hyphae before, during and after sporulation. The hyphae were fixed to preserve the time point's developmental stage using methanol, and then stained. To observe any differences in cell wall and DNA distribution, two different fluorescent dyes were used on each cover slip sample. The dyes were Wheat Germ Agglutinin (WGA) with an Alexa Fluor 488 conjugate, and propidium iodide (PI).

The cover slips were viewed using fluorescence light microscopy at x100 magnification using a phase contrast filter and under two different waves of UV light so to highlight areas of cell wall growth (WGA) and DNA (PI), with images taken at all three channels (Figures 5.7 and 5.8).

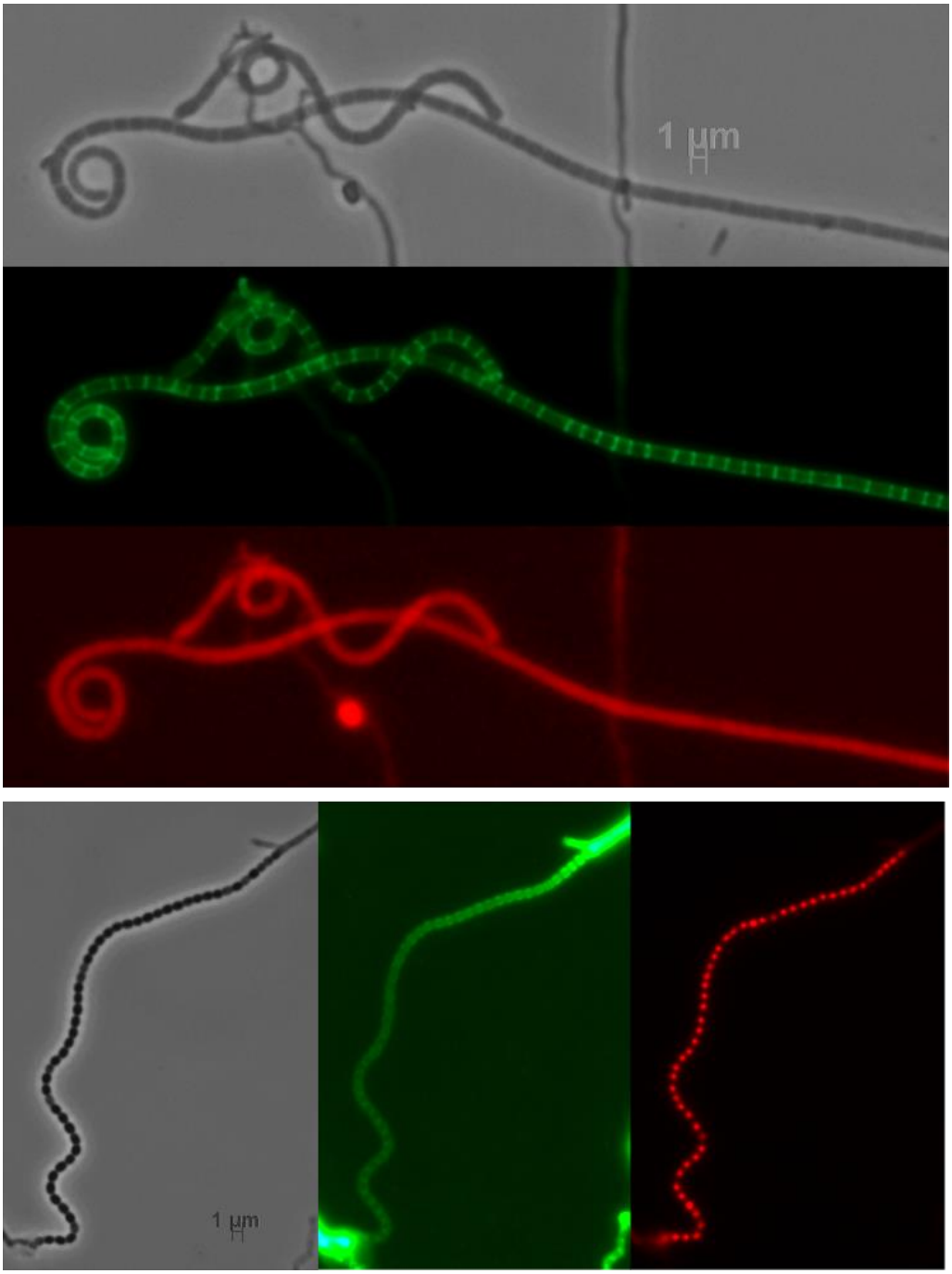


Figure 5.7: Δ*SCO2078* viewed using epi-fluorescence microscopy. Aerial hyphae for Δ*SCO2078* were imaged using phase-contrast (top and left panels), UV light to excite green fluorophore of WGA (middle panels), and UV light to excite red fluorophore of PI (bottom and right panels).

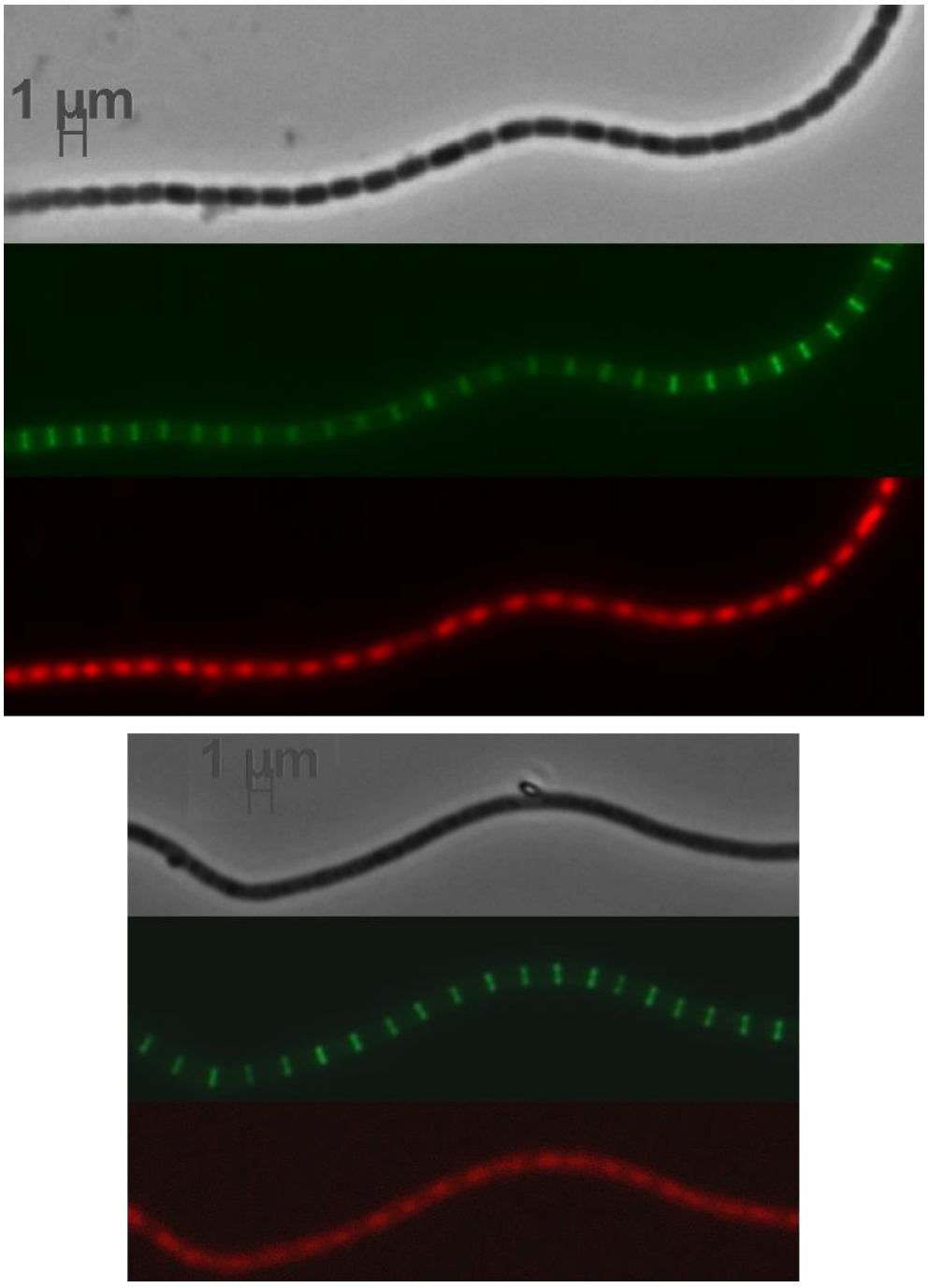


Figure 5.8: Δ*SCO2078* viewed via epi-fluorescence microscopy (top set panels) compared to the wild-type M145 (bottom set panels). Top grey panels are phase contrast images, middle green panels are WGA stained, and bottom red are PI stained.

After the initial observations of the strains at the various time points, it seemed that Δ*SCO2078* and M145 were similar (Figure 5.8), but there were some subtle differences in the distance between sporulation septa (Figure 5.7 top panel) within the aerial hyphae which prompted further analysis of the images.

To quantitatively analyse any potential differences the images were scaled and measured using AxioVision software. The measurements taken were the distance from the middle of one septum to the middle of the adjacent septum. These distances were measured at the stages when the septa where still being formed in the aerial hyphae as this point of development would show the septa clearly, as the WGA-Alexa Fluor 488 dye would stain strongly due to both of WGA's targets being present in high amounts. Later stages of aerial hyphae development would show septa, but weakly, and at earlier time points the septa would not yet be present.

Septa to septa distances were chosen to be measured as they would give indication to future spore size and therefore if the septa localisation had been affected. The data was then collected and processed into frequency graphs, so to easily observe any differences (Figure 5.9).

After this analysis, it was found that the Δ*SCO2078* mutant and wild-type M145 strains do exhibit some differences with their respective average sporulation septa to septa distance and thus spore size (Figure 5.9). The modal value for the septa to septa distances for M145 was 1.3 µm with an average distance of 1.21 µm, while modal distance was smaller for Δ*SCO2078* at 1.1 µm with an average distance of 1.15 µm. Additionally, a larger range of septa lengths was observed for Δ*SCO2078*, with the smallest lengths observed for Δ*SCO2078* being almost half the size of the smallest lengths recorded for M145. However, the upper range of both strains did not differ greatly. There was an overall shift of frequency towards smaller lengths in the Δ*SCO2078* strain. (Figure 5.9)

This means that Δ*SCO2078* and M145 strains do differ, on a microscopic level, suggesting that the absence of SCO2078 from the *S. coelicolor* genome somehow affects septa to septa differences in aerial hyphae, and therefore spore size, though other stages of development do not seem to be affected. Earlier mentioned was a study in which a gene encoding an *SCO2078* homologue, *ylmG*, was knocked out of *A. thaliana (Kabeya et al., 2010)*. The effect observed by knocking out the *Streptomyces SCO2078* is very different from the effect observed when a knockout of *ylmG* of *A. thaliana* was characterised. This latter mutation resulted in nucleoids taking on higher order structures. If the Δ*SCO2078* mutant

resulted in higher order structures within DNA then the possibility of multiple chromosomes or larger DNA packets within individual spores would have been expected, but this was not observed.

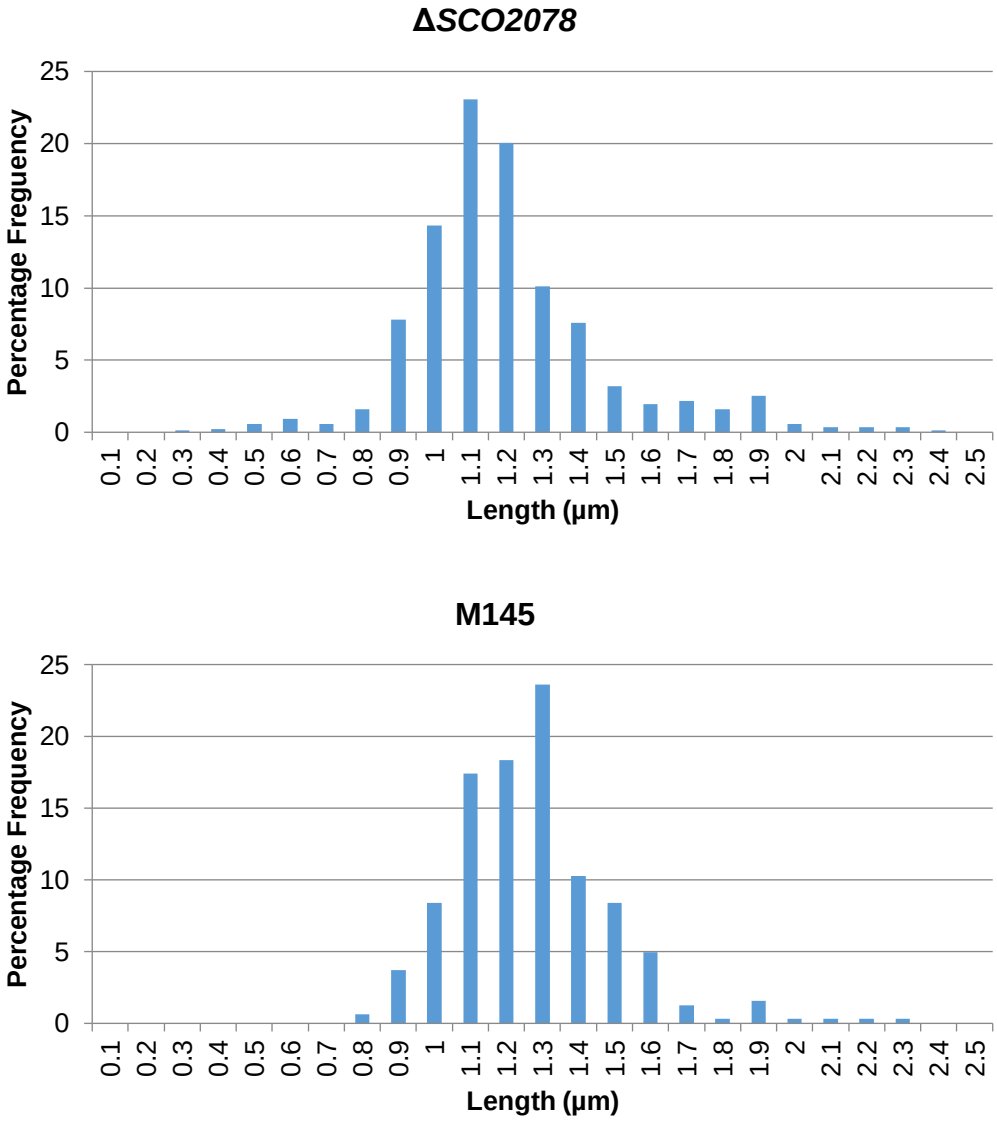


Figure 5.9: **Septa to septa distances of aerial hyphae in Δ*SCO2078* compared those in M145**. Δ*SCO2078* shows a shift towards smaller compartment sizes compared to M145. 872 samples were measured for Δ*SCO2078*, and 406 samples for M145.

The phenotypic differences between the wild-type and the Δ*SCO2078* knockout produced are subtle. This subtle difference and that *SCO2078* potentially contains a transcriptional start site for the essential gene *divIVA*, led us to consider that *SCO2078* may have not been fully replaced with an apramycin resistance

cassette. Therefore, the mutant strain was again tested for the presence of the apramycin resistance cassette and the absence of *SCO2078.*

### 5.2.3. Confirming the Δ*SCO2078* knockout mutant

To confirm if the Δ*SCO2078* strain is a true knockout mutant a series of PCRs were designed and implemented.

The *SCO2078* gene was originally knocked out using the Redirect Technology (Gust et al., 2002), in which the entire gene is replaced by an apramycin resistance cassette. The genome organisation can be tested performing a set of PCR reactions using chromosomal DNA isolated from both the wild-type and mutant strains.

To confirm that the *SCO2078* gene was replaced by the apramycin resistance cassette in the mutant strains, different primer pairs were designed to test for the presence or absence of the *SCO2078* gene, and for the presence or absence of the apramycin cassette at the correct gene location (Figure 5.10 and Table 5.2).

Table 5.2: **The oligonucleotide primer pairs and the expected PCR products used confirm the presence or absence of *SCO2078* and the apramycin resistance cassette.**

| | **Primer Pairs** | **Expected sizes using the wild-type chromosomal DNA and the 4A10 cosmid** | **Expected sizes using the Δ*SCO2078* chromosomal DNA and the cosmid DNA 4A10 Δ*SCO2078*** |
|---|---|---|---|
| 1 | 2078 XbaBgl FRW<br>sepF 3 END | 421 bp | No product |
| 2 | 2078 XbaBgl FRW<br>2078 3 END | 779 bp | 1877 bp |
| 3 | 2078 XbaBgl FRW<br>Apra 5' Rev | No product | 417 bp |
| 4 | Apra 3' FRW<br>2078 3 END | No product | 309 bp |

As the knock out process requires two double crossover steps, once in the cosmid and then after the conjugation, to successfully knockout the gene, DNA from both double crossover stages was tested. This required the cosmids 4A10 and 4A10/Δ*SCO2078,* and chromosomal DNA from wild-type M145 and three putative Δ*SCO2078* strains.

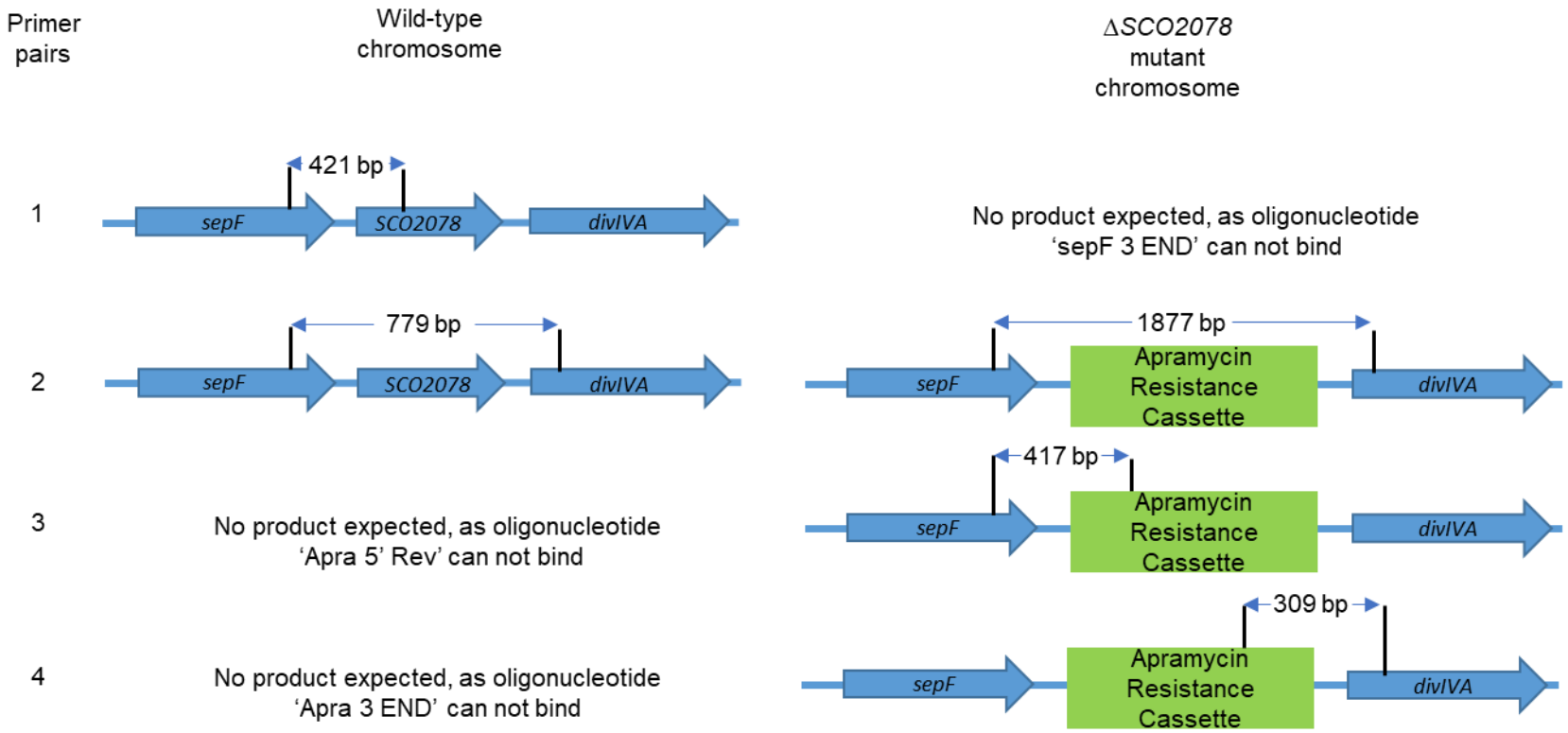


**Figure 5.10: Oligonucleotides that were designed to distinguish between the wild-type and mutant chromosomes are shown.**

The first primer pair, 2078 XbaBlg FRW and sepF 3 END, with sepF 3 END priming inside the *SCO2078* gene (Figure 5.10), should generate a 421 bp product when using the wild-type chromosome as a template during the PCR, but there should be an absence of product when using the Δ*SCO2078* mutant as a template, as sepF 3 END should not prime if the gene is completely replaced by the apramycin resistance cassette. The second primer pair, 2078 XbaBgl FRW and 2078 3 END, both prime outside the *SCO2078* gene location. This means there should be a product generated in the PCR using both the wild-type and mutant chromosomes as templates. The wild-type chromosome template would give a 779 bp product while the mutant should give a larger 1877 bp product as the apramycin resistance cassette is larger than the *SCO2078* gene (Table 5.2). The third primer pair, 2078 XbaBgl FRW and Apra 5' Rev, should only give a 417 bp product when using the mutant chromosome template as the Apra 5' Rev should only prime to the apramycin resistance cassette. The last primer pair, Apra 3' FRW and 2078 3 END should again confirm the presence of the apramycin cassette in the mutant and the absence in the wild-type, as the primer Apra 3' FRW should only anneal to the complementary sequence in the mutant chromosome.

The PCR reactions were optimised, taking into consideration the melting temperature of the oligonucleotides and the length of the expected products. For the second primer pair, where the expected sizes of the products are very different (779 bp and 1877 bp), 2078 XbaBgl FRW and 2078 3 END, two different PCR conditions were designed, which were optimised for either the short or long product length.

**The apramycin resistance cassette is present in the mutant strains**

The presence of the apramycin resistance cassette within the Δ*SCO2078* strains was confirmed by the third and fourth primer pair PCRs. The third primer pair only shows a singular product when the mutant chromosomes were used as templates for the PCR and the product is approximately the correct size of 417 bp (Figure 5.11 and Table 5.2). There is, as predicted, no product for the wild-type chromosomes as the oligonucleotide Apra 5 Rev requires the apramycin resistance cassette to be present to anneal, therefore the PCR products cannot be produced when only one oligo of the primer pair (2078 XbaBgl FRW) corresponds to the DNA.

Figure 5.11 section 4 shows, when the mutant strains were used as PCR templates the results were strong singular bands at the correct size of 309 bp (Table 5.2). The wild-type DNA when used in the fourth primer pair PCR reaction should

not give the 309 bp band. This is the case for both the wild-type M145 and wild-type 4A10 cosmid, with the wild-type M145 lane being completely clear of bands. There are two bands seen for the wild-type 4A10, but they are approximately ~200 bp and ~1000 bp in length (respectively), and therefore differ greatly from the 309 bp band that indicates the presence of the apramycin resistance cassette being present in the wild-types. The presence of these extra bands is thought to be due to non-specific binding of the oligonucleotides, as the 4A10 cosmid is 43 Kbp in length and could contain similar sequences (in part) to the apramycin resistance cassette.

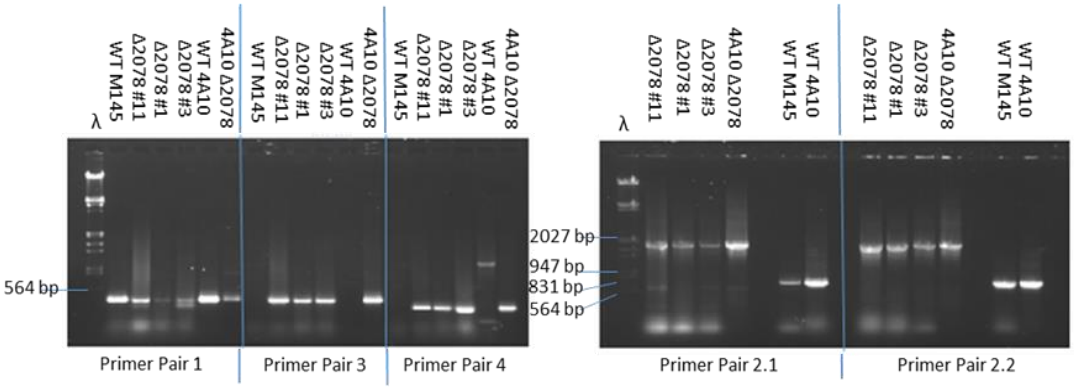


Figure 5.11: Wild-type and Δ*SCO2078* mutant DNA templates show that the absence and presence of the apramycin resistance cassette and 2078. The DNA template are shown above the lanes and the primer pairs used in the PCR can be seen from the number below the images, which correspond directly to Table 5.2. The ladder used was lambda DNA digested with EcoRI and HindIII. There are multiple putative Δ*SCO2078* mutants, with Δ*SCO2078* #11, #1 and #3 being used in this series of experiments.

Though the presence of the apramycin resistance cassette has been confirmed through PCRs 3 and 4, the full replacement of the *SCO2078* gene and therefore the absence of *SCO2078* sequence needs to be confirmed. This was done using the PCRs 1 and 2.

The first primer pair PCR should show a product that is only present for the wild-type templates, however, Figure 5.11 shows otherwise. The wild-type chromosomal templates do show the correct bands as expected, but there are also bands present for each of the mutants tested. These bands, though not as strong as the ones present for the wild-types, do seem to be at 421 bp which is the predicted size if the *SCO2078* gene was still present (Table 5.2). However, other bands can be seen for some of the mutants. The cosmid Δ*SCO2078* mutant also has a band at ~850 bp and Δ*SCO2078* #1 and #11 both have a band ~320 bp in length. The Δ*SCO2078* #3 has an additional band ~1100 bp in length. These multiple products

from the mutant templates suggest non-specific binding, though the bands that are equal to the wild-type 421 bp implies that the mutants may contain the *SCO2078* gene or at least a partial *SCO2078*, as the oligo sepF 3 END only requires 119 bp of the end of *SCO2078* to completely anneal.

The idea that the apramycin resistance cassette did not fully replace the *SCO2078* gene is further suggested by the results of the second PCR. When the conditions were optimised for the longer bands in the PCR 2.1, all the samples gave the expected results of the shorter 779 bp fragments for the wild-type templates and the larger 1877 bp fragments for the mutants (Table 5.2). However, optimisation of the PCR conditions, to show the smaller bands characteristic of the wild-type strain clearly when the mutant strains were tested (Figure 5.11). These bands seem to be slightly smaller than the bands expected for the wild-type products. This again suggests that the apramycin resistance cassette might not have fully replaced the *SCO2078* gene.

The gel electrophoresis of the PCR results seems to suggest that the apramycin resistance cassette was introduced into the putative mutants, but the *SCO2078* gene may have not been fully replaced.

However, this may not be the case, and it is possible that the apramycin resistance cassette did fully replace the *SCO2078* gene, but only in a low number of the *Streptomyces* spores used in the conjugation. The DNA templates used in the PCRs to test for the absence and presence of the *SCO2078* gene was collected initially from spore preps from multi-genomic plates. Therefore, it is possible that the DNA tested could be a mix of strains, which could explain why certain bands were present in the PCR using 2078 XbaBgl FRW and 2078 3 END. The strains present could be a mixture of the knockout mutant, in which the *SCO2078* gene is fully replaced, and another strain in which the *SCO2078* gene and the apramycin resistance cassette are both present. This is possible if during the knockout process a single recombination event took place, instead of a double recombination event which is required to remove the *SCO2078* gene. The single recombination event would transfer apramycin resistance to the cell and therefore it could not be used to select between the single and double recombinants, making this event hard to detect.

To test if this is the case, the mutant strain Δ*SCO2078* #3 was subject to a series of experiments to see if it is possible to separate the putative Δ*SCO2078* spores from any of the original mixed stocks. Single colonies from the Δ*SCO2078*

#3 stock were used to generate five new stocks. These were used to collect chromosomal DNA and DNA preps which were then tested using the same PCR conditions and oligonucleotides used above for the PCR sets 1, 2.1 and 2.2. The PCR conditions 3 and 4 were not retested, as they are only indicative of the presence of the apramycin resistance cassette at the correct location, but they are unable to establish the absence of the wild-type copy. The Δ*SCO2078* #3 strains were being used to attempt to separate the potentially mixed stocks, as the PCR products of the original Δ*SCO2078* **#**3 mutant did not give strong 'wild-type bands', suggesting that, if the DNA original tested is a mix of the knockout and the single recombination mutant, then there are less single recombination samples in these stocks then compared to the Δ*SCO2078* #11 mutant. However, there was not enough time to characterise the five new stocks generated from the original Δ*SCO2078* #3 stock by streaking for several rounds of colonies.

## 5.3. Introducing the *SCO2078* gene into Δ*SCO2078* and the wild-type M145 strains

The *SCO2078* gene was reintroduced into the putative Δ*SCO2078* mutant and the wild-type M145. A similar construct design was used to carry the *SCO2078* gene as the *sepF* constructs described in Chapter 3.

### 5.3.1. Construct generation

The plasmid pMS82 was used as the vector for cloning of the *SCO2078* gene. The description of the plasmid pMS82 is found in Chapter 3.

The *SCO2078* gene was generated using high fidelity PCR with the primers designed to anneal to sequences either side of *SCO2078* (Table 5.3 and Figure 5.12). The size of the PCR generated fragment is 779 bp, with the *SCO2078* gene itself only 258 bp. The construct was designed to contain some of the upstream sequence of *SCO2078* in order to allow potential close promoters to be included in the construct fragments. As the promoter or potentially multiple promoters for *SCO2078* had not yet been identified, an estimation on the promoter location had to be made.

The forward oligonucleotide 2078 XbaBgl FRW was designed previously and contains XbaI and BglII restriction sites, however, these sites were not used in this set of experiments.

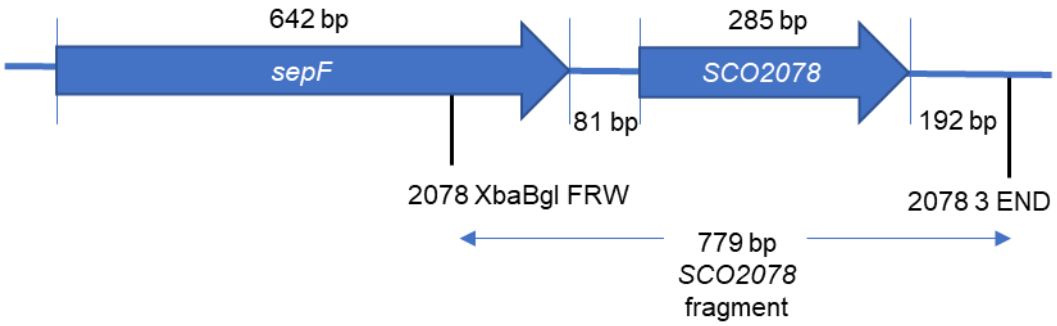


Figure 5.12: **The fragment design for *SCO2078*.** The names and positions of the oligonucleotides used to generate the construct pMS82-SCO2078 and the surrounding DNA region from the 4A10 cosmid are shown. The positions of the oligonucleotides are shown by the black lines. Measurements of DNA fragments are shown in base pairs.

Table 5.3: **The oligonucleotide primer pairs and the expected size of the PCR product** when using the wild-type 4A10 cosmid DNA as a template.

| | **Primer Pair** | **Expected size of fragments** |
|---|---|---|
| *SCO2078* | 2078 XbaBgl FRW<br>2078 3 END | 779 bp |

### Generation of the pMS82-SCO2078 plasmid

High fidelity Phusion PCR was performed using the primer pairs (Table 5.3) to produce a DNA fragment carrying *SCO2078*. The PCR product was confirmed through gel electrophoresis (Figure 5.13) and was then phosphorylated with T4 kinase and phenol extracted.

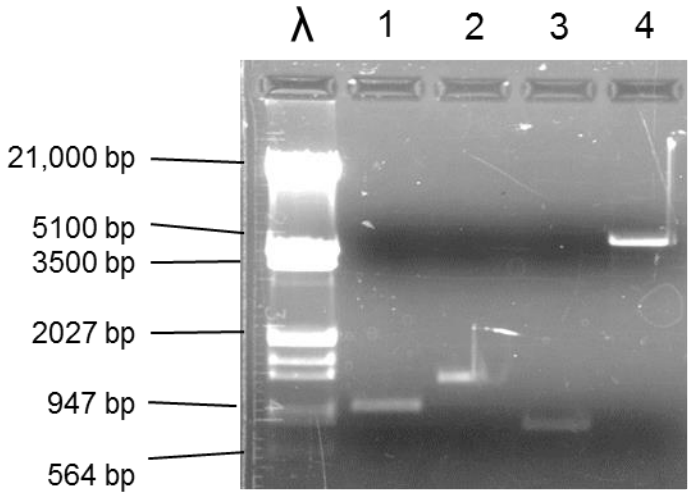


Figure 5.13: **The Gel Electrophoresis of the Phusion PCR products.** The sizes of the PCR Phusion product for *SCO2078* is in lane 3, and the pMS82 plasmid after digestion with EcoRV and gel extraction is in Lane 4. (The other lanes contain PCR products not relevant to this chapter). Lambda DNA was digested with EcoRI and HindIII and used as a size marker.

The DNA fragments generated by the Phusion PCR were introduced into the pMS82 vector which had been digested with EcoRV (Figure 5.13). The vector was dephosphorylated beforehand to block relegation of pMS82 as the single digestion with EcoRV generated blunt ended products, which without dephosphorylation would have re-joined during ligation.

The ligation reaction set up between the de-phosphorylated pMS82 and the phosphorylated PCR product were desalted and introduced into *E. coli* DH5α competent cells using electroporation.

**Confirmation of the Recombinant Clones**

The transformed DH5α cells were selected for on a growth medium of LB lacking salt but containing hygromycin. The resulting colonies were then screened using colony PCR, to ensure selected colonies did contain the *SCO2078* DNA and not a copy of a self-ligated plasmid.

The colony PCR used the same primer pairs that were used to produce the PCR product, therefore the expected sizes should be as shown in table 5.3. After a series of colony PCRs positives were found for the clone containing pMS82-SCO2078 (Figure 5.14).

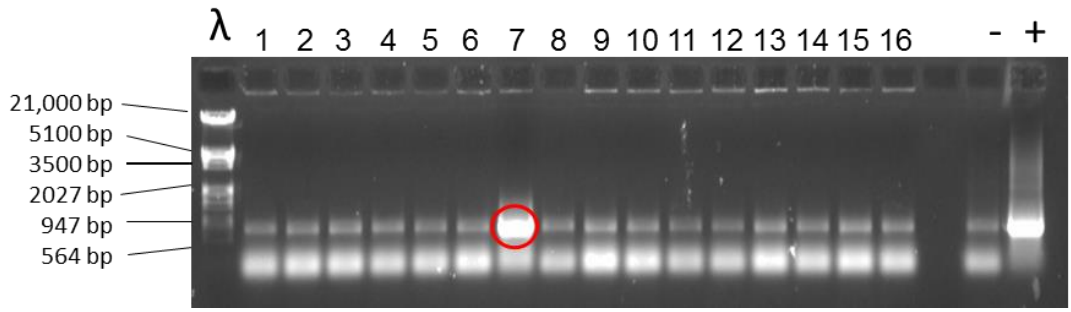


Figure 5.14: Colony PCR for screening for recombinant clones. Lambda DNA digested with EcoRI and HindIII was used as a size marker. The positive clone was recognised by its strong PCR product which is the same size as the positive control. One positive recombinant clone was found to carry *SCO2078* as shown by the red circle (Lane 7). The positive control was pGEM-2078 generated earlier and the negative control was pMS82/ftsZ-2080 a plasmid that did not contain the *SCO2078* gene.

**Sequencing and confirmation of the pMS82-SCO2078 plasmid**

In order to confirm the putative positive clone, a plasmid preparation was performed and the plasmid was sequences. The sequencing confirmed the pMS82-SCO2078 plasmid carrying the *SCO2078* gene.

**Conjugating the fragments into *S. coelicolor***

The *E. coli* strain ET12567 (pUZ8002) was chosen to be transformed with the pMS82-SCO2078, and act as the donor during conjugation. This is as it contains the pUZ8002 plasmid which facilitates the conjugation of pMS82 by providing the *tra* gene which is required in order to transfer the DNA between the donor ET12567 and receiver *Streptomyces*. This mobilises the pMS82, but pUZ8002 is not able to cross into *Streptomyces* ensuring only the plasmid of interest is transferred. Additionally, *Streptomyces* does not readily accept all donors during conjugations, due to a system in which it will restrict certain methylated DNA (González-Cerón et al., 2009). ET12567 (pUZ8002) is able to bypass this problem as it is methylation deficient (Gregory et al., 2003).

The conjugations set up were using the *Streptomyces* strains Δ*SCO2078* and the wild-type M145. Each of these strains were conjugated with the construct pMS82-SCO2078 and an empty pMS82 vector to act as control. The exconjugants were selected using hygromycin.

Selected exconjugants were stored as spore preparations and were characterised by first monitoring their growth. It was expected that the introduction of pMS82-SCO2078 into the knockout strain should return the knocked-out strain to a wild-type phenotype. The Δ*SCO2078* strain should also be complemented by the *SCO2078*, though the effects may not be as observable as the differences between the knockout and wild-type are not easily marked.

Additionally, the introduction of the constructs into the wild-type M145 strain could give an indication of the dosage effects, as the *SCO2078* gene would be duplicated.

### 5.3.2. Characterising the conjugated strains

The Δ*SCO2078* strain when conjugated with pMS82-2078 showed no major differences in its appearance when grown on SFM medium, however, this was expected as the Δ*SCO2078* and the wild-type are macroscopically very similar.

When pMS82-SCO2078 was introduced into the wild-type M145, there were no obvious changes in the appearance of the vegetative or aerial hyphae.

The exconjugant strains were also investigated though microscopy analysis to see if the Δ*SCO2078* strain had been returned to the full wild-type phenotype after pMS82-SCO2078 was introduced. The strains were streaked and collected into spore preparations. From these similar amounts of each strain was used to grow material for cover slip microscopy. Several time points were tested so to compare the strains to their non-conjugated counterparts. Each cover slip was stained with WGA-Alexa 488 and PI, as before, to detect any change in cell wall growth and DNA distribution. The morphology of stage was also noted, so to detect any unexpected differences due to the conjugations.

**The strain M145 carrying pMS82**

This strain was generated to see if the pMS82 vector affected *Streptomyces* growth in any way, and to verify that any differences seen when using pMS82 derivatives were due to the gene inserted and not because of the presence of the vector.

The wild-type and M145/pMS82 are very similar, though septa to septa length analysis has shown that there are some small differences between the two strains (Figure 5.15). Septa to septa measurements were also performed to quantify any

subtle differences observed (Figure 5.18). The M145/pMS82 strain seems to have a modal length 0.2 μm smaller than the wild type, and the range of septa length is somewhat larger for M145/pMS82 compared to the wild-type M145.

The small differences between the two strains do not seem significant, therefore it will be assumed any differences in the other strains are due to the effects of the presence of the cloned gene, and not the presence of pMS82.

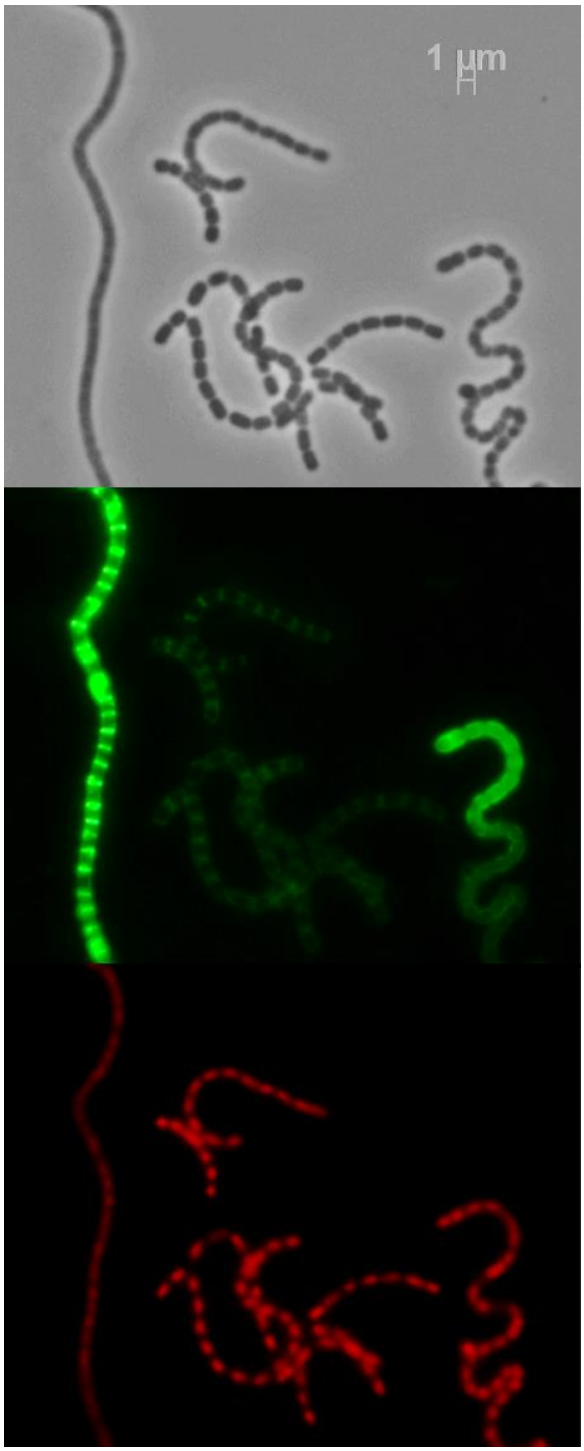


Figure 5.15: M145/pMS82 was viewed using epi-fluorescence microscopy after 48 hrs of growth on SFM medium supplemented with hygromycin. Top: phase-contrast image, middle: WGA stained, and bottom: PI stained images.

**The strain M145 carrying pMS82-2078**

The M145/pMS82-2078 strain shows a fairly normal distribution of septa to septa lengths, with a mode of 1.1 µm and the mean of 1.18 µm. There is a small secondary peak at 1.8 µm-1.9 µm when the septal distances were measured (Figure 5.16). The septa are clear and show a strong WGA signal (Figure 5.16)

This seems to suggest that doubling the gene copies, hence possibly increasing the levels of SCO2078 does not significantly affect the morphology of hyphae.

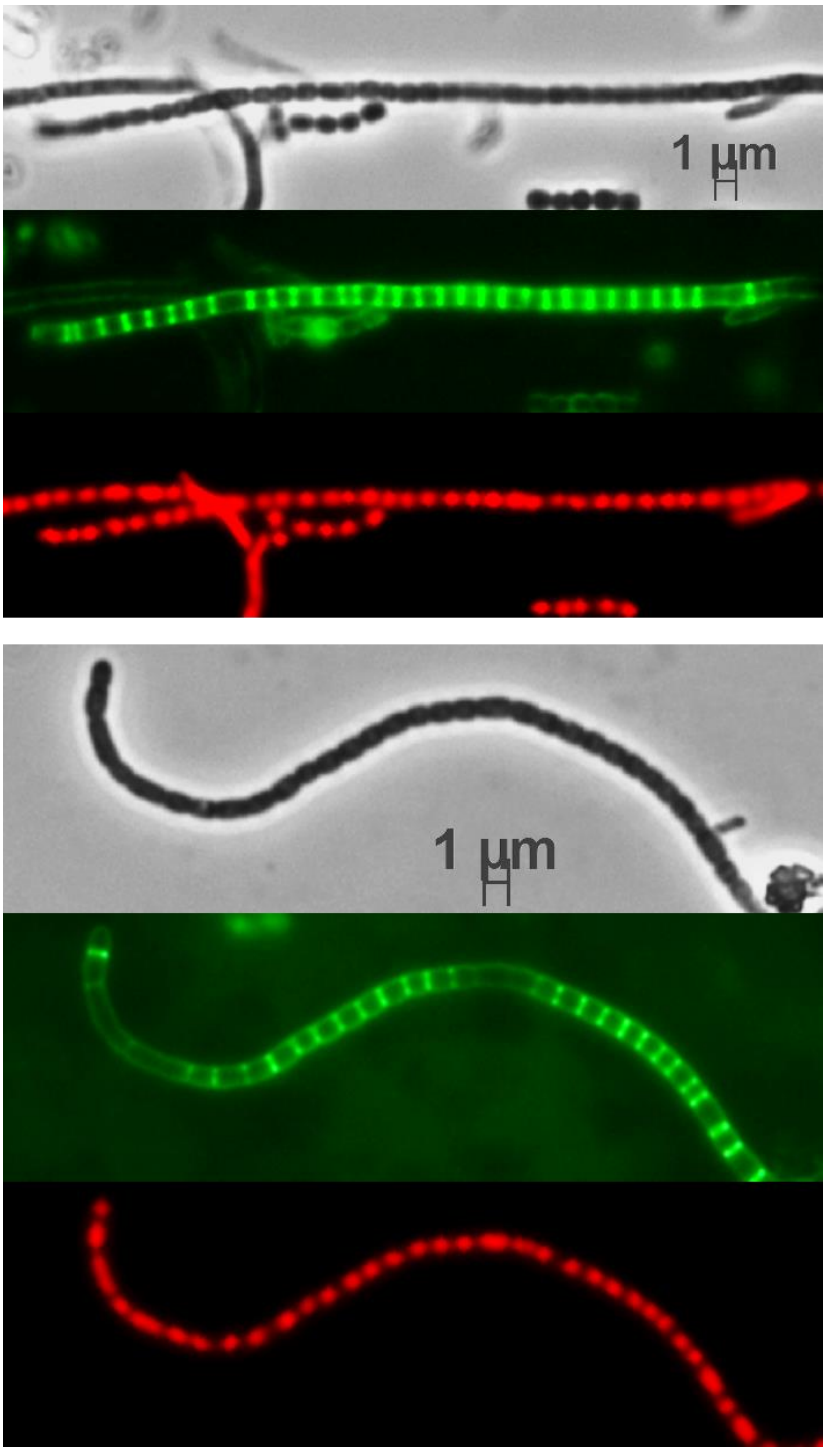


Figure 5.16: M145/pMS82-2078 viewed using epi-fluorescence microscopy. Aerial hyphae are shown after 48 hrs of growth on SFM medium supplemented with hygromycin. Top: phase-contrast image, middle: WGA stained, and bottom: PI stained image.

**The strain Δ*SCO2078* carrying pMS82-2078**

Microscopically Δ*SCO2078*/pMS82-2078 seemed mostly similar to the wild-type M145, though there was a number of spore compartments which contained two to three chromosomes each within the mature aerial hyphae. Septa to septa length analysis showed that there was a larger range of septa to septa distances compared to the wild-type and M145/pMS82 strains (Figure 5.18). The modal length for Δ*SCO2078*/pMS82-2078 was 1.2 µm, with a much smaller secondary peak at 2.6 µm, which seems to be due to the number of double-length spore compartments (An example of which can be seen in the bottom panel of Figure 5.17). This could also explain why the range of septa to septa lengths is higher than the wild-type.

In all it seems that the conjugation resulted in a mostly complemented phenotype, though the presence of the smaller second peak indicates that the introduction of the *SCO2078* gene did not entirely restore the strain to wild-type state. This could be due an absent promoter for *SCO2078*. Another possibility is that the absence of *SCO2078* somehow affects the gene downstream to it, which is *divIVA*. Though this not likely as DivIVA depletion affects hyphae morphology and growth, and not DNA distribution.

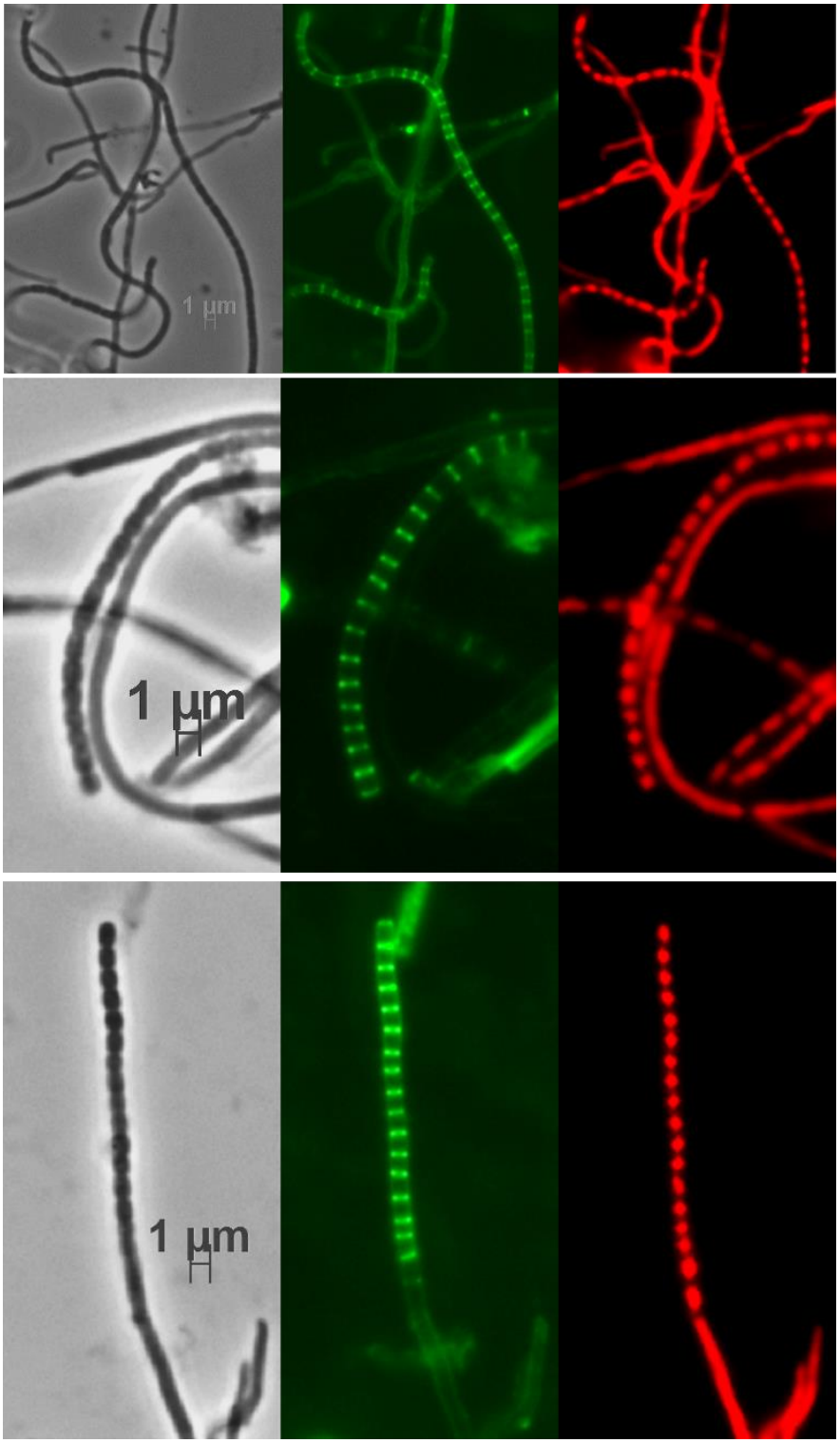


Figure 5.17: Δ*SCO2078*/pMS82-2078 viewed using epi-fluorescence microscopy after 48 hrs growth on SFM medium supplemented with hygromycin. Left: phase contrast image, middle: WGA stained, and right: PI stained images.

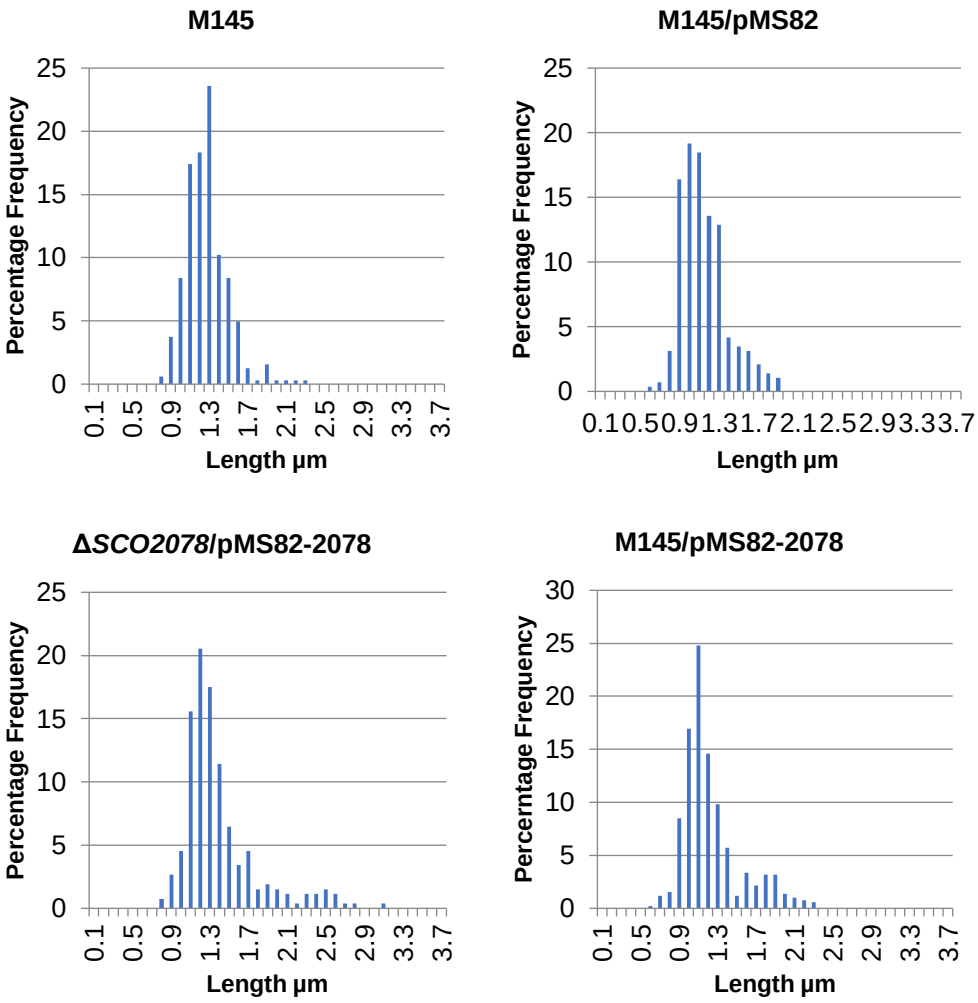


Figure 5.18: **The percentage frequency graphs for the various strains.** The lengths are measured in µm.

## 5.4. Testing the effect of *SCO2078* overexpression

After the attempted knocking out of *SCO2078* did not result in any significant changes in phenotype, the gene was then subject to overexpression. Previous studies of the *SCO2078* homologue, *ylmG* in *A. thalina* (Kabeya et al., 2010), has shown overexpression to affect chloroplast division and nucleoid distribution, as opposed to the knockout which resulted in more compact nucleoids. Therefore, it was next tested whether overexpressing *SCO2078* in *S. coelicolor* result in defects in cell division or genome packaging.

To overexpress *SCO2078,* the tipA system of pIJ6902 was used, as described in Chapter 4. It was hoped that overexpression of *SCO2078* would give an insight to its role, regarding cell division and growth.

### Primer design

The primers used to generate the *SCO2078* fragment were the same as those used to generate the original pMS82-2078 intended for complementation, namely 2078 XbaBgl FRW and 2078 3 END.

The presence of an XbaI site in the forward primer would be utilised when cloning the PCR product into the XbaI site of pIJ6902 (Figure 4.2). The oligonucleotide pairs and the expected size of the PCR product are found in Table 5.4.

Table 5.4: **The oligonucleotide primer pairs and the expected sizes of the PCR product**.

| | **Primer Pair** | **Expected size of fragment** |
|---|---|---|
| *SCO2078* | 2078 XbaBgl FRW<br>2078 3 END | 779 bp |

### Generation of the Overexpression Construct

Using the primers pairs from table 5.4 and with a high fidelity Phusion PCR, the cloned fragment was produced (Figure 5.20, top). To introduce the PCR generated fragment into pIJ6902, an EcoRI site would be required at the 5' end of the fragment, but the 2078 3 END primer did not contain EcoRI sites. Therefore, the fragment was first cloned into the pGEM plasmid (Figure 5.19) before subsequent cloning steps into pIJ6902, as pGEM contains a EcoRI site downstream the MCS to be used (Figure 5.19).

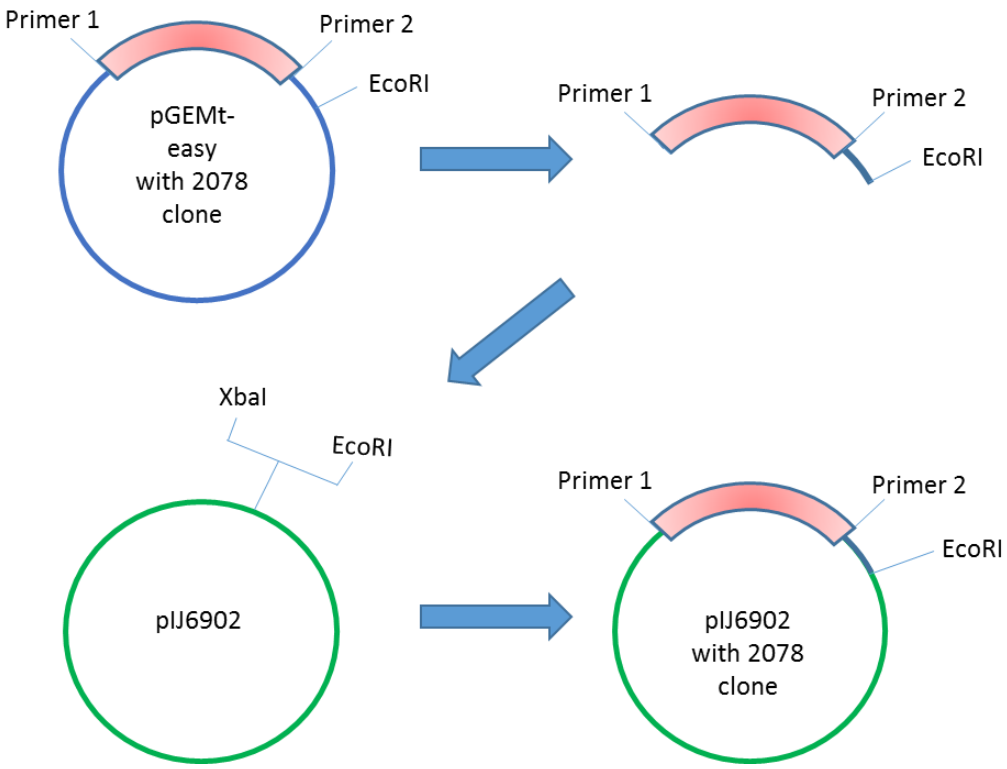


Figure 5.19: The transfer of the PCR product carrying *SCO2078* from pGEM to pIJ6902. The pink box indicates the PCR product, which includes *SCO2078* and an upstream and downstream region surrounding the gene. The pGEM plasmid sequences are marked by a blue line, pIJ6902 plasmid sequences are shown by a green line.

The pGEM plasmid (Kobs, 1997) has several T-residues as 5' overhangs as this plasmid is designed for direct cloning of any PCR product generated by standard Tag polymerase, which adds 'A's (Adenine) to its 5' ends. However, to generate our PCR product standard Tag polymerase was not used, instead, the high fidelity Phusion polymerase was used as it can generate blunt ended DNA products. In order to clone this blunt ended DNA into the pGEM plasmid, the *SCO2078* DNA had to be 'A-tailed' using dATP and GoTaq Polymerase. After a ligation of the A-tailed fragment and pGEM followed by transformation into *E. coli* DH5α, the resulting colonies were selected on ampicillin containing LB medium. The colonies that contained recombinant plasmids were identified using blue-white screening in the presence of IPTG and X-Gal. The white colonies were further screened for the presence of the fragment via colony PCR using the primers DIR and REV, which prime in the pGEM vector on either side of the cloned fragment (Figure 5.20).

The larger bands of ~1.1 kbp on the image show that the *SCO2078* fragment was inserted into pGEM, with the smaller ~300 bp bands confirming that the primers annealed but the colony did not carry the *SCO2078* fragment (Figure 5.20).

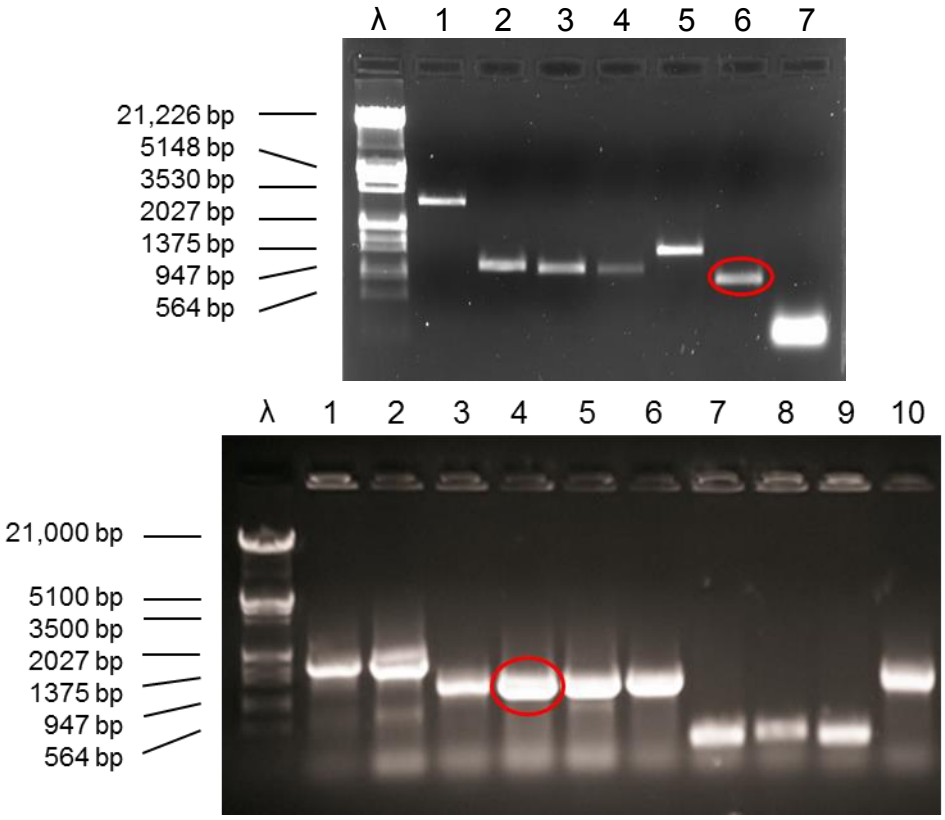


Figure 5.20: Generation of the pGEM-SCO2078 clone. Top: The results of the gel extraction confirming the *SCO2078* fragment; red circle represents the relevant PCR product in lane 6. The products in the other lanes are not relevant to this study. The *SCO2078* Phusion PCR product was phenol extracted, and then was run on an ethidium bromide gel and then gel extracted. The eluted product for SCO2078 was then A-tailed via another PCR, for ligation as the pGEM plasmid is T-tailed. Bottom: The colony PCR results for *SCO2078*, a positive PCR is circled red (Lane 4). The size of the PCR product containing the *SCO2078* gene is the size of insert (2078: 779 bp) with an additional 314 bp, as the primer DIR and Rev are positioned 314 bp apart within pGEM. Lanes 3-6 and 10 all contain positive results for pGEM-SCO2078 with products at 1093 bp, while lanes 7-9 are negative colonies which do not contain *SCO2078* but do contain pGEM. The lanes 1 and 2 contain larger sized products than expected and therefore may contain the pGEM vector with multiple *SCO2078* fragments. Lambda DNA digested with EcoRI and HindIII was used a size marker.

One of the successful colonies was selected (Figure 5.20) for inoculation and subsequent plasmid preparation. The pGEM-SCO2078 plasmid was then digested with EcoRI and XbaI so to excise the fragment with had been extended by less than ten nucleotides to include the EcoRI site.

The pIJ6902 plasmid was also digested with EcoRI and XbaI. After the digestion the pGEM-SCO2078 fragment and pIJ6902 were run on gels to confirm their sizes, and gel extracted to purify the DNA.

Ligations between the *SCO2078* fragment and pIJ6902 then took place, and the ligations were desalted through columns twice, before being electroporated into DH5α cells. The transformant cells were then plated onto LB medium containing apramycin.

**Confirmation of the Recombinant Clones**

Colonies were then screened for the presence of the *SCO2078* fragment using colony PCR.

The primer used for the colony PCR were tfd and 2078 XbaBgl FRW, where the tfd primer anneals within the pIJ6902 plasmid (Figure 4.2) and the 2078 XbaBgl FRW primer anneals within the cloned PCR fragment (Table 5.5).

Table 5.5: **The oligonucleotide primer pairs used in the colony PCR and the expected sizes of the colony PCR products**.

| | **Primer Pair** | **Expected size of fragments** |
|---|---|---|
| *SCO2078* | 2078 XbaBgl FRW<br>tfd | 947 bp |

The colony PCR was analysed on an agarose gel (Figure 5.21), which identified several positive colonies.

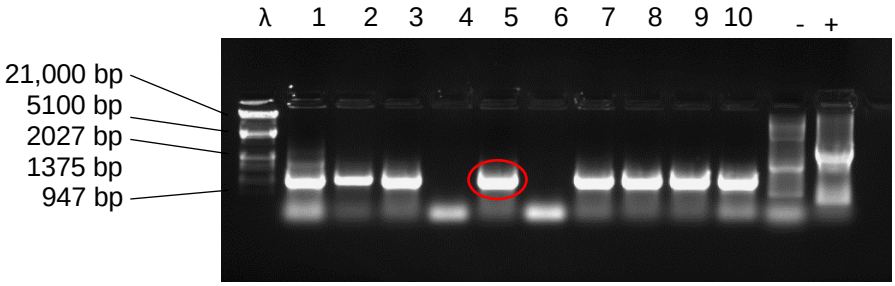


Figure 5.21: **Gel electrophoresis of colony PCRs for the generation of pIJ6902-SCO2078.** The expected size of a PCR product carrying *SCO2087* is 947 bp. Lambda DNA digested with EcoRI and HindIII was used as a size marker in the first lane. The positive control for SCO2078 was the confirmed pIJ6902 *sepF-SCO2078* clone which generates a larger DNA product of 1589 bp and the negative control was an empty pIJ6902 vector. The colony that was used further is marked by a red circle in lane 5.

### Sequencing and confirmation of the fragments within pIJ6902

Colony number 5 for the pIJ6902-SCO2078 construct was chosen to be carried further, and underwent plasmid preparations, which were then sequenced to confirm the sequence of the inserts.

The *SCO2078* clone was sequenced with the oligonucleotides tfd and t0, which anneal to the pIJ6902 vector. These primers anneal a small distance from either side of the insert (Figure 5.22). Sequencing confirmed that the clones were correct.

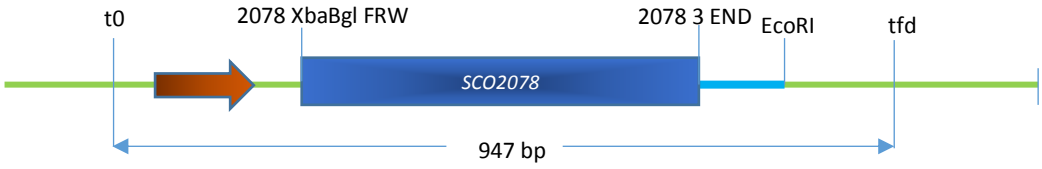


Figure 5.22: The **expected orientation of the *SCO2078* fragment derived from pGEM (blue).** The t0 and tfd primers used to confirm the presence of the fragment are marked, as well as the primers which were used to construct the fragments.

Once confirmed the plasmid pIJ6902-SCO2078 was introduced into the wild-type M145 and Δ*SCO2078 S. coelicolor* strains via conjugation. This process was

the same as described in Chapter 4. Spore stocks for representative exconjugants of both strains were collected.

**Testing the effect of overproduction of SCO2078 on growth and morphology of *S. coelicolor***

The strains I characterised were Δ*SCO2078*/pIJ6902, Δ*SCO2078*/pIJ6902-SCO2078, M145/pIJ6902 and M145/pIJ6902-SCO2078. The strains containing the pIJ6902 vector were used as controls. Firstly, all four strains were grown on three different types of media (SFM, MMM, MMG), with a different carbon source for each minimal media, as described in Chapter 4. In addition, each media was tested either by the presence or absence of the tipA inducer thiostrepton.

As the SCO2078 protein may have a function within aerial hyphae, potentially with genome packaging during sporulation, thiostrepton was directly applied onto the aerial surface of the strains. This followed the way in which the overexpression experiments for *sepF*, with varying amounts of thiostrepton being added to the strains at four different developmental time points.

***SCO2078* overexpression by thiostrepton applied in the media does not result in significant phenotypic changes**

The strains were observed over 8 days at 24 hour intervals, while grown at 30°C in the appropriate media either in the presence or absence of thiostrepton (Figure 6.23).

As expected, the upregulation of the expression of *SCO2078* did not result in any obvious macroscopic changes. However, the Δ*SCO2078*/pIJ6902 and Δ*SCO2078*/pIJ6902-SCO2078 do seem to be darker than the M145/pIJ6902 and M145/pIJ6902-SCO2078 strains at day 3 and 4, on both the un-induced and induced plates (Figure 5.23). This may suggest that these strains develop slightly faster than their corresponding controls.

Similarly to the SFM medium, the MMM plates (Figure 5.24) and the MMG plates (Figure 5.25) also fail to show any major differences between the strains.

The lack of differences suggests that the overproduction of SCO2078 is neither beneficial or detrimental to growth.

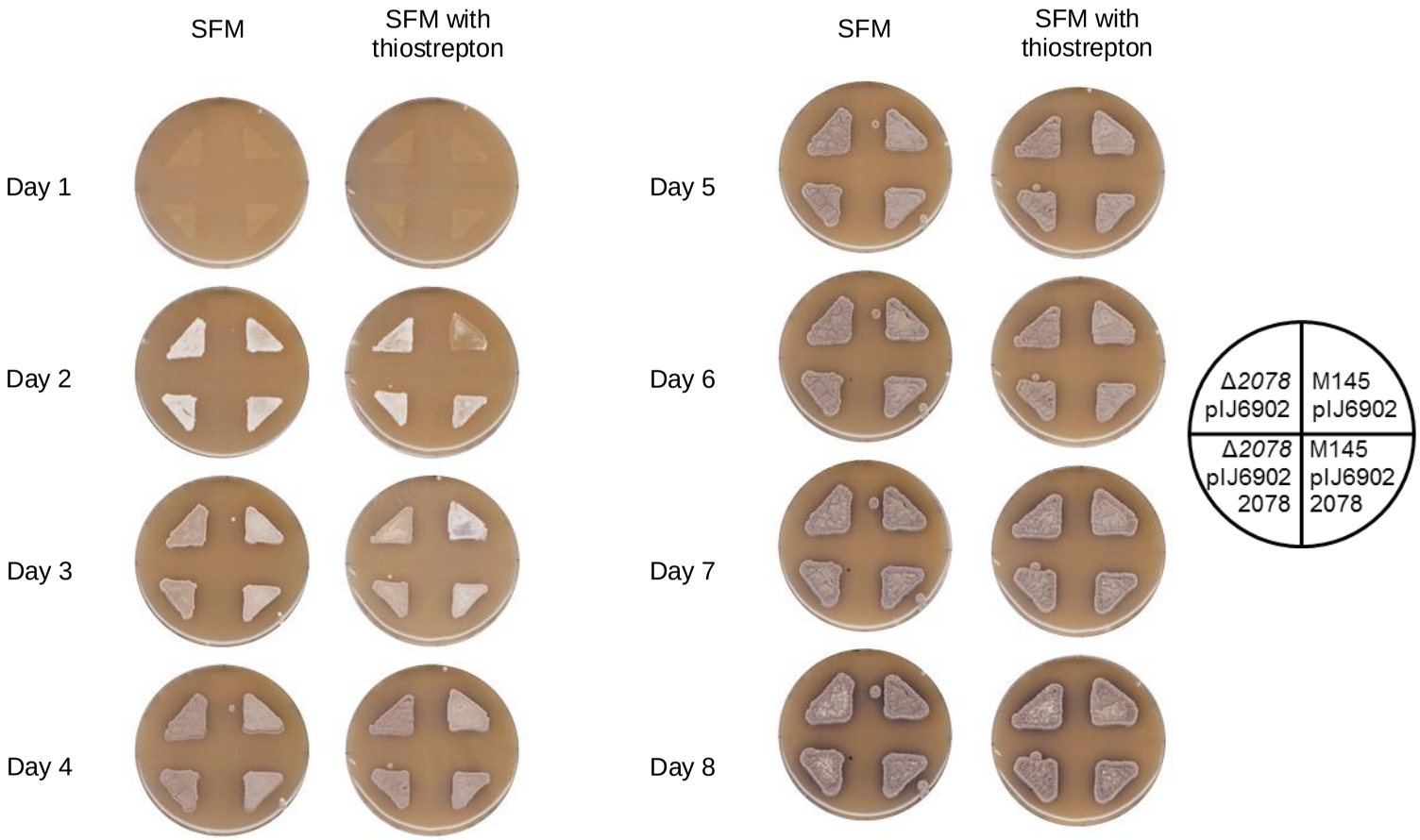


Figure 5.23: Scanned images of the strains, grown over 8 days on SFM medium at 30°C. Explanation of the strains inoculated is shown on the right.

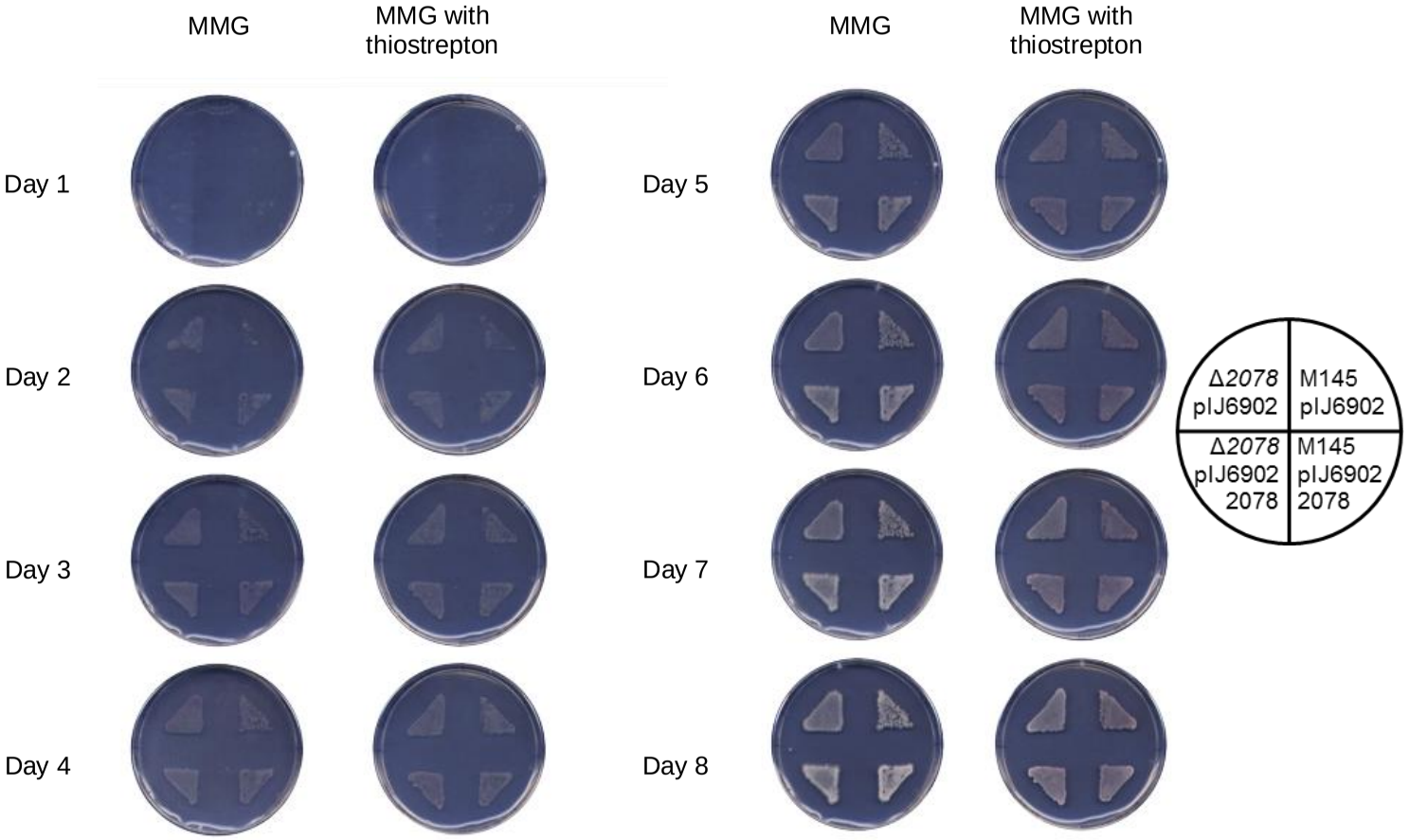


Figure 5.24: Scanned images of the strains, grown over 8 days at 30°C on MMG medium. Explanation of the strains inoculated is shown on the right.

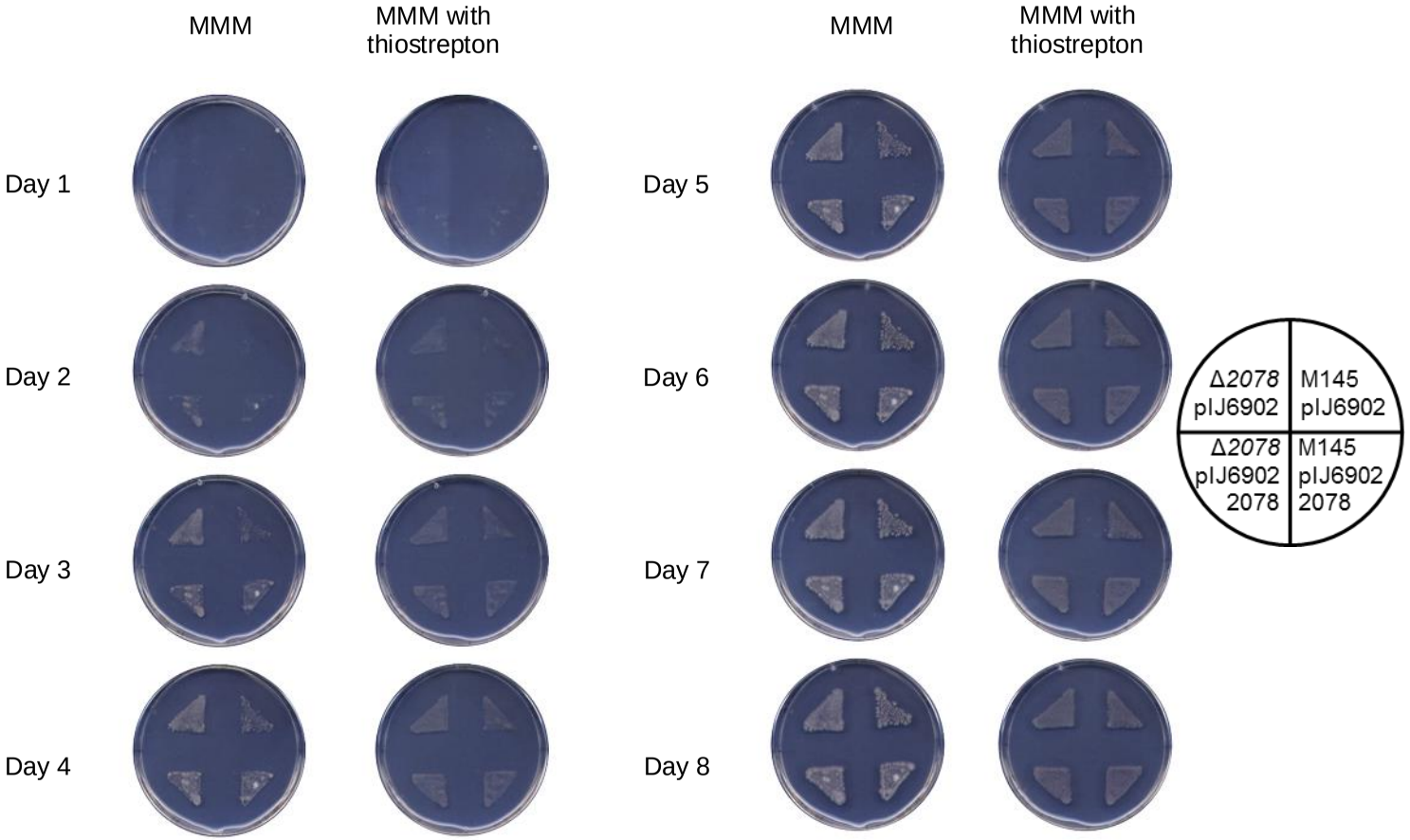


Figure 5.25: Scanned images of the strains, over 8 days at 30°C on MMM medium. Explanation of the strains inoculated is shown on the right.

### *SCO2078* overexpression attempt through directly adding thiostrepton to the aerial hyphae

As explored in Chapter 4, the overexpression of a gene within the pIJ6902 vector may be dependent on the placement, and therefore the availability, of the inducer thiostrepton. As seen for the strain Δ*sepF*/pIJ6902-sepF, thiostrepton is not effective within the growth media when its effect is expected in the aerial hyphae, very likely because the thiostrepton is not transported to the aerial hyphae. However, thiostrepton added directly to the strain through droplets over the surface of the inoculates strains did result in phenotypic change when *sepF* overexpression was induced (Chapter 4).

The *sepF* and *SCO2078* genes are both thought to be important during development of the aerial hyphae. SepF is required for septum formation and SCO2078, if studies on its YlmG homologue within plants are comparable, could be involved in chromosome packaging. This only occurs in the aerial hyphae during sporulation, as before this point the genetic material of *S. coelicolor* is continuous and uncondensed within the hyphae.

Therefore, the overexpression strains produced for *SCO2078* were also tested through 'thiostrepton drop' experiments. The experiments were conducted the same way as the thiostrepton drop experiments for *sepF*.

The phenotype of the strains Δ*SCO2078*/pIJ6902-SCO2078 together with Δ*SCO2078*/pJI6902 were monitored on SFM medium. After inoculating a confluent lawn, thiostrepton was then added to the plates in varying amounts at different time points. The different amounts of thiostrepton, 5 µg, 10 µg, 25 µg, and 50 µg, was delivered directly to the aerial hyphae in droplets, with a water only droplet used as a control.

As with the *sepF* series of overexpression experiments, the strains were exposed to thiostrepton at different developmental time points. These were at inoculation, vegetative, early aerial, and late aerial stages, and these relate to 0 hr, 28 hr, 51 hr, and 69 hrs (respectively) after inoculation.

The strains were grown at 30°C for 5 days and were monitored throughout that time (Figure 5.26 and Figure 5.27).

### *SCO2078* overexpression does not result in any major phenotypic change

Both the Δ*SCO2078*/pIJ6902 and Δ*SCO2078*/pIJ6902-2078 strains grew well on the medium in a very similar.

At day three all patches to where thiostrepton was added were negatively affected, with an inhibition of growth within these areas. The Δ*SCO2078*/pIJ6902 strain plate 0 hrs after inoculation seemed to show a larger area affected by thiostrepton compared to Δ*SCO2078*/pIJ6902-2078.

At day 4, the areas where thiostrepton was added show some differences depending on the strains tested. The Δ*SCO2078*/pJ6902-2078 strain has darker areas within these patches, with the best examples of these seen in the plates to which thiostrepton was added at 0 hrs and 28 hrs after inoculation. Interestingly, for both strains the 51 hr plates are very similar and do not show any signs of growth impairment through the addition of thiostrepton or otherwise. The images taken the day before do show that the 51 hr plates were initially negatively affected by the presence of thiostrepton, but by day 4 this time point shows the least observable change.

At day 5 the strains look very similar, and most of the patches have recovered showing growth. Some of these patches have growth delays, but these areas are where the highest amount of thiostrepton, 50 µg, was added. In these patches the areas are still slightly darker for Δ*SCO2078*/pIJ6902-2078 compared to Δ*SCO2078*/pIJ6902. Additionally, the 51 hr plate for Δ*SCO2078*/pIJ6902-2078 shows darker brown areas for all the amounts of thiostrepton added compared to its water control and Δ*SCO2078*/pIJ6902. This suggests that potentially this is the developmental time where the possible overproduction of SCO2078 affects growth most. Other time points tested show lighter patches at thiostrepton drop points at day 5.

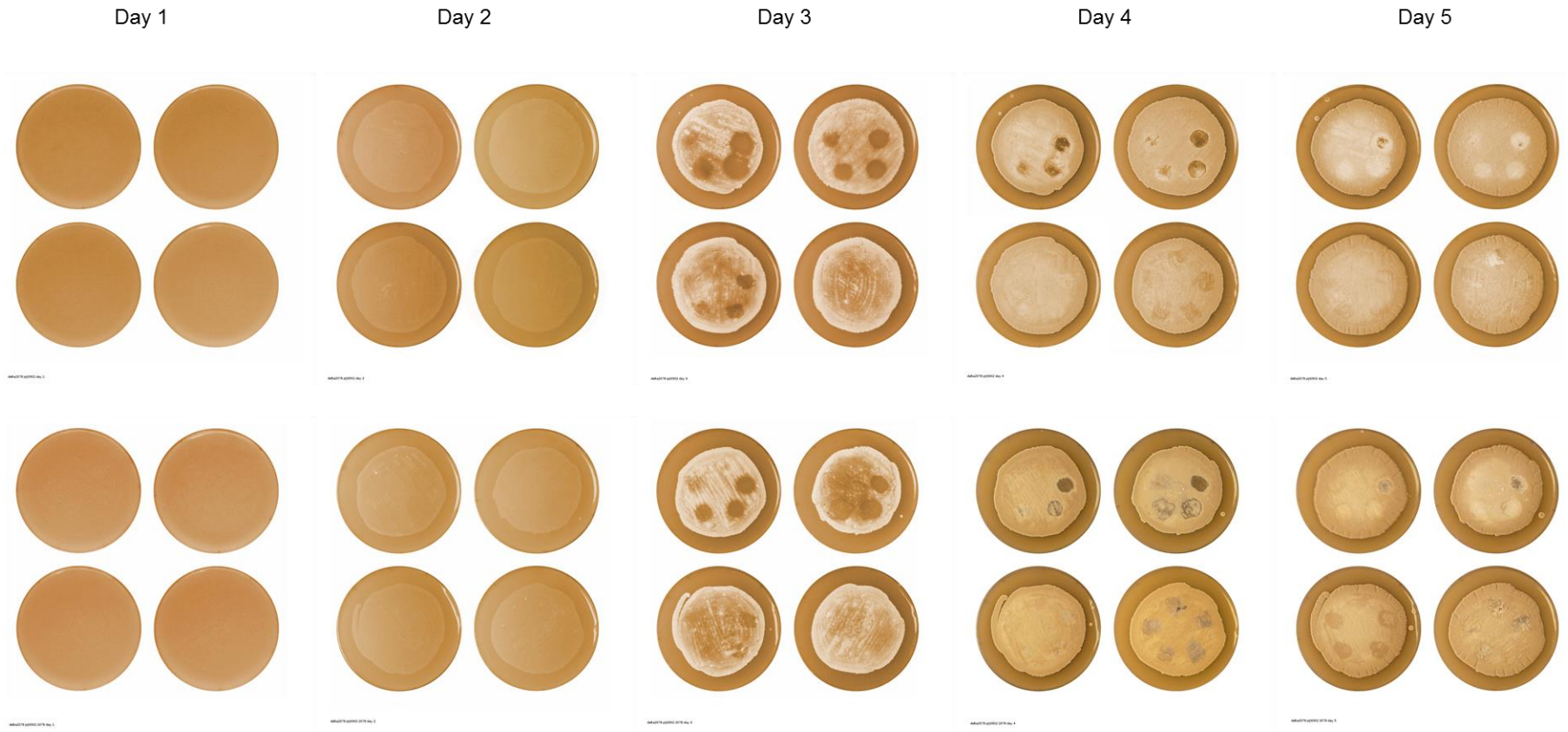


Figure 5.26: The effects of different amounts of thiostrepton applied at different developmental points, viewed after 5 days. The strains are Δ*SCO2078*/pIJ6902 (top row) and Δ*SCO2078*/pIJ6902-2078 (bottom row).

Δ*SCO2078*/pIJ6902

Δ*SCO2078*/pIJ6902-2078

Figure 5.27: The effects of different amounts of thiostrepton applied at different developmental points, viewed after 5 days. The strains are Δ*SCO2078*/pIJ6902 (left) and Δ*SCO2078*/pIJ6902-2078 (right).

## 5.5. Summary

This chapter focused on the characterisation of the *SCO2078* gene, which is located between the *sepF* and *divIVA* genes in the *S. coelicolor* chromosome.

Bioinformatic analysis of the gene and gene product were performed, results of which suggested that *SCO2078* might have a role to play in cell division. Eukaryotic homologues of SCO2078 present the protein as involved in nucleoid division and distribution. As it is believed that the eukaryotic homologues, which are used within chloroplasts, originated from bacteria, then the role of SCO2078 could also be shared. However, the experiments carried out on *SCO2078* did not result in a clear phenotype for any of the generated strains.

In this chapter the characterisation of the previously generated *SCO2078* knockout mutant was begun. The strain was monitored both macroscopically and microscopically, with the phenotypes of the *SCO2078* knockout mutant together with the wild-type strain recorded. No major differences between the strains were macroscopically noted, but a subtle difference was observed when quantifying septal distances that were measured during sporulation.

An extensive array of PCR reactions were performed to confirm the *SCO2078* knockout mutant, after chromosomal DNA was extracted from both the mutant and the wild-type strains. It was confirmed that as a result of the knockout generation, the apramycin resistance cassette was successfully integrated at the correct chromosomal site, potentially replacing the native copy of *SCO2078.* When primer pairs that were external to the deleted region of *SCO2078* were used, single PCR products for both the wild-type and the knockout strains were observed, which corresponded to their expected distinct sizes. However, when primers internal to *SCO2078* were used, which should have only produced a PCR product when wild-type chromosomal DNA was used as the template, weak PCR products of similar sizes to that of PCR products expected for the wild-type DNA were observed when chromosomal DNA of the *SCO2078* knockout mutant was tested. This work was unable to fully confirm whether those weak PCR products were PCR artefacts or whether the presence of the weak PCR products implied that the *SCO2078* gene has not been fully knocked out. As *Streptomyces* grows as long, multi-genomic hyphal filaments, it is conceivable that in our *SCO2078* knockout mutant might have a mixture of wild-type and knocked out chromosomes. This will have to be established in the future using an independent method, for example using Southern blotting.

Also tested was the effect of overexpression of *SCO2078* using the inducible plasmid pIJ6902. After extensive tests performed, no significant macroscopic differences were found when comparing the phenotypes of induced or uninduced strains. In the future, the microscopic studies of *SCO2078* overexpression should also be carried out to test whether DNA distribution was different in the overexpression strain.

## Chapter 6. DivIVA and cell wall synthesis

### 6.1. Introduction

*Streptomyces*, like other Gram-positive bacteria, contains a homologue of *divIVA*. In many bacteria, such as *B. subtilis*, *divIVA* is required for cell division, however, in *Streptomyces* DivIVA is a key player in growth. DivIVA in *Streptomyces* contains two coiled coil structures, which are present in all DivIVA homologues, and a highly conserved 20 amino acid stretch located in the N-terminal domain. It is thought that it is these conserved areas of DivIVA make the protein functional, as deletions of these stretches affect the cells negatively. Deletion of the N-terminal or a coil region results in a non-functioning protein, and as *divIVA* is an essential gene strains containing non-functioning DivIVA are not viable. The amino acids between the two coils of DivIVA, 66-201, are *Streptomyces* specific and shown not be essential, as deletions in this area of *divIVA* did not affect the *Streptomyces* growth (Wang et al., 2009).

According to Flardh (2003) in *Streptomyces*, *divIVA* overexpression or under expression will result in phenotypes differing from the wild-type (Flärdh, 2003). Overexpression can lead to over branching, with the branches not being fully developed. Also, the tips differ from the wild-type as they are swollen in appearance. (Flärdh, 2003)

The function of DivIVA in *Streptomyces* differs from that of *B. subtilis*, as it is thought to be involved in MreB independent cell growth and establishing polarity of cells. It has been shown to be involved in the growing tips of mycelium hyphae, where it collects in a ‘cap like’ fashion, where it is part of the Tip Organising Centre (TIPOC). The TIPOC has not been fully described but is thought to contain proteins involved in polar apical cell growth including DivIVA and two other coiled coil proteins; Scy and FilP. One model points to DivIVA as the recruiter of other cell machinery and thus initiates cell wall changes in the *Streptomyces*. DivIVA is thought to influence cell shape determination as it affects cell wall synthesis and branches have been noted to prefer starting on curved areas of hyphae and this is thought to be due to DivIVA.

DivIVA has also been shown to collect in small foci along lateral cell walls, marking sites of future branching. These foci have been shown to grow in size as

more DivIVA aggregates at future branching sites, some of which comes from the apical growth tip.

The *divIVA* homolog in *Streptomyces* is known as *SCO2077* and is located downstream of *ftsZ* (*SCO2082*) (Figure 6.1). It is within the core conserved genome of *Streptomyces* indicating the essential nature of the gene. The *SCO2082* to *SCO2077* stretch of genome is unidirectional and a transcriptional stop point occurs after *divIVA*. The promoter for *divIVA* is not yet described.

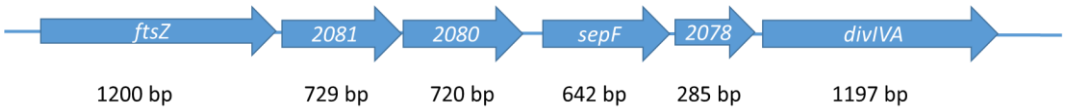


Figure 6.1: The six genes within the cell division and growth cluster of *S. coelicolor*. The *divIVA* gene is the last in the cluster.

DivIVA localisation has been previously described in the hyphae of *Streptomyces*, using a *divIVA*-eGFP construct (M145 KF59) monitored through fluorescent microscopy techniques (Flärdh, 2003). It is mainly concentrated in the growing tips and future branching sites, with little scattering. Therefore, it can be associated with cell wall synthesis. However, the localisation of DivIVA in stress conditions has not been attempted. It is possible that under stress conditions that DivIVA will not localise as expected, and that secondary pathways involved in growth maybe be utilised.

To test this, two 'stress factors' where chosen, a lower than optimum temperature and a growth medium containing a cell wall synthesis inhibitor. Additionally, M145 KF59 may not entirely act as the wild-type M145 should under these conditions, therefore it would be useful to have M145 under the same conditions to act as a control. The aim would be to show areas of cell wall synthesis, through DivIVA localisation (in M145 KF59) or cell wall precursor staining (M145). This would only be tested in the vegetative stage of *S. coelicolor* as it is the only stage at which branching normally occurs.

### 6.2. M145 and M145 KF59 under stress conditions

To test M145 and M145 KF59, each strain was grown on separate sterile cellophane disks placed on SFM plates, with the media for M145 KF59 containing kanamycin to ensure M145 KF59 retained *divIVA*-eGFP. Each plate was inoculated

with an equal number of spores, which were spread evenly and confined to the area of the cellophane disks. The spores were then placed at 30°C, to grow in optimum conditions for 18 hrs. At this point the spores had germinated and started to form a mycelium of near equal density for both strains.

The cellophane disks, which now carried the vegetative mycelium, were divided into halves and placed onto separate SFM or SFM and kanamycin plates dependent on strain. The strains where then subject to the stress conditions. To test the effect of temperature the cellophane disks carrying the strains where divided onto two plates, one which was kept at the optimum 30°C and another which was precooled and kept at 4°C. The lower temperature was chosen to be 4°C as it was significantly lower than 30°C, but high enough to allow the tested strains (M145 and M145 KF59) to survive and grow. Additionally, this temperature could be experienced by *Streptomyces* when in their native soil environments, so the bacteria may have existing pathways to deal with this change in temperature. However, the abrupt nature of the temperature change should be stressful on the strains.

To test the effect of cell wall synthesis inhibition on the localisation of DivIVA, the Gram-positive antibiotic bacitracin was added to the SFM plates. Bacitracin inhibits cell wall synthesis by binding to lipid carrier undecaprenol pyrophosphate, which is required for the cycling of lipid II. Without lipid II being transported peptidoglycan synthesis is disrupted, thus inhibiting cell wall synthesis. Though bacitracin is an antibiotic, sub-lethal levels were used, and the minimum inhibitory concentration was reached. The cellophane halves containing the strains were then placed onto SFM plates containing bacitracin or plates absent of bacitracin as a control.

Both stress conditions were then used in conjunction with one another, producing four environments for the strains: an optimum growth condition of 30°C with no bacitracin present in growth media, 30°C with bacitracin present in growth media, 4°C with no bacitracin present in growth media, and, 4°C with bacitracin present in the media.

The strains were then grown in their respective conditions and were viewed at 3 hrs and 5 hrs after being transferred to the test conditions.

To evaluate any changes in DivIVA localisation and cell wall synthesis the strains were viewed via fluorescence microscopy. Squares of cellophane containing the strains were removed from each plate and prepared into slides. The various samples for M145 KF59 were not stained or fixed, but viewed directly under UV

light, which allowed the GFP tag of DivIVA to clearly be seen. The M145 samples were also not fixed, but they did require staining. To see areas affected by new cell wall synthesis the stain was required to specifically target only these areas. Therefore vancomycin, which is an antibiotic which affects Gram-positive bacteria and is a cell wall synthesis inhibitor, was used as a dye. Vancomycin binds to lipid II, inhibiting peptidoglycan synthesis, so would be able to show the areas at which cell wall synthesis is taking place. The vancomycin used is attached to a fluorescent dye (BODIPY FL), the dye is also hydrophobic, allowing it to stain lipids. Therefore, it should not affect the action of vancomycin. BODIPY FL has an emission maximum of 512 nm and this gives it a green fluorescence.

### 6.2.1. The effect of various conditions on M145 KF59

#### 30°C without Bacitracin

In optimum conditions of 30°C with no cell wall synthesis inhibitors present the M145 KF59 vegetative hyphae grew as expected. The localisation of DivIVA-eGFP in M145 KF59 has been previously described and this was seen in the control sample. The expected areas of fluorescence are the tip ends, with the signal being 'cap' shaped (Flärdh, 2003). Other points of fluorescence are thought to mark the sites of future branches. (Hempel et al., 2008)

The signal from DivIVA-eGFP was concentrated at the tips of the growing hyphae. The fluorescence was seen in 'cap' like shapes which followed the growing tip of 'active' hyphae. Fluorescence signal was also seen in dense foci at certain sites on the cell wall behind the growing tip. This is thought to be the site of future branching, with immature branches showing the cap like signal at their apical tips. Some other areas of fluorescence were also noted, but these were not as bright or large as the other foci and caps, suggesting that the signal was caused by scattered DivIVA, which may have been in transit to growing tips or branching sites. Another potential cause of this low-level fluorescence could be the natural background fluorescence seen in *Streptomyces*. This fluorescence pattern and thus DivIVA-eGFP localisation was seen in samples 3 hrs and 5 hrs after cellophane transfer (Figures 6.2 and 6.3). In all, the strongest fluorescence was seen in the 'caps' at the tips, with some other limited numbers of smaller foci seemly scattered throughout the hyphae.

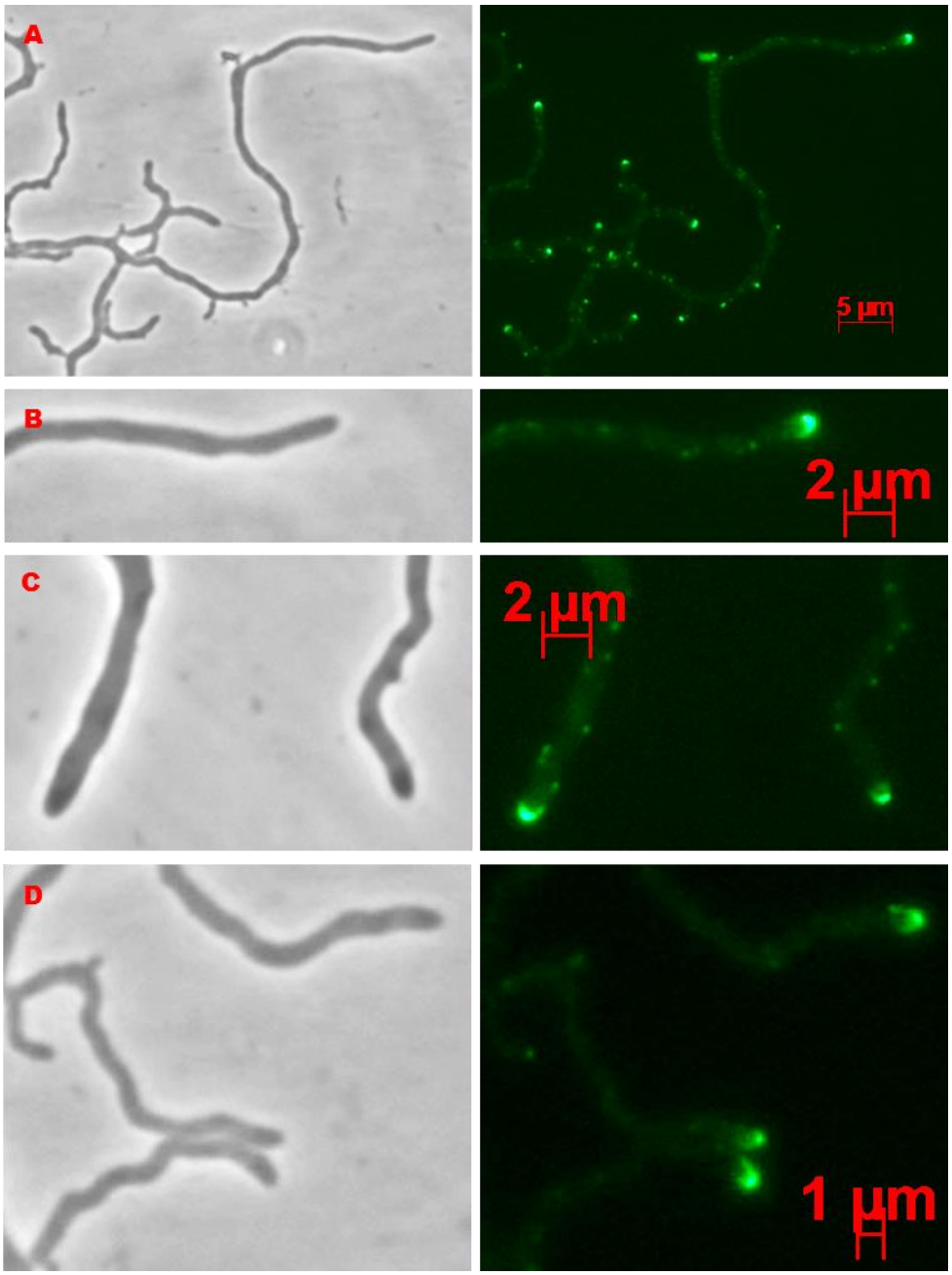


**Figure 6.2**: Microscopy images of M145 KF59 samples exposed to SFM at 30°C for 3 hrs. Phase contrast images on left, eGFP on right. A: shows fluorescence at hyphal tips and future branching points. B: shows a DivIVA-eGFP fluorescence 'cap' at a growing hyphal tip. C: shows fluorescence at tip ends and small foci with the hypha. D: shows the DivIVA-eGFP 'caps' mark the edge of the tips and are more concentrated at the upmost ends of the hyphae tips.

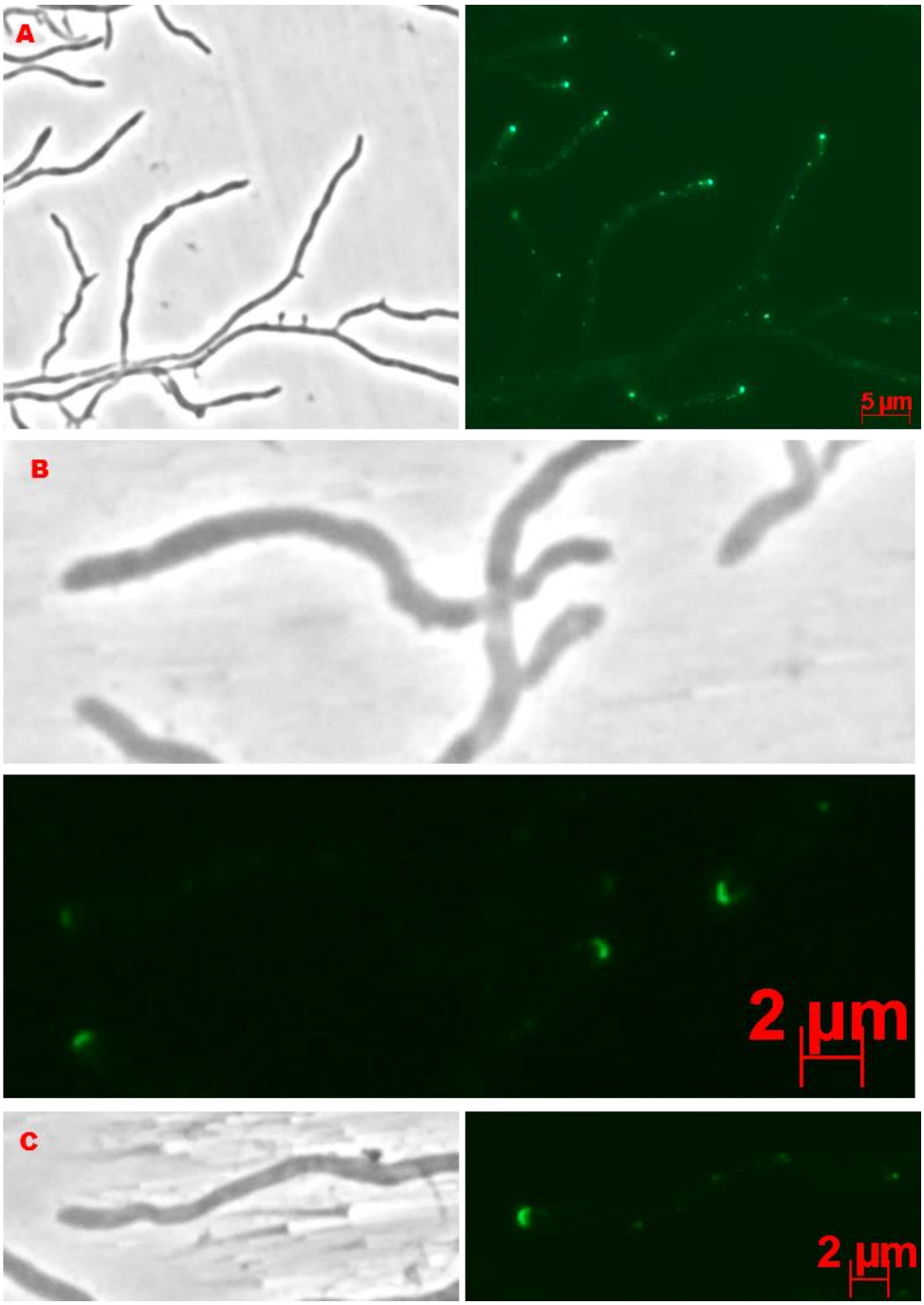


**Figure 6.3**: Microscopy images of M145 KF59 samples exposed to SFM at 30°C for 5 hrs. Phase contrast images on left, eGFP on right. A: shows fluorescence mainly at the end of hyphae and at potential branching points. B: shows DivIVA-eGFP localising at the edges of the tips to form 'caps' at the ends of the growing hyphae. C: shows a fluorescence 'cap' at the end of hypha followed by small foci within the hypha.

**4°C without Bacitracin**

When M145 KF59 was exposed to lower temperatures there was a change in the fluorescence signals seen in the 3 hr and 5 hr samples tested (Figures 6.4 and 6.5).

Tips do show signal, though the strong ‘cap’ like signal pattern seen at optimum conditions seems to be reduced. Caps are present, but the signal is not always even, with certain areas of the cap showing greater fluorescence (which may be due to DivIVA-eGFP concentrations being focused in one area). At some tips the ‘cap’ shape of fluorescence is not seen, but instead a small point of fluorescence is present.

Additionally, smaller foci are also seen, in a range of fluorescence levels. The foci signals are not greater in brightness than clear tip signals, though they are more numerous. Previously, these smaller signals were in low amounts, but after exposure to 4°C for 3 hrs or 5 hrs DivIVA-eGFP seems to aggregate into more and smaller foci. These foci are throughout the hyphae, though do seem to occur commonly near growing tips. Additionally, these foci can be quite close to one another, clustering at the ends of tips. The drop in temperature for M145 KF59 ultimately results in more scattered foci and signals, with less ‘cap’ tip signals, with the differences being more apparent in samples exposed to lower temperatures for a longer period of time.

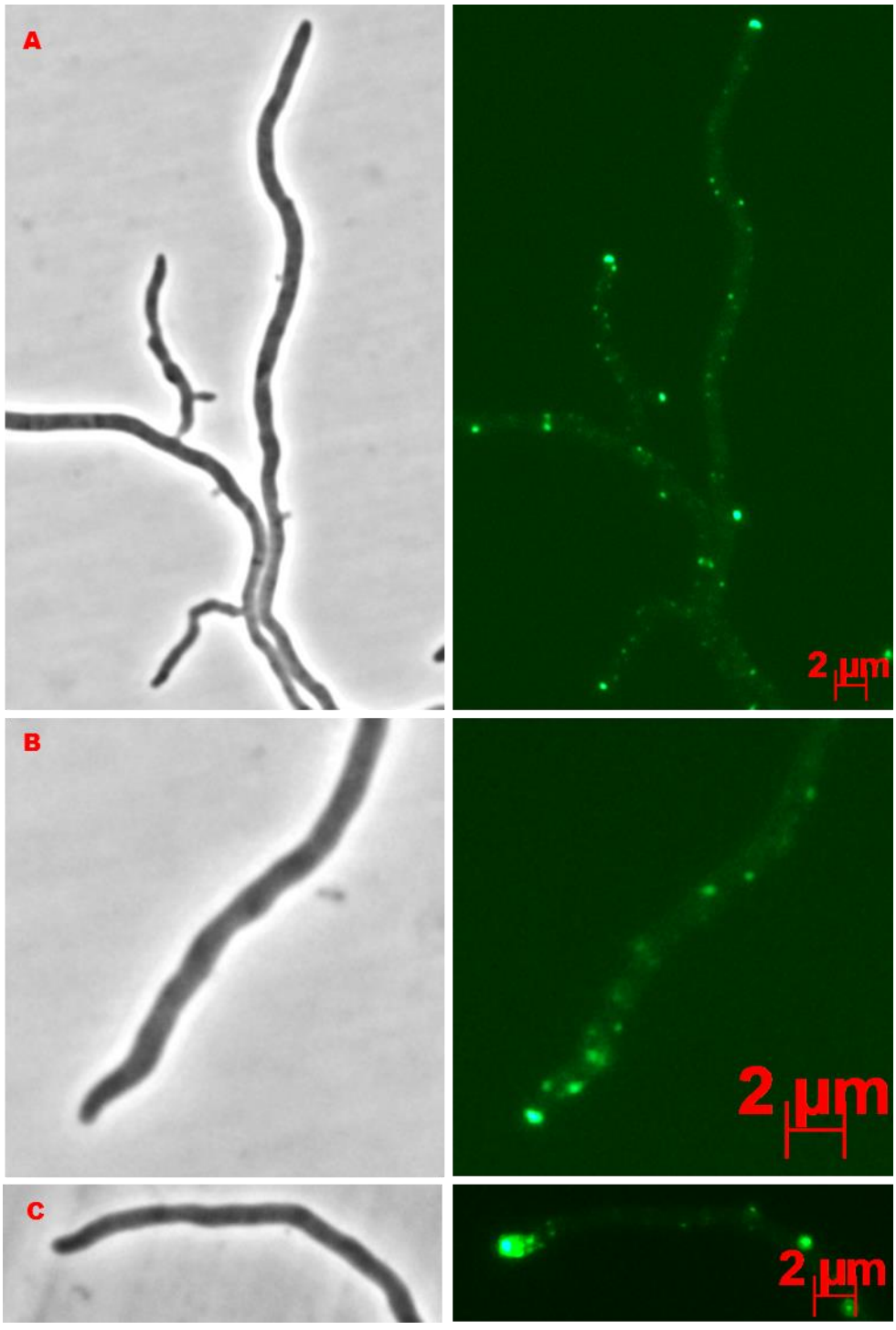


**Figure 6.4**: Microscopy images of M145 KF59 samples exposed to SFM at 4°C for 3 hrs. Phase contrast images on left, eGFP on right. A: shows fluorescence at hyphal tips and scattered foci throughout the hyphae. B: shows DivIVA-eGFP fluorescence is not necessarily 'cap' shaped at the tips. There are also small foci behind the growing tip. C: shows fluorescence at the tip end with many small foci trailing directly behind the main tip foci. Other larger foci are present further down the hyphae (possible branch site).

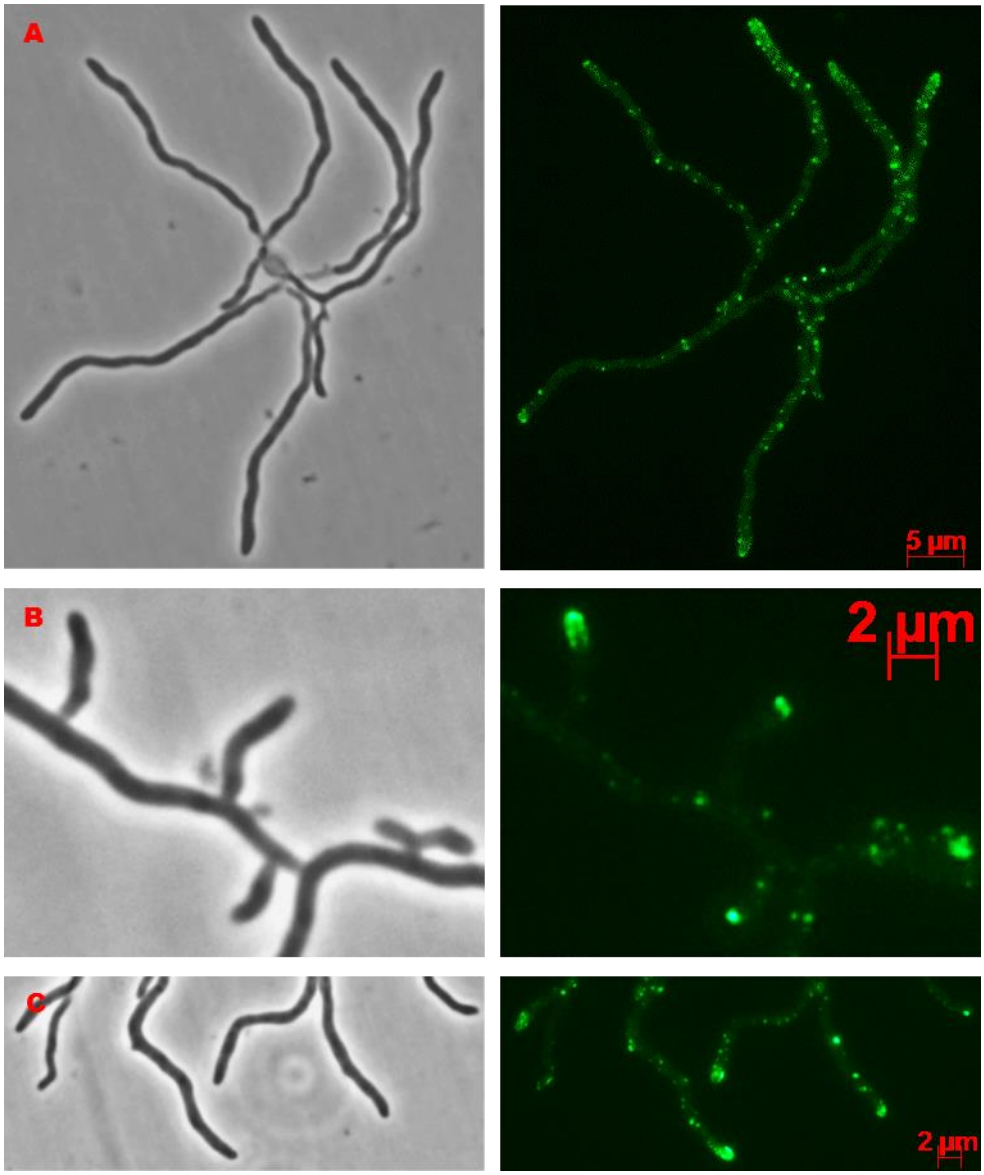


**Figure 6.5**: Microscopy images of M145 KF59 samples exposed to SFM at 4°C for 5 hrs. Phase contrast images on left, eGFP on right. A: shows there are many points of fluorescence throughout the hyphae, with tips having a concentration of foci compared to elsewhere in the hyphae. B: shows different shaped DivIVA-eGFP foci at the tip ends, with one almost 'cap' shaped and the other flat. Other foci are present in the hyphae in various sizes. C: shows tip foci and a possible branch site. Other smaller foci are present, some in close proximity to the growing ends.

**30°C with Bacitracin**

For M145 KF59 samples exposed to bacitracin but kept at 30°C, the DivIVA-eGFP signal again differs from the signal pattern seen in the hyphae kept at optimum conditions. However, the differences are slight, as signal is seen in the expected areas of the tips and scattered throughout the hyphae. The cap structure of the signals is not seen, with tip signals being broken up into two or more strong foci. The foci are at the leading edges of the tip, and at times are seen to be accompanied by smaller foci (Figure 6.6). The foci in the hyphae are numerous and seem to be scattered throughout the hyphae in a random pattern. Interestingly, some foci within the vegetative hyphae have strong signals, which match the intensity of the tip foci (Figures 6.6 and 6.7). These foci could be marking the future branching sites, and therefore have a signal as strong as the tip foci as they too are destined to be growing tips. This is also seen in the samples kept at optimum conditions, however, the number of strong foci seems to higher for samples exposed to bacitracin.

There are no visible differences between the samples tested for 3 hrs and 5 hrs. Suggesting that the effect of bacitracin on divIVA-localisation occurs before 3 hrs of exposure and is then maintained, and not increased in intensity, after this point. Interestingly, the strong foci found within the hyphae (and not tips) after 3 hrs of exposure to bacitracin, which may have been marking the site of future branches, have not resulted in an increase of branches after 5 hrs of exposure to bacitracin.

In all, the DivIVA-eGFP signals in M145 KF59 kept at 30°C and those seen in similar samples with the addition of bacitracin do not seem to differ significantly, though the latter conditions contain signals that may suggest more future branching.

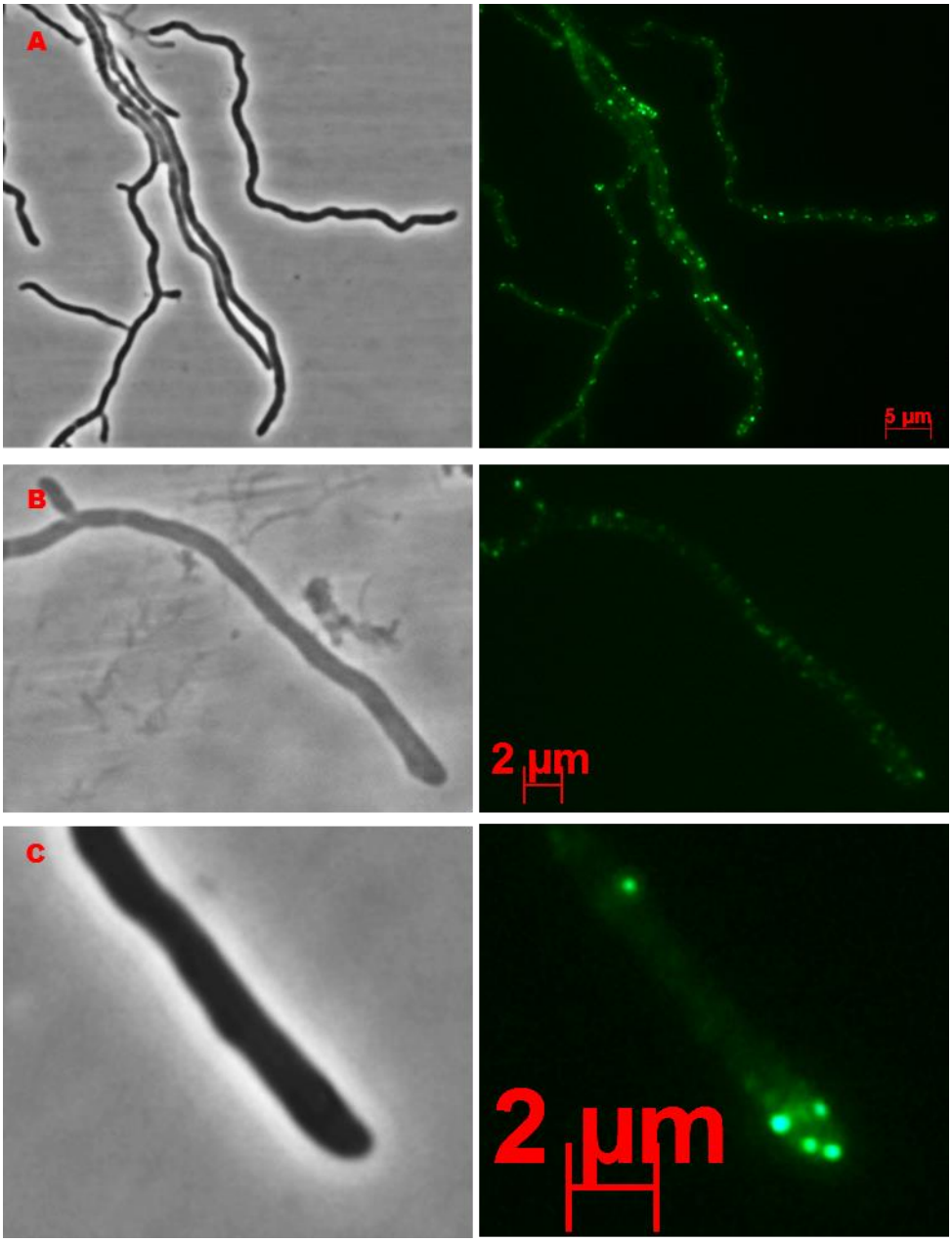


**Figure 6.6**: Microscopy images of M145 KF59 samples exposed to SFM containing bacitracin at 30°C for 3 hrs. Phase contrast images on left, vancomycin stained on right. A: shows many strong foci throughout the hyphae, with no clear concentration of foci at tip ends. B: shows a hypha with many small foci within it. The tip end is absent of a strong fluorescence signal, 'cap' shaped or otherwise. C: shows a hyphal end with four distinct points of fluorescence. Other weaker points of fluorescence can also be seen.

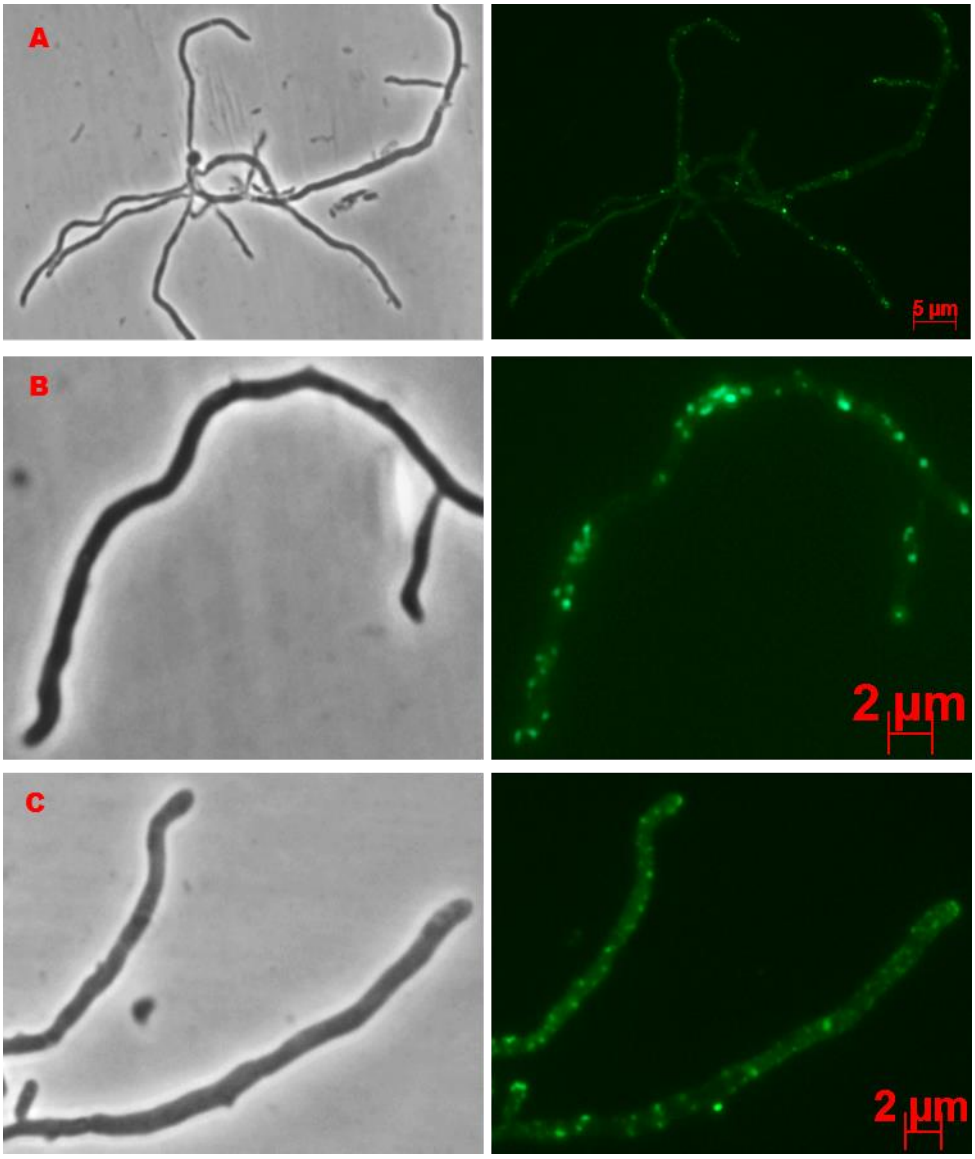


**Figure 6.7**: Microscopy images of M145 KF59 samples exposed to SFM containing bacitracin at 30°C for 5 hrs. Phase contrast images on left, vancomycin stained on right. A: shows many foci throughout a sample, with an absence of a clear localisation pattern. B: shows a hypha with many scattered foci signals and small sections without any fluorescence. The tip ends have foci, but the DivIVA-eGFP florescence is not concentrated. C: shows two hyphae with many scattered foci signals. The ends do not show a 'cap' like fluorescent pattern or stronger foci. There are many small foci present.

**4°C with Bacitracin**

When both stress factors are applied to M145 KF59 for 3 hrs and 5 hrs, there is again a slight change in DivIVA-eGFP signalling. As compared with the previous factors when applied individually, signals do not appear as strong in the tips of the vegetative hyphae. The cap shape of fluorescence is rarely seen, with foci at growing tips instead (Figures 6.8 and 6.9). However, at the tips there seems to be one 'dominant' or 'stronger' foci, then seen when M145 KF59 is exposed to bacitracin only. Smaller foci are seen in further behind the lead tip foci, something noted when M145 KF59 was exposed only to lower temperatures.

Other foci are also seen, scattered throughout the hyphae. These foci do not match the tip foci in intensity, with the hyphae foci being smaller. From these smaller hyphae, some are distinctive from the rest due to their slight increase in signal strength. These foci can be seen at areas where the hyphae bend, suggesting that they may be marking possible branching sites.

The DivIVA-eGFP signal in the hyphae noted shares a closer resemblance with the DivIVA-eGFP signals noted for M145 KF59 after exposure to 4°C, than bacitracin. However, tip signals though not 'cap' like resemble the control M145 KF59 (kept at 30°C and not exposed to bacitracin), as they are strongest signals seen the in the mycelium and not accompanied with other closely grouped foci, phenotypic traits that are not seen in the other conditions tested.

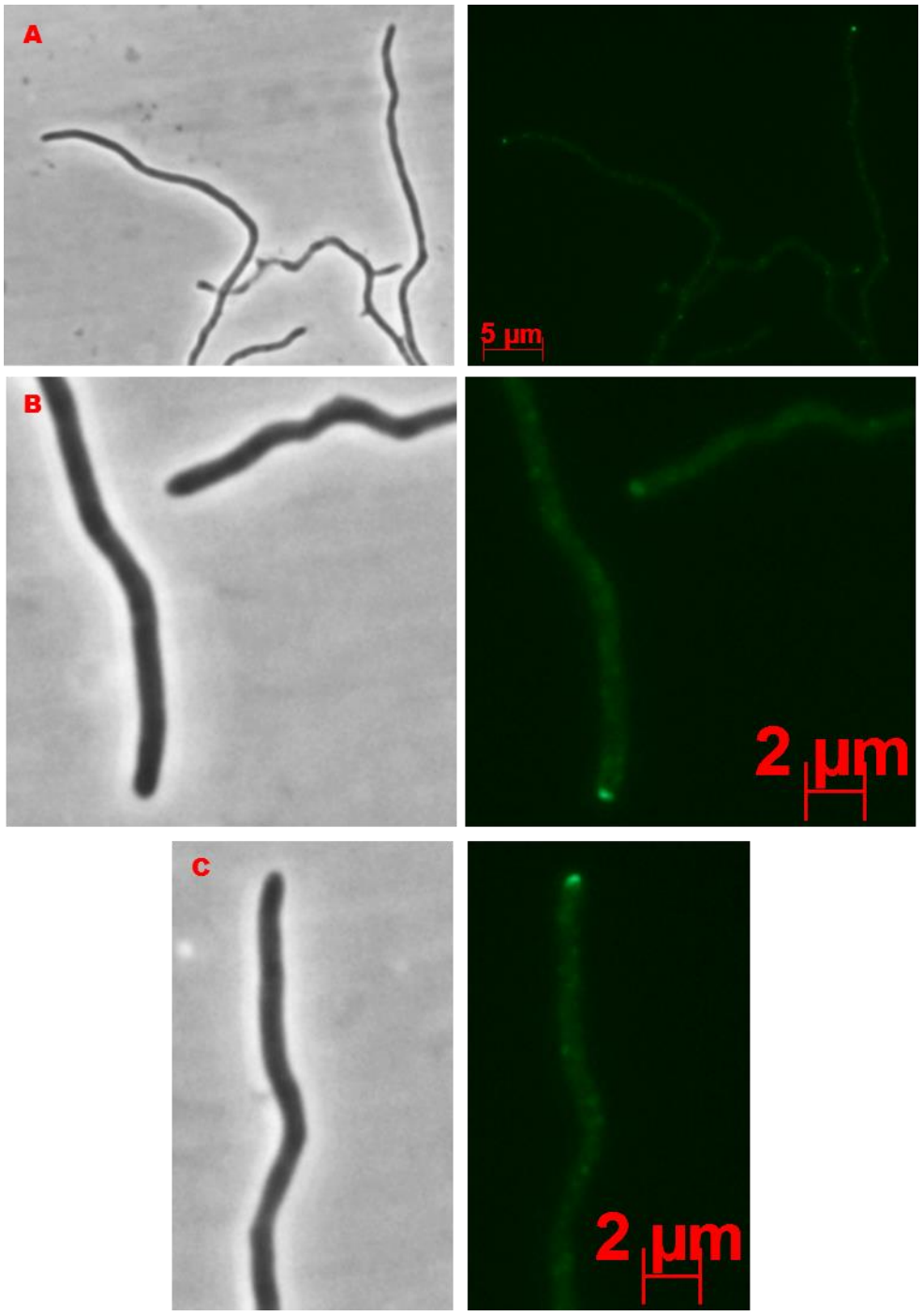


**Figure 6.8**: Microscopy images of M145 KF59 samples exposed to SFM containing bacitracin at 4°C for 3 hrs. Phase contrast images on left, vancomycin stained on right. A: shows a weak scattered fluorescence signal throughout the hyphae. The tip ends have a relatively stronger fluorescence than the rest of the hyphae. B: shows scattered foci throughout the hypha. Both have weak tip end signals. C: shows a hypha with weak foci scattered throughout. A tip signal can be observed.

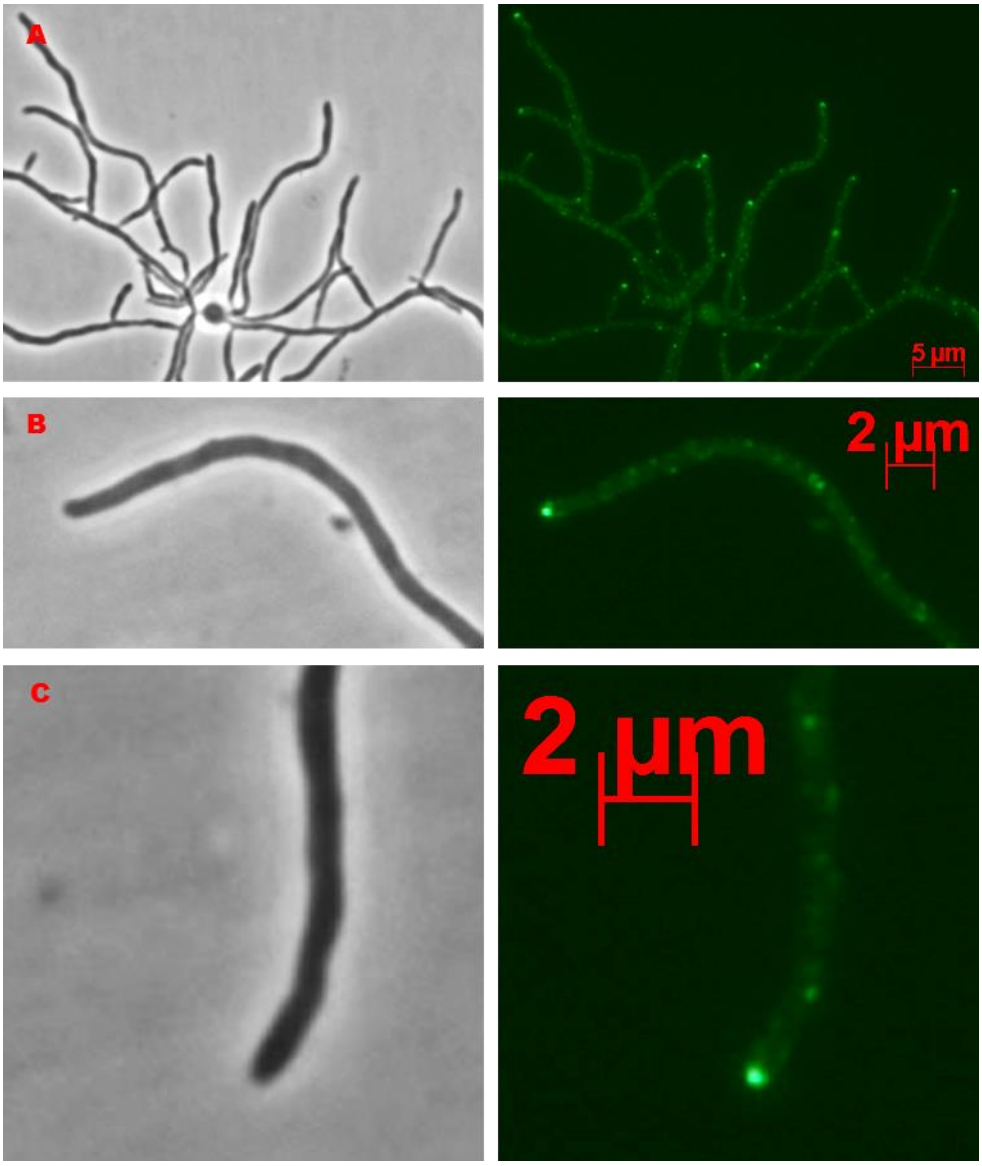


**Figure 6.9**: Microscopy images of M145 KF59 samples exposed to SFM containing bacitracin at 4°C for 5 hrs. Phase contrast images on left, vancomycin stained on right. A: shows scattered foci throughout the hyphae. Tip ends of the hypha do show stronger signal relative to the rest of the hyphae. B: shows a hypha with a strong fluorescence signal at the tip end. The rest of the hypha has small scattered foci throughout, with some weak foci close to the tip end. C: shows a hypha with a strong round fluorescence signal at the tip end. Scattered foci are throughout the hypha.

### 6.2.2. The effect of various conditions on M145

#### 30°C without bacitracin

M145 was used to describe any differences between the wild-type and M45 KF59 regarding cell wall synthesis. The vancomycin staining for M145 in optimum conditions, showed that the areas of cell wall synthesis were the growing tips, at some areas of the established hyphae cell wall (which are thought to be areas where branching will take place), and within vegetative crosswalls or septa (Figure 6.10 and 6.11). These signals were strong and distinct from background fluorescence.

Tip signals were ‘cap’ like, and covered the area expected as seen by DivIVA-eGFP in M145 KF59, indicating that this area of cell wall synthesis was paired with DivIVA as previously described.

The other foci were smaller than the cap signals and seen throughout the hyphae. Some of these foci were noted to be situated on raised areas of the hyphae, which may have been the start of new branches. This again is expected, and works well with the idea that DivIVA is linked to cell wall synthesis.

However, there were new structures which showed strong signals for cell wall synthesis, not seen in fluorescence microscopy for M145 KF59. These signals spanned the width of the vegetative hyphae and ranged from very narrow to large structures. The fluorescence intensity was matched to that of the tip signals, and the structures were spaced throughout the hyphae. The distances between the structures varied greatly, and did not seem to follow a set pattern of placement. The structures placement, shape and size suggest that they are crosswalls. Crosswalls are found in wild-type *Streptomyces* and their function is thought to be linked compartmentalising vegetative hyphae. The strong signals associated with the crosswalls suggest that they are areas of active cell wall synthesis, and the absence of signal for crosswalls in M145 KF59 suggest that crosswall synthesis is not linked with *divIVA*.

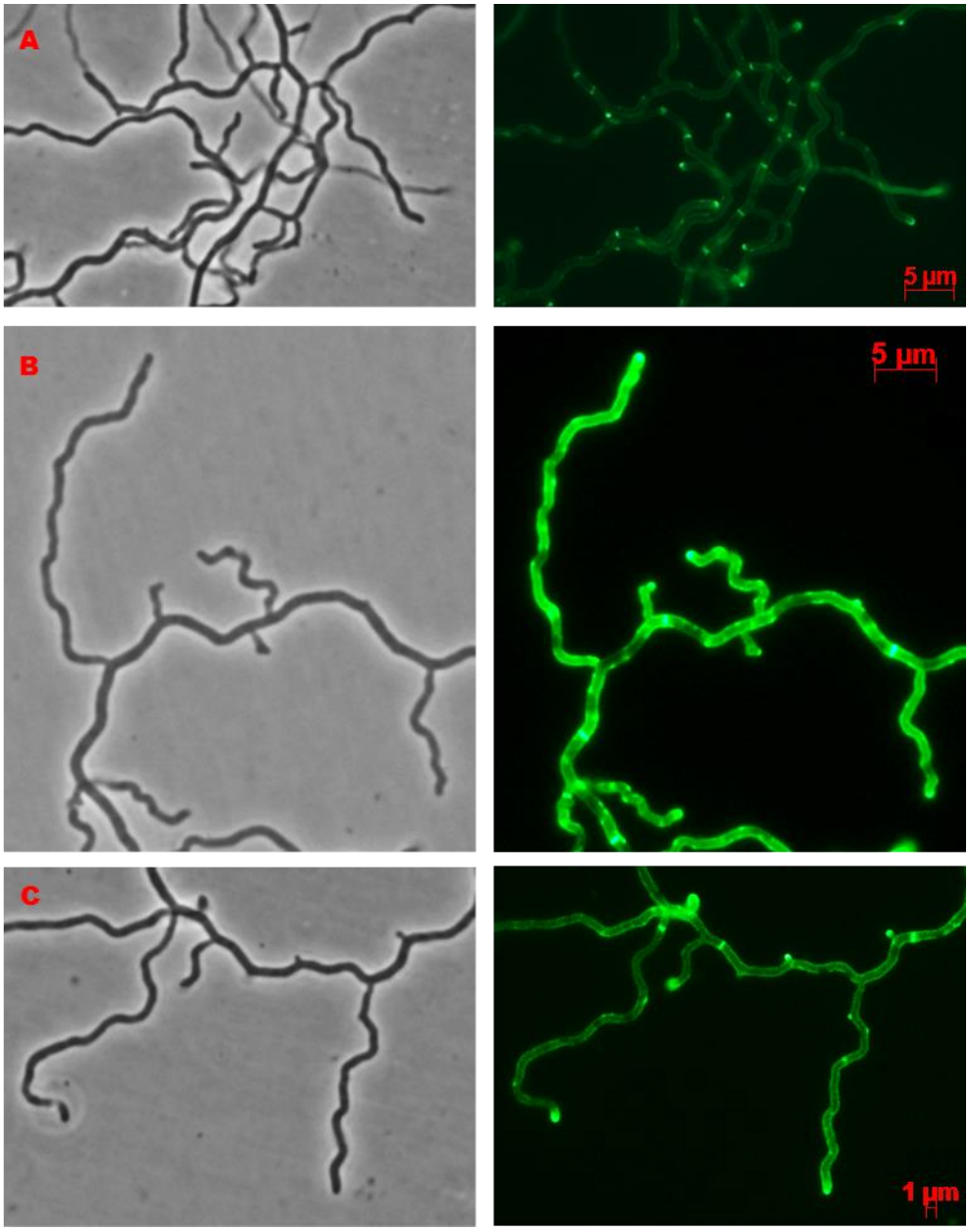


**Figure 6.10**: Microscopy images of M145 (wild-type) samples exposed to SFM at 30°C for 3 hrs and stained with vancomycin. Phase contrast images on left, vancomycin stained on right. A: shows that the vancomycin has strongly stained tip ends and crosswalls. B: shows fluorescence at tip ends and crosswalls. C: shows fluorescence at hyphal ends and crosswalls. The cell wall of the samples is also clearly seen.

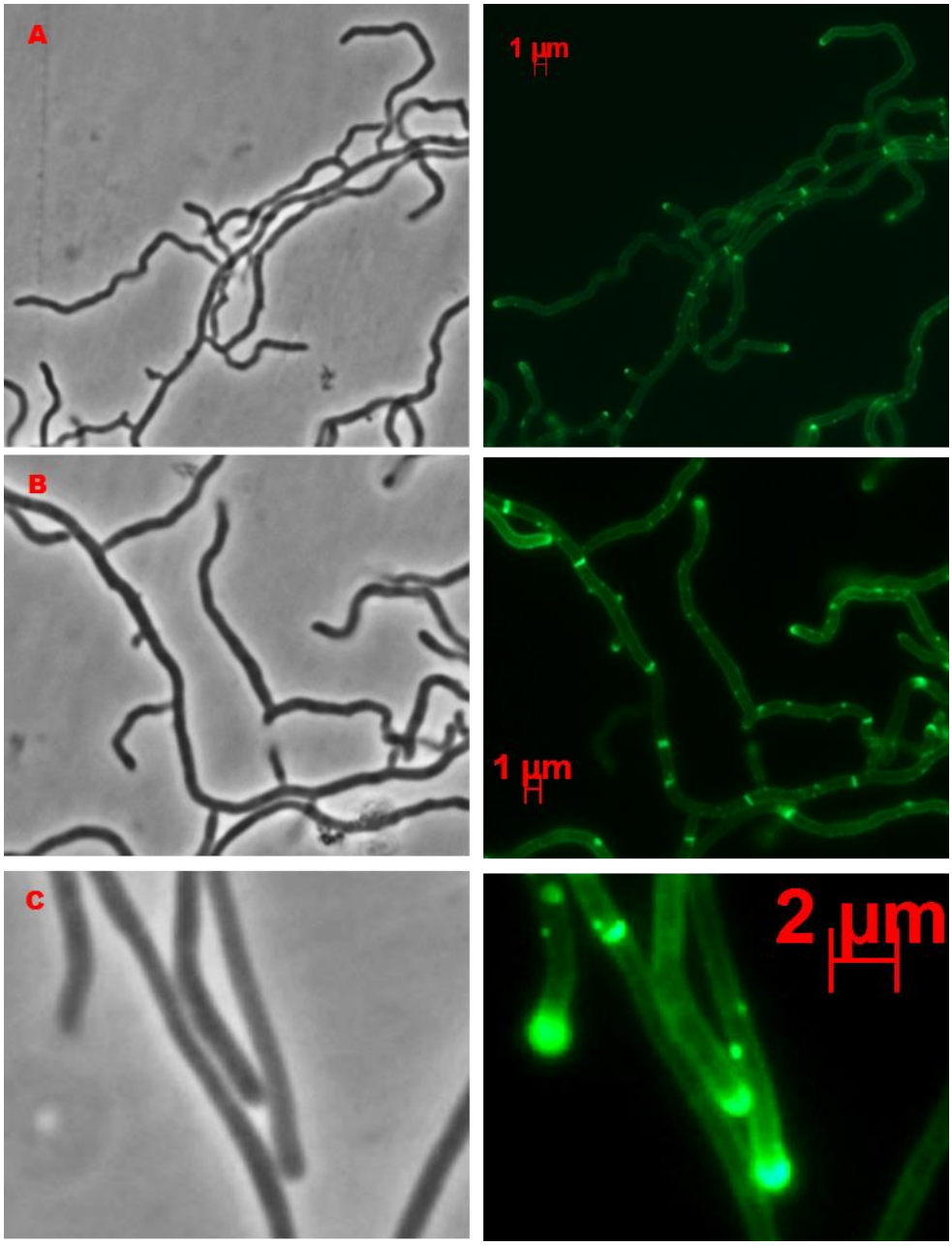


**Figure 6.11**: Microscopy images of M145 (wild-type) samples exposed to SFM at 30°C for 5 hrs and stained with vancomycin. Phase contrast images on left, vancomycin stained on right. A: shows fluorescence at tip ends in mature and newer hyphae. Crosswalls are also present. B: shows multiple crosswalls within the mature vegetative hyphae. Growing tips have strong fluorescence signal, and there are smaller foci within the hyphae (possible branch sites). C: shows that the vancomycin has adhered to the growing tips in a 'cap' shape. A crosswall is visible, as are two small foci which may be future branch sites.

**4°C without Bacitracin**

When M145 was exposed to 4°C, the three main areas of fluorescence; tips, crosswalls and branching sites, were easily observable (Figures 6.12 and 6.13).

Tip signals still showed a cap like structure and were strong areas of signal after 3 hrs of exposure to the lower temperature. Though caps were present, they did not fully resemble the control. Instead of the fluorescence being evenly spread through the edges of the tips, fluorescence seems to be concentrated to one edge more than the other (Figure 6.12.B, C). After 5 hrs of expose to 4°C, the M145 samples showed an additionally fluorescence pattern to the previous caps and elongated caps. Some samples had tip ends with a large amount of fluorescence starting from the tip end and trailing 1 or 2 µm (Figures 6.12.B and 6.13.B).

Crosswall signals were also seen, in similar intensity and placement as that seen when M145 was in optimum conditions. The number and placement of the crosswalls is visually similar to the control samples. The crosswalls do not seem to affect pattern of fluorescence for the other points.

However, the smaller branching site foci show as slight difference in shape. Previously, the foci were almost circular in shape, with some foci seeming slightly stretched as they followed the cell wall as it curved. When exposed to lower temperatures, the ‘stretched’ foci seem more numerous than circular foci, even on relatively straight stretched of hyphae. The foci signal strength seems to be on par with the foci seen in optimum conditions, however, there may be a slight increase in foci.

Ultimately, exposing M145 to lower temperatures for 3 hrs or 5 hrs does not seem to significantly change cell wall synthesis patterns as shown through vancomycin staining of the samples. This differs slightly from M145 KF59 being exposed to 4°C, though both samples were not greatly affected by the change in temperature when compared to the relative controls.

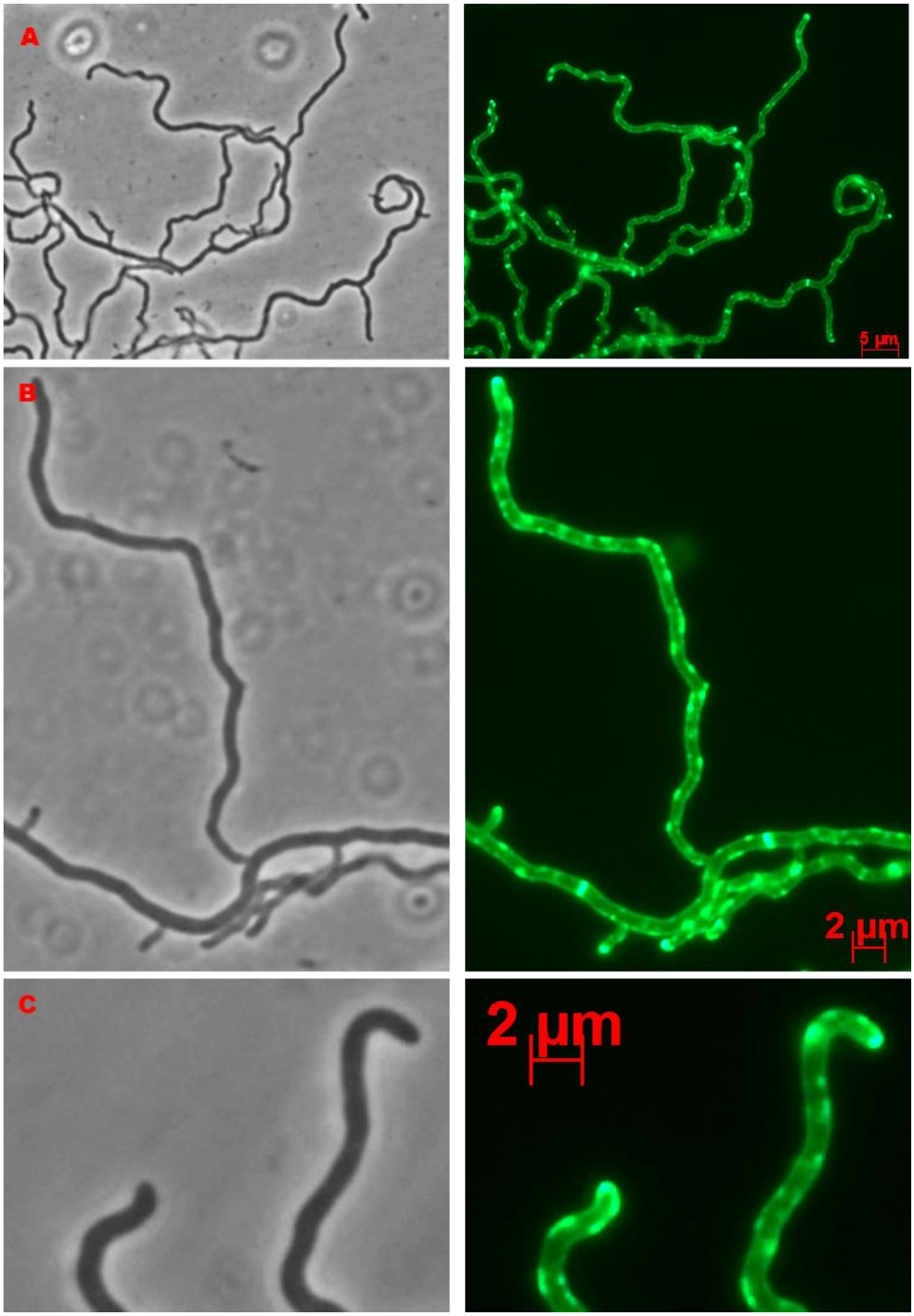


**Figure 6.12**: Microscopy images of M145 (wild-type) samples exposed to SFM at 4°C for 3 hrs and stained with vancomycin. Phase contrast images on left, vancomycin stained on right. A: shows multiple hyphae, all of which have fluorescence at crosswalls, tip ends, and scatter throughout the hyphae. B: shows that there are many foci of varying sizes within the hyphae. Crosswalls show a strong signal, comparable to the signal strength of the tip foci. There are strong foci trailing close to the tip end. C: shows that some tip ends have a 'cap' shaped fluorescence pattern. There are foci close to the tip ends, which seem to mostly aggregate to one side of the tip. Other smaller foci are also present within the hyphae. Some of these foci appear to be one long point of fluorescence; however, closer observation shows that they are separate small 'dot' foci.

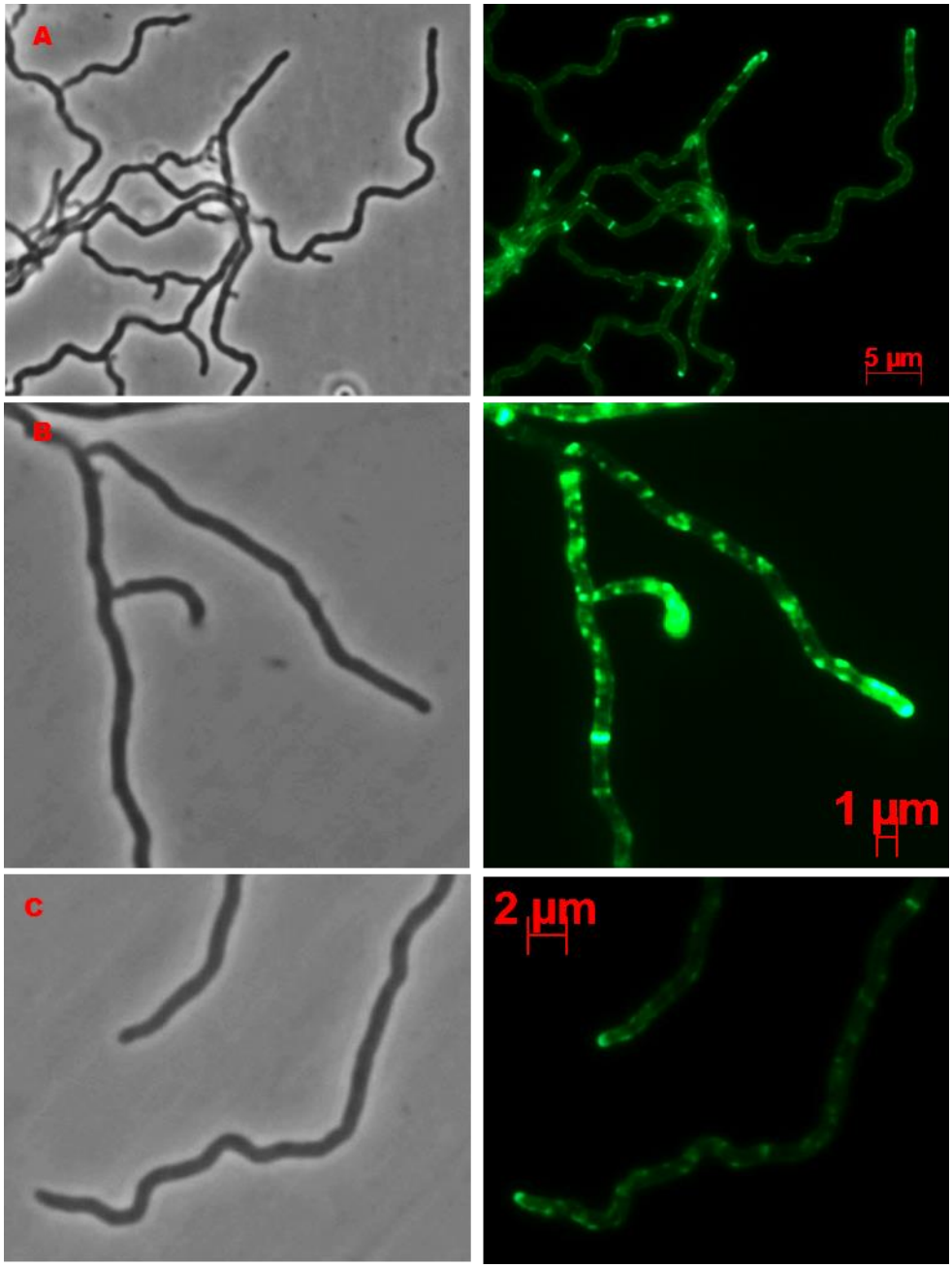


**Figure 6.13**: Microscopy images of M145 (wild-type) samples exposed to SFM at 4°C for 5 hrs stained with vancomycin. Phase contrast images on left, vancomycin stained on right. A: shows fluorescence varies at tip ends. Some tips show a strong signal at the ends only, but other samples show tips with fluorescence trailing the ends of the hyphae. Crosswalls are strongly stained. B: shows tips can have a fluorescence pattern which is strong but not confined to the ends of the tips. Other strong foci not joined to the tip signal can also be observed close to the ends. Weaker foci are spread throughout the hyphae. Crosswalls are easily observable. C: shows some tips have a fluorescence pattern close to 'cap' shaped. Other foci are scattered throughout the hyphae.

**30°C with Bacitracin**

A large phenotypic change is seen when M145 is exposed to bacitracin. There is 'explosion' of branching, as it documented clearly in samples exposed to bacitracin for 3 hrs or 5 hrs (Figures 6.14 and 6.15). Numerous branches are established, all of which show strong apical growth as seen by their intense tip fluorescence. The fluorescence signals are cap like in shape and free from other smaller foci, and usually have a 'foci free' area behind them. The additional branches are positioned at various areas along the hyphae and are closer together than normally seen in M145. The branches also grow in various directions and on different planes. Of the newer branches, larger branches may contain only a few foci or crosswall signals (Figure 6.15.C). Hyphae which were established before the M145 samples were exposed to bacitracin have a different phenotype. These hyphae are distinguished from newer branches as they are much longer and are sometimes thicker than the surrounding hyphae, have a different vancomycin staining pattern and have new branches growing from them. The older hyphae seem to have stopped growing apically, as branches are seen close to their tips and their tip signal is scattered, though their tip sections do show strong fluorescence signals. It is possible that parts of the established hyphae are being 'recycled', such as cell wall synthesis lipids, to allow for the branching occurring. As the branching seen is in high levels, cell wall machinery and cell wall components would also be required in high levels. Therefore, hyphae tips which have encountered as problem, such as a cell wall synthesis disruptor, may have their cell wall components recalled allowing for other branches to develop as these new branches may have more success in growing. As the new branches can grow it suggests that the cell wall synthesis pathway has been slightly adjusted for the subsequent growth after bacitracin exposure.

The older hyphae also contain numerous crosswall signals. The crosswalls are relatively close together and show a strong fluorescence. Some crosswalls are thicker than previously seen, though in shape most resemble crosswalls seen in optimum conditions. This increase of crosswalls could be to increase compartmentalisation in the hyphae. This could be in an attempt to stop the cell wall synthesis disruptor, bacitracin, from travelling to the rest of the hyphae. However, in this experiment the whole of the hyphae is exposed to bacitracin, not just the apical tips or small sections of the hyphae, as would have been the conditions outside of the lab if *S. coelicolor* encountered bacitracin producing bacteria (such as *Bacillus subtilis var Tracy*). This could account for the dramatic rise in the number of

crosswalls and branches throughout the mycelium. It is possible that the branching may have been limited to an area close to the tip, if *S. coelicolor* was exposed to bacitracin in a natural environment.

Additionally, M145 when exposed to bacitracin does not seem to increase foci scattering, as seen in M145 KF59. Inversely, foci scattering is limited, with foci scattering is only seen in the older hyphae at the tip ends, which was described earlier. The decrease in smaller foci could be due to the increase of branches and crosswalls. The cell wall synthesis seen at the smaller foci would be required at the other active areas of cell wall growth, and the synthesis components could have been recruited to these areas.

The changes seen in M145 are significant compared to M145 KF59, as the latter did not show an increase in branching. Though, there was an increase in signals within the hyphae of M145 KF59 when exposed to bacitracin, which may have allowed for an increase in branching at a later date.

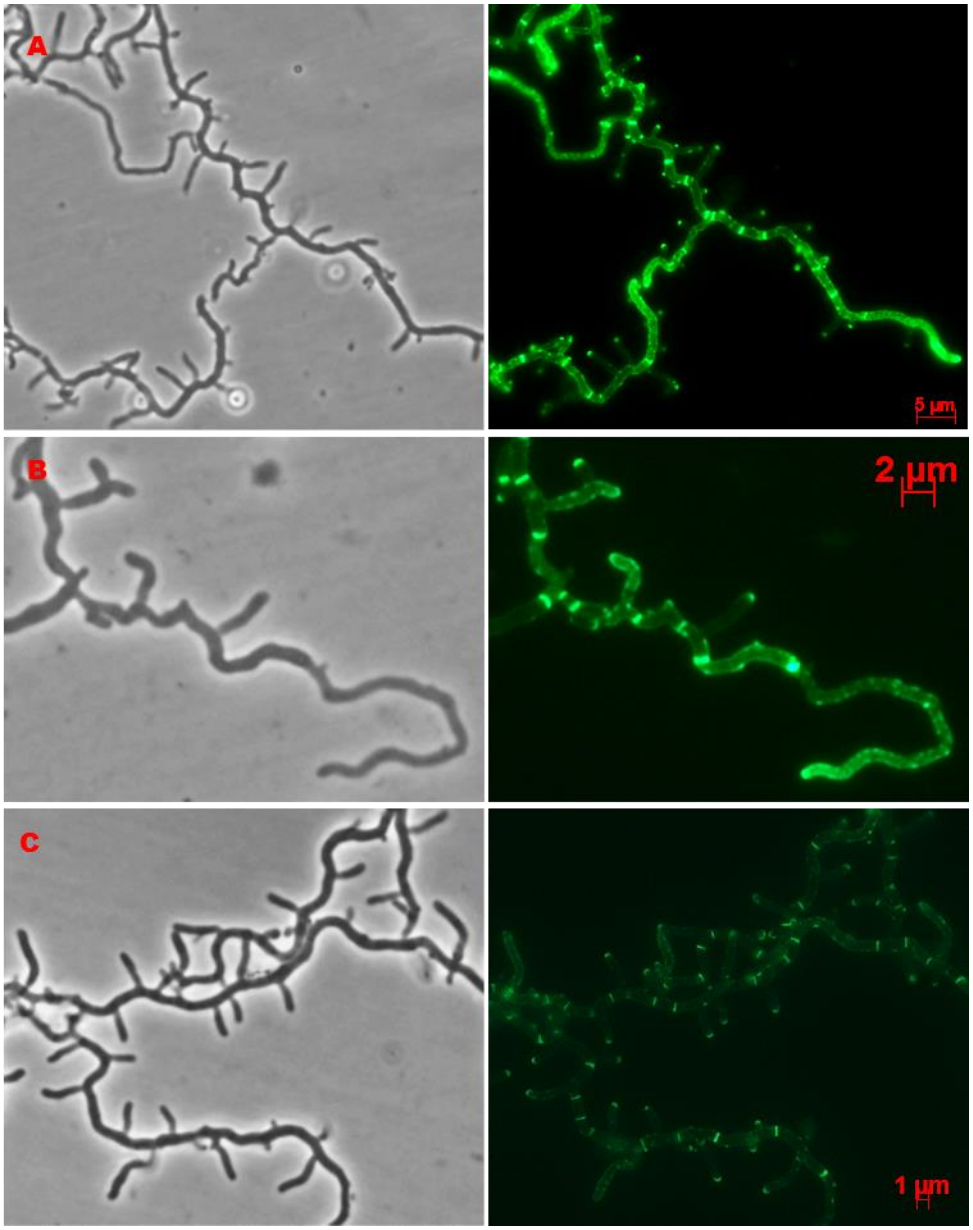


**Figure 6.14**: Microscopy images of M145 (wild-type) samples exposed to SFM containing bacitracin at 30°C for 3 hrs stained with vancomycin. Phase contrast images on left, vancomycin stained on right. All panels show samples with multiple new branches. A: shows the main mature hypha, which the new branches are growing from, has a strong signal through and has a concentrated signal closer to the tip ends. Crosswalls in this hypha are clearly observable. The new branches have clear growing end signals, with the rest of the new hyphae being relatively clear of fluorescence. B: shows many crosswalls within close proximity. The new branches have 'cap' shaped fluorescence signal. The old hypha has dispersed and scattered fluorescence throughout the hypha past the final crosswall. C: shows many new branches and crosswalls within the older hypha. The new branches show clear 'cap' signals and scattering is absent.

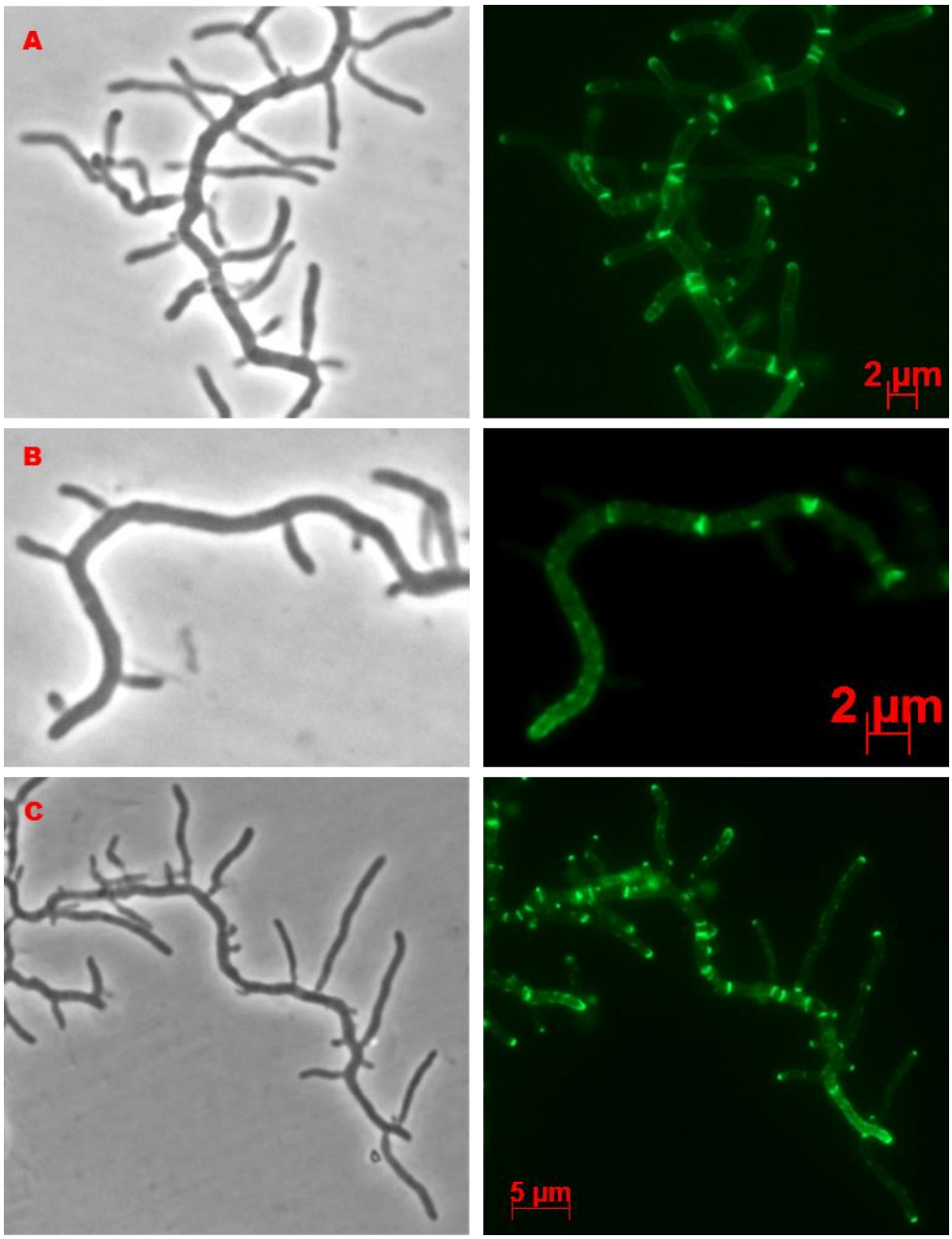


**Figure 6.15**: Microscopy images of M145 (wild-type) samples exposed to SFM containing bacitracin at 30°C for 5 hrs stained with vancomycin. Phase contrast images on left, vancomycin stained on right. New branches can be seen in all the panels. A: many branches in close proximity have formed from the mature hypha. The branches show a clear and strong 'cap' fluorescence. Additionally, there are many crosswalls, with some examples being close together. B: shows an older hypha with scattered signal throughout. C: shows many new branches of varying sizes. The longer of the new branches have foci (which may be future branch sites). Many crosswalls are seen in the main branch.

**4°C with Bacitracin**

When M145 was exposed to both stress factors, lower temperatures and a cell wall synthesis disruptor, the cell wall synthesis pattern changed once again, with distinct fluorescence patterns from the control and the previous samples. The signals measured from M145 at 4°C and exposed to bacitracin were limited to the crosswalls. Other areas of growth or cell wall synthesis as shown by vancomycin staining were not seen. There are no additional branches, scattered foci or tip signals (Figures 6.16 and 6.17).

In some samples there does seem to be a slightly increase in fluorescence at the tip ends. However, this signal may not be due to vancomycin staining but natural background *Streptomyces* fluorescence. The hyphae are generally smooth and bar the absence of fluorescence signal as seen in the conditions, seem typical of hyphae of that age. The signal that is seen is only at crosswalls, and the fluorescence seems to match its counterpart in the M145 control in intensity. There does not seem to be any increase in crosswalls when compared to the control, and crosswalls do not follow a clear placement pattern within the hyphae.

This different to M145 KF59, which showed some signal in the tips and foci scattering. However, the signal seen in the M145 KF59 strain from DivIVA-eGFP, which was scattered in the hyphae, may not be linked with cell wall synthesis. Instead it could be from ‘free’ DivIVA-eGFP which had aggregated in sufficient amounts to be observable, but were not required by the cell machinery as cell wall synthesis is not taking place. This would mean that the hyphae from M145 KF59 is similar to that of M145 as both do not have cell wall synthesis taking place at branching sites. However, tip signal is seen in M145 KF59, unlike M145, when exposed to bacitracin and 4°C. The signal could be explained as DivIVA-eGFP that is not being utilised in cell wall synthesis. It is possible DivIVA is at the tip site, but it is not initiating cell wall synthesis, which would explain why the tip signal is not in a cap like shape, as the DivIVA is not being used as an active part of the TIPOC.

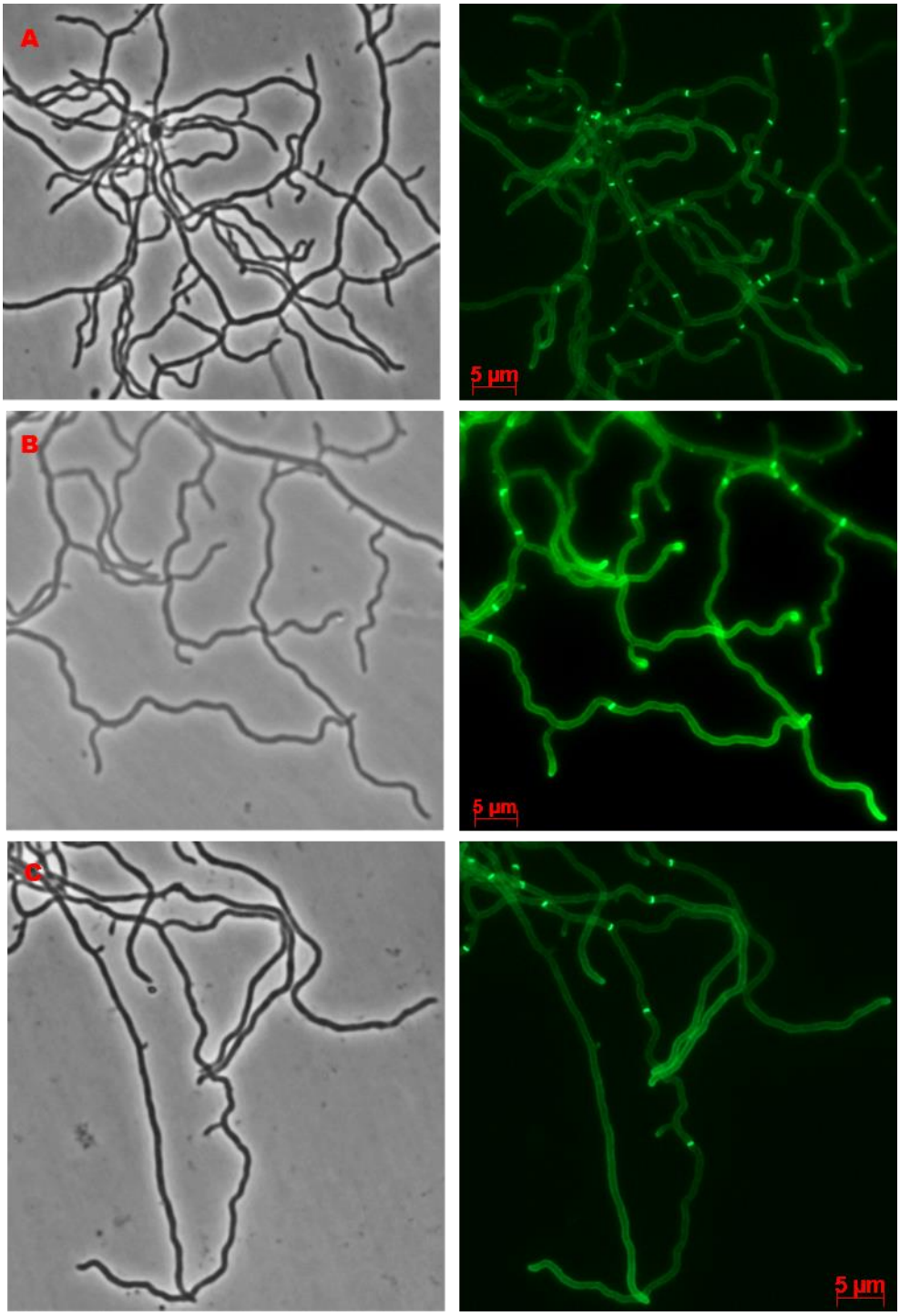


**Figure 6.16**: Microscopy images of M145 (wild-type) samples exposed to SFM containing bacitracin at 4°C for 3 hrs and stained with vancomycin. Phase contrast images on left, vancomycin stained on right. A: shows there is only evidence of vancomycin staining at crosswalls. B: shows strong fluorescence at crosswalls, with some possible fluorescence at tip ends. C: fluorescence is only seen at crosswalls.

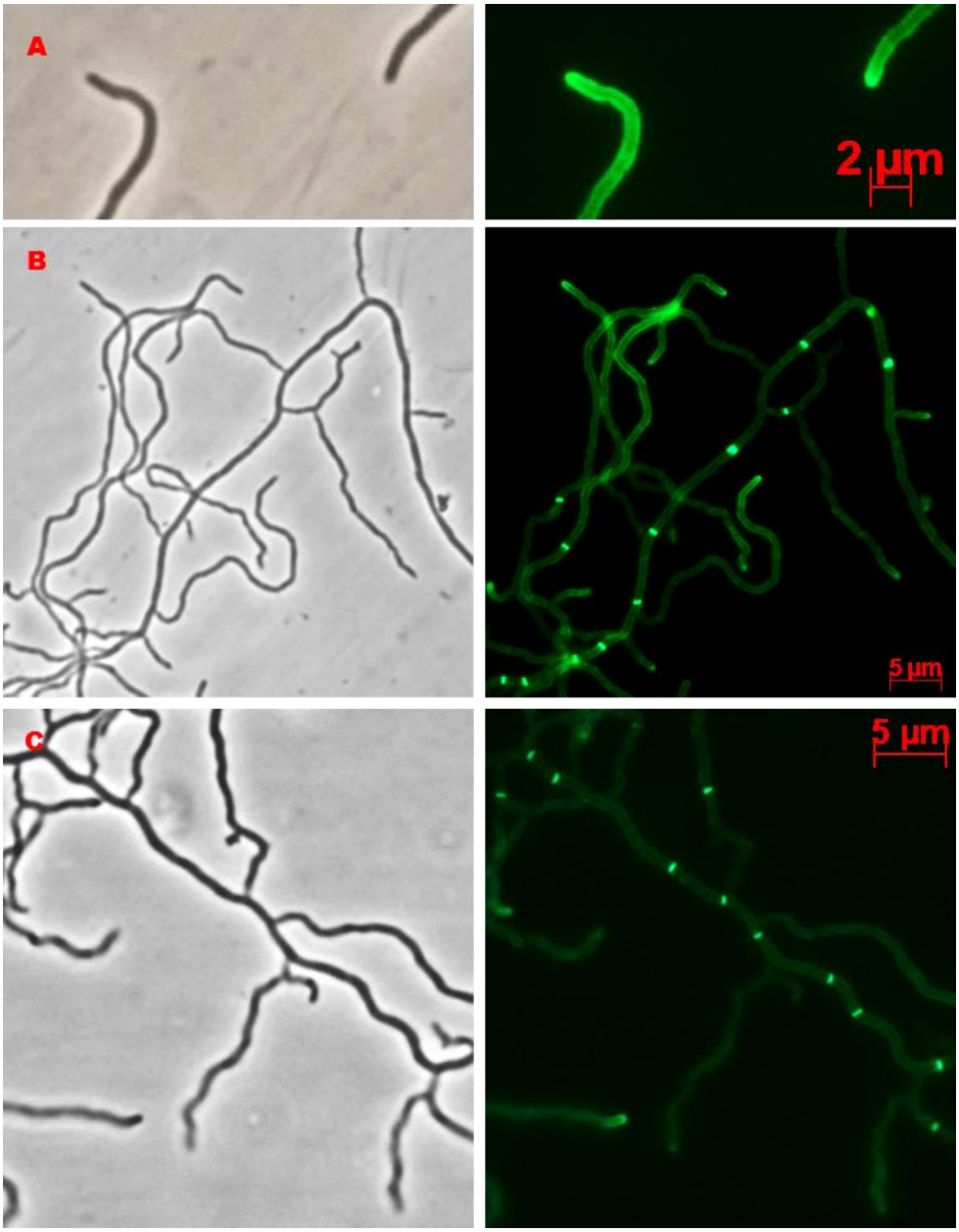


**Figure 6.17**: Microscopy images of M145 (wild-type) samples exposed to SFM containing bacitracin at 4°C for 5 hrs and stained with vancomycin. Phase contrast images on left, vancomycin stained on right. A: shows some possible 'cap' shaped fluorescence at tip ends. B: shows fluorescence at crosswalls only. C: shows fluorescence at crosswalls. The distribution and number of crosswalls seem to be relatively normal.

### 6.3. Summary

The effects of the stress conditions tested on the two strains did not always result in similar outcomes.

One of the most distinct phenotypes was the extra branching of the vegetative hyphae, only seen when M145 was exposed to bacitracin at 30°C. This does not occur in M145 KF59, however, some microscopy data suggests that there is the future possibility of additional branches, due to the increase of foci which are similar to foci seen at future branching sites. When comparing these two sets of conditions it is important to note that the only true difference between the samples is the eGFP fused to DivIVA in M145 KF59. While M145 is exposed to another 'stress factor', in the form of its cell wall dye of vancomycin, it is not substantial. Vancomycin is a cell wall inhibitor so could be working in a compound affect with bacitracin. However, it is only used as a cell wall stain in this experiment, and therefore only exposed to M145 from a maximum of 5 minutes. While this is optimum time for vancomycin to penetrate the cell wall and thus act indicator of active cell wall growth, it is not enough time for the downstream effects of the vancomycin induced cell wall inhibition to manifest. Even if the downstream effects had been put into motion this would not result in branching, as this growth process takes much longer than five minutes.

This suggests that that the addition of GFP to DivIVA in the KF59 construct affects normal functioning of DivIVA and results in larger morphological changes when the strain is exposed to stress conditions.

Another obvious phenotype was the increase of crosswalls seen in stress conditions as recorded in M145.

M145 and M145 KF59 also differed in the areas that cell wall growth was indicated, with emphasis on the lack of crosswalls seen in M145 KF59. Crosswalls were not present in the M145 KF59 strain tested, however, crosswalls were present in every sample of M145 tested. This could possibly be due to two main reasons. Either that M145 KF59 does not contain crosswalls. Or that the DivIVA-eGFP fluorescence in M145 KF59 did not show crosswalls. It seems unlikely that M145 KF59 does not contain crossswalls, as crosswalls are seen in healthy *Streptomyces*. Crosswalls are not seen in *sepF* impaired strains, but M145 KF59 does contain a *sepF* gene so should be able to produce crosswalls. This leaves the other theory that DivIVA-eGFP does not show crosswalls as it does not localise to crosswalls. This form of growth may not be DivIVA dependent, and therefore is not

highlighted by DivIVA-eGFP in fluorescence microscopy. This indicates that not all forms of cell wall synthesis are linked with DivIVA.

In summary, it seems that M145 and M145 KF59 differ when exposed to stress conditions which may be due to the influence of the DivIVA-eGFP fusion. Additionally, *divIVA* may not be linked to cell wall synthesis in all cases, suggesting that other cell wall synthesis pathways are used in conjunction to *divIVA* dependent growth.

## Chapter 7. Discussion

Cell division is a complex and essential process in the majority of bacteria, however, there is still much that is not known about the molecular mechanism of cell division. One of the obstacles to studying cell division is that division mutants are not viable in most of the model organisms, such as *E. coli* or *B. subtilis*. To truly understand cell division, studies should focus more on model organisms such as *S. coelicolor*, due to their early development and growth not being reliant on cell division, hence knockout mutations of cell division genes are not lethal and affect only the late stages of development, sporulation. The key to understanding cell division, is linked with proteins which associate and form the division site.

In *S. coelicolor* the cluster containing *ftsZ* and *divIVA* is important for the normal growth and division of the cell. The FtsZ protein is a driver of cell division, and without its proper placement and polymerisation into stable Z-rings, cell division cannot take place. DivIVA is the driver of polar cell growth, and essential in *Streptomyces*. Therefore, further investigation of DivIVA was performed using DivIVA-GFP fusion strain, M145 KF59, to test the effects of the addition of the cell wall synthesis inhibitor bacitracin and a sudden change from optimum to low temperatures on vegetative growth. The effects of bacitracin and low temperatures varied greatly, but the most significant and interesting difference was between M145 KF59 and the wild-type M145. This may be due to the M145 KF59 strain, which has previously been used to show the localisation of DivIVA (Flardh et el., 2003), and carries a DivIVA-GFP fusion in addition to a wild-type DivIVA copy. The presence of more than one copy of DivIVA might had an effect on the growth and branching of the M145 KF59 strain compared to the wild-type.

The importance of the proteins DivIVA and FtsZ might indicate that the other proteins encoded within this cluster also have roles within cell division or growth. One of these proteins is SepF, which had been previously shown in *B. subtilis* to be a FtsZ membrane anchoring protein (Hamoen et al., 2006; Gundogu et al., 2011; Duman et al., 2013). Due to the role of SepF in *B. subtilis*, and the fact that *S. coelicolor* contains three homologues of SepF, strongly suggested that SepF is important in *Streptomyces*. Additionally, other proteins associated with tethering FtsZ to the membrane, such as FtsA, are not present in *Streptomyces*, despite its large genome. This led to the investigation into the role of one of the three SepFs of *S. coelicolor*, SepF2, through knockout and complementation studies.

During the investigation of SepF2 during inducible overexpression attempts, it became apparent that *sepF* overexpression can be affected by a number of factors. Firstly, thiostrepton, which is the inducer of the tipA promoter which controls expression within the pIJ6902 overexpression vector, may not be free to travel between the 'tissues' or compartments of *S. coelicolor*. This is a problem as the inducer can be introduced in the growth medium of *Streptomyces*, but it will not be able to travel to the aerial hyphae. If the proteins to be overexpressed are needed in the aerial hyphae, then adding thiostrepton to the solid medium might not be sufficient to achieve expression in the aerial hyphae. Secondly, overexpression constructs need to be carefully designed, to maximise ribosome binding to ensure high translation initiation rates. If these rates of translation are low, then over all expression efficiency is also low.

Additionally, *SCO2078* was investigated due to its gene location in the cell division and growth cluster of *S. coelicolor*. The role of SCO2078 is still relatively unknown, though the study by Kabeya et al (2010) determining the role of its homologues within plant chloroplasts and cyanobacteria was an interesting insight to its potential roles, although at present we cannot say whether the roles in DNA compaction and segregation described is also true in *Streptomyces.*

**DivIVA is not necessarily linked to all mechanisms of cell wall growth**

DivIVA is an essential protein for *Streptomyces*, and important in polar growth. However, it may not be required for all forms of growth within *Streptomyces*. When comparing the areas of cell wall growth between the wild-type M145 and M145 KF59, with its GFP tagged DivIVA, there was one large difference. Crosswalls which are a form of vegetative septa, could be clearly seen in M145 through vancomycin staining, but were not present in M145 KF59 when viewed via fluorescence microscopy.

As DivIVA was not shown to localise to the vegetative crosswalls, it suggests that the formation of crosswalls is independent of DivIVA. However, as seen when comparing M145 and M145 KF59 under various 'stress' conditions, the two strains do not always have the same morphology. This suggests that M145 KF59 does not act as wild-type strain at all times, but instead that in the presence of DivIVA-GFP DivIVA localisation is impaired under stress conditions. Therefore, the lack of DivIVA-GFP localisation at crosswalls may be partly due to the nature of the mutant itself, and not that DivIVA is not linked to the growth of crosswalls.

**Lateral hyper-branching due to spontaneous nucleation as a result of disturbing the TIPOC**

Lateral hyper branching was documented in M145 when the strain was exposed to bacitracin for over 3 hrs, with the strongest evidence for hyper-branching seen after the samples were exposed to the cell wall synthesis inhibitor for 5 hrs. The samples all exhibited extra branches, which grew at irregular distances between branchpoints. The distances between branches were also small, with branches occurring close together and, in some cases, very close to the tip of the branch they were growing off.

The change in branch to branch distances and the event of hyper-branching seen in M145 exposed to bacitracin suggests that there has been a change in the mechanism of branching control. Normally, branch to branch distances are tightly controlled, with the size of the TIPOC regulating distances. The mechanisms require the TIPOC to reach a minimum size before a new branch site can be placed or developed, ensuring that branches do not grow close to the tip or too close one another (Richards *et al.*, 2012).

However, when M145 is exposed to bacitracin the tip foci, as shown through vancomycin staining, are affected, with the tip foci being smaller, diffused or in some cases not present. The tip foci show areas of cell wall growth, which is normally controlled by and corresponds to the TIPOC. Therefore, changes to the tip foci indicate that the TIPOC is also affected.

If the TIPOC directly corresponds to the tip foci, it should also be smaller when the tip foci are affected. This would mean that the minimum size of the TIPOC for branching initiation would not be reached, so branching should not occur let alone hyper-branching. However, increased branching and irregular branch to branch distances are seen in every M145 sample exposed to bacitracin. This suggest that another, non-dominant, mechanism for branching has been utilised by M145 when exposed to the cell wall inhibitor.

Literature has documented lateral hyper-branching previously, in cases where *divIVA*, a key component of the TIPOC, has been overexpressed in *Streptomyces*. This form of branching was the result of ‘spontaneous nucleation’. It is thought that the excess DivIVA allows TIPOCs to form throughout the hyphae in a non-predetermined fashion, resulting in multiple new branching sites. (Flärdh, 2003)

This may be the same mechanism that results in M145 hyper-branching when exposed to bacitracin. Bacitracin does not directly interfere with DivIVA or gene expression, but it does inhibit growth. It is possible that the inhibition of growth at the tips of M145, which is seen through the lack of tip foci, translates to the lack of TIPOC at the hyphae tips. This would suggest that DivIVA is no longer within the strong TIPOC complexes usually documented as cap-like foci at the tip ends. Therefore, DivIVA would not be concentrated at the tip ends, but is instead 'free' to travel within the hyphae. This extra, cytoplasmic DivIVA could mirror circumstances where *divIVA* is overexpressed, thus allowing 'spontaneous nucleation' to take place.

Initially, the 'spontaneous nucleation' mechanism was thought to be irrelevant effect occurring during *divIVA* overexpression in vegetative hyphae (Flardh, 2003). However, it may serve as an alternative method for vegetative growth when main tip growth is not feasible. Though the example of M145 exposed to bacitracin is within laboratory conditions, it is not unnecessarily seen in the natural environment of *S. coelicolor*. As *Streptomyces* is a soil bacterium it is in a competitive environment containing many other bacteria. Therefore, *Streptomyces* could be exposed to other bacteria which can produce metabolites which affect normal growth. This would suggest that *Streptomyces* would require an alternative method for vegetative mycelium development.

Without this secondary growth pathway, *Streptomyces* would not be able to develop in areas of high competition. Therefore, this shows the importance of 'spontaneous nucleation', and highlights that *S. coelicolor* may contain multiple pathways for branching and growth for its vegetative stage.

Additionally, the idea that excess free DivIVA being present in hyphae with impaired or absent tip foci, and thus absent TIPOCs, may explain the higher amount of hyphae foci found in M145 KF59 exposed to bacitracin when compared to controls. The increase in scattered foci within the hyphae suggests that there could be many branching sites. This should result in hyper-branching as seen in M145 when exposed to bacitracin. However, it seems that in M145 KF59 only the precursor of hyper-branching occurs; spontaneous nucleation forming multiple TIPOCs throughput the hyphae. The next step of the branches forming may not occur as DivIVA-eGFP, which is present in M145 KF59, may not be neutral, and therefore not act as DivIVA naturally would in all situations.

**SepF is essential for septa formation**

The absence of *sepF* within *S. coelicolor* resulted in the absence of septa, in both the vegetative and aerial hyphae. This indicates that *sepF* is essential in the formation of septa and crosswalls. The absence of *sepF*, and therefore septa, caused several other macroscopic and microscopic changes.

The absence of septa stopped the formation of spores. Septa are required in spore formation, as they help form pre-spore compartments. Pre-spore compartments contain the future spore's packaged genetic material, and septa form the walls of pre-spores. The pre-spores then undergo a constriction process in which spores are formed and can separate from the spore chain. This process is the only true form of cell division that takes places in the *Streptomyces* life cycle. However, without SepF, septa are not formed, therefore the walls of the pre-spores and subsequent spores are also not formed, thus preventing sporulation. Therefore, *sepF* is essential for spore formation and thus cell division in *S. coelicolor*.

Without SepF, no other visible septa like structures are seen, however, the aerial hyphae does attempt spore formation. Evidence for this is the occasional partial constriction or 'pinching' of the cell wall seen in some aerial hyphae samples. This may be due to the natural constricting forces applied to spores, suggesting that this process is independent of septa formation and SepF.

**Absence of SepF may cause increased cell lysis**

Within the vegetative and aerial samples of the Δ*sepF* strain more lysis was seen than in wild-type samples.

This suggests that SepF may have a structural role in *S. coelicolor*. It is possible that the crosswalls in vegetative hyphae support cell wall development. However, as crosswalls are not seen in the formation of aerial hyphae, it suggests that crosswalls have another role. This role may be the formation of compartments in the mycelium. As mentioned in Chapter 4, crosswalls may act as partitions between compartments within vegetative hyphae. This could be to prevent the transport of foreign or harmful proteins or compounds. Therefore, an absence of crosswalls would allow lysis-inducing particles to travel within the mycelium and even to the aerial hyphae. Thus, the strain would be lysis-prone. Therefore, it suggests that crosswalls have a protective function, and their absence results in a lysis prone mutant.

**Absence of SepF increases Actinorhodin Production**

The *sepF* mutant was also distinct due to its blue colour, as opposed to the wild-type grey-brown. The blue pigment produced by the Δ*sepF* strain is actinorhodin. Actinorhodin is naturally produced by *S. coelicolor*, however, it is not produced in quantities large enough to change the colour of *S. coelicolor* or stain its surrounding media on a macroscopically observable scale, as seen in the *sepF* knockout mutant. This suggests that Δ*sepF* overproduces actinorhodin. As noted in Chapter 4, the role of actinorhodin is not fully defined in *S. coelicolor*.

The metabolite may be produced as a form of defence, as actinorhodin has antibacterial properties. However, the effectiveness of actinorhodin as an antibiotic is questionable. Past studies are limited, and it is thought that actinorhodin is only effective on some Gram-positive bacteria (Wright e Hopwood, 1976; Nass *et al.*, 2017).

It is possible the overproduction of actinorhodin in Δ*sepF* may act as a signal to other *Streptomyces*. It has been observed that different *Streptomyces* species can induced changes in species such as *S. coelicolor* without being in physical contact (Romero *et al.*, 2011). This shows secreted molecules can act as signalling molecules. The paper also showed that the *Streptomyces* species acted against *S. coelicolor*, but it is possible *S. coelicolor* could also act against *S. coelicolor* and other species.

The signal that Δ*sepF* may be trying to convey through actinorhodin overexpression could be one that denotes stress. In certain stress conditions were growth is limited, through limited resources such as nitrogen, phosphate or trace elements, can result in the production of actinorhodin and other associated blue pigments (Leonid *et al.*, 1996).

Additionally, it is possible that actinorhodin is visible in the mutant, not only because it is overproduced, but due to the absence of septa and crosswalls. It may be produced at levels normally seen in the wild-type, but when in the wild-type actinorhodin is not free to move through vegetative compartments or aerial hyphae. As the mutant does not produce septa and crosswalls, then actinorhodin may travel. This could be the reason for the colour change of the aerial hyphae from white to blue as the mutant matures.

Additionally, the spore sheaf contributes to the wild-type colouring of mature *S. coelicolor*. As this is absent in the mutant, the aerial cannot become ‘grey’, but

must remain white. This white colouring would be more susceptible to being dyed by the actinorhodin than the grey spore sheaf. Therefore, actinorhodin which has travelled, as it is not impended by crosswalls, may stain the mutant's aerial hyphae and been more easily observed.

This study does not suggest that SepF directly supresses actinorhodin production, but that the absence of SepF either causes actinorhodin to be overproduced as the mutant is 'stressed' or that the absence of crosswalls allows the movement and travel of actinorhodin.

**The absence of *sepF* results in delayed development**

The Δ*sepF* strain grew and developed at a slower rate than the wild-type. There are several potential reasons for this, which may be working in conjunction.

Firstly, as previously discussed, the Δ*sepF* strain is more prone to lysis. The areas which undergo lysis can be large and encompass the majority of the mycelium, or relatively small and only affect singular branches, however, all areas once had active growth. This use and subsequent waste of energy for growth may divert resources required for normal development and growth. This energy dissipation could result in slower overall growth for the strain.

Secondly, it has been proposed that the production of secondary metabolites may slow the rate of growth. The Δ*sepF* strain may be an actinorhodin overproducer, and it is thought that the activation of ACT pathway may have a secondary function of slowing down growth in *S. coelicolor* (Esnault *et al.*, 2017). As Δ*sepF* overproduces actinorhodin this would have a greater growth slowing effect than seen for normal levels of actinorhodin production.

Lastly, Δ*sepF* development is incomplete as the strain cannot complete its life cycle, as sporulation cannot take place. This means that the aerial hyphae are unable to fully mature. The strain attempts to sporulate, as seen by the partial constriction of areas which should contain spores in a wild-type strain. As spores are unable to be formed, development is halted.

**There are multiple promoters for *sepF***

Attempts to complement the *sepF* knockout strain with the gene and adjoining upstream region only resulted in partial complementation. Septa were formed but were irregular in width and distances between aerial septa varied. Some examples of the septa formed did not span the width of the aerial hyphae. This suggested that the cloned fragment used for complementation was not fully expressed as though it did contain a promoter it did contain not all the promoters that *sepF* requires for full expression. Additionally, *sepF* had been predicted to contain two promoters, as documented in a *S. coelicolor* wide mapping paper (Jeong *et al.*, 2016).

This was investigated further in a separate study within the research group, and the *sepF* knockout strain was shown to be fully complemented after *sepF* and an upstream region containing the second half of the adjacent gene (*SCO2078*) was used (Tan et al., unpublished).

**Expression of *sepF* is regulated and highly dynamic**

In a further attempt to restore the Δ*sepF* mutant to a wild-type phenotype, the *sepF* fragment P1sepF, containing the *sepF* gene and an upstream region containing only one promoter for *sepF,* was introduced into the overexpression plasmid pIJ6902. This construct was also used to investigate the effect of *sepF* overexpression. The *sepF* gene in the pIJ6902-P1sepF construct would then be under the control of two promoters, one native and the other an inducible tipA promoter.

The two promoters working in tandem in the Δ*sepF*/pIJ6902-P1sepF strain resulted in growth that, when observed macroscopically, resembled the wild-type, as grey pigment associated with spore production was being produced in the previously spore-less strain. By the addition of varying levels of tipA inducer thiostrepton to the strain, the strength of the pigment could be changed. Higher amounts of thiostrepton resulted in darker, greyer, hyphal lawns (though amounts above 25 µg resulted in a different phenotype for the strain – see below). The time at which the tipA inducer thiostrepton was added also affected the Δ*sepF*/pIJ6902-P1sepF strain macroscopically. When the inducer thiostrepton was added to very early development, such as germination, developmental delays were seen. If the

inducer was added 51 hrs after inoculation then the resulting aerial hyphae was darker than when added at earlier or later time points (Figure 5.10)

When the Δ*sepF*/pIJ6902-P1sepF was observed microscopically, it became apparent that none of the range of thiostrepton added, and thus the levels of *sepF* expression, and the times at which tipA was induced by thiostrepton resulted in a wild-type phenotype. The septa observed in the aerial hyphae were irregular for the low and high amounts of thiostrepton added. This was seen for all the developmental points tested for Δ*sepF*/pIJ6902-P1sepF. Therefore, it seems that the level of SepF must be accurate and carefully controlled to result in a wild-type phenotype.

**Increased *sepF* expression can compensate for the developmental delay caused by the addition of the inducer thiostrepton**

Also described in Chapter 5 is the development delay caused by thiostrepton on the strains *ΔsepF*/pIJ6902-P1sepF and *ΔsepF*/pIJ6902. Both strains show a delay in growth when thiostrepton is added to the strains 0 hrs and 28 hrs after inoculation (Figure 5.14). This delay may be caused by the antibiotic action of the thiostrepton, as the water controls did not affect development, and as it is seen in control strain (*ΔsepF*/pIJ6902) it was accounted for in analysis of the strains.

Interestingly, the patches to which thiostrepton was added at 0 hrs and 28 hrs after inoculation are almost as dark grey as the patches to which thiostrepton was added 51 hrs and 69 hrs after inoculation by day 5. The areas which differed from the later induced plates are different due to the possible negative side effect of *sepF* overexpression (see next page). This indicates that the previous developmental delay due to thiostrepton addition at early stages of strain growth had been overcome.

This in turn suggest that *sepF* expression, as certain levels, may accelerate development to encourage aerial growth and spore production. This would mark SepF as a driver of aerial development and sporulation. However, the *sepF* expression could be having a greater effect on vegetative development and cause the ending of the stage to occur earlier.

**Overexpression of *sepF* at high levels during early developmental stages may be harmful to *S. coelicolor***

As seen in Chapter 5, *sepF* overexpression in the *ΔsepF*/pIJ6902-P1sepF strain can cause a 'black' phenotype (Figures 5.14 and 5.15). These areas had high amounts of thiostrepton added at 0 hrs after inoculation to induce high levels of *sepF* expression. This phenotype was not seen in the water controls or in the control strain *ΔsepF*/pIJ6902. The delay on development seen through the influence of thiostrepton differs from this phenotype, as the other strains did not turn black and the phenotype does not recover.

This black phenotype may have been the result of excessive amount of SepF being produced. This may have been detrimental, as it has been shown that overexpression of *sepF* in *Mycobacterium smegmatis* blocks cell division, and results in longer filamentous cells. Some of the cells, when over 15 µm, also showed branch-like structures (Gola *et al.*, 2015). The increase in cell length is also seen when *sepF* is overproduced in *B. subtilis*. In *B. subtilis* it has been shown that high levels of *sepF* do not impact Z-ring formation but may instead interfere with later cell division proteins and thus block cell division (Gao *et al.*, 2017).

This may be the reason why the 'black' phenotype does not fully recover, even after 4 and 5 days of growth which is the expected time for aerial hyphae to form. At this point the control strain has mostly recovered from the development delay of thiostrepton and has a full lawn. The *ΔsepF*/pIJ6902-P1sepF strain however, is different. The areas to which *sepF* overexpression induction had taken place at 28 hrs, 51 hrs and 69 hrs are fully recovered by day 5 and exhibited the grey colouring associated with mature spore producing aerial hyphae. Conversely, the 0 hrs examples for the thiostrepton amounts of 25 µg and 50 µg have turned black, though the outer areas of the patches are grey. This suggests that *sepF* overexpression only results in a 'black' phenotype if overexpression takes place soon after inoculation of spores. This is the developmental point at which *ΔsepF*/pIJ6902-P1sepF is the most vulnerable to the negative effects of high levels of SepF.

**Thiostrepton requires direct contact with aerial hyphae to induce overexpression**

As previously discussed in Chapter 5, overexpression of *sepF* was subject to a number of conditions. Thiostrepton, an inducer for the tipA promoter which acts as the second promoter of the *sepF* clone in the vector pIJ6902, was not utilised by *Streptomyces* in initial experiments. However, the exposure of the tested strain to thiostrepton did result in the overexpression of *sepF* when its application was revised.

Originally, thiostrepton was introduced to *Streptomyces* through its growth media. Therefore, it was only exposed to the vegetative hyphae, as they grow in and on the growth medium. This did not cause any phenotypic changes to the strains tested. When thiostrepton was directly applied to the strains, through 'drop application', phenotypic changes were documented, and *sepF* was overexpressed.

Drop application allowed thiostrepton to directly contact the aerial hyphae. Aerial hyphae are the main areas of *Streptomyces* which require *sepF*, and were only able to express *sepF* after they were directly exposed to the inducer. This suggests that membranes or 'tissues' of *Streptomyces* require direct contact with agents such as thiostrepton to affect inducible promoters in overexpression systems.

Additionally, the idea that crosswalls or other semi-permeable membranes within the vegetative hyphae could stop the transport of thiostrepton should be explored. It was touched upon in Chapter 5, that thiostrepton should in theory travel from the media to throughout the bacterium. However, this travel could be prevented by semi-permeable barriers, which naturally occur with *S. coelicolor*. The barriers may act to prevent the movement of harmful substances to the unaffected areas of the organism. Thiostrepton may have been treated as a harmful or unwanted substance, as it is an antibiotic. This would mean that when thiostrepton was present in the media its travel and uptake was restricted to only the vegetative hyphae that it was in direct contact with. The inducer was unable to travel to the aerial hyphae, where it would have had the greatest phenotypic effect.

**Effectiveness of Overexpression Systems in *Streptomyces* may be limited by Inefficient Ribosome Binding**

Also discussed in Chapter 5 is that the success of overexpression systems in *S. coelicolor* is variable. Past experiments have shown that similar genes, which result in structurally similar proteins, can not necessarily be overexpressed or even just expressed, by using the same overexpression system.

This study investigated the variable overexpression vector pIJ6902 which allows genes to be cloned under the control of inducible promoter tipA, and is one of the few variable overexpression systems available to *Streptomyces*. Previous overexpression experiments of different genes had been of mixed success when using pIJ6902. However, with the system able to overexpression *sepF*, the tipA promoter was assumed to be able to transcribe a gene, such as *sepF*, inserted downstream of it.

This logically left translation as the limiting factor in achieving *Streptomyces* gene overexpression when using pIJ6902. This was determined to be the case when testing *sepF* overexpression using different *sepF* constructs, as only constructs containing an upstream native promoter or RBS site were expressed. Overexpressing the gene in isolation was not achievable.

This was thought to be due the structure of the mRNA transcripts produced by the constructs. The transcripts would have variable accessibility to their start sites due to having either a stem or loop in the immediate or upstream binding area. Transcripts without a loop at their start site would impend ribosomal binding. This would result in a lower transcription initiation rate (TIR), which would affect the efficiency at which the mRNA was translated.

To test if the differences in expression of the *sepF* in its various constructs was due to differences in TIRs and mRNA structure, the constructs were run in specialised software for predicting TIRs. This showed that TIRs did vary, and that higher TIRs can be achieved through careful design of the constructs. Constructs can be designed to contain a ribosomal binding site which would increase TIR, and thus would overcome the problem of *Streptomyces* overexpression in pIJ6902.

**The Role of *SCO2078* is still unclear**

The investigation into *SCO2078* was to determine its role with *Streptomyces*, as the gene is within the cell division and growth cluster which suggests that it has a role either in cell growth or division. However, its role still remains unclear, though bioinformatics and plant homologues point to a potential role in organising chromosomes.

Gene knockouts were attempted for *SCO2078*; however, the resulting strains did not show any obvious macroscopic or macroscopic differences to the wild-type. Further investigation suggested that the gene might not have been truly knocked out. It is possible that a partial knockout occurred, but this has not been confirmed at this point.

It is thought that *SCO2078* could not be knocked out as it was predicted to contain a transcription start site for the essential gene *divIVA* (Jeong et al., 2016). This suggests that knocking out *SCO2078* would essentially result in a *divIVA* knockout, and *divIVA* is established as an essential gene (Flardh, 2003). This could also explain why *SCO2078*, which may not have an important role in *Streptomyces* development, is in the cell division and growth cluster.

As knockout generation was not feasible, *SCO2078* was overexpressed. The gene was overexpressed in using three methods. The initial method of repeating the gene within the wild-type, did not result in any phenotypic differences.

The gene was then overexpressed using the variable expression system of pIJ6902 and the inducible promoter tipA. As the gene was shown to have expression during all stages of growth, it was exposed to the overexpression inducer in its media and through direct dropping of the inducer onto the strain. Different time points for overexpression and levels of overexpression were tested, but the phenotype did not differ from the wild-type.

This suggests that overexpressing *SCO2078* is not harmful or beneficial *Streptomyces*. This may be as the protein produced is not being utilised, as it may require other proteins or complexes to be used. It is also possible that it may be regulated in other ways, with the proteins regulating *SCO2078* also being expressed at higher levels to counteract the effects of *SCO2078* overexpression.

**References**


Adams, D. W. and J. Errington (2009). "Bacterial cell division: assembly, maintenance and disassembly of the Z ring." Nat Rev Microbiol 7(9): 642-653.

Addinall, S. G. and J. Lutkenhaus (1996). "FtsA is localized to the septum in an FtsZ-dependent manner." J Bacteriol 178(24): 7167-7172.

Adler, H. I., W. D. Fisher, A. Cohen and A. A. Hardigree (1967). "MINIATURE escherichia coli CELLS DEFICIENT IN DNA." Proc Natl Acad Sci U S A 57(2): 321-326.

Alyahya, S. A., R. Alexander, T. Costa, A. O. Henriques, T. Emonet and C. Jacobs-Wagner (2009). "RodZ, a component of the bacterial core morphogenic apparatus." Proc Natl Acad Sci U S A 106(4): 1239-1244.

An, J. Y., T. G. Kim, K. R. Park, J. G. Lee, H. S. Youn, Y. Lee, J. Y. Kang, G. B. Kang and S. H. Eom (2013). "Crystal structure of the N-terminal domain of MinC dimerized via domain swapping." J Synchrotron Radiat 20(Pt 6): 984-988.

Arjes, H. A., B. Lai, E. Emelue, A. Steinbach and P. A. Levin (2015). "Mutations in the bacterial cell division protein FtsZ highlight the role of GTP binding and longitudinal subunit interactions in assembly and function." BMC Microbiol 15: 209.

Ausmees, N. (2013). "Coiled coil cytoskeletons collaborate in polar growth of Streptomyces." Bioarchitecture 3(4): 110-112.

Bagchi, S., H. Tomenius, L. M. Belova and N. Ausmees (2008). "Intermediate filament-like proteins in bacteria and a cytoskeletal function in Streptomyces." Mol Microbiol 70(4): 1037-1050.

Barka, E. A., P. Vatsa, L. Sanchez, N. Gaveau-Vaillant, C. Jacquard, J. P. Meier-Kolthoff, H. P. Klenk, C. Clément, Y. Ouhdouch and G. P. van Wezel (2016). "Taxonomy, Physiology, and Natural Products of Actinobacteria." Microbiol Mol Biol Rev 80(1): 1-43.

Beall, B. and J. Lutkenhaus (1992). "Impaired cell division and sporulation of a Bacillus subtilis strain with the ftsA gene deleted." J Bacteriol 174(7): 2398-2403.

Bendezú, F. O., C. A. Hale, T. G. Bernhardt and P. A. de Boer (2009). "RodZ (YfgA) is required for proper assembly of the MreB actin cytoskeleton and cell shape in E. coli." EMBO J 28(3): 193-204.

Bentley, S. D., K. F. Chater, A. M. Cerdeño-Tárraga, G. L. Challis, N. R. Thomson, K. D. James, D. E. Harris, M. A. Quail, H. Kieser, D. Harper, A. Bateman, S. Brown, G. Chandra, C. W. Chen, M. Collins, A. Cronin, A. Fraser, A. Goble, J. Hidalgo, T. Hornsby, S. Howarth, C. H. Huang, T. Kieser, L. Larke, L. Murphy, K. Oliver, S. O'Neil, E. Rabbinowitsch, M. A. Rajandream, K. Rutherford, S. Rutter, K. Seeger, D. Saunders, S. Sharp, R. Squares, S. Squares, K. Taylor, T. Warren, A. Wietzorrek, J. Woodward, B. G. Barrell, J. Parkhill and D. A. Hopwood (2002). "Complete genome

sequence of the model actinomycete Streptomyces coelicolor A3(2)." Nature 417(6885): 141-147.

Bernander, R. (2003). "The archaeal cell cycle: current issues." Mol Microbiol 48(3): 599-604.

Bernhardt, T. G. and P. A. de Boer (2005). "SlmA, a nucleoid-associated, FtsZ binding protein required for blocking septal ring assembly over Chromosomes in E. coli." Mol Cell 18(5): 555-564.

Bi, E. F. and J. Lutkenhaus (1991). "FtsZ ring structure associated with division in Escherichia coli." Nature 354(6349): 161-164.

Bibb, M. J., G. R. Janssen and J. M. Ward (1985). "Cloning and analysis of the promoter region of the erythromycin resistance gene (ermE) of Streptomyces erythraeus." Gene 38(1-3): 215-226.

Bignell, C. and C. M. Thomas (2001). "The bacterial ParA-ParB partitioning proteins." J Biotechnol 91(1): 1-34.

Bork, P., C. Sander and A. Valencia (1992). "An ATPase domain common to prokaryotic cell cycle proteins, sugar kinases, actin, and hsp70 heat shock proteins." Proc Natl Acad Sci U S A 89(16): 7290-7294.

Bottomley, A. L., A. T. F. Liew, K. D. Kusuma, E. Peterson, L. Seidel, S. J. Foster and E. J. Harry (2017). "Coordination of Chromosome Segregation and Cell Division in." Front Microbiol 8: 1575.

Brown, P. J., D. T. Kysela and Y. V. Brun (2011). "Polarity and the diversity of growth mechanisms in bacteria." Semin Cell Dev Biol 22(8): 790-798.

Buchan, D. W., F. Minneci, T. C. Nugent, K. Bryson and D. T. Jones (2013). "Scalable web services for the PSIPRED Protein Analysis Workbench." Nucleic Acids Res 41(Web Server issue): W349-357.

Buske, P. J. and P. A. Levin (2012). "Extreme C terminus of bacterial cytoskeletal protein FtsZ plays fundamental role in assembly independent of modulatory proteins." J Biol Chem 287(14): 10945-10957.

Buss, J., C. Coltharp, T. Huang, C. Pohlmeyer, S. C. Wang, C. Hatem and J. Xiao (2013). "In vivo organization of the FtsZ-ring by ZapA and ZapB revealed by quantitative super-resolution microscopy." Mol Microbiol 89(6): 1099-1120.

Bérdy, J. (2005). "Bioactive microbial metabolites." J Antibiot (Tokyo) 58(1): 1-26.

Bérdy, J. (2012). "Thoughts and facts about antibiotics: where we are now and where we are heading." J Antibiot (Tokyo) 65(8): 385-395.

Cabré, E. J., B. Monterroso, C. Alfonso, A. Sánchez-Gorostiaga, B. Reija, M. Jiménez, M. Vicente, S. Zorrilla and G. Rivas (2015). "The Nucleoid Occlusion SlmA

Protein Accelerates the Disassembly of the FtsZ Protein Polymers without Affecting Their GTPase Activity." PLoS One 10(5): e0126434.

Cambridge, J., A. Blinkova, D. Magnan, D. Bates and J. R. Walker (2014). "A replication-inhibited unsegregated nucleoid at mid-cell blocks Z-ring formation and cell division independently of SOS and the SlmA nucleoid occlusion protein in Escherichia coli." J Bacteriol 196(1): 36-49.

Carballido-López, R., A. Formstone, Y. Li, S. D. Ehrlich, P. Noirot and J. Errington (2006). "Actin homolog MreBH governs cell morphogenesis by localization of the cell wall hydrolase LytE." Dev Cell 11(3): 399-409.

Cava, F., E. Kuru, Y. V. Brun and M. A. de Pedro (2013). "Modes of cell wall growth differentiation in rod-shaped bacteria." Curr Opin Microbiol 16(6): 731-737.

Celler, K., R. I. Koning, J. Willemse, A. J. Koster and G. P. van Wezel (2016). "Cross-membranes orchestrate compartmentalization and morphogenesis in Streptomyces." Nat Commun 7: ncomms11836.

Cha, J. H. and G. C. Stewart (1997). "The divIVA minicell locus of Bacillus subtilis." J Bacteriol 179(5): 1671-1683.

Chater, K. F., S. Biró, K. J. Lee, T. Palmer and H. Schrempf (2010). "The complex extracellular biology of Streptomyces." FEMS Microbiol Rev 34(2): 171-198.

Chen, Y., H. Huang, M. Osawa and H. P. Erickson (2017). "ZipA and FtsA* stabilize FtsZ-GDP miniring structures." Sci Rep 7(1): 3650.

Chiu, M. L., M. Folcher, T. Katoh, A. M. Puglia, J. Vohradsky, B. S. Yun, H. Seto and C. J. Thompson (1999). "Broad spectrum thiopeptide recognition specificity of the Streptomyces lividans TipAL protein and its role in regulating gene expression." J Biol Chem 274(29): 20578-20586.

Claessen, D., W. de Jong, L. Dijkhuizen and H. A. Wösten (2006). "Regulation of Streptomyces development: reach for the sky!" Trends Microbiol 14(7): 313-319.

Colletti, K. S., E. A. Tattersall, K. A. Pyke, J. E. Froelich, K. D. Stokes and K. W. Osteryoung (2000). "A homologue of the bacterial cell division site-determining factor MinD mediates placement of the chloroplast division apparatus." Curr Biol 10(9): 507-516.

Coltharp, C. and J. Xiao (2017). "Beyond force generation: Why is a dynamic ring of FtsZ polymers essential for bacterial cytokinesis?" Bioessays 39(1): 1-11.

Combes, P., R. Till, S. Bee and M. C. Smith (2002). "The streptomyces genome contains multiple pseudo-attB sites for the (phi)C31-encoded site-specific recombination system." J Bacteriol 184(20): 5746-5752.

Cordell, S. C., R. E. Anderson and J. Löwe (2001). "Crystal structure of the bacterial cell division inhibitor MinC." EMBO J 20(10): 2454-2461.

Cuthbertson, L. and J. R. Nodwell (2013). "The TetR family of regulators." Microbiol Mol Biol Rev 77(3): 440-475.

Dajkovic, A., S. Pichoff, J. Lutkenhaus and D. Wirtz (2010). "Cross-linking FtsZ polymers into coherent Z rings." Mol Microbiol 78(3): 651-668.

Dalton, K. A., A. Thibessard, J. I. Hunter and G. H. Kelemen (2007). "A novel compartment, the 'subapical stem' of the aerial hyphae, is the location of a sigN-dependent, developmentally distinct transcription in Streptomyces coelicolor." Mol Microbiol 64(3): 719-737.

Dangel, V., L. Westrich, M. C. Smith, L. Heide and B. Gust (2010). "Use of an inducible promoter for antibiotic production in a heterologous host." Appl Microbiol Biotechnol 87(1): 261-269.

Daniel, R. A. and J. Errington (2003). "Control of cell morphogenesis in bacteria: two distinct ways to make a rod-shaped cell." Cell 113(6): 767-776.

de Boer, P., R. Crossley and L. Rothfield (1992). "The essential bacterial cell-division protein FtsZ is a GTPase." Nature 359(6392): 254-256.

de Boer, P. A. (2016). "Classic Spotlight: Discovery of ftsZ." J Bacteriol 198(8): 1184.

den Hengst, C. D., N. T. Tran, M. J. Bibb, G. Chandra, B. K. Leskiw and M. J. Buttner (2010). "Genes essential for morphological development and antibiotic production in Streptomyces coelicolor are targets of BldD during vegetative growth." Mol Microbiol 78(2): 361-379.

Di Ventura, B., B. Knecht, H. Andreas, W. J. Godinez, M. Fritsche, K. Rohr, W. Nickel, D. W. Heermann and V. Sourjik (2013). "Chromosome segregation by the Escherichia coli Min system." Mol Syst Biol 9: 686.

Domínguez-Escobar, J., A. Chastanet, A. H. Crevenna, V. Fromion, R. Wedlich-Söldner and R. Carballido-López (2011). "Processive movement of MreB-associated cell wall biosynthetic complexes in bacteria." Science 333(6039): 225-228.

Du, S., K. T. Park and J. Lutkenhaus (2015). "Oligomerization of FtsZ converts the FtsZ tail motif (conserved carboxy-terminal peptide) into a multivalent ligand with high avidity for partners ZipA and SlmA." Mol Microbiol 95(2): 173-188.

Duman, R., S. Ishikawa, I. Celik, H. Strahl, N. Ogasawara, P. Troc, J. Löwe and L. W. Hamoen (2013). "Structural and genetic analyses reveal the protein SepF as a new membrane anchor for the Z ring." Proc Natl Acad Sci U S A 110(48): E4601-4610.

Ebersbach, G., E. Galli, J. Møller-Jensen, J. Löwe and K. Gerdes (2008). "Novel coiled-coil cell division factor ZapB stimulates Z ring assembly and cell division." Mol Microbiol 68(3): 720-735.

Egan, A. J., R. M. Cleverley, K. Peters, R. J. Lewis and W. Vollmer (2017). "Regulation of bacterial cell wall growth." FEBS J 284(6): 851-867.

Erdmann, N., T. Petroff and B. E. Funnell (1999). "Intracellular localization of P1 ParB protein depends on ParA and parS." Proc Natl Acad Sci U S A 96(26): 14905-14910.

Erickson, H. P. (2001). "The FtsZ protofilament and attachment of ZipA--structural constraints on the FtsZ power stroke." Curr Opin Cell Biol 13(1): 55-60.

Erickson, H. P. (2017). "How bacterial cell division might cheat turgor pressure - a unified mechanism of septal division in Gram-positive and Gram-negative bacteria." Bioessays 39(8).

Erickson, H. P. (2017). "The discovery of the prokaryotic cytoskeleton: 25th anniversary." Mol Biol Cell 28(3): 357-358.

Erickson, H. P., D. E. Anderson and M. Osawa (2010). "FtsZ in bacterial cytokinesis: cytoskeleton and force generator all in one." Microbiol Mol Biol Rev 74(4): 504-528.

Errington, J., R. A. Daniel and D. J. Scheffers (2003). "Cytokinesis in bacteria." Microbiol Mol Biol Rev 67(1): 52-65, table of contents.

Esnault, C., T. Dulermo, A. Smirnov, A. Askora, M. David, A. Deniset-Besseau, I. B. Holland and M. J. Virolle (2017). "Strong antibiotic production is correlated with highly active oxidative metabolism in Streptomyces coelicolor M145." Sci Rep 7(1): 200.

Espah Borujeni, A., A. S. Channarasappa and H. M. Salis (2014). "Translation rate is controlled by coupled trade-offs between site accessibility, selective RNA unfolding and sliding at upstream standby sites." Nucleic Acids Res 42(4): 2646-2659.

Finn, R. D., P. Coggill, R. Y. Eberhardt, S. R. Eddy, J. Mistry, A. L. Mitchell, S. C. Potter, M. Punta, M.
Qureshi, A. Sangrador-Vegas, G. A. Salazar, J. Tate and A. Bateman (2016). "The Pfam protein families database: towards a more sustainable future." Nucleic Acids Res 44(D1): D279-285.

Flärdh, K. (2003). "Essential role of DivIVA in polar growth and morphogenesis in Streptomyces coelicolor A3(2)." Mol Microbiol 49(6): 1523-1536.

Flärdh, K. (2003). "Growth polarity and cell division in Streptomyces." Curr Opin Microbiol 6(6): 564-571.

Flärdh, K. (2010). "Cell polarity and the control of apical growth in Streptomyces." Curr Opin Microbiol 13(6): 758-765.

Flärdh, K. and M. J. Buttner (2009). "Streptomyces morphogenetics: dissecting differentiation in a filamentous bacterium." Nat Rev Microbiol 7(1): 36-49.

Flärdh, K., E. Leibovitz, M. J. Buttner and K. F. Chater (2000). "Generation of a non-sporulating strain of Streptomyces coelicolor A3(2) by the manipulation of a developmentally controlled ftsZ promoter." Mol Microbiol 38(4): 737-749.

Flärdh, K., D. M. Richards, A. M. Hempel, M. Howard and M. J. Buttner (2012). "Regulation of apical growth and hyphal branching in Streptomyces." Curr Opin Microbiol 15(6): 737-743.

Fuchino, K., S. Bagchi, S. Cantlay, L. Sandblad, D. Wu, J. Bergman, M. Kamali-Moghaddam, K. Flärdh and N. Ausmees (2013). "Dynamic gradients of an intermediate filament-like cytoskeleton are recruited by a polarity landmark during apical growth." Proc Natl Acad Sci U S A 110(21): E1889-1897.

Gamba, P., J. W. Veening, N. J. Saunders, L. W. Hamoen and R. A. Daniel (2009). "Two-step assembly dynamics of the Bacillus subtilis divisome." J Bacteriol 191(13): 4186-4194.

Gao, Y., M. Wenzel, M. J. Jonker and L. W. Hamoen (2017). "Free SepF interferes with recruitment of late cell division proteins." Sci Rep 7(1): 16928.

Gerdes, K., M. Howard and F. Szardenings (2010). "Pushing and pulling in prokaryotic DNA segregation." Cell 141(6): 927-942.

Gola, S., T. Munder, S. Casonato, R. Manganelli and M. Vicente (2015). "The essential role of SepF in mycobacterial division." Mol Microbiol 97(3): 560-576.

González-Cerón, G., O. J. Miranda-Olivares and L. Servín-González (2009). "Characterization of the methyl-specific restriction system of Streptomyces coelicolor A3(2) and of the role played by laterally acquired nucleases." FEMS Microbiol Lett 301(1): 35-43.

Grantcharova, N., U. Lustig and K. Flärdh (2005). "Dynamics of FtsZ assembly during sporulation in Streptomyces coelicolor A3(2)." J Bacteriol 187(9): 3227-3237.

Gray, D. I., G. W. Gooday and J. I. Prosser (1990). "Apical hyphal extension in Streptomyces coelicolor A3(2)." J Gen Microbiol 136(6): 1077-1084.

Gregory, M. A., R. Till and M. C. Smith (2003). "Integration site for Streptomyces phage phiBT1 and development of site-specific integrating vectors." J Bacteriol 185(17): 5320-5323.

Guan, F., J. Yu, Y. Liu, Y. Li, X. H. Feng, K. C. Huang, Z. Chang and S. Ye (2018). "Lateral interactions between protofilaments of the bacterial tubulin homolog FtsZ are essential for cell division." Elife 7.

Gueiros-Filho, F. J. and R. Losick (2002). "A widely conserved bacterial cell division protein that promotes assembly of the tubulin-like protein FtsZ." Genes Dev 16(19): 2544-2556.

Gupta, S., S. K. Banerjee, A. Chatterjee, A. K. Sharma, M. Kundu and J. Basu (2015). "Essential protein SepF of mycobacteria interacts with FtsZ and MurG to regulate cell growth and division." Microbiology 161(8): 1627-1638.

Gust, B., T. Kieser and K. Chater (2003). PCR targeting system in Streptomyces coelicolor A3(2). John Innes Centre.

Gust, B., T. Kieser and K. Chater, F. (2002). REDIRECT technology: PCR-targeting system in Streptomyces Coelicolor. Norwich, UK, The John Innes Centre.

Gündoğdu, M. E., Y. Kawai, N. Pavlendova, N. Ogasawara, J. Errington, D. J. Scheffers and L. W.
Hamoen (2011). "Large ring polymers align FtsZ polymers for normal septum formation." EMBO J 30(3): 617-626.

Haeusser, D. P. and W. Margolin (2016). "Splitsville: structural and functional insights into the dynamic bacterial Z ring." Nat Rev Microbiol 14(5): 305-319.

Haeusser, D. P., V. W. Rowlett and W. Margolin (2015). "A mutation in Escherichia coli ftsZ bypasses the requirement for the essential division gene zipA and confers resistance to FtsZ assembly inhibitors by stabilizing protofilament bundling." Mol Microbiol 97(5): 988-1005.

Haeusser, D. P., R. L. Schwartz, A. M. Smith, M. E. Oates and P. A. Levin (2004). "EzrA prevents aberrant cell division by modulating assembly of the cytoskeletal protein FtsZ." Mol Microbiol 52(3): 801-814.

Hajduk, I. V., C. D. Rodrigues and E. J. Harry (2016). "Connecting the dots of the bacterial cell cycle: Coordinating chromosome replication and segregation with cell division." Semin Cell Dev Biol 53: 2-9.

Hale, C. A. and P. A. de Boer (1999). "Recruitment of ZipA to the septal ring of Escherichia coli is dependent on FtsZ and independent of FtsA." J Bacteriol 181(1): 167-176.

Hale, C. A., A. C. Rhee and P. A. de Boer (2000). "ZipA-induced bundling of FtsZ polymers mediated by an interaction between C-terminal domains." J Bacteriol 182(18): 5153-5166.

Hamoen, L. W., J. C. Meile, W. de Jong, P. Noirot and J. Errington (2006). "SepF, a novel FtsZ-interacting protein required for a late step in cell division." Mol Microbiol 59(3): 989-999.

Hanahan, D. (1983). "Studies on transformation of Escherichia coli with plasmids." J Mol Biol 166(4): 557-580.

Hempel, A. M., S. B. Wang, M. Letek, J. A. Gil and K. Flärdh (2008). "Assemblies of DivIVA mark sites for hyphal branching and can establish new zones of cell wall growth in Streptomyces coelicolor." J Bacteriol 190(22): 7579-7583.

Hofmann, K. and W. Stoffel (1993). "TMbase - A database of membrane spanning proteins segements." Biol. Chem. Hoppe Seyler 374.

Holmes, N. A., J. Walshaw, R. M. Leggett, A. Thibessard, K. A. Dalton, M. D. Gillespie, A. M.
Hemmings, B. Gust and G. H. Kelemen (2013). "Coiled-coil protein Scy is a key component of a multiprotein assembly controlling polarized growth in Streptomyces." Proc Natl Acad Sci U S A 110(5): E397-406.

Hopwood, D. A. (1999). "Forty years of genetics with Streptomyces: from in vivo through in vitro to in silico." Microbiology 145 ( Pt 9): 2183-2202.

Hsiao, N. H., S. Nakayama, M. E. Merlo, M. de Vries, R. Bunet, S. Kitani, T. Nihira and E. Takano (2009). "Analysis of two additional signaling molecules in Streptomyces coelicolor and the development of a butyrolactone-specific reporter system." Chem Biol 16(9): 951-960.

Hu, Z., E. P. Gogol and J. Lutkenhaus (2002). "Dynamic assembly of MinD on phospholipid vesicles regulated by ATP and MinE." Proc Natl Acad Sci U S A 99(10): 6761-6766.

Hu, Z., A. Mukherjee, S. Pichoff and J. Lutkenhaus (1999). "The MinC component of the division site selection system in Escherichia coli interacts with FtsZ to prevent polymerization." Proc Natl Acad Sci U S A 96(26): 14819-14824.

Huang, J., J. Shi, V. Molle, B. Sohlberg, D. Weaver, M. J. Bibb, N. Karoonuthaisiri, C. J. Lih, C. M. Kao, M. J. Buttner and S. N. Cohen (2005). "Cross-regulation among disparate antibiotic biosynthetic pathways of Streptomyces coelicolor." Mol Microbiol 58(5): 1276-1287.

Ikeda, H., J. Ishikawa, A. Hanamoto, M. Shinose, H. Kikuchi, T. Shiba, Y. Sakaki, M. Hattori and S.
Omura (2003). "Complete genome sequence and comparative analysis of the industrial microorganism Streptomyces avermitilis." Nat Biotechnol 21(5): 526-531.

Iniesta, A. A. (2014). "ParABS system in chromosome partitioning in the bacterium Myxococcus xanthus." PLoS One 9(1): e86897.

Ishikawa, S., Y. Kawai, K. Hiramatsu, M. Kuwano and N. Ogasawara (2006). "A new FtsZ-interacting protein, YlmF, complements the activity of FtsA during progression of cell division in Bacillus subtilis." Mol Microbiol 60(6): 1364-1380.

Ito, T., N. Uozumi, T. Nakamura, S. Takayama, N. Matsuda, H. Aiba, H. Hemmi and T. Yoshimura (2009). "The implication of YggT of Escherichia coli in osmotic regulation." Biosci Biotechnol Biochem 73(12): 2698-2704.

Jakimowicz, D. and G. P. van Wezel (2012). "Cell division and DNA segregation in Streptomyces: how to build a septum in the middle of nowhere?" Mol Microbiol 85(3): 393-404.

Jensen, S. O., L. S. Thompson and E. J. Harry (2005). "Cell division in Bacillus subtilis: FtsZ and FtsA association is Z-ring independent, and FtsA is required for efficient midcell Z-Ring assembly." J Bacteriol 187(18): 6536-6544.

Jeong, Y., J. N. Kim, M. W. Kim, G. Bucca, S. Cho, Y. J. Yoon, B. G. Kim, J. H. Roe, S. C. Kim, C. P. Smith and B. K. Cho (2016). "The dynamic transcriptional and translational landscape of the model antibiotic producer Streptomyces coelicolor A3(2)." Nat Commun 7: 11605.

Jones, L. J., R. Carballido-López and J. Errington (2001). "Control of cell shape in bacteria: helical, actin-like filaments in Bacillus subtilis." Cell 104(6): 913-922.

Juarez, J. R. and W. Margolin (2012). "A bacterial actin unites to divide bacterial cells." EMBO J 31(10): 2235-2236.

Jyothikumar, V., E. J. Tilley, R. Wali and P. R. Herron (2008). "Time-lapse microscopy of Streptomyces coelicolor growth and sporulation." Appl Environ Microbiol 74(21): 6774-6781.

Kabeya, Y., H. Nakanishi, K. Suzuki, T. Ichikawa, Y. Kondou, M. Matsui and S. Y. Miyagishima (2010). "The YlmG protein has a conserved function related to the distribution of nucleoids in chloroplasts and cyanobacteria." BMC Plant Biol 10: 57.

Kanehisa, M. and S. Goto (2000). "KEGG: kyoto encyclopedia of genes and genomes." Nucleic Acids Res 28(1): 27-30.

Kanehisa, M., Y. Sato, M. Kawashima, M. Furumichi and M. Tanabe (2016). "KEGG as a reference resource for gene and protein annotation." Nucleic Acids Res 44(D1): D457-462.

Kang, C. M., S. Nyayapathy, J. Y. Lee, J. W. Suh and R. N. Husson (2008). "Wag31, a homologue of the cell division protein DivIVA, regulates growth, morphology and polar cell wall synthesis in mycobacteria." Microbiology 154(Pt 3): 725-735.

Kawai, K., G. Wang, S. Okamoto and K. Ochi (2007). "The rare earth, scandium, causes antibiotic overproduction in Streptomyces spp." FEMS Microbiol Lett 274(2): 311-315.

Kelemen, G. H. (2017). "Intermediate Filaments Supporting Cell Shape and Growth in Bacteria." Subcell Biochem 84: 161-211.

Kemp, J. T., A. Driks and R. Losick (2002). "FtsA mutants of Bacillus subtilis impaired in sporulation." J Bacteriol 184(14): 3856-3863.

Kim, E. S., J. Y. Song, D. W. Kim, K. F. Chater and K. J. Lee (2008). "A possible extended family of regulators of sigma factor activity in Streptomyces coelicolor." J Bacteriol 190(22): 7559-7566.

King, A. A. and K. F. Chater (1986). "The expression of the Escherichia coli lacZ gene in Streptomyces." J Gen Microbiol 132(6): 1739-1752.

Kleckner, N. E., K. Chatzi, M. A. White, J. K. Fisher and M. Stouf (2018). "Coordination of Growth, Chromosome Replication/Segregation, and Cell Division in." Front Microbiol 9: 1469.

Kloosterman, T. G., R. Lenarcic, C. R. Willis, D. M. Roberts, L. W. Hamoen, J. Errington and L. J. Wu (2016). "Complex polar machinery required for proper chromosome segregation in vegetative and sporulating cells of Bacillus subtilis." Mol Microbiol 101(2): 333-350.

Kobs, G. (1997). Cloning Blunt-End DNA Fragments into the pGEM -T vector Systems. Promega Notes Magazine: 15.

Kormanec, J. and B. Sevcikova (2002). "The stress-response sigma factor sigma(H) controls the expression of ssgB, a homologue of the sporulation-specific cell division gene ssgA, in Streptomyces coelicolor A3(2)." Mol Genet Genomics 267(4): 536-543.

Krogh, A., B. Larsson, G. von Heijne and E. L. Sonnhammer (2001). "Predicting transmembrane protein topology with a hidden Markov model: application to complete genomes." J Mol Biol 305(3): 567-580.

Krupka, M., E. J. Cabré, M. Jiménez, G. Rivas, A. I. Rico and M. Vicente (2014). "Role of the FtsA C terminus as a switch for polymerization and membrane association." MBio 5(6): e02221.

Krupka, M., M. Sobrinos-Sanguino, M. Jiménez, G. Rivas and W. Margolin (2018). "Escherichia coli ZipA Organizes FtsZ Polymers into Dynamic Ring-Like Protofilament Structures." MBio 9(3).

Kruse, T., J. Bork-Jensen and K. Gerdes (2005). "The morphogenetic MreBCD proteins of Escherichia coli form an essential membrane-bound complex." Mol Microbiol 55(1): 78-89.

Król, E., S. P. van Kessel, L. S. van Bezouwen, N. Kumar, E. J. Boekema and D. J. Scheffers (2012). "Bacillus subtilis SepF binds to the C-terminus of FtsZ." PLoS One 7(8): e43293.

Käll, L., A. Krogh and E. L. Sonnhammer (2005). "An HMM posterior decoder for sequence feature prediction that includes homology information." Bioinformatics 21 Suppl 1: i251-257.

Laloux, G. and C. Jacobs-Wagner (2014). "How do bacteria localize proteins to the cell pole?" J Cell Sci 127(Pt 1): 11-19.

Leonid, B. V., F.-M. A. Miguel, H. K. Jan, M. Francisco, H. A. David and D. Lubbert (1996). "Production of Actinorhodin-Related "Blue Pigments" by Streptomyces coelicolor A3(2)." Journal of Bacteriology 178(8): p. 2233-2244.

Letek, M., M. Fiuza, E. Ordóñez, A. F. Villadangos, A. Ramos, L. M. Mateos and J. A. Gil (2008). "Cell growth and cell division in the rod-shaped actinomycete Corynebacterium glutamicum." Antonie Van Leeuwenhoek 94(1): 99-109.

Letek, M., E. Ordóñez, J. Vaquera, W. Margolin, K. Flärdh, L. M. Mateos and J. A. Gil (2008). "DivIVA is required for polar growth in the MreB-lacking rod-shaped actinomycete Corynebacterium glutamicum." J Bacteriol 190(9): 3283-3292.

Levin, P. A., I. G. Kurtser and A. D. Grossman (1999). "Identification and characterization of a negative regulator of FtsZ ring formation in Bacillus subtilis." Proc Natl Acad Sci U S A 96(17): 9642-9647.

Liu, Z., A. Mukherjee and J. Lutkenhaus (1999). "Recruitment of ZipA to the division site by interaction with FtsZ." Mol Microbiol 31(6): 1853-1861.

Livny, J., Y. Yamaichi and M. K. Waldor (2007). "Distribution of centromere-like parS sites in bacteria: insights from comparative genomics." J Bacteriol 189(23): 8693-8703.

Loose, M. and T. J. Mitchison (2014). "The bacterial cell division proteins FtsA and FtsZ self-organize into dynamic cytoskeletal patterns." Nat Cell Biol 16(1): 38-46.

Lussier, F. X., F. Denis and F. Shareck (2010). "Adaptation of the highly productive T7 expression system to Streptomyces lividans." Appl Environ Microbiol 76(3): 967-970.

Lutkenhaus, J. (2012). "The ParA/MinD family puts things in their place." Trends Microbiol 20(9): 411-418.

Löwe, J. and L. A. Amos (1998). "Crystal structure of the bacterial cell-division protein FtsZ." Nature 391(6663): 203-206.

MacNeil, D. J., K. M. Gewain, C. L. Ruby, G. Dezeny, P. H. Gibbons and T. MacNeil (1992). "Analysis of Streptomyces avermitilis genes required for avermectin biosynthesis utilizing a novel integration vector." Gene 111(1): 61-68.

Makarova, K. S., N. Yutin, S. D. Bell and E. V. Koonin (2010). "Evolution of diverse cell division and vesicle formation systems in Archaea." Nat Rev Microbiol 8(10): 731-741.

Margolin, W. (2001). "Bacterial cell division: a moving MinE sweeper boggles the MinD." Curr Biol 11(10): R395-398.

Margolin, W. (2003). "Bacterial division: the fellowship of the ring." Curr Biol 13(1): R16-18.

Margolin, W. (2005). "FtsZ and the division of prokaryotic cells and organelles." Nat Rev Mol Cell Biol 6(11): 862-871.

Margolin, W. (2009). "Sculpting the bacterial cell." Curr Biol 19(17): R812-822.

Marschall, L., P. Sagmeister and C. Herwig (2017). "Tunable recombinant protein expression in E. coli: promoter systems and genetic constraints." Appl Microbiol Biotechnol 101(2): 501-512.

McCormick, J. R. (2009). "Cell division is dispensable but not irrelevant in Streptomyces." Curr Opin Microbiol 12(6): 689-698.

McCormick, J. R., E. P. Su, A. Driks and R. Losick (1994). "Growth and viability of Streptomyces coelicolor mutant for the cell division gene ftsZ." Mol Microbiol 14(2): 243-254.

Meinhardt, H. and P. A. de Boer (2001). "Pattern formation in Escherichia coli: a model for the pole-to-pole oscillations of Min proteins and the localization of the division site." Proc Natl Acad Sci U S A 98(25): 14202-14207.

Meniche, X., R. Otten, M. S. Siegrist, C. E. Baer, K. C. Murphy, C. R. Bertozzi and C. M. Sassetti (2014). "Subpolar addition of new cell wall is directed by DivIVA in mycobacteria." Proc Natl Acad Sci U S A 111(31): E3243-3251.

Mikuni, S., K. Kodama, A. Sasaki, N. Kohira, H. Maki, M. Munetomo, K. Maenaka and M. Kinjo (2015). "Screening for FtsZ Dimerization Inhibitors Using Fluorescence Cross-Correlation Spectroscopy and Surface Resonance Plasmon Analysis." PLoS One 10(7): e0130933.

Monahan, L. G. and E. J. Harry (2013). "Identifying how bacterial cells find their middle: a new perspective." Mol Microbiol 87(2): 231-234.

Monahan, L. G., A. T. Liew, A. L. Bottomley and E. J. Harry (2014). "Division site positioning in bacteria: one size does not fit all." Front Microbiol 5: 19.

Mosyak, L., Y. Zhang, E. Glasfeld, S. Haney, M. Stahl, J. Seehra and W. S. Somers (2000). "The bacterial cell-division protein ZipA and its interaction with an FtsZ fragment revealed by X-ray crystallography." EMBO J 19(13): 3179-3191.

Mukherjee, A., K. Dai and J. Lutkenhaus (1993). "Escherichia coli cell division protein FtsZ is a guanine nucleotide binding protein." Proc Natl Acad Sci U S A 90(3): 1053-1057.

Mukherjee, P., K. Sureka, P. Datta, T. Hossain, S. Barik, K. P. Das, M. Kundu and J. Basu (2009). "Novel role of Wag31 in protection of mycobacteria under oxidative stress." Mol Microbiol 73(1): 103-119.

Mura, A., D. Fadda, A. J. Perez, M. L. Danforth, D. Musu, A. I. Rico, M. Krupka, D. Denapaite, H. T. Tsui, M. E. Winkler, P. Branny, M. Vicente, W. Margolin and O. Massidda (2016). "Roles of the essential protein FtsA in cell growth and division in Streptococcus pneumoniae." J Bacteriol.

Ochi, K. and T. Hosaka (2013). "New strategies for drug discovery: activation of silent or weakly expressed microbial gene clusters." Appl Microbiol Biotechnol 97(1): 87-98.

Oliva, M. A., S. Halbedel, S. M. Freund, P. Dutow, T. A. Leonard, D. B. Veprintsev, L. W. Hamoen and

J. Löwe (2010). "Features critical for membrane binding revealed by DivIVA crystal structure." EMBO J 29(12): 1988-2001.

Omura, S., H. Ikeda, J. Ishikawa, A. Hanamoto, C. Takahashi, M. Shinose, Y. Takahashi, H. Horikawa,
H. Nakazawa, T. Osonoe, H. Kikuchi, T. Shiba, Y. Sakaki and M. Hattori (2001). "Genome sequence of an industrial microorganism Streptomyces avermitilis: deducing the ability of producing secondary metabolites." Proc Natl Acad Sci U S A 98(21): 12215-12220.

Osteryoung, K. W., K. D. Stokes, S. M. Rutherford, A. L. Percival and W. Y. Lee (1998). "Chloroplast division in higher plants requires members of two functionally divergent gene families with homology to bacterial ftsZ." Plant Cell 10(12): 1991-2004.

Petersen, T. N., S. Brunak, G. von Heijne and H. Nielsen (2011). "SignalP 4.0: discriminating signal peptides from transmembrane regions." Nat Methods 8(10): 785-786.

Pichoff, S. and J. Lutkenhaus (2002). "Unique and overlapping roles for ZipA and FtsA in septal ring assembly in Escherichia coli." EMBO J 21(4): 685-693.

Pichoff, S., B. Shen, B. Sullivan and J. Lutkenhaus (2012). "FtsA mutants impaired for self-interaction bypass ZipA suggesting a model in which FtsA's self-interaction competes with its ability to recruit downstream division proteins." Mol Microbiol 83(1): 151-167.

Procópio, R. E., I. R. Silva, M. K. Martins, J. L. Azevedo and J. M. Araújo (2012). "Antibiotics produced by Streptomyces." Braz J Infect Dis 16(5): 466-471.

Randich, A. M. and Y. V. Brun (2015). "Molecular mechanisms for the evolution of bacterial morphologies and growth modes." Front Microbiol 6: 580.

RayChaudhuri, D. (1999). "ZipA is a MAP-Tau homolog and is essential for structural integrity of the cytokinetic FtsZ ring during bacterial cell division." EMBO J 18(9): 2372-2383.

RayChaudhuri, D. and J. T. Park (1992). "Escherichia coli cell-division gene ftsZ encodes a novel GTP-binding protein." Nature 359(6392): 251-254.

Redenbach, M., H. M. Kieser, D. Denapaite, A. Eichner, J. Cullum, H. Kinashi and D. A. Hopwood (1996). "A set of ordered cosmids and a detailed genetic and physical map for the 8 Mb Streptomyces coelicolor A3(2) chromosome." Mol Microbiol 21(1): 77-96.

Renner, L. D., P. Eswaramoorthy, K. S. Ramamurthi and D. B. Weibel (2013). "Studying biomolecule localization by engineering bacterial cell wall curvature." PLoS One 8(12): e84143.

Richards, D. M., A. M. Hempel, K. Flärdh, M. J. Buttner and M. Howard (2012). "Mechanistic basis of branch-site selection in filamentous bacteria." PLoS Comput Biol 8(3): e1002423.

Rodríguez-García, A., P. Combes, R. Pérez-Redondo and M. C. Smith (2005). "Natural and synthetic tetracycline-inducible promoters for use in the antibiotic-producing bacteria Streptomyces." Nucleic Acids Res 33(9): e87.

Romero, D., M. F. Traxler, D. López and R. Kolter (2011). "Antibiotics as signal molecules." Chem Rev 111(9): 5492-5505.

Romero-Rodríguez, A., B. Ruiz-Villafán, V. H. Tierrafría, R. Rodríguez-Sanoja and S. Sánchez (2016). "Carbon Catabolite Regulation of Secondary Metabolite Formation and Morphological Differentiation in Streptomyces coelicolor." Appl Biochem Biotechnol 180(6): 1152-1166.

Rowlett, V. W. and W. Margolin (2015). "The Min system and other nucleoid-independent regulators of Z ring positioning." Front Microbiol 6: 478.

Ruiz-Avila, L. B., S. Huecas, M. Artola, A. Vergoñós, E. Ramírez-Aportela, E. Cercenado, I. Barasoain, H. Vázquez-Villa, M. Martín-Fontecha, P. Chacón, M. L. López-Rodríguez and J. M. Andreu (2013). "Synthetic inhibitors of bacterial cell division targeting the GTP-binding site of FtsZ." ACS Chem Biol 8(9): 2072-2083.

Ryding, N. J., T. B. Anderson and W. C. Champness (2002). "Regulation of the Streptomyces coelicolor calcium-dependent antibiotic by absA, encoding a cluster-linked two-component system." J Bacteriol 184(3): 794-805.

Saalbach, G., A. M. Hempel, M. Vigouroux, K. Flärdh, M. J. Buttner and M. J. Naldrett (2013). "Determination of phosphorylation sites in the DivIVA cytoskeletal protein of Streptomyces coelicolor by targeted LC-MS/MS." J Proteome Res 12(9): 4187-4192.

Salis, H. M., E. A. Mirsky and C. A. Voigt (2009). "Automated design of synthetic ribosome binding sites to control protein expression." Nat Biotechnol 27(10): 946-950.

Schirner, K. and J. Errington (2009). "Influence of heterologous MreB proteins on cell morphology of Bacillus subtilis." Microbiology 155(Pt 11): 3611-3621.

Scholtissek, S. and F. Grosse (1987). "A cloning cartridge of lambda t(o) terminator." Nucleic Acids Res 15(7): 3185.

Schumacher, M. A. (2017). "Bacterial Nucleoid Occlusion: Multiple Mechanisms for Preventing Chromosome Bisection During Cell Division." Subcell Biochem 84: 267-298.

Schwedock, J., J. R. McCormick, E. R. Angert, J. R. Nodwell and R. Losick (1997). "Assembly of the cell division protein FtsZ into ladder-like structures in the aerial hyphae of Streptomyces coelicolor." Mol Microbiol 25(5): 847-858.

Shih, Y. L., X. Fu, G. F. King, T. Le and L. Rothfield (2002). "Division site placement in E.coli: mutations that prevent formation of the MinE ring lead to loss of the normal midcell arrest of growth of polar MinD membrane domains." EMBO J 21(13): 3347-3357.

Shih, Y. L. and L. Rothfield (2006). "The bacterial cytoskeleton." Microbiol Mol Biol Rev 70(3): 729-754.

Shiomi, D., H. Mori and H. Niki (2009). "Genetic mechanism regulating bacterial cell shape and metabolism." Commun Integr Biol 2(3): 219-220.

Singh, J. K., R. D. Makde, V. Kumar and D. Panda (2008). "SepF increases the assembly and bundling of FtsZ polymers and stabilizes FtsZ protofilaments by binding along its length." J Biol Chem 283(45): 31116-31124.
Strakova, E., J. Bobek, A. Zikova and J. Vohradsky (2013). "Global features of gene expression on the proteome and transcriptome levels in S. coelicolor during germination." PLoS One 8(9): e72842.

Suefuji, K., R. Valluzzi and D. RayChaudhuri (2002). "Dynamic assembly of MinD into filament bundles modulated by ATP, phospholipids, and MinE." Proc Natl Acad Sci U S A 99(26): 16776-16781.

Szklarczyk, D., J. H. Morris, H. Cook, M. Kuhn, S. Wyder, M. Simonovic, A. Santos, N. T. Doncheva, A.
Roth, P. Bork, L. J. Jensen and C. von Mering (2017). "The STRING database in 2017: quality-controlled protein-protein association networks, made broadly accessible." Nucleic Acids Res 45(D1): D362-D368.

Szwedziak, P., Q. Wang, S. M. Freund and J. Löwe (2012). "FtsA forms actin-like protofilaments." EMBO J 31(10): 2249-2260.

Taghbalout, A., L. Ma and L. Rothfield (2006). "Role of MinD-membrane association in Min protein interactions." J Bacteriol 188(8): 2993-3001.

Takano, E. (2006). "Gamma-butyrolactones: Streptomyces signalling molecules regulating antibiotic production and differentiation." Curr Opin Microbiol 9(3): 287-294.

Takano, E., J. White, C. J. Thompson and M. J. Bibb (1995). "Construction of thiostrepton-inducible, high-copy-number expression vectors for use in Streptomyces spp." Gene 166(1): 133-137.

Thanbichler, M. (2010). "Synchronization of chromosome dynamics and cell division in bacteria." Cold Spring Harb Perspect Biol 2(1): a000331.

Tiyanont, K., T. Doan, M. B. Lazarus, X. Fang, D. Z. Rudner and S. Walker (2006). "Imaging peptidoglycan biosynthesis in Bacillus subtilis with fluorescent antibiotics." Proc Natl Acad Sci U S A 103(29): 11033-11038.

Tonthat, N. K., S. T. Arold, B. F. Pickering, M. W. Van Dyke, S. Liang, Y. Lu, T. K. Beuria, W. Margolin and M. A. Schumacher (2011). "Molecular mechanism by which the nucleoid occlusion factor, SlmA, keeps cytokinesis in check." EMBO J 30(1): 154-164.

Tonthat, N. K., S. L. Milam, N. Chinnam, T. Whitfill, W. Margolin and M. A. Schumacher (2013). "SlmA forms a higher-order structure on DNA that inhibits cytokinetic Z-ring formation over the nucleoid." Proc Natl Acad Sci U S A 110(26): 10586-10591.

Toro, E. and L. Shapiro (2010). "Bacterial chromosome organization and segregation." Cold Spring Harb Perspect Biol 2(2): a000349.

van Wezel, G. P., J. White, P. Young, P. W. Postma and M. J. Bibb (1997). "Substrate induction and glucose repression of maltose utilization by Streptomyces coelicolor A3(2) is controlled by malR, a member of the lacI-galR family of regulatory genes." Mol Microbiol 23(3): 537-549.

Varma, A. and K. D. Young (2009). "In Escherichia coli, MreB and FtsZ direct the synthesis of lateral cell wall via independent pathways that require PBP 2." J Bacteriol 191(11): 3526-3533.

Vats, P., Y. L. Shih and L. Rothfield (2009). "Assembly of the MreB-associated cytoskeletal ring of Escherichia coli." Mol Microbiol 72(1): 170-182.

Vecchiarelli, A. G., J. C. Havey, L. L. Ing, E. O. Wong, W. G. Waples and B. E. Funnell (2013). "Dissection of the ATPase active site of P1 ParA reveals multiple active forms essential for plasmid partition." J Biol Chem 288(24): 17823-17831.

Viollier, P. H., W. Minas, G. E. Dale, M. Folcher and C. J. Thompson (2001). "Role of acid metabolism in Streptomyces coelicolor morphological differentiation and antibiotic biosynthesis." J Bacteriol 183(10): 3184-3192.

Vitha, S., J. E. Froehlich, O. Koksharova, K. A. Pyke, H. van Erp and K. W. Osteryoung (2003). "ARC6 is a J-domain plastid division protein and an evolutionary descendant of the cyanobacterial cell division protein Ftn2." Plant Cell 15(8): 1918-1933.

Walshaw, J., M. D. Gillespie and G. H. Kelemen (2010). "A novel coiled-coil repeat variant in a class of bacterial cytoskeletal proteins." J Struct Biol 170(2): 202-215.

Wang, S. B., S. Cantlay, N. Nordberg, M. Letek, J. A. Gil and K. Flärdh (2009). "Domains involved in the in vivo function and oligomerization of apical growth determinant DivIVA in Streptomyces coelicolor." FEMS Microbiol Lett 297(1): 101-109.

Wang, X., J. Huang, A. Mukherjee, C. Cao and J. Lutkenhaus (1997). "Analysis of the interaction of FtsZ with itself, GTP, and FtsA." J Bacteriol 179(17): 5551-5559.

Ward, J. M., G. R. Janssen, T. Kieser, M. J. Bibb and M. J. Buttner (1986). "Construction and characterisation of a series of multi-copy promoter-probe plasmid

vectors for Streptomyces using the aminoglycoside phosphotransferase gene from Tn5 as indicator." Mol Gen Genet 203(3): 468-478.

Wasserstrom, S., N. Grantcharova, W. Ubhayasekera, N. Ausmees, L. Sandblad and K. Flärdh (2013). "Non-sporulating ftsZ mutants in Streptomyces coelicolor reveal amino acid residues critical for FtsZ polymerization dynamics." Microbiology 159(Pt 5): 890-901.

Weiss, D. S. (2004). "Bacterial cell division and the septal ring." Mol Microbiol 54(3): 588-597.

Willemse, J., J. W. Borst, E. de Waal, T. Bisseling and G. P. van Wezel (2011). "Positive control of cell division: FtsZ is recruited by SsgB during sporulation of Streptomyces." Genes Dev 25(1): 89-99.

Wu, L. J. and J. Errington (2004). "Coordination of cell division and chromosome segregation by a nucleoid occlusion protein in Bacillus subtilis." Cell 117(7): 915-925.

Wu, L. J. and J. Errington (2011). "Nucleoid occlusion and bacterial cell division." Nat Rev Microbiol 10(1): 8-12.

Yagüe, P., J. Willemse, R. I. Koning, B. Rioseras, M. T. López-García, N. Gonzalez-Quiñonez, C. Lopez-Iglesias, P. V. Shliaha, A. Rogowska-Wrzesinska, A. J. Koster, O. N. Jensen, G. P. van Wezel and Á. Manteca (2016). "Subcompartmentalization by cross-membranes during early growth of Streptomyces hyphae." Nat Commun 7: 12467.

Yu, Z., S. Vodanovic-Jankovic, N. Ledeboer, S. X. Huang, S. R. Rajski, M. Kron and B. Shen (2011). "Tirandamycins from Streptomyces sp. 17944 inhibiting the parasite Brugia malayi asparagine tRNA synthetase." Org Lett 13(8): 2034-2037.

# Appendix

The genes surrounding the *S. coelicolor sepF* genes (SepF homologues are marked in bold), shown in numerical 'SCO number' order. The gene size is given amino acids (AA) and taken from StrepDB. The gene function data was collected from StreptDB (column 3) and possible domains, families and homologues of each gene is given in column 4. This information was collected by conducting protein BLAST searches using the amino acid sequence of each respective gene. Bit scores and E values are also provided for the recorded top results. The protein BLASTs excluded results from *Streptomycetales*.

| Gene identifier | Size | Gene function (StreptDB) | Additional information |
|---|---|---|---|
| *SCO1744* | 388 AA | Possible two-component system sensor kinase<br>Similar to putative sensor kinases involved in global regulation of antibiotic synthesis | Multidomain: COG4585<br>Superfamily/specific hit: HisKA 3 and HATPase c, contains: Mg2+ binding site<br>Top results: histidine kinase domain-containing protein, then two-component sensor histidine kinase<br>Bit score: 377 / 376<br>E value: 3e-126 / 7e-126 |
| *SCO1745* | 221 AA | Probable two-component system response regulator<br>Similar to *E. coli* nitrate response regulator | Multidomain: Citb<br>Superfamily: REC and HTH, specific hit: REC and LuxR C like, contains: intermolecular recognition site, phosphorylation site, dimerisation site, DNA binding residues, active site<br>Top results: DNA binding response regulator, then putative two-component system response regulator LuxR,<br>Bit score: 352 / 331<br>E value: 2e-121 / 7e-133 |
| *SCO1746* | 300 AA | Highly similar to extracellular serine protease<br>Contains pFam match to trypsin | Multidomain: trypsin, family/specific hit: Pro Al protease,<br>Top result: serine proteases<br>Bit score: 427<br>E value: 1e-148 |
| *SCO1747* | 283 AA | Hypothetical protein (conserved)<br>Probable CDS | Superfamily and specific hit: DUF1684<br>Top result: protein of unknown function<br>Bit score: 371<br>E value: 3e-127 |
| *SCO1748* | 159 AA | Probable expression regulator fragment<br>Highly similar to metallothionein-like proteins, probable expression regulator | No conserved domains detected<br>Top result: hypothetical protein<br>Bit score: 476<br>E value: 4e-165 |
| ***SCO1749 / sepF1*** | **146 AA** | **Conserved hypothetical protein<br>Similar to mycobacterium** | **Part of DUF552 Superfamily/DUF552 family<br>Non-specific hit of ylmF** |

| | | **tuberculosis MTCY270.21** | **Top result: sepF** |
|---|---|---|---|
| *SCO1750* | 397 AA | Probable acyl coA dehydrogenase<br>Similar to many dehydrogenases | Multidomain: CaiA<br>Superfamily; ACAD<br>Also contains: active site<br>Top result: acyl-CoA dehydrogenase<br>Bit score: 734<br>E value: 0.0 |
| *SCO1751* | 534 AA | Probable transmembrane transport protein<br>Contains possible hydrophobic membrane spanning regions | Multidomain: PRK14995<br>Superfamily: MF5<br>Also contains: putative substrate translocation pore<br>Top result: transporter<br>Bit score: 720<br>E value: 0.0 |
| *SCO1752* | 396 AA | Possible integral membrane protein<br>Contains possible hydrophobic membrane spanning regions | Superfamily: PMT 2 Top result: hypothetical protein, then membrane protein/<br>Bit score: 522<br>E value: 0.0 |
| *SCO1753* | 340 AA | Possible integral membrane protein<br>Contains pFam match to PAP2 superfamily/PF01569<br>Contains possible membrane spanning regions | Multidomain: PgpB<br>Superfamily/specific hit: PAP2 like 2, also contains: active site<br>Top result: membrane protein, hypothetical protein, then phosphoesterase PA-phosphatase related protein<br>Bit score: 477 / 470 / 411<br>E value: 3e-167 / 3e-164 / 2e-141 |
| *SCO1754* | 71 AA | Hypothetical protein | Superfamily: Inhibitor I78<br>Top result: Proteinase inhibitor I78<br>Bit score: 122<br>E value: 4e-35 |
| *SCO1755* | 282 AA | Conserved hypothetical protein | No putative conserved domains detected (only 20 hits in total)<br>Top result: hypothetical protein,<br>Some results indicated glycosyl transferase<br>Bit score: 320 / 70.1<br>E value: 5e-107 / 5e-10 |

| Gene identifier | Size | Gene function (StreptDB) | Additional information |
|---|---|---|---|
| *SCO2074* | 204 AA | Probable signal peptidase, possible hydrophobic membrane spanning regions, pFam match to peptidase A8 and SPase II | Superfamily: peptidase A8, domain: PRK14764<br>Top result: Signal peptidase II<br>Bit score: 299<br>E value: 3e-101 |
| *SCO2075* | 239 AA | Probable DNA binding protein, N-terminus is similar to histone-like proteins as it contains 13 degenerate AAKK repeats (like karP in chlamydia trachomatis), c-terminus similar to *E. coli* DskA, contains probable coiled-coil, contains pFam match to prokaryotic dskA/traR C4 type zinc finger | Superfamily: HC2 and zf-dskA traA<br>Specific hit: DskA<br>Top result: DNA binding protein / transcription regulator<br>Bit score: 318 / 285<br>E value: 1e-105 / 2e-93 |
| *SCO2076* | 1047 AA | Possible isoleucyl-tRNA sythetase<br>Contains pFam match to PF00133<br>tRNA-synt 1 | Multidomain: ileS<br>Superfamily: nt trans and anticodon Ia like<br>Specific hits: IleRS core and anticodon Ia likeABEc<br>Also contains: tRNA binding surface, anticodon binding site, KMSKS motif, HIGH motif, active site<br>Top result: isoleucyl-tRNA sythetase<br>Bit score: 1993<br>E value: 0.0 |
| *SCO2077 / DivIVA* | 398 AA | Hypothetical protein, contains probable coiled-coils, | Superfamilies: PRK14127 and vATP-synt E and SPFH like<br>Specific hit: DivI1A domain<br>Top result: cell division protein DivIVA<br>Bit score: 488<br>E value: 3e-169 |
| *SCO2078* | 94 AA | Putative membrane protein, contains possible hydrophobic membrane spanning regions | Superfamily: YGGT<br>Specific hit: YGGT<br>Top result: Protein of unknown function YGGT<br>/ membrane protein<br>Bit score: 173 / 147<br>E value: 7e-55 1e-44 |
| ***Sco2079 / sepF2*** | **213 AA** | **Conserved hypothetical protein<br>N-terminus is Asp- and Glu-rich** | **Superfamily: DUF552<br>Top result: cell division protein SepF<br>Bit score: 419<br>E value: 3e-148** |
| *SCO2080* | 239 AA | Conserved hypothetical protein, contains pFam match to PF01168 UPF0001, PS01211 | Superfamily: PLPDE III<br>Specific hit: PLPDE III YBL036c like<br>Also: catalytic residue Pyridoxal 5'-phosphate binging site<br>Top result: YggS family pyridoxal phosphate enzyme<br>Bit score: 402 |

| | | | |
|---|---|---|---|
| | | | E value: 7e-141 |
| *SCO2081* | 242 AA | Conserved hypothetical protein | Superfamily/specific hit: Cu-oxidase 4<br>Top result: laccase<br>Bit score: 397<br>E value: 1e-138 |
| *SCO2082 / ftsZ* | 399 AA | ftsZ, with ftsZ protein signatures 1 and 2 | Multidomain: PRK09330, Superfamily: Tubulin FtsZ CetZ-like,<br>Specific hit: FtsZ type 1, contains SulA interaction site<br>Top result: cell division protein FtsZ<br>Bit score: 657<br>E value: 0.0 |
| *SCO2083 / ftsQ* | 264 AA | ftsQ, required for efficient sporulation but not growth and viability, contains possible hydrophobic membrane spanning region | Superfamilies: SURF Ag VNR and FtsQ,<br>specific hits: POTRA 1 and FtsQ<br>Top result: cell division protein FtsQ<br>Bit score: 372<br>E value: 6e-128 |
| *SCO2084 / murG* | 364 AA | Probable UDP-N-acetylglucosamine-N-acetylmuramyl-(pentapeptide) pyrophosphoryl-undecaprenol N-acetylglucosamine transferase | multidomain: murG, superfamily: glycosyltransferase GTB type, specific hit: GT1 MurG, contains: homodimer interface, active site<br>Top result: UDP- N-acetylglucosamine-N-acetylmuramyl-(pentapeptide) pyrophosphoryl-undecaprenol N-acetylglucosamine transferase<br>Bit score: 683<br>E value: 0.0 |

| Gene identifier | Size | Gene function (StreptDB) | Additional information |
|---|---|---|---|
| *SCO5962* | 196 AA | Probable transcriptional regulator, part of MerR family. Contains MerR family signature, helix-turn-helix motif and pFam match to MerR | Multidomain – SoxR, specific hit– HTH No1A AlbR, may have DNA binding residues and putative dimer interface<br>Top result: transcriptional regulator<br>Bit score: 184<br>E value: 9e-56 |
| *SCO5963* | 191 AA | Possible membrane protein | Hit: Ion trans 2<br>Top result: membrane family protein,<br>Bit score: 176<br>E value: 2e-53 |
| *SCO5964* | 452 AA | Probable membrane protein<br>Contains zinc-binding region and possible hydrophobic membrane spanning regions | Hit: voltage gated –cic (CIC chloride channel)<br>Top result: hypothetical protein,<br>Putative ion channel protein<br>Bit score: 314 / 298<br>E value: 9e-100 / 2e-93 |
| *SCO5965* | 155 AA | Possible integral membrane protein<br>Contains possible hydrophobic membrane spanning regions | No putative conserved domains detected<br>Top result: hypothetical protein,<br>Then membrane protein<br>Bit score: 159<br>E value: 2e-47 |
| *SCO5966* | 1032 A | Possible oxidase<br>pFam match to PF02913 FAD-oxidase | Specific hits; FAD-binding-4, FAD-oxidase-C, Fer4-8<br>Top result- demethylmenaguinone methyltransferase<br>Also, FAD-linked oxidase<br>Bit score: 1558<br>E value 0.0 |
| ***sCO5967 / sepF3*** | **136 AA** | **Conserved hypothetical protein**<br>**Similar to 2SC134.02** | **DUF552 Superfamily, DUF552**<br>**Top result- Actinobacteria bacterium OK006**<br>**228 bits**<br>**E value: 2e-75** |
| *SCO5968* | 402 AA | Possible bldA-regulated nucleotide binding protein<br>No significant database matches | Superfamily: P-loop NTPase, specific hit: AAA 23,<br>Top result: hypothetical protein, then biotin transporter BioY<br>Bit score: 541 / 541<br>E value: 0.0 / 0.0 |
| *SCO5969* | 117 AA | Conserved hypothetical protein | Hits: NTP-PPase RS21 C6 like, with chemical substrate binding site, homodimer interface, oligomer interface, metal binding site<br>Top result: nucleotide pyrophosphohydrolase<br>Bit score: 182<br>E value: 1e-57 |
| *SCO5970* | 156 AA | Unknown, no sign database | No putative domains detected |

| | | | |
|---|---|---|---|
| | | matches | and only 5 matches in total (all hypothetical proteins)<br>Bit score: 214<br>E value: 3e-69 |
| *SCO5971* | 307 AA | Conserved hypothetical protein<br>Contains pFam match to bacterial luciferase | Superfamily: flavin utilising monoxygenases, specific hit: F420 Rv1855c<br>Top result: putative oxidoreductase, then many LLM class F420-dependent oxidoreductase<br>Bit score: 565 / 563<br>E value: 0.0 / 0.0 |
| *SCO5972* | 307 AA | Hypothetical protein with conserved region | Superfamilies: Hen1 L and AdoMet MTases, specific hits: Hen1 L and adoMet MTases, also contains s-adenosylmethionine binding site<br>Top result: 3'terminal RNA ribose 2'-O-methyltransferase Hen1<br>Bit score: 781<br>E value: 0.0 |
| *SCO5973* | 842 AA | Possible phosphatase<br>Similar to protein serine-threonine phosphatase from Anabaena | Superfamilies: p-loop NTPase and MPP superfamily,<br>specific hit: MPP Prp like,<br>also contains putative RNA binding site, metal binding site, active site<br>Top result: polynucleotide kinase-phosphatase<br>Bit score: 1516<br>E value: 0.0 |